Modelling the effects of submerged breakwaters in a wave basin

2DH-simulations of tests with Delft2D-MOR

Volume I: Report

J. Schaap

Master thesis
August 1997

TU Delft
Technische Universiteit Delft

Faculteit der Civiele Techniek

Modelling the effects of submerged breakwaters in a wave basin

2DH-simulations of tests with Delft2D-MOR

Volume I: Report

J. Schaap

Master thesis
August 1997

Delft University of Technology
Faculty of Civil Engineering

Supervision:

prof. ir. K. d'Angremond
dr. ir. N. Booij
dr. ir. J. van de Graaff
dr. ir. J.A. Roelvink
ir. S.C. van der Biezen

Abstract

This report is the result of a master thesis of the author, student at Delft University of Technology, Faculty of Civil Engineering.

In this report a simulation of tests with submerged breakwaters, parallel to the shoreline, in a wave basin, are carried out with the morphodynamic model Delft2D-MOR. This 2-dimensional horizontal model was developed by DELFT HYDRAULICS.
The aim of this thesis is to find out whether and how this model is able to simulate these tests with submerged breakwaters, and to investigate the effects of these breakwaters on profile development.

The conditions of the experiments are used as input for the model. One simulation without breakwaters and two simulations with different breakwater configurations are carried out.

Comparison of model results with measurement data from the experiments shows that the model is able to simulate some hydrodynamic and morphological processes induced by the submerged breakwaters. Wave heights in the vicinity of the obstacles are reduced because of wave dissipation over the breakwaters. Flow circulation patterns occur induced by water level gradients.
Sediment is mainly transported from behind the breakwaters towards and through the gaps seaward.

However, there are still quite some differences between model and experimental results. Large amounts of sediment are eroded near the shoreline and close behind the breakwaters, which was not measured during the experiments.
Apparently inaccuracies in modelling appear at the boundary of sea and land (original dry points remain dry, bottom gradients are irrealistic large), and at the location of submerged breakwaters where the modelling of wave behaviour is not adequate.
Also problems with resolution of computational grid arise at the location of submerged breakwaters. A higher resolution is needed in order to compute realistic flow velocities close behind the submerged breakwaters.

Obviously a lot of work has to be done to improve the 2DH model results such that it can be a useful tool for modelling the effects of submerged breakwaters on a beach profile.

Contents

Abstract
List of tables
List of figures

1 Introduction **1-1**

2 Human Capital and Mobility Programme **2-1**

3 Submerged offshore breakwaters **3-1**

3.1 Introduction 3-1
3.2 Effects on waves 3-1
3.2.1 Transmission and reflection 3-1
3.2.2 Diffraction 3-2
3.3 Effects on water level (wave set-up) 3-3
3.4 Effects on currents 3-6
3.4.1 Longshore currents 3-6
3.4.2 Onshore-offshore currents 3-6
3.5 Effects on morphology 3-7

4 Aims and restrictions of this study **4-1**

4.1 Introduction 4-1
4.2 Aims of this study 4-1
4.3 Starting-points and limiting conditions 4-1
4.4 Choice of experiments for comparison 4-1

5 Experiments **5-1**

5.1 Introduction 5-1
5.2 Lay-out of the wave basin 5-1
5.3 Configurations and dimensions of the submerged breakwaters 5-3
5.4 Sand profile 5-4
5.5 Orientation 5-4
5.6 Measurements 5-5
5.6.1 Profile measurements 5-5
5.6.2 Fluid velocity measurements 5-5
5.6.3 Wave height measurements 5-6
5.7 Test schedule 5-6

Contents (continued)

6 Description of Delft2D-MOR **6-1**

6.1 The compound model Delft2D-MOR 6-1
6.2 Modules, input files and data communication 6-3

7 WAVES (HISWA) **7-1**

7.1 Physical background 7-1
7.1.1 General 7-1
7.1.2 Directional spreading 7-3
7.1.3 Bottom refraction 7-3
7.1.4 Wave generation by wind 7-4
7.1.5 Bottom dissipation 7-4
7.1.6 Surf dissipation and added white-capping 7-4
7.1.7 Current dissipation (wave blocking) 7-5
7.1.8 Dissipation and transmission through and over an obstacle 7-6
7.1.9 Dissipation due to vegetation 7-6
7.2 Numerical background 7-7

8 Flow module (Delft3D-FLOW) **8-1**

8.1 Description of Delft3D-FLOW 8-1
8.1.1 Physical background 8-1
8.1.2 Numerical background 8-2
8.1.3 Grid definition 8-3

9 Transport module (TRSTOT) **9-1**

9.1 Introduction 9-1
9.2 Bijker formula 9-1
9.2.1 Bed load transport 9-1
9.2.2 Suspended load transport 9-3

10 Bottom module (BOTTOM) **10-1**

10.1 Introduction 10-1
10.2 Physical background 10-2
10.3 Numerical background 10-3

Contents (continued)

11 Determination of HISWA parameters 11-1

11.1 Introduction 11-1
11.2 Wave height H_s 11-1
11.3 Wave period T 11-2
11.4 Angle of incidence θ_0 11-2
11.5 Directional spreading of wave energy 11-2
11.6 Breaking parameters 11-4
11.6.1 Input for HISWA calibration 11-4
11.6.2 Calibration results 11-5
11.7 Friction parameters 11-9

12 2DH-simulations of initial hydrodynamic processes in the wave basin 12-1

12.1 Introduction 12-1
12.2 Used process tree 12-1
12.3 Input description 12-2
12.3.1 WAVES input 12-2
12.3.2 FLOW input 12-4
12.3.3 TRSTOT input 12-5
12.4 Results 12-6
12.4.1 Case A3: No breakwaters 12-6
12.4.2 Case C3: Two breakwaters 12-10
12.4.3 Case D3: Three breakwaters 12-14

13 2DH-simulation of hydrodynamic and morphological processes in the wave basin without breakwaters 13-1

13.1 Introduction 13-1
13.2 Used process tree 13-1
13.3 Input description 13-3
13.4 Results 13-3
13.5 Conclusions and remarks 13-7

14 2DH-simulation of hydrodynamic and morphological processes in the wave basin with two breakwaters 14-1

14.1 Introduction 14-1
14.2 Used process tree 14-1
14.3 Input description 14-1

Contents (continued)

14.4 Results 14-1
14.5 Conclusions and remarks 14-10

15 2DH-simulation of hydrodynamic and morphological processes in the wave basin with three breakwaters 15-1

15.1 Introduction 15-1
15.2 Used process tree 15-1
15.3 Input description 15-1
15.4 Results 15-1
15.5 Conclusions and remarks 15-9

16 General discussion of the simulation results 16-1

17 Sensitivity analysis 17-1

17.1 Introduction 17-1
17.2 Shallow water breaking index γ_s 17-1
17.2.1 Introduction 17-1
17.2.2 Results 17-1
17.3 Dissipation coefficient α 17-5
17.3.1 Introduction 17-5
17.3.2 Results 17-5
17.4 Breakwater crest enlargement 17-7
17.4.1 Introduction 17-7
17.4.2 Results 17-7

18 Conclusions and recommendations 18-1

Acknowledgements

References

Appendices

List of tables

5.1 Measured cross sections
5.2 Test schedule

List of figures

3.1 Parameters determining the wave climate behind the breakwater

5.1 Lay-out of the basin
5.2 Breakwater configuration 1
5.3 Breakwater configuration 2
5.4 Cross section of submerged breakwater
5.5 Axis system

6.1 General structure of Delft2D-MOR
6.2 Example of a process tree
6.3 Modules and input files of Delft2D-MOR

8.1 Staggered grid in Delft3D-FLOW

11.1 Generated wave field at t = 6 min 26 s
11.2 Generated and measured wave heights at x = 3.0 m and t = 6 min 26 s
11.3 Generated wave field at t = 32 min 09 s
11.4 Generated and measured wave heights at x = 12.5 m and t = 32 min 09 s
11.5 Generated and measured wave heights at x = 3.0 m

12.1 Process tree
12.2 History current u
12.3 History water level
12.4 Initial wave height
12.5 Initial dissipation
12.6 Initial water level
12.7 Initial wave height at x = 12.5 m and x = 20.0 m
12.8 Initial dissipation at x = 12.5 m and x = 20.0 m
12.9 Initial water level at x = 12.5 m and x = 20.0 m
12.10 Initial wave height at x = 15.5 m and x = 20.0 m
12.11 Initial dissipation at x = 15.5 m and x = 20.0 m
12.12 Initial water level at x = 15.5 m and x = 20.0 m

13.1 Process tree
13.2 Wave height after 0.0 and 7.5 hours at x = 15.5 m
13.3 Dissipation after 0.0 and 7.5 hours at x = 15.5 m
13.4 Water level after 0.0 and 7.5 hours at x = 15.5 m
13.5 Computed profile development at x = 15.5 m
13.6 Measured profile development at x = 15.5 m

List of figures (continued)

14.1 Wave height after 0.0 and 7.5 hours at x = 20.0 m
14.2 Dissipation after 0.0 and 7.5 hours at x = 20.0 m
14.3 Wave height after 0.0 and 7.5 hours at x = 12.5 m
14.4 Dissipation after 0.0 and 7.5 hours at x = 12.5 m
14.5 Water level after 0.0 and 7.5 hours at x = 20.0 m
14.6 Water level after 0.0 and 7.5 hours at x = 12.5 m
14.7 Computed profile development at x = 12.5 m
14.8 Measured profile development at x = 12.5 m
14.9 Computed profile development at x = 20.0 m
14.10 Measured profile development at x = 20.0 m

15.1 Process tree
15.2 Wave height after 0.0 and 7.5 hours at x = 20.0 m
15.3 Dissipation after 0.0 and 7.5 hours at x = 20.0 m
15.4 Wave height after 0.0 and 7.5 hours at x = 15.5 m
15.5 Dissipation after 0.0 and 7.5 hours at x = 15.5 m
15.6 Water level after 0.0 and 7.5 hours at x = 20.0 m
15.7 Water level after 0.0 and 7.5 hours at x = 15.5 m
15.8 Computed profile development at x = 15.5 m
15.9 Measured profile development at x = 15.5 m
15.10 Computed profile development at x = 20.0 m
15.11 Measured profile development at x = 20.0 m

17.1 Wave height at x = 15.5 m
17.2 Dissipation at x = 15.5 m
17.3 Dissipation at x = 20.0 m
17.4 Wave height at x = 15.5 m
17.5 Dissipation at x = 15.5 m
17.6 Dissipation at x = 15.5 m

1 Introduction

Unprotected sandy beaches often suffer from erosion due to wave attack, tides and currents. Several measures can be taken to prevent this, like artificial beach nourishments, application of groynes, revetments and (submerged) breakwaters.
There is not much known about the effect of submerged breakwaters until so far. Therefore some experiments with submerged, discontinuous breakwaters were carried out in a wave basin in the Laboratory of Fluid Mechanics of Delft University of Technology. The results of these experiments, carried out by Van der Biezen and De Later, were described by De Later (1996). These results consist of measurements on wave heights, currents (velocity and direction) and sediment transports.

In this report a comparison of the experimental results to results with a computer model is presented. The computer model used is Delft2D-MOR developed by DELFT HYDRAULICS.
The aim of this study is to find out whether and how a recent developed computer model, Delft2D-MOR, is able to simulate the hydrodynamic and morphological processes that were present during the experiments with submerged breakwaters in the wave basin. The main focus is on morphology. Besides, an intercomparison of the computer model results for different cases with and without breakwaters is made in order to predict effects of different breakwater configurations on morphology.

This report has the following lay-out.
In Chapter 2 information is given about the framework in which this study is carried out.
Chapter 3 gives relevant information about the most important hydrodynamic and morphological processes in the nearshore region and the influences of submerged offshore breakwaters on these processes.
Objective, starting-points and limiting conditions are described in Chapter 4 in which also the restrictions of this study are given.
In Chapter 5 a description of the experiments is given (lay-out of the basin, configuration of the breakwaters, sand profile, initial conditions, test schedule).
Information about Delft2D-MOR, the computer model used, is given in Chapter 6.
In the next chapters the different modules are described. In Chapter 7 the wave module, in Chapter 8 the flow module, in Chapter 9 the sediment transport module and finally the bottom module in Chapter 10. In Chapter 11 the determination of HISWA parameters is described.
The 2DH-simulation of initial hydrodynamic processes in the wave basin is described in Chapter 12.
Chapter 13, 14 and 15 contain the simulations of the tests without breakwaters, with two breakwaters and with three breakwaters respectively. In these simulations the movable bed is taken into account. The results are qualitatively compared to the tests.
A sensitivity analysis of some parameters and other modelling aspects is carried out in Chapter

17. These parameters directly influence the computed wave heights and flow field and also the computed sediment transports and morphology. The possibility of getting better simulation results is investigated. For this purpose also a computation with wider breakwater crests is carried out.
Finally, in Chapter 18 conclusions and recommendations are given.

2 Human Capital and Mobility Programme

The tests mentioned in Chapter 1 were carried out within the framework of the Dynamics of Beaches project. This project is part of the HCM-framework of the European Union. This particular project is a co-operation of six universities:

- Aristotle University of Thessaloniki (Greece)
- University of Ghent (Belgium)
- University of Liverpool (United Kingdom)
- University College of Cork (Ireland)
- Delft University of Technology (The Netherlands)
- Universitat Politecnico de Catalunya (Spain)

The objective of the Dynamics of Beaches project is to improve the existing knowledge on physical processes pertaining to the nearshore region (including the surf zone). Four of the above mentioned universities will carry out tests within their experimental facilities. These tests will cover three areas:

- Hydrodynamics: water motion
- Morphodynamics: sediment motion (bed and suspended transport and resulting bottom evolution)
- Structural effects: all tests will be performed with and without a submerged breakwater with a view to assess the physical impact of this structure on the nearshore zone

3 Submerged offshore breakwaters

3.1 Introduction

Submerged breakwaters, also called reef breakwaters or sills, are breakwaters with a construction height which is less than the water depth. They are generally shore-parallel and built nearshore. The main purpose of these structures is to reduce the effects of offshore sediment movement caused by waves and currents. A submerged breakwater allows better water exchange between the inner and outer zone than emerged breakwaters.
In this chapter the influence of submerged breakwaters on the nearshore hydrodynamic and morphological processes is described.

3.2 Effects on waves

The main aim of an offshore breakwater is to dissipate wave energy (and thus diminishing the wave height) and to change wave and current patterns. The offshore breakwater has effect on a number of hydrodynamic processes which contribute to these goals: transmission, reflection and diffraction.

3.2.1 Transmission and reflection

If a wave meets a (submerged) breakwater which has a steep slope, the wave will partly dissipate (by breaking) and partly reflect. The steeper the slope the larger the wave reflection. The ratio of the incoming wave height and the reflected wave height is called the reflection coefficient K_r:

$$K_r = \frac{H_r}{H_i} \tag{3.1}$$

in which H_r is the reflected wave height and H_i the incoming wave height.

Part of the wave energy is transmitted into the lee of the breakwater. The magnitude of transmission can be expressed in the transmission coefficient K_t, which yields:

$$K_t = \frac{H_t}{H_i} \tag{3.2}$$

in which H_t is the transmitted wave height and H_i the incoming wave height.

The effectiveness of the submerged breakwaters can be determined in terms of the transmission coefficient K_t which can be expressed as follows: $\{K_t\} = f(H_i/\lambda, b/\lambda, \{h-d\}/h, h/\lambda, s)$, see Figure 3.1.

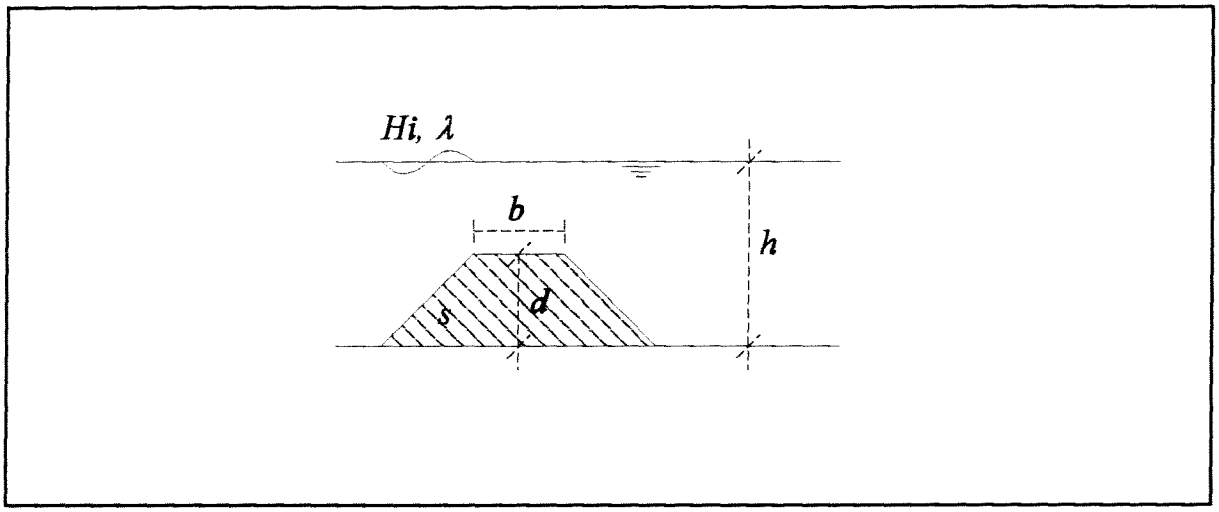

Figure 3.1: Parameters determining the wave climate behind the breakwater

in which:	H_i	=	incoming wave height
	λ	=	wave length
	b	=	crest width of the breakwater
	h	=	water depth at the location of the breakwater
	d	=	breakwater height
	s	=	shape parameter

Research results show that submergence (h-d) and crest width b are the most important parameters.

3.2.2 Diffraction

Diffraction causes wave energy bending around the tip of an offshore breakwater and penetrating into the sheltered area. This can be explained by looking at the different zones. The submerged breakwater creates a more or less sheltered area with reduced wave heights in the lee of the breakwater while the waves approaching the beach pass the breakwater unchanged in the exposed area. This leads to a variation in wave energy along a wave crest going from the exposed area into the sheltered area. This will cause transport of wave energy into the sheltered area, so that bending waves develop with diminishing wave heights going from the exposed to the sheltered area.

3.3 Effects on water level (wave set-up)

Waves influence the mean condition (averaged in time) of the medium in which they propagate. The mean effect of the waves can be expressed in extra terms in the mass and the momentum balance of the medium. Because of the change in the mass and momentum balance, the medium behaves differently compared to when waves are absent. The wave-induced contribution of horizontal momentum is referred to as the radiation stress, defined as:

$$S_{XX} = \int_0^{h+\eta} (p + \rho_w U^2)\,dz - \int_0^{h} p_0\,dz \qquad (3.3a)$$

$$= (2n-1/2)E \qquad (3.3b)$$

$$S_{YY} = (n-1/2)E \qquad (3.4)$$

in which:

S_{XX}	=	principal radiation stress acting on a plane parallel to the wave crest
S_{YY}	=	principal radiation stress acting on a plane perpendicular to the wave crest
h	=	water depth
η	=	instantaneous water level
p	=	pressure
p_0	=	pressure if waves are absent
ρ_w	=	mass density of water
n	=	ratio of wave group velocity to wave celerity c_g/c
E	=	wave energy given by:

$$E = \frac{1}{8}\rho_w g H^2 \qquad (3.5)$$

where g is the acceleration due to gravity and H is the wave height.

Obviously, the most important factor that influences the radiation stress is the wave height, via the wave energy. In shallow water this wave energy is very dependent upon the water depth when breaking occurs.
Radiation stress influences physical processes mainly in areas where wave conditions change.

Such areas are locations where wave refraction, diffraction, shoaling or breaking occurs (e.g. near (submerged) breakwaters).

In the case of a uniform beach with normal incident waves, the wave heights change due to shoaling and breaking. The radiation stress gradient should in this case be balanced by a horizontal pressure gradient resulting from a water surface slope. The momentum balance yields:

$$\frac{dS_{XX}}{dx} + \rho_w g(h+\eta)\frac{d\eta}{dx} = 0 \qquad (3.6)$$

in which:

S_{XX}	=	principal radiation stress acting on a plane parallel to the wave crest
x	=	horizontal coordinate perpendicular to the coast
h	=	water depth
η	=	averaged water level change caused by the waves
ρ_w	=	mass density of water
g	=	acceleration due to gravity

In the region outside the surf zone, the energy dissipation can be neglected. The energy balance then reduces to E.n.c. = constant = $E_0.n_0.c_0$, from which the variation of E with x can be calculated. Using the initial condition that η=0 in deep water, the result is:

$$\eta = -\frac{1}{8}\frac{kH^2}{\sinh 2kh} \qquad (3.7)$$

in which:

η	=	averaged water level change caused by the waves
H	=	local wave height
h	=	local water depth
k	=	wave number

This equation shows a lowering of the mean water level towards the shore (set-down).
In very shallow water (kh << 1) equation (3.7) can be approximated to:

$$\eta = -\frac{1}{16}\frac{H^2}{h} \tag{3.8}$$

The resulting water level change immediately seaward of the breaker zone follows from the substitution of breaking conditions ($H = H_b = \gamma h_b$):

$$\eta_b = -\frac{1}{16}\frac{H_b^2}{h_b} = -\frac{1}{16}\gamma^2 h_b \tag{3.9}$$

where the subscript b refers to conditions at the outer edge of the breaker zone.

Because of the breaking waves in the surf zone the wave height here will decrease, and as a consequence so will the radiation stress S_{XX}. The radiation stress S_{XX} in the surf zone can be determined using equation (3.3) and the (breaking) condition $H(x) = \gamma h(x)$ with the shallow water approximation n=1.
This yields:

$$S_{XX} = \frac{3}{16}\gamma^2 \rho g (h+\eta)^2 \tag{3.10}$$

Substitution of this expression in the equation (3.6) results in an equation for the gradient of the wave set-up. Integration of this equation from the breaker point to the point of maximum set-up gives the change of averaged water level across the surf zone $\Delta\eta$:

$$\Delta\eta = \frac{3}{8}\gamma^2 h_b \tag{3.11}$$

The wave set-up at the water line is the difference between the wave set-down at the breaker point and this maximum set-up:

$$\eta_s = \eta_b + \Delta\eta \approx \frac{5}{16}\gamma H_b \tag{3.12}$$

If a submerged breakwater is placed in a cross-shore profile, a sheltered area is generated in the lee of the breakwater in which the wave heights are reduced. Wave breaking over the submerged breakwater induces a wave set-up over the breakwater. The wave set-up increases going from the exposed area to the axis of symmetry in the lee of the breakwater. The water level difference strongly depends on the wave height difference between the wave height in the exposed and in the sheltered area, which, in turn, depends on the geometry of the breakwater.

3.4 Effects on currents

3.4.1 Longshore currents

The wave set-up gradient is a driving force for currents in the zone between breakwaters and shoreline. In longshore direction there is not an opposing thrust to balance the gradient in the mean water level. This pressure gradient therefore induces a longshore current flowing parallel to the shore from the sheltered area into the exposed area.

In the case of waves arriving obliquely to the coast, there would also be a radiation shear stress component acting parallel to the shore. This radiation shear stress S_{xy} is given by:

$$S_{xy} = En\sin(\theta)\cos(\theta) \qquad (3.13)$$

In the experiments waves were generated with a propagation direction perpendicular to the shoreline.
Because of the small amount of diffraction due to the breakwater the direction of the waves changes only slightly. Therefore the radiation shear stress component is very small in case of this study and longshore are mainly generated by effects of the submerged breakwaters.

3.4.2 Onshore-offshore currents

Water particles do not describe exactly closed orbital trajectories, but they have a second-order mean Lagrangian velocity in the direction of the wave propagation, called the Stokes drift. Assuming a condition of zero mass flux at each location, there must be a return flow (opposite to the direction of the wave propagation), the undertow. The Stokes drift acts between wave crest and trough level, the undertow below the wave trough level. Dean et al. (1995) interpreted experimental data on a submerged breakwater. They found that the water which is transported over the breakwater as mass transport, is ponded up due to the return flow being impeded by the presence of the breakwater, resulting in a portion being redirected as longshore currents.
Hattori and Sakai (1994) highlight the influence of the return flow over the crest upon the incoming waves. Permeability of the structure plays an important role in reduction of the

strength of this return flow yielding changes in the breaker height and breaking position as well as the breaker type.
Seelig and Walton (1980) developed a simple theory in the case of segmented submerged breakwaters. Water is transported over the structure until either a gap or the breakwater ends are reached. Then the impounded water is released to the offshore region. According to Seelig and Walton's approach it is possible to estimate the strength of the seaward flowing currents. To reduce return currents the crest elevation may be raised, the gaps between the segments may be enlarged or the permeability of the structure may be increased.

3.5 Effects on morphology

The above described effects of submerged breakwaters on waves, water level and currents have their influence on morphology. This influence has been examined by many investigators. Laboratory experiments in a wave flume show that the submerged breakwater is an excellent holding tool for the sand contained in the surf zone (Chiaia et al., 1992). However it did not reduce the retreat of the shore line.
Laboratory test with segmented submerged breakwaters pointed out the importance of the ratio between the breakwater length and the gap width upon the wave transmission and sediment transport (Sawaragi, 1992). A strong return flow through the breakwater gap develops which carries sediment offshore and reduces the sand level behind the structure.

Results from tests within the framework of the Dynamics of Beaches project have been reported by Prinos et al. (1995). In 2DV tests it has been shown that less sediment is transported offshore as a result of placing a submerged breakwater and that this material is deposited behind the structure. In these tests the 3D-effects, such as the influence of gaps, return currents, longshore currents, are not taken into account. 3D-tests with multiple segmented submerged breakwaters carried out by De Later and Van der Biezen (here reference is made to Chapter 5) show that sediment is removed from behind the structures and transported through the gaps. Moreover, the overall transported sand volumes seem to be larger with the presence of breakwaters than without.
It is clear that the breakwater length/gap width ratio mainly determines the effects of submerged breakwaters on morphology. Longer breakwater lengths or smaller gaps will result in stronger currents through the gaps which will remove more sediment.

Much more research is required to examine the effects of submerged breakwaters on hydro- and morphodynamics. For this purpose a computer model which is able to simulate these processes would be a useful tool.

4 Aims and restrictions of this study

4.1 Introduction

In this chapter a description is made of the aim of this study and the starting-points and limiting conditions that are posed. In section 4.4 three experiments are chosen for (inter)comparison with the computer model Delft2D-MOR.

4.2 Aims of this study

In this study the results of tests with submerged breakwaters in a wave basin with regular waves and the simulation results of Delft2D-MOR are compared. The simulation results are intercompared in order to give an opinion about the influence of the breakwaters on hydrodynamic and morphological aspects. However, the main focus is on morphology.
The aims of this study are to find out whether and how Delft2D-MOR is able to simulate the tests and whether the model can be useful for further research on (submerged) breakwaters. (For this purpose also the computer model CREON (developed by Gao, Radder and Booij) is used).
Besides, recommendations will be given for further research.

4.3 Starting-points and limiting conditions

- It is assumed that test results are reliable, so these are not checked.
- It is assumed that computer models Delft2D-MOR, HISWA and CREON do not make computation errors.
- Parameters and dimensions will not be scaled back to prototype values.
- The comparison between experiments and simulation results will mainly focus on morphology.
- The consequence of the use of numerical schemes in the computer models is not investigated.

4.4 Choice of experiments for comparison

Out of the nine different experiments with and without breakwaters carried out by De Later and Van der Biezen three experiments have been chosen for (inter)comparison with the computer model Delft2D-MOR. These experiments are A3, C3 and D3. General information about the wave conditions and basin lay-out in these experiments are given in appendix A1, A2 and A3.

The experiments C1 and D1 with H_i = 0.08 m and experiments C2 and D2 with H_i = 0.10 m showed that the incident waves are not (hardly) influenced by the breakwaters (no breaking). Apparently these relatively small waves hardly feel the breakwaters. The experiments C3 and D3 with H_i = 0.12 m showed that the waves are influenced by the breakwaters. These waves partially break as they run over the breakwaters.
Since the aim of this study is to investigate the possibility of modelling submerged breakwaters and simulate their effects on morphology, it is desired that the submerged breakwaters do have a significant effect on morphology (and on wave heights, currents and sediment transports). Therefore the choice has been made to use experiments C3, D3 (and A3) for comparison with model results.

5 Experiments

5.1 Introduction

The experiments were carried out by De Later and Van der Biezen in a wave basin of the Labatory of Fluid Mechanics of Delft University of Technology. In this basin regular waves were generated, perpendiculary incoming on a sloping concrete and sand profile. Experiments were done with two configurations of submerged breakwaters and without breakwaters. The model of the breakwaters had a scale of 1:15. Other parameters (related to waves, sand) had not been scaled with respect to some prototype.

5.2 Lay-out of the wave basin

The lay-out of the basin is shown in Figure 5.1.

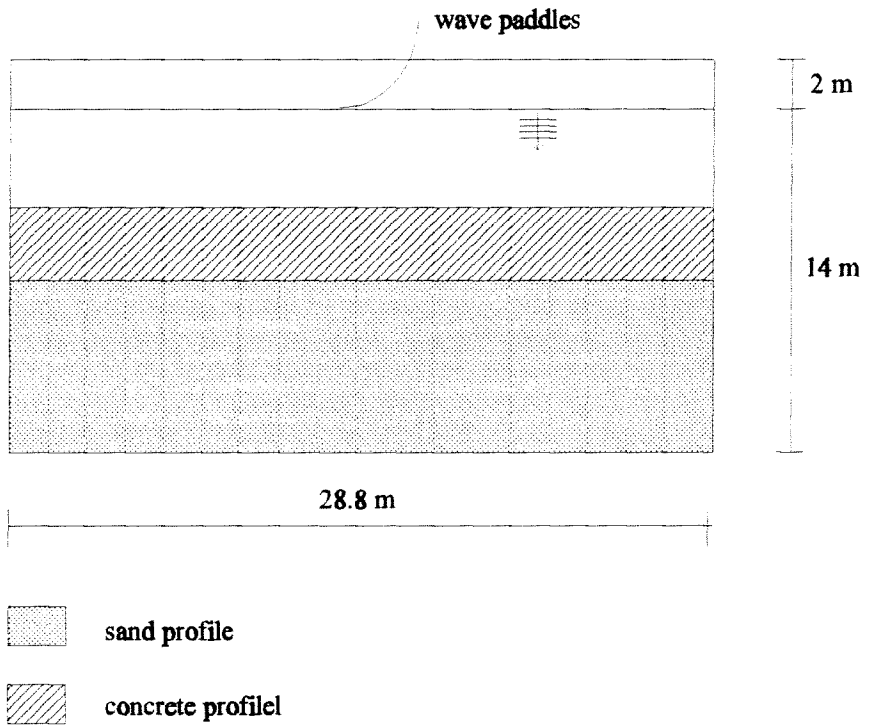

Figure 5.1: Lay-out of the basin

The basin floor has been made of concrete. On behalf of the experiments a concrete slope of 1:13 has been created on top of a part of this floor. The concrete slope, on which the breakwaters are based, is the lowest part of the total slope. It guarantees stability under the breakwaters.

5.3 Configurations and dimensions of the submerged breakwaters

In the experiments two configurations of submerged breakwaters have been applied.
The first configuration is shown in Figure 5.2.

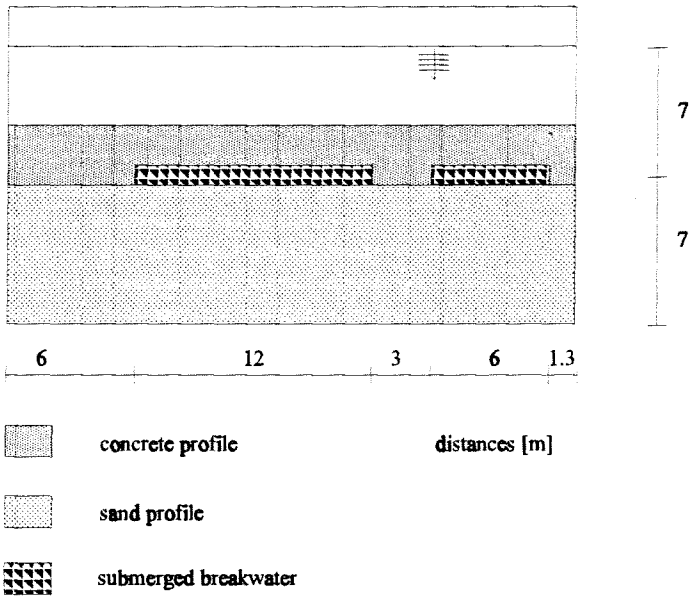

Figure 5.2: Configuration 1

The first configuration consists of two submerged breakwaters, one with a length of 12 m and one of 6 m, with inbetween these a gap with a length of 3 m.
The second configuration, as shown in Figure 5.3, consists of three submerged breakwaters with a length of 6 m, with inbetween these breakwaters gaps with lengths of 3 m.

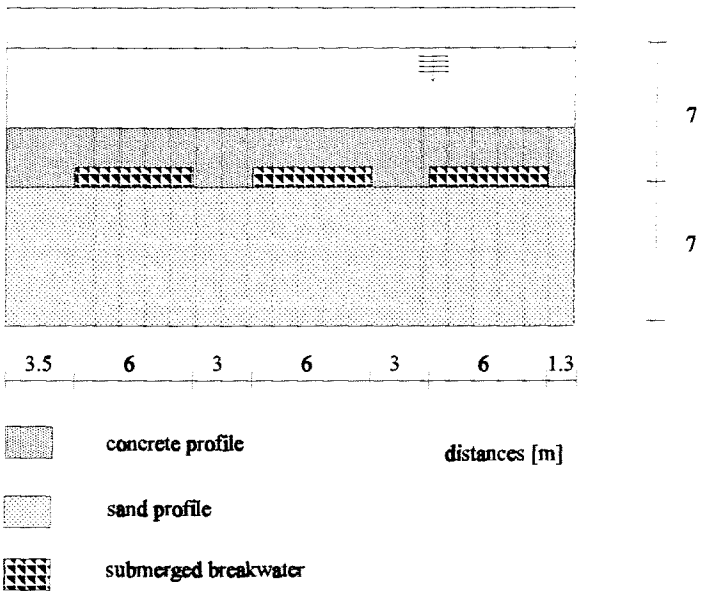

Figure 5.3: Configuration 2

The submerged breakwaters consist of an impermeable core with a surrounding armour layer of two layers of rock (D_{n50} = 0.05 m, ρ = 2650 kg/m^3), designed according to the stability formulae of Van der Meer.

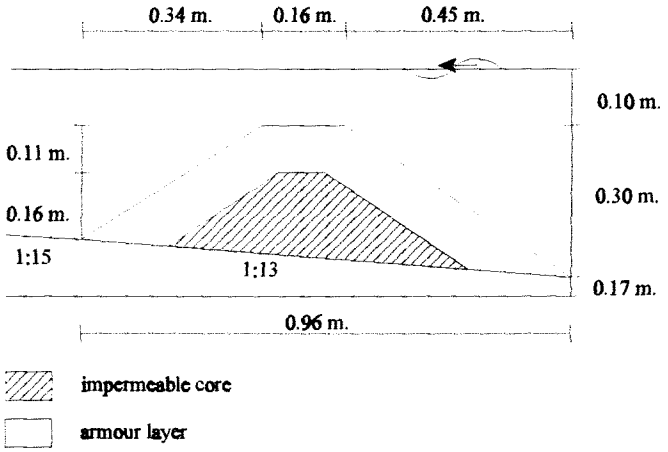

Figure 5.4: Cross section of submerged breakwater

The water depth over the crest (= head) of the breakwaters is 0.10 m and the water depth at the upwave toe is 0.40 m. The cross-section of a breakwater is shown in Figure 5.4 . Both the upwave and downwave slope of the breakwaters are 2:3.

5.4 Sand profile

The (initial) slope of the sand profile behind the breakwaters is 1:15. The sand has a grain diameter D_{50} of 75 μm. This diameter is relatively small compared to the diameter of sand that can be found on beaches. The reason for applying this smaller diameter is that in this case the ratio of bottom transport and suspended transport is closer to the value which would be found if the experiments were done at scale 1:1. Applying scaled wave parameters and unscaled sand parameters would result in a decreased amount of suspended transport compared to the amount of bottom transport, because of the decrease of wave energy.

5.5 Orientation

The same axis system as in the experiments is used for this study: the y-axis direction is the opposite of the propagation direction (with y = 0 m at the beach and y = 14 m where the waves are generated). See Figure 5.5.

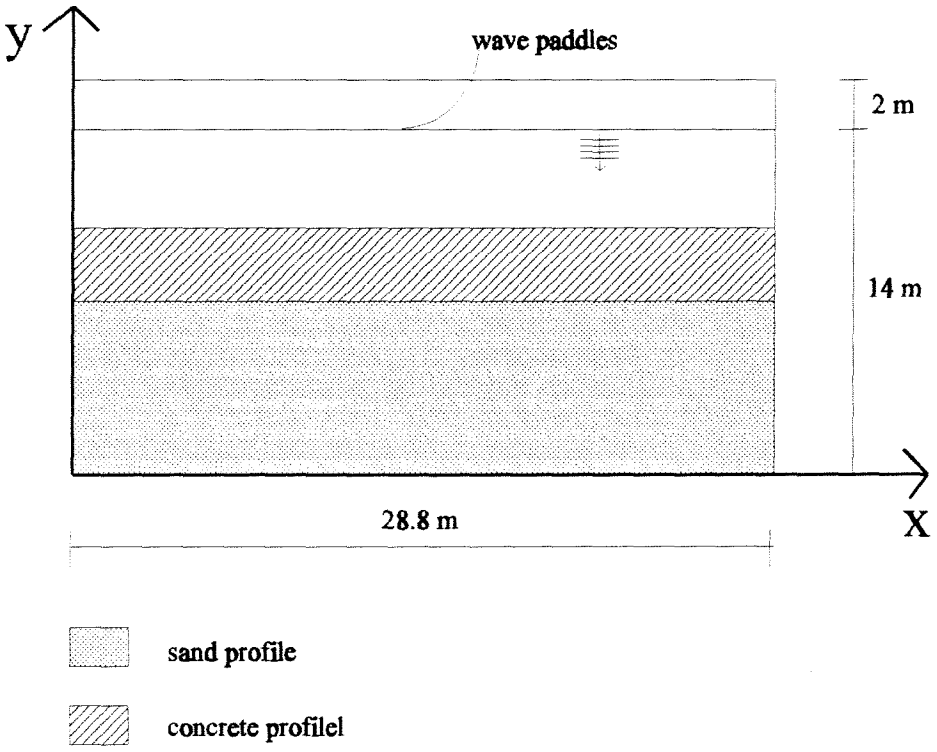

Figure 5.5: Axis system

This orientation and definition of the axes is used throughout this whole report unless indicated otherwise.

5.6 Measurements

5.6.1 Profile measurements

An electrical profile follower (Profo) has been used for measuring the bottom profiles.
(For information about this instrument reference is made to De Later (1996)).
During every experiment each profile (= cross-section) has been measured five times:

profo measurement 1 at t = 0.0 hrs.
profo measurement 2 at t = 0.5 hrs.
profo measurement 3 at t = 1.5 hrs.
profo measurement 4 at t = 3.5 hrs.
profo measurement 5 at t = 7.5 hrs.

During the experiments without breakwaters profo measurements were carried out every meter, from cross section x = 2.5 m to x = 26.5 m. During the experiments with breakwaters profo measurements were also carried out every meter, except near the gaps where an interval of 0.5 m was applied.
In case of measuring landward of a breakwater, the start position was y = 7.10 m and in case of measuring between breakwaters y = 10.34 m. The final position depended on the position of the waterline (either y = 0.92 m or y = 1.23 m).

5.6.2 Fluid velocity measurements

In order to measure flow velocities electromagnetic fluid-velocity meters (EMS) were used.
(For information about this instrument reference is made to De Later (1996)).
During the experiments four velocity meters were used. The position of these meters were:

EMS 1: y = 4.86 m
EMS 2: y = 5.76 m
EMS 3: y = 6.66 m
EMS 4: y = 8.41 m

EMS 1, 2 and 3 were positioned landward of the breakwater, EMS 4 was positioned seaward of the breakwater. In the cross-sections as given in Table 5.1 velocity measurements were carried out:

Tests without breakwaters Tests with two breakwaters	Tests with three breakwaters
cross-section x = 3.0 m	cross-section x = 12.5 m
cross-section x = 6.5 m	cross-section x = 14.0 m
cross-section x = 12.5 m	cross-section x = 15.5 m
cross-section x = 20.0 m	cross-section x = 17.0 m
cross-section x = 24.5 m	cross-section x = 18.5 m
	cross-section x = 20.0 m

Table 5.1: Measured cross sections

In the first interval (from 0 to 0.5 hrs.) only one cross-section was measured. In the next interval (from 0.5 to 1.5 hrs.) the other profiles were measured. In the other intervals (from 1.5 to 3.5 hrs. and from 3.5 to 7.5 hrs.) all cross-sections were measured.

5.6.3 Wave height measurements

In order to measure wave heights wave probes were used. (For information about this instrument reference is made to De Later (1996)).
During the experiments six wave probes were used. Two of them were located in front of the wave generator, in the corners of the basin, while the other four were positioned on the bridge. The wave probes in front of the wave generator stayed there during the entire experiment. The wave probes on the bridge measured the same cross-sections as the velocity meters (see Table 5.1). Every five minutes another cross-section was measured.
The y-positions on the bridge of these wave probes are the same as for the velocity meters.

5.7 Test schedule

The first series of experiments (A) is without breakwaters. This series was carried out in order to obtain a reference for the experiments with breakwaters. The second series of experiments (C) was carried out with two breakwaters (configuration 1), the third series with three breakwaters (configuration 2).
Each series consisted of three different experiments, every experiment with a different wave height. The three wave heights used are 0.08 m, 0.10 m and 0.12 m with all waves having a period of 1.55 s.
This results in the following schedule (Table 5.2):

		wave heights		
		0.08 m	0.10 m	0.12 m
without breakwaters	experiment	A1	A2	A3
breakwater configuration 1	experiment	C1	C2	C3
breakwater configuration 2	experiment	D1	D2	D3

Table 5.2: Test schedule

6 Introduction to the numerical model Delft2D-MOR

6.1 The compound model Delft2D-MOR

The model Delft2D-MOR, developed by DELFT HYDRAULICS, is essentially a model system existing of separate modules for the physical processes: waves, currents, sediment transport and bottom change.
The general structure of the compound morphological model is shown in Figure 6.1:

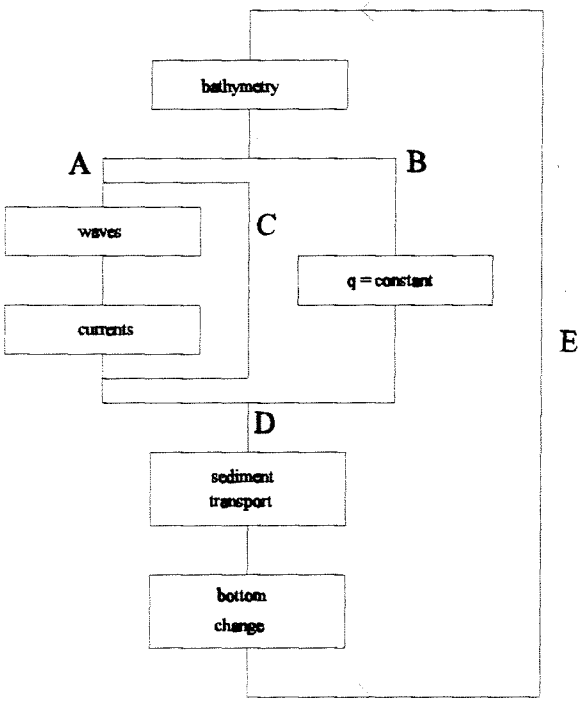

Figure 6.1: General structure of Delft2D-MOR

Two alternative main routes (A and B) are present for the computation of sediment transports and bottom level changes. Only route A is used: first wave and flow computations are made on the initial topography. The wave-induced forces resulting from the wave computation serve as input for the flow computation. If current-refraction must be taken into account, the results of the flow computation can be used again for a next wave computation (route C). Next, the sediment transport rate is determined (route D), followed by the computation of the bottom changes. These changes will be superimposed on the original bathymetry (route E).The next cycle starts.
The routes which should be followed in the model must be specified by a user-supplied process tree. This tree consists of a set of nodes and branches. These branches and nodes are numbered

from left top right, starting with all the end nodes. The graphical representation of such a tree is usually top-down. An example of a process tree is given in Figure 6.2:

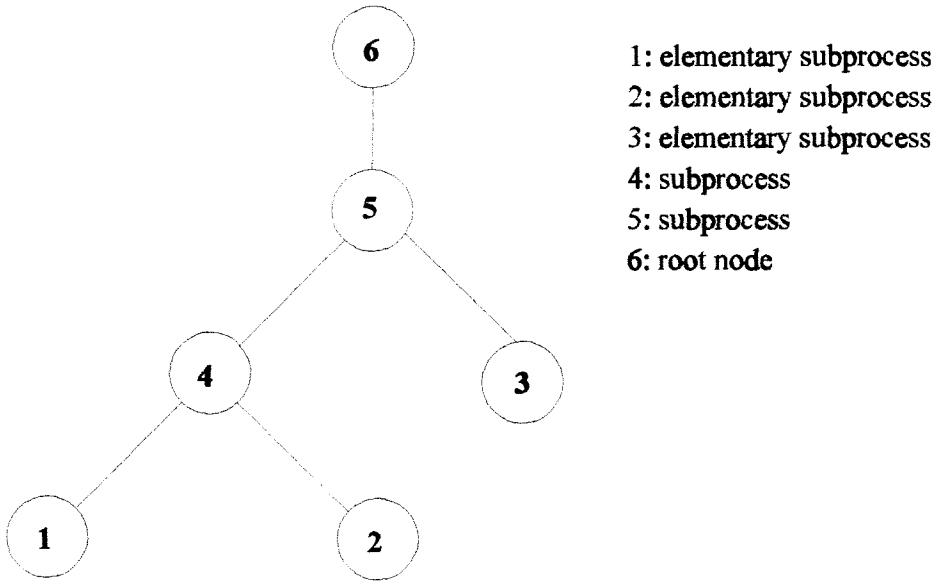

Figure 6.2: Example of a process tree

The elementary subprocesses (nodes 1, 2 and 3) contain the actual calls to the modules (waves, flow, sediment transport, bottom change). One elementary subprocess can contain 1 to 4 calls to modules. So the process tree allows the user to construct a specific tree suitable for the problem of interest.
Higher processes are built up by combining elementary processes. The link between a process and a lower process is a branch. The processes are called nodes. In the process tree parent and child nodes can be identified. A branch connects two nodes, one of which will be the parent node and one the child node. A node can be a parent node and child node at the same time (in the example above nodes 4 and 5). A node without a parent node will be the root node (in the example above: node 6).
Each branch of the process tree corresponds to a controller. This controller controls the execution of the elementary process or subprocess to be associated with the child node of that branch. The control criterium of each particular controller should be specified by the user.

The execution of a simulation is the climbing up and down the branches of the tree. The process tree starts at the top, at the root node (node 6), by activating the subprocess (node 5) connected to the root node. Next, the controller checks if the node below left has to be executed, and so on till all elementary subprocesses satisfy their own stop criteria.
Each process can be executed more than one time.

6.2 Modules, input files and data communication

The present implementation of the system includes the following modules:

- WAVES: computes wave field parameters (such as wave height, wave period) for a given set of current fields and a given bed level
- FLOW: computes the flow field development (velocities, water level) for a given bed level and wave forces
- TRSTOT: computes the sediment transport for a given flow field development
- TRSSUS: computes the sediment transport with a separate approach for the bed load and suspended sediment transport for a given time dependent flow field, or computes the silt transport
- BOTTOM: computes the bed level variation for a given sediment transport

A module will use data generated by one or more of the other modules and will read these data from a central communication file. The data computed by the module which are of interest for one of the other modules will be written to that central communication file. A general process simulation consists of subsequent executions of the separate modules in any required order, accounting for back-coupling effects. The total time to be simulated will be split up into separate time intervals, for which modules can be executed. The module MORSYS will control this process of splitting up of the time and will control the module executions according to the user-defined process specification, given in the MORSYS input file. All other modules have their own input file with its own specifications (Figure 6.3)

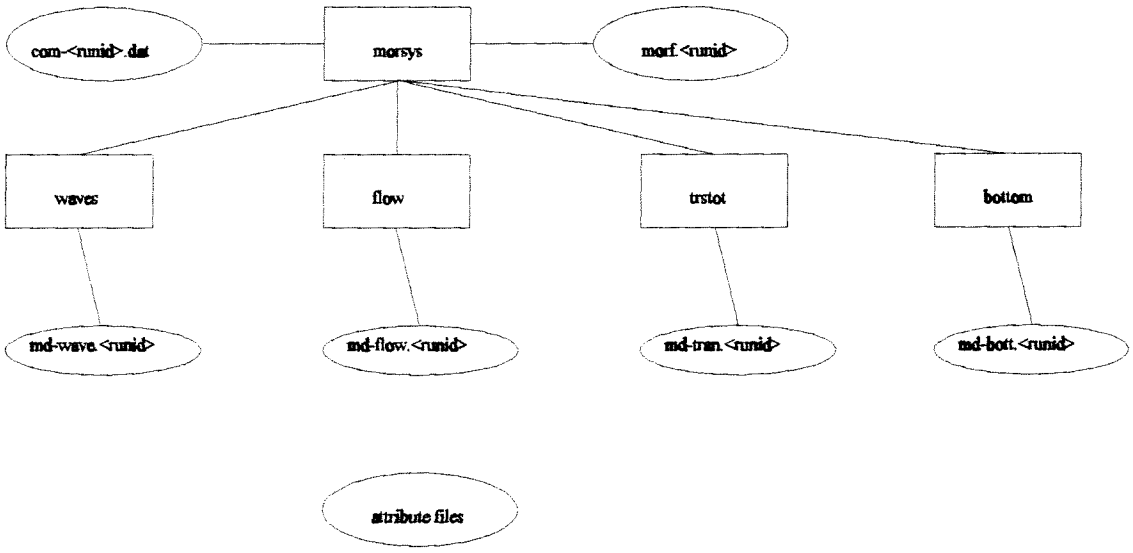

Figuur 6.3: Modules and input files of Delft2D-MOR

7 WAVES (HISWA)

7.1 Physical background

7.1.1 General

In HISWA (HIndcast for Shallow-water WAves) the wave propagation is determined across a grid according to the Eulerian approach of the action balance of the waves. The wave action is a function of the spatial coordinates (x,y) and of the spectral wave direction (θ). In this approach all wave information is available at the mesh-points of a regular grid.

The action density A is defined a:

$$A(\omega,\theta)=\frac{E(\omega,\theta)}{\sigma} \tag{7.1}$$

in which E is the wave energy density, θ the spectral wave direction and σ is the relative frequency defined as $\sigma = \omega - k.U$, where ω is the wave frequency, k the wave number and U the current velocity.

The action balance is then (without the notation for the independent variables):

$$\frac{\partial A}{\partial t}+\frac{\partial}{\partial x}(c_x A)+\frac{\partial}{\partial y}(c_y A)+\frac{\partial}{\partial \theta}(c_\theta A)+\frac{\partial}{\partial \omega}(c_\omega A)=T \tag{7.2}$$

The first term in this equation represents the local rate of change of action density. The other terms on the left-hand side represent the net transport of action in x-, y-, θ-, and ω-domain respectively. The total effect of generation and dissipation of action is represented by the source term T.
This action balance has been simplified in the following manner:
Neglecting time dependent parameters (assuming that the time scale of the wave propagation over the model area is small compared to that of the local wind field or currents), the first and fifth term on the left-hand side get out of the action balance which makes the model stationary.
Parametrisation of the remaining action balance is the second simplification. Therefore two directional wave functions are defined: the directional action spectrum $A_0(\theta)$, resulting from the integration of the action density $A(\omega,\theta)$ over the total frequency domain, and a mean wave frequency as a function of spectral direction $\omega_0(\theta)$.

$$A_0(\theta)=m_0(\theta) \tag{7.3}$$

$$\omega_0(\theta)=\frac{m_1(\theta)}{m_0(\theta)} \tag{7.4}$$

in which the moments m_n of the action density spectrum are defined as:

$$m_n(\theta)=\int_0^\infty \omega^n A(\omega,\theta)d\omega \tag{7.5}$$

When the zero-th and first order moments of the action density spectrum are used, the following equations remain of the action balance (without the notation of the independent variable):

$$\frac{\partial}{\partial x}(c_{0x}^{\cdot} m_0)+\frac{\partial}{\partial y}(c_{0y}^{\cdot} m_0)+\frac{\partial}{\partial \theta}(c_{0\theta}^{\cdot} m_0)=T_0 \tag{7.6}$$

$$\frac{\partial}{\partial x}(c_{0x}^{\cdot\cdot} m_1)+\frac{\partial}{\partial y}(c_{0y}^{\cdot\cdot} m_1)+\frac{\partial}{\partial \theta}(c_{0\theta}^{\cdot\cdot} m_1)=T_1 \tag{7.7}$$

where $c_{0x}^{\cdot}$, $c_{0y}^{\cdot}$ and $c_{0\theta}^{\cdot}$ are the propagation speeds of wave action in x-, y- and θ-space respectively. Similarly $c_{0x}^{\cdot\cdot}$, $c_{0y}^{\cdot\cdot}$ and $c_{0\theta}^{\cdot\cdot}$ are the propagation speeds of the mean wave frequency in x-, y- and θ-space respectively. T_0 and T_1 are the source terms.

With these final two equations HISWA computes for given x,y the propagation of the frequency-integrated energy density and the mean wave frequency for each spectral direction.

The physical phenomena which are accounted for in HISWA are:

- directional spreading
- refractive propagation
- current refraction
- wave generation by wind
- bottom dissipation
- dissipation by wave breaking
- current dissipation
- dissipation and transmission through and over an obstacle
- dissipation due to vegetation

Diffraction is not taken into account. Therefore in this study the lack of wave energy penetrating into the lee of the breakwater is to some extent compensated by directional spreading. Booij et al. (1992) show that in areas where refraction occurs this will give plausible results.

7.1.2 Directional spreading

HISWA takes into account a directional spreading of wave energy. The distribution of this wave energy over the directional sectors is characterized by a function $D(\theta) = A\cos^{ms}(\theta-\theta_0)$ inside the domain $-90^0 < \theta < 90^0$ and $D(\theta) = 0$ outside this domain. It is clear that the distribution function is mainly determined by the parameter *ms*. A larger value of *ms* means a higher peak in the function (the wave energy is more concentrated around the main propagation direction θ_0 of the waves. A smaller value of *ms* means the opposite.

7.1.3 Bottom refraction

In HISWA wave propagation is computed for each of the above described wave components. In the basic evolution equations (7.6) and (7.7), this propagation is separated in rectilinear propagation and refraction.

Rectilinear propagation
The first of these two, represented by c_x and c_y (in both equations) gives propagation in x,y-space based on linair wave theory, including bottom and current induced shoaling. These propagation speeds are determined with the mean wave frequency (different values) in different spectral directions). Refraction is modelled as a continuous directional shifting of wave energy as explained next.

Refraction
Refraction is commonly defined as the change in propagation direction due to variation of phase speed along the wave crest. A curving wave ray implies that the direction of wave propagation changes while travelling along the ray. In other words, the energy transport continuously changes direction while travelling through the area of interest. This can be conceived as the energy travelling not only through the geographic area but also (and

simultaneously) from one direction to another. This permits the Eulerian approach that has been taken in HISWA: the energy propagates not along rays but across a grid covering the area, while refraction is accounted for by shifting energy from one direction to another during propagation. This is expressed in the basic evolution equations (7.6) and (7.7) with the speed c_θ (in both equations).

7.1.4 Wave generation by wind

This process has been modelled in HISWA, but it is irrelevant to this study.

7.1.5 Bottom dissipation

In shallow water some wave energy is dissipated in HISWA by bottom friction. The dissipation is determined with a fairly conventional formulation for periodic waves (quadratic friction law) with the appropriate parameters adapted to suit a random wave field in an ambient current field. The energy dissipation per unit time (S) for one wave component (i.e. one spectral direction) is calculated with:

$$S(\theta) = -U^2_{bot1} * [c_{fw} * U_{bot2} + c_{fc} * U_{curr}]/g \qquad (7.8)$$

where c_{fw} en c_{fc} are the friction coefficients for the waves and the current respectively, U_{bot1} and U_{bot2} are measures for the orbital velocity at the bottom, U_{cur} is the current velocity in the direction of θ and g is gravitational acceleration.

The mean wave frequency per spectral wave direction is affected by bottom friction in HISWA assuming that the wave energy dissipation due to bottom friction affects only the energy at low frequencies. For this purpose the spectrum is assumed to be:

$E = C * k^{-n}$ for $k >= k_{peak}$

$E = 0$ for $k < k_{peak}$

where k is the wave number and k_{peak} is the peak wave number.

7.1.6 Surf dissipation and added white-capping

In extremely shallow water or if a certain wave steepness is exceeded (in deep or shallow water), the waves will break. The bottom induced wave breaking is called surf breaking while the steepness induced breaking is called white-capping. The corresponding energy dissipation is determined in HISWA with a bore-model (Battjes and Janssen, 1979) for those waves which

are higher than some threshold value. Only the total rate of energy dissipation is thus determined. The total energy dissipation thus obtained is distributed over the wave directions proportional to the existing directional energy distribution. The directional characteristics of the waves in HISWA are therefore not affected by breaking.

The procedure for the computation of surf breaking or white-capping consists of a few separate steps. First the maximum wave height H_m that can exist at the given depth or steepness is determined. The value of H_m is the smallest value of [γ_s * depth] and [γ_d / k], where k is the wave number and γ_s and γ_d are coefficients which the user of HISWA may choose.

Next the fraction of breaking waves is detemined from:

$$\frac{(1-Q_b)}{\ln(Q_b)} = -8\frac{E_{tot}}{H_m^{\,2}} \tag{7.9}$$

where Q_b represents the fraction of waves that is breaking and E_{tot} the total wave energy.

The dissipation for one directional component per unit time is calculated with:

$$S(\theta) = -\alpha Q_b f_{av}(\theta) H_m^{\,2} \frac{E(\theta)}{(8\pi E_{tot})} \tag{7.10}$$

where $E(\theta)$ and $f_{av}(\theta)$ are the energy density and the average frequency respectively of that component.

7.1.7 Current dissipation (wave blocking)

In a strong adverse current some wave energy is carried away by the current. This is energy which in a fully spectral model (all directions and frequencies included) is carried by wave components which cannot travel against the current (propagation speed less than current speed). This energy is removed from the wave field in the HISWA model through high frequency dissipation.

For the computation of the current dissipation for a directional component, a critical frequency f_c is determined. This is the lowest frequency that cannot travel against the current. In HISWA the energy carried by the frequencies higher than the critical frequency is assumed to be dissipated. If the waves propagate against an increasing opposing current, the critical frequency f_c decreases and the high-frequency energy decreases accordingly.

This dissipation is equal to the decrease of the total energy of the following spectrum as the critical frequency decreases:

$E(f,\theta) = C(\theta) * f^n$ for $f_{peak} < f < f_c$

$E(f,\theta) = 0$ for $f < f_{peak}$ and for $f > f_c$

with constant $C(\theta)$.

7.1.8 Dissipation and transmission through and over an obstacle

HISWA is able to model the effect of breakwaters and other obstacles which are too narrow to be considered as features of the bottom grid.
If there is an obstacle in the computational area, it will affect the wave field in two ways. First it will reduce the wave height locally along its length, and second it will cause diffraction around its end(s). HISWA is not able to take into account diffraction, but in case of an irregular wave field, it can reasonably account for waves around an obstacle if the directional spectrum of incoming waves is not too narrow.

The transmission is completely determined by the transmission coefficient K_t, being a function of wave height and the crest submergence. K_t is the ratio of the transmitted wave height and the wave height at the upwave side of the dam. The following expression for K_t (Seelig 1979) is used in in HISWA:

$$K_t = 0.5[1 - \sin(\frac{\pi}{2\alpha}(\frac{F}{H_i} + \beta))] \qquad (7.11)$$

with $-\beta-\alpha < F/H_i < \alpha-\beta$, $F = h-d$

where H_i is the wave height at the upwave side of the dam, h is the crest level of the dam, d is the water level and the coefficients α and β depend on the shape of the dam.

It is assumed that the transmission coefficient is independent of the direction of the waves and that the frequency remains unchanged over an obstacle.

7.1.9 Dissipation due to vegetation

This process has been modelled in HISWA, but it is irrelevant to this study.

7.2 Numerical background

The evolution equations used in HISWA (equations 7.6 and 7.7) are partial differential equations of the first order with the two horizontal coordinates (x and y) and the spectral wave direction (θ) as independent variables. The dependent variables are the action density $A_0(x,y,\theta)$ and the mean frequency (action averaged) per spectral wave direction $\omega_m(x,y,\theta)$. The state in a point (x,y,θ)-space is determined only by what happens in the up-wave direction of this point.

The computational region is a rectangle covered with a rectangular grid. One of the axes (x-axis) is chosen in the down-wave direction (i.e. roughly the mean wave direction); lateral (normal) to the x-axis is the y-axis. The computation starts at the up-wave boundary x = 0 and proceeds in positive x-direction. After the states in all points on a line in y-direction have been determined, the computation proceeds with the next line in the grid (see Figure 7.1).

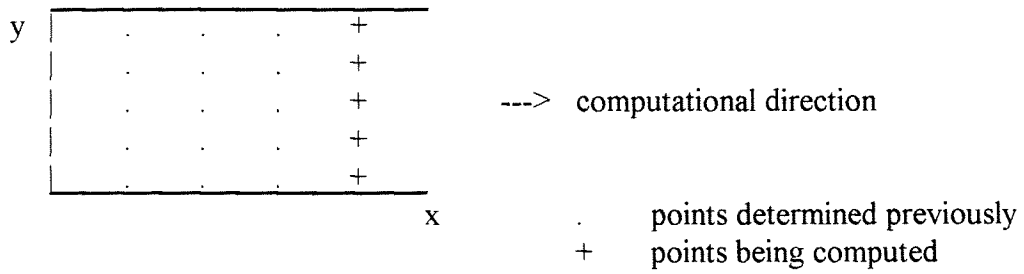

Figure 7.1: Computational grid

For the propagation in x-y space an explicit scheme is used (leap-frog), in θ-direction a fully implicit scheme is used (backward Euler). This has certain consequences. Since the numerical scheme is explicit in x-y space, the computation is only stable under the condition that the ratio of the forward step (i.e. the step in x-direction) and the lateral step (step in y-direction) is smaller than a certain limit. The stability condition is:

$$\frac{|c_y \Delta x|}{|c_x \Delta y|} \leq 1 \qquad (7.12)$$

where Δx and Δy are the step sizes in x- and y-direction respectively and c_x and c_y are the energy transport velocities in x- and y-direction respectively (group velocity of the mean frequency in the HISWA computations).

In cases without current this is equivalent with:

$$\frac{\Delta x}{\Delta y} \leq cotg\,\theta \qquad (7.13)$$

where θ is the discrete spectral wave propagation direction. A consequence of this condition is that waves can be computed only in a sector narrower than 180°. For economic computations a compromise must be made between the maximum value of θ (as large as possible to have a large directional sector to encompass as much as possible of the directional energy distribution) and a large Δx (in order to speed up the computation).

The up-wave boundary wave conditions should be provided by the user.
The lateral boundaries are partially reflecting (from 0 to 100% reflection). No wave energy crosses the lateral boundaries from outside the computational area. The down-wave boundary is always fully absorbing (no energy entering the area).

8 Flow module (Delft3D-FLOW)

The flow module in Delft2D-MOR consists of the Delft3D-FLOW model (formerly known as TRISULA). The model simulates the non-steady flow and water level variation (also from wave forcing).
Delft3D-FLOW includes effects of waves, wind and density differences.

8.1 Description of Delft3D-FLOW

8.1.1 Physical background

The 2DH-version of the Delft3D-FLOW model solves the unsteady shallow water equations. In this approach the vertical momentum equation is reduced to the hydrostatic pressure relation. Vertical accelerations are assumed to be small compared to the gravitational acceleration and are not taken into account. The momentum equations in x- and y-direction are depth-averaged. These equations are:

Conservation of momentum in x-direction (depth-averaged):

$$\frac{\partial u}{\partial t}+u\frac{\partial u}{\partial x}+v\frac{\partial u}{\partial y}+g\frac{\partial \eta}{\partial x}-fv+\frac{g u|U|}{C^2(d+\eta)}-\frac{F_x}{\rho_w(d+\eta)}-\nu\left(\frac{\partial^2 u}{\partial x^2}+\frac{\partial^2 u}{\partial y^2}\right)=0 \qquad (8.1)$$

Conservation of momentum in y-direction (depth-averaged):

$$\frac{\partial v}{\partial t}+u\frac{\partial v}{\partial x}+v\frac{\partial v}{\partial y}+g\frac{\partial \eta}{\partial y}-fu+\frac{g v|U|}{C^2(d+\eta)}-\frac{F_y}{\rho_w(d+\eta)}-\nu\left(\frac{\partial^2 v}{\partial x^2}+\frac{\partial^2 v}{\partial y^2}\right)=0 \qquad (8.2)$$

The depth-averaged continuity equation is given by:

$$\frac{\partial \eta}{\partial t}+\frac{\partial (d+\eta)u}{\partial x}+\frac{\partial (d+\eta)v}{\partial y}=0 \qquad (8.3)$$

in which:

C	=	Chézy coefficient
d	=	bottom depth
f	=	Coriolis parameter $2\omega\sin\phi$, in which ϕ is the geographic latitude and ω is the earth's angular frequency
$F_{x,y}$	=	x- en y-component of external forces
g	=	acceleration due to gravity
u,v	=	depth averaged velocity in x- and y-direction
U	=	magnitude of total velocity, $U = (u^2 + v^2)^{1/2}$
ρ_w	=	mass density of water
ν	=	diffusion coefficient or eddy viscosity
η	=	water level variation

The main physical phenomena which are accounted for in Delft3D-FLOW are:

- tidal forcing
- the effect of the earth's rotation (Coriolis force)
- density differences
- wind shear stress on the water surface
- bed shear stress on the bottom
- influence of the waves on the bed shear stress
- wave-induced stresses and mass fluxes

Mass flux
In Delft3D-FLOW the user has the option to in- or exclude the effect of mass transport by waves (see section 3.4.2 for a brief explanation of mass transport). If mass transport is not taken into account the total flux velocities are defined with the equations described above. If mass transport is included in the computations the same equations are used for the computation of the total flux velocities, but then these velocities have to be interpreted in a different way: the total flux velocity $\tilde{U}$ (in x-direction) is defined as $\tilde{U} = U + U_s$, in which U is the Eulerian mean velocity and U_s the mass flux velocity (in x-direction). (The same holds for the y-direction).
From this relation the Eulerian mean flow velocity can be defined. The Eulerian flow velocity is used for the computation of sediment transport rates. In this report this Eulerian flow is called return flow (if the effect of mass flux is included in the computation).

8.1.2 Numerical background

The equations for the water levels are solved with an Alternating Direction Implicit (ADI) technique, Stelling (1984). This means that water levels and velocities in the x-direction are implicitly solved in the first half time step. For more details about this numerical method reference is made to the Delft3D-FLOW manual and to Stelling (1984).

8.1.3 Grid definition

In the horizontal plane Delft3D-FLOW uses a staggered grid. Each cell contains a water level point, a point for the bottom depth, a point for the velocity in x-direction (u-velocity) and a point for the velocity in y-direction (v-velocity). The points in a grid cell all have the same indices (i,j). This is made more clear in Figure 8.1:

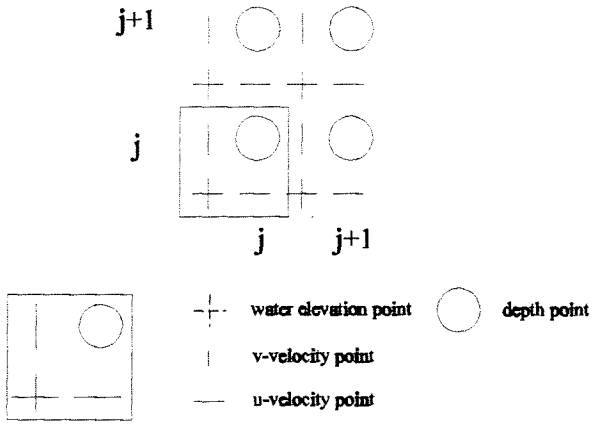

Figure 8.1: Staggered grid in Delft3D-FLOW

At the end of the computation the velocities are known at the velocity points. These values will be transformed to the water level point by averaging. For the x-component this holds:

$$u(i,j) = \frac{u(i-1,j)+u(i,j)}{2} \qquad (4.4)$$

and for the y-component:

$$v(i,j) = \frac{v(i-1,j)+v(i,j)}{2} \qquad (4.5)$$

So in the end all properties except the bottom depths are known at the coordinates of the water level points.

9 Transport module (TRSTOT)

9.1 Introduction

The transport module determines the sediment transport using time-dependent flow and effects of a wave field. The magnitude of the sediment transport will be computed by use of a selected sediment transport relation. In this study the Bijker formula will be used. This transport relation accounts for bed load and suspended load computations of the total sediment transport. Since the focus of the experiments was on profile development, only the total sediment transport will be used. Therefore the module TRSTOT (for computation of total sediment transport) is applied.

9.2 Bijker formula

Bijker introduced wave influence via a modification of the bottom shear stress in an existing sediment transport formula for currents. He chose the Kalinske-Frijlink formula for the bed load transport and coupled this to the Einstein formula for suspended sediment transport.

9.2.1 Bed load transport

The layer in which the bed load takes place is taken equal to the bottom roughness r. Waves contribute considerably to the amount of sediment transport. Bijker assumed that the waves only contribute to the stirring up of sediment rather than the transport. This stirring effect has been taken into account by a modification of the bed shear stress. In case of waves and current the bed shear stress increases considerably. With this increase the bed load transport rate increases too.

Bijker calculated separately the velocities of waves and currents at some height above the bed. After superposition of these two velocity vectors the total velocity is substituted into the formula of the bottom shear stress:

$$\tau_{cw}=\rho_w \kappa^2 U_{cw}^2 \qquad (9.1)$$

in which ρ_w is the water density, κ the Von Karman constant and U_{cw} the velocity which represents the combination of waves and currents at a specified height above the bed.

Due to oscillating wave motion the direction of this bottom shear stress varies with time. However, the only important condition for the stirring of the bed material is the exceeding of

the critical velocity regardless of its direction. So it is sufficient to know the mean shear stress. The time-averaged value of the bed shear stress finally yields:

$$\overline{\tau_{cw}}=[1+\frac{1}{2}(\xi\frac{\hat{u}_0}{U})^2]\tau_c \tag{9.2}$$

in which:

$$\tau_c=\rho_w U_{*c}^2 \tag{9.3}$$

$$\xi=C\sqrt{\frac{f_w}{2g}} \tag{9.4}$$

U_{*c}	=	shear stress current velocity at the bed
U	=	the depth-averaged current velocity
$\hat{u}_0$	=	maximum wave velocity amplitude immediately above the boundary layer
C	=	Chézy factor
f_w	=	friction factor
g	=	acceleration due to gravity

The bed load transport in terms of the mean bed shear stress yields:

$$S_b=b.d_{50}.\frac{U}{C}\sqrt{g}.\exp\left[-0.27\frac{\Delta.d_{50}.\rho_w.g}{\mu.\overline{\tau_{cw}}}\right] \tag{9.5}$$

in which:

S_b	=	bed load transport per unit width
b	=	constant
d_{50}	=	median grain size
Δ	=	relative sediment density $(\rho_s-\rho_w)/\rho_w$
μ	=	ripple factor

As mentioned above the waves only contribute to the stirring effect. Transport by waves due to asymmetry of the orbital motion is therefore neglected in the approach of Bijker.

9.2.2 Suspended load transport

The suspended load transport in the layer between the water surface and the bottom layer is determined by:

$$S_s = \int_r^h c(z)U(z)dz \tag{9.6}$$

in which the velocity U is taken equal to the Prandtl-Von Karman logarithmic profile, and the concentration distribution is given by:

$$c(z) = c_a \left[\frac{r}{h-r}\frac{h-z}{z}\right]^{z_*} \tag{9.7}$$

in which r is the bottom layer thickness, h the water depth and c_a is the bed load concentration.

The exponential part z_* is the Rouse number given by:

$$z_* = \frac{w}{\kappa\sqrt{\tau_{cw}/\rho_w}} \tag{9.7}$$

where κ is the Von Karman constant and w is the fall velocity of the grains.

The bed load concentration is assumed to have a constant value over the entire thickness of the bed transport layer, r. This concentration can then be determined from:

$$c_a = \frac{S_b}{\int_0^r U dz} \tag{9.8}$$

10 Bottom module (BOTTOM)

10.1 Introduction

The bottom module computes the bottom changes from the transport rates following from the transport module. These changes are next superimposed on the original bottom which gives the new bottom.

10.2 Physical background

The determination of the bottom level changes is based on the conservation of sediment mass:

$$\frac{\partial z_b}{\partial t}-(\frac{\partial S_x}{\partial x}+\frac{\partial S_y}{\partial y})=0 \qquad (10.1)$$

in which z_b is the bottom level and S_x and S_y the sediment transport in x- and y-direction respectively. This sediment transport includes the volume of the pores.

10.3 Numerical background

The above mentioned continuity equation is solved using the explicit FTCS (Forward-Time Central Space) scheme. In fact, a Lax-like scheme is applied because the FTCS scheme generates negative diffusion. To compensate for that a Lax correction has been applied by introducing positive diffusion in the form of an artificial down slope term in the transport rates.

Since the sediment transport rates are known at the water level points of the Delft3D-FLOW grid, the bottom module computes with the FTCS scheme the bottom changes at the bottom points of the Delft3D-FLOW grid using the sediment transport values at the four surrounding water level points. This yields:

$$\frac{z_{b_{ij}}^{n+1}-z_{b_{ij}}^{n}}{\Delta t}=\frac{(S_{x_{i+\frac{1}{2},j+\frac{1}{2}}}^{*n}-S_{x_{i-\frac{1}{2},j+\frac{1}{2}}}^{*n})+(S_{x_{i+\frac{1}{2},j-\frac{1}{2}}}^{*n}-S_{x_{i-\frac{1}{2},j-\frac{1}{2}}}^{*n})}{2\Delta x}+$$

$$+\frac{(S_{y_{i+\frac{1}{2},j+\frac{1}{2}}}^{*n}-S_{y_{i-\frac{1}{2},j+\frac{1}{2}}}^{*n})+(S_{y_{i+\frac{1}{2},j+\frac{1}{2}}}^{*n}-S_{y_{i-\frac{1}{2},j+\frac{1}{2}}}^{*n})}{2\Delta y} \tag{10.2}$$

Since the FTCS scheme is an explicit scheme the Courant number should be less than one. On the other hand, the Courant number should not be much lower than one as low Courant numbers will generally induce numerical diffusion. In order to ensure this stability criterium the time step used in the bottom module can be determined by the module by specifying the maximum Courant number which may not be exceeded. The result of this is a varying time step during the simulation run. For a given Courant number the maximum allowed time step follows from the minimum value of the stability criterium:

$$\sigma = c\frac{\Delta t}{\Delta x} \rightarrow \Delta t = \sigma\frac{\Delta x}{c} \tag{10.3}$$

in which σ is the user-specified Courant number, Δx the grid spacing and c the propagation speed of the bed level. The smallest value of Δt throughout the field finally determines the time step for updating the bottom level.

The above mentioned bed level celerity c can be seen as the propagation speed of bed level disturbances and is determined by assuming that the sediment transport relation can be written as:

$$S = aU^{b} \tag{10.4}$$

in which a and b are constants. After a bit of algebra the bed level celerity can then be written as:

$$c = \frac{b|S|}{h} \tag{10.5}$$

in which:

b = power of the used transport formula
h = waterdepth

The optimal time step now follows from:

$$\Delta t = \frac{\sigma}{b} \frac{\Delta x h}{S} \qquad (10.6)$$

11 Determination of HISWA parameters

11.1 Introduction

In this chapter the input parameters for HISWA are determined. The aim is to determine the wave parameters in a way that a reasonable wave field is created, i.e. the wave field as measured and expected for the conditions in the wave basin.
In section 11.2, 11.3 and 11.4 the wave height parameter H_s, the wave period parameter T and the angle of wave incidence of the waves are determined.
Next, in section 11.5, a suitable directional spreading of wave energy is chosen in order to model the (small amount of) diffraction behind the breakwaters. This is done with the aid of the computer model CREON.
In section 11.6 the breaker parameters are determined. The values of these parameters are obtained by comparing the generated wave fields with wave height measurements.
Finally, in section 11.7, the friction parameters are chosen.

11.2 Wave height H_s

In HISWA the incident wave height has to be defined as a significant wave height. The significant wave height is a statistical parameter, defined as the mean wave height of the highest one third waves, and is therefore not suitable to describe a monochromatic wave field. Because of the difference between regular and irregular waves, the most satisfying relation between these phenomena depends on the application. In this case it could be a rational approach to equal the mean total energy in both regular and irregular waves. For sinusoidal, non breaking waves in deep water this yields:

$$H_m = \frac{H_{m0}}{\sqrt{2}} \qquad (11.1)$$

In deep water H_{m0} is approximately equal to H_s, but in shallow water and for breaking waves the difference between H_{m0} en H_s can be at least 30%. However, the use of this approach in shallow water may be reasonable.
This approach has been applied in HISWA, where the monochromatic wave height H_m = 0.12 m has been modelled as H_s = 0.17 m.

11.3 Wave period T

In the experiments a wave period of 1.55 s was generated. This value has been used for the mean wave period as defined in HISWA, namely the inverse of the mean frequency of the energy density spectrum.

11.4 Angle of incidence θ_0

In the experiments the generated waves propagated perpendicularly to the shoreline. Therefore the angle of incidence θ_0 is 0 degrees.

11.5 Directional spreading of wave energy

In the experiments there was no directional spreading of wave energy. The breakwaters, however, force the waves to diffract around the tip, causing a directional spread of wave energy. HISWA does not take into account diffraction, but the effects of that phenomenon, namely the lateral transmisson of energy through the wave rays and the penetration of wave energy into the lee of the breakwaters, can be compensated by the use of directional spreading of wave energy. The magnitude of this directional spreading has to be chosen such that it simulates the phenomenon of diffraction reasonably.

Another computer model, CREON (developed by Gao, Radder and Booij), a computer model that is able to simulate both regular and irregular waves and does take into account diffraction, was used for a reference. This model is briefly described in Appendix B.
At first, the same input was used for HISWA and CREON with the initial bottom profile and dimensions of the basin.
First runs with HISWA and CREON showed, also in the case of very accurate calculations (relatively small numerical stepsizes), a remarkable difference in the development of wave height in the direction of propagation: an increasing difference in wave height in the areas where shoaling occurs. This difference cannot be caused by physical or numerical approximations in both models.

A test was carried out in order to find out which model shows the effects of shoaling correctly. Therefore obstacles and the effect of wave breaking were left out of the computation in both models. A simple bottom profile was chosen in order to simplify the manual calculation.
The test showed (see Appendix C) that the HISWA shoaling curve is almost equal to the manually calculated curve and the CREON curve is not. The shoaling effect in CREON is clearly less. (Besides, the wave height decreases when the breaking depth is reached, which indicates that wave breaking is still taken into account).
There are three possible explanations for the fact that CREON does not show the right shoaling curve:

- the phenomenon of shoaling is not correctly modelled
- an error in the computer program
- the output data are not generated correctly

Following runs with HISWA and CREON were carried out with a non-sloping bottom profile to exclude the effect of shoaling. The conditions of the experiments were chosen as input, but the breakwaters were situated differently. There is only one gap in between the breakwaters. The runs with HISWA were carried out with directional spreadings of 17.1, 12.4 and 10.2 degrees (*ms* = 10, 20, 30 respectively) and a sector of 150 degrees, divided into 60 sectors of 2.5 degrees. This resolution has been chosen such that the continuous curve of the distribution function $D(\theta)$ is described reasonably well by the numerical, discontinuous 'curve'. Especially in the case of strongly peaked directional spreadings, when most of the energy is concentrated in a very narrow sector, this accurate resolution is needed.

It is of importance that the generated waves in HISWA and CREON have the same wave length. This wave length depends on the parameter cfae, the ratio of the mean frequency of an energy spectrum (f_E) and the mean frequency of an action spectrum (f_A): $f_E = f_A$ * cfae. This ratio depends on the spectral shape that has been chosen.
The parameter cfae has been chosen such that in HISWA and CREON the initial wave length is equal.

CREON	**HISWA**
wave height H_m = 0.12 m wave period T = 1.55 s propagation direction θ_0= 0 reflecting lateral walls	wave height H_s = 0.17 m wave period T = 1.55 s propagation direction θ_0= 0 reflecting lateral walls cfae = 1.05 varying directional spreading

Lay-out:

no bottom slope

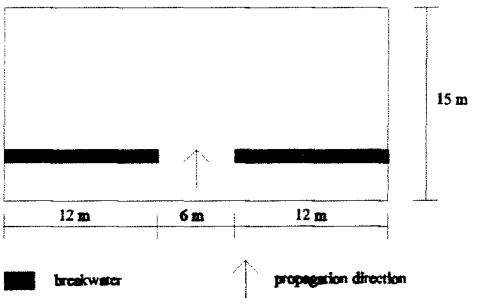

Runs with HISWA and CREON have been carried out with submerged breakwaters with crests 0.10 m below still water level. The wave field behind the breakwaters is determined by transmission and diffraction.
Results of these calculations are shown in Appendix D. The CREON wave field and HISWA wave fields with ms = 10, 20, and 30 have been plotted. The HISWA wave field with ms = 30 seems to correspond to the CREON wave field reasonably well. Therefore this value has been chosen in order to model diffraction in all other computations.

11.6 Breaking parameters

The breaking paramaters used by HISWA are the shallow water breaking index γ_s, the deep water breaking index γ_d and the dissipation coefficient α.
The index γ_s is defined as H_b/h_b, in which H_b is the height of the breaking wave and h_b the water depth where breaking occurs. Given the bathymetry it defines the wave height when waves break and the location of the breaker point.
The index γ_d, being the wave steepness H/L, has no influence on the process of breaking in the wave basin, since depth induced breaking rules the process in shallow water.
The coefficient α is used in equation (7.10) as a switch to adjust the magnitude of dissipation for different circumstances.
The parameters γ_s and α determine the wave height development from the sea towards the shore. They are calibrated, as described in sections 11.6.1 and 11.6.2, to suit the wave height measurements carried out in the wave basin at different times, at different locations.

11.6.1 Input for HISWA calibration

Bottom
The bottom consists of concrete and sand. At t=0 the bottom profile was measured. Next, waves were generated and wave heights were measured. The initial bottom profile is known, but the waves and currents, inducing sediment transport, cause the bottom profile to change in time. It was not possible to measure all wave heights in the chosen sections at one time, which means that the wave field at one time is not known (measured).
The first measurements in the last measured sections were carried out only after minutes. Therefore it is impossible to relate these measured wave heights to the initial bottom profile (and to the first measured wave heights in the first sections).
At t = 0:30 hrs. the second, and at t = 1:30 hrs. the third profile measurement was carried out. These measurements have been used for an approximation of the bottom profile between t = 0 and t = 1:30 hrs. This is done by linear interpolation, which has no physical background, but it is the only possibility to estimate the bottom profile at all points of time from t = 0 to t = 1:30 hrs.

Input grid
The dimensions of the input grid are 10.1 m in wave propagation direction (y-direction) and 24.00 m in the x-direction. The origin of the grid is at (x,y) = (2.5, 3.6). The mesh size in y-direction was chosen 0.1 m and in x-direction 0.5 m.

Computational grid
The computational grid has the same dimensions, mesh sizes and origin as the input grid. In θ-direction a sector of 150° has been chosen, divided into 60 segments of 2.5°. This resolution is chosen such that the continuous curve of the directional spreading function is reasonably described by the numerical discontinuous curve.

Lateral boundaries
The lateral boundaries of the computational grid are fully reflecting.

11.6.2 Calibration results

Since at only a few locations on both sides of the breakwater the wave heights were measured, very little is known about the wave field that was present during the experiments, especially in the region between breakwaters and the shoreline. Therefore the focus was on fitting a curve through the measurement data and model the dissipation due to the breakwaters as accurate as possible. For this purpose theoretical proposed values for γ_s and α could not be used.
Several combinations of γ_s and α, some without physical significance, were chosen in order to create a wave field that corresponds reasonably well to the measured wave heights.
Finally a good correspondence of the generated wave field with the measured wave data was found with $\gamma_s = 2.0$ and $\alpha = 8.0$. The value of α is very large compared to values that are more likely to describe wave dissipation well ($\alpha \sim 1$ to 2), but in this case this large value seems to describe wave dissipation at the breakwater reasonably well.

First it was checked which combination of γ_s and α could be used to generate a wave field that corresponds reasonably well to the measured wave heights in the case of the presence of breakwaters. For this purpose measurements of experiment C3 ($H_m = 0.12$ m, two breakwaters) were used.
During experiment C3 the first reliable wave measurements in a gap were carried out in cross-section x = 3.0 m at t = 6:26 mins. Assuming the bottom changes were small, the measured initial bathymetry was used as input in HISWA. The measured wave heights were compared to the generated wave heights in HISWA, using the picture of the generated wave field and the picture of the wave height development.
In the case of $\gamma_s = 2.0$ and $\alpha = 8.0$ the generated wave field is shown in Figure 11.1.
The generated and measured wave heights in cross section x = 3.0 m are shown in Figure 11.2.

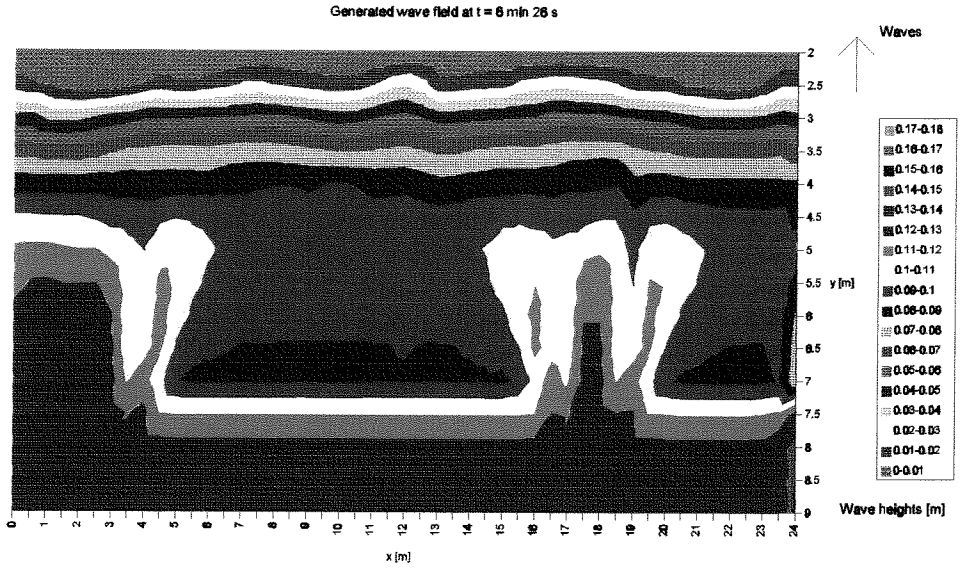

Figure 11.1: Generated wave field at t = 6 min 26 s

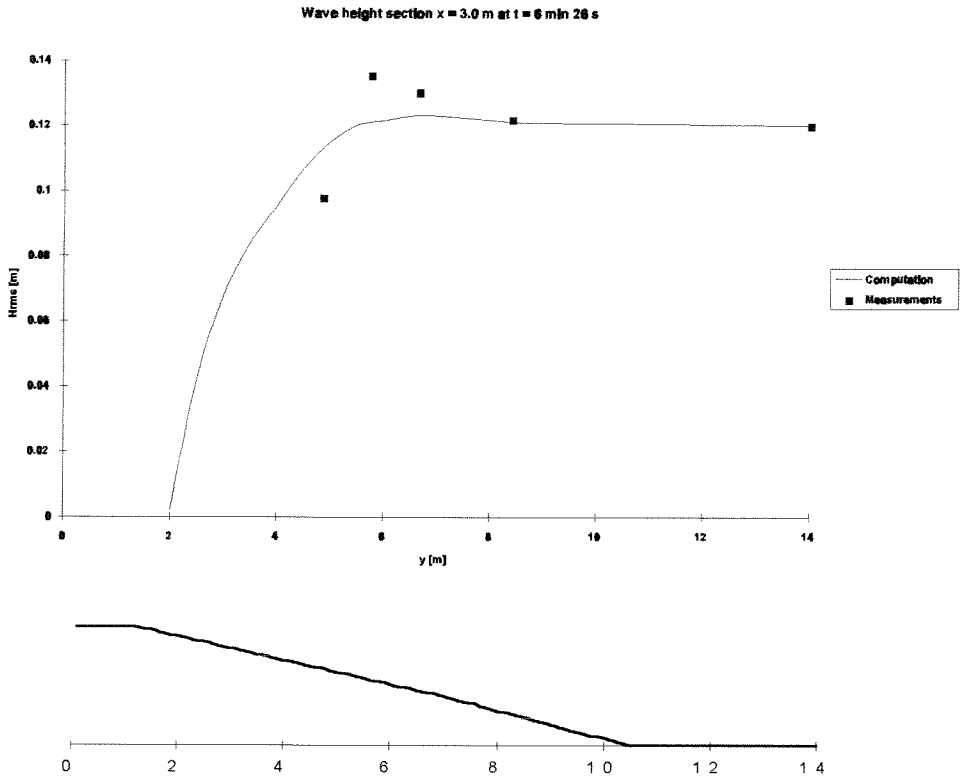

Figure 11.2: Generated and measured wave heights at x = 3.0 m and t = 6 min 26 s

Figure 11.2 shows that the computed wave height curve is not able to follow the measurements, but differences between measured and computed wave heights are small.

The first reliable wave measurements in a cross-section over a breakwater were carried out in cross-section x = 12.5 m at t = 32:09 mins. The interpolated bathymetry of t = 32:09 mins. was used as input in HISWA. Again the measured wave heights were compared to the generated wave heights in HISWA. In the case of $\gamma_s = 2.0$ and $\alpha = 8.0$ the generated wave field is shown in Figure 11.3.

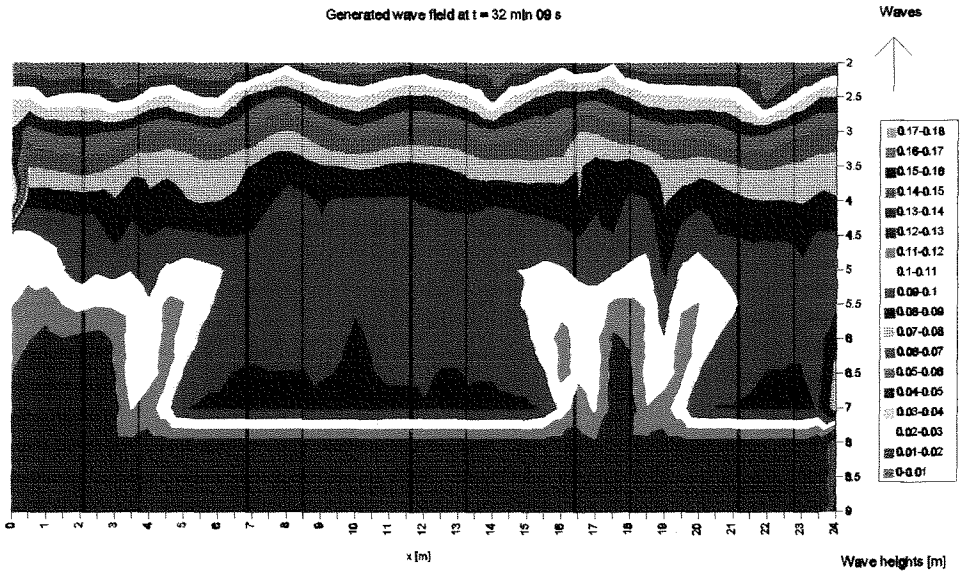

Figure 11.3: Generated wave field at t = 32 min 09 s

The generated and measured wave heights in cross section x = 12.5 m are shown in Figure 11.4.
The curve in Figure 11.4 follows the measurements very well such that it can be assumed that the wave height decay over the breakwater is modelled reasonably well:

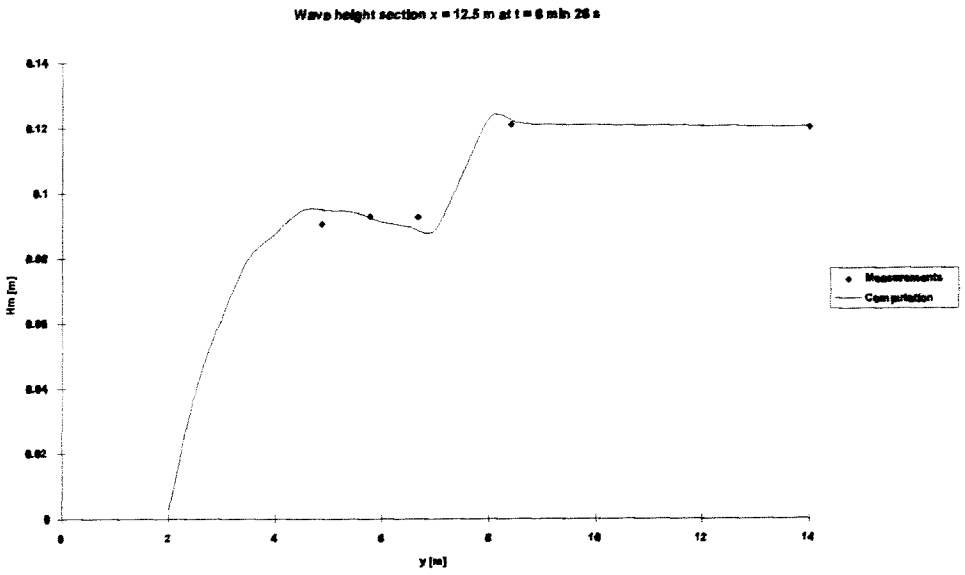

Figure 11.4: Generated and measured wave heights at x = 12.5 m and t = 32 min 09 s

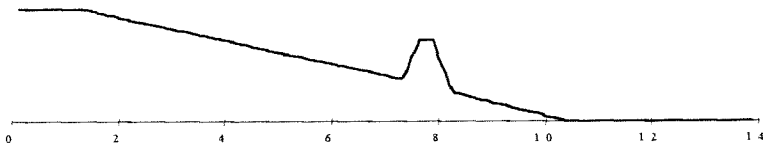

Next it was checked if it was possible to generate a wave field with $\gamma_s = 2.0$ and $\alpha = 8.0$ that corresponds reasonably well to the measured wave heights in the case of absence of breakwaters. For this purpose measurements of experiment A3 (H = 0.12 m, no breakwaters) were used.
During experiment A3 the first reliable wave measurements were carried out in cross-section x = 3.0 m at t = 6:31 and t = 13:03 mins. Assuming the bottom changes are small, the measured initial bathymetry was used as input in HISWA. The measured wave heights at t = 6:31 and t = 13:03 mins. were averaged in order to obtain one set of wave measurement data in cross-section x = 3 m. These measured wave heights were compared to the generated wave heights in HISWA, using the picture of the wave height development. The generated and measured wave heights in cross section x = 3.0 m are shown in Figure 11.5.
Also in this case the curve follows the measurents reasonably well, which indicates that with the chosen values of α and γ_s the wave height in the basin without breakwaters can be modelled.

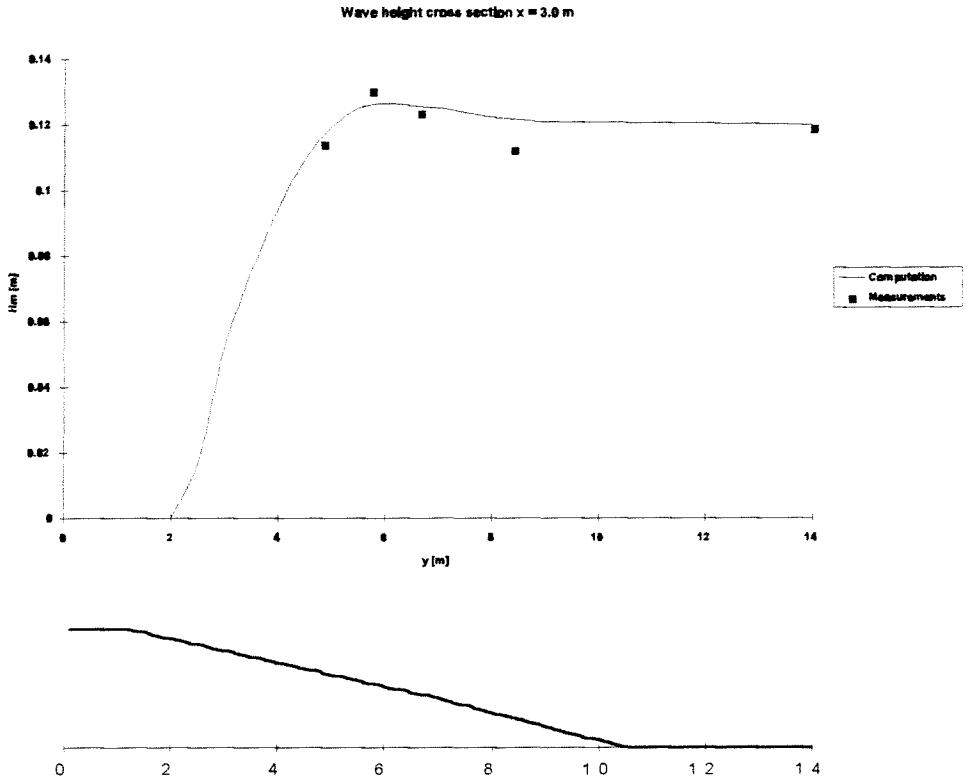

Figure 11.5: Generated and measured wave heights at x = 3.0 m

With the values for γ_s and α, being 2 and 8 respectively, it is assumed that the wave field is modelled reasonably well (knowing that the high value of α has no physical significance).

11.7 Friction parameters

In HISWA the magnitude of bottom friction is determined by two parameters in equation (7.8), namely c_{fw} en c_{fc}, being the friction parameter for waves and for currents respectively. In HISWA these parameters have a default value of 0.01 and 0.005 respectively. These default values have been used, because the influence of bottom friction on waves in this experiment, in which waves travel only a short distance, can be neglected.

12 2DH-simulations of initial hydrodynamic processes in the wave basin

12.1 Introduction

The initial (fixed bed) computations are carried out to obtain the initial wave field, flow field and sediment transports for all cases, i.e. experiment A3, C3 and D3 (for the meaning of these codes reference is made to section 5.7).
Intercomparison of the model results can lead to an opinion about the influence of the two configurations of breakwaters on sediment transports and morphology. These results also serve as the starting-point from which parameter sensitivity research is done (Chapter 17).
In section 12.2 the process tree that is used for these computations is given. The input description can be found in section 12.3. Finally, in section 12.4, the results are discussed.

12.2 Used process tree

The process tree of this computation is presented below:

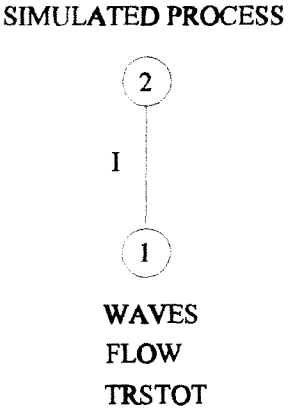

Figure 12.1: Process tree

First WAVES is called for the computation of the (initial) wave field. For this computation only a zero time step is needed, because the wave field is stationairy.
Next FLOW is called in order to compute the current field and the waterlevel. After 200 timesteps of 0.6 seconds (i.e. 2 minutes process time), the current field and water level is stationair, as can be seen from Figure 12.2 and 12.3, and the computation ends.

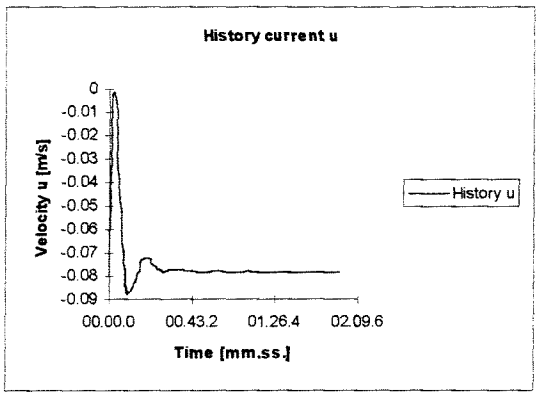

Figure 12.2: History current u

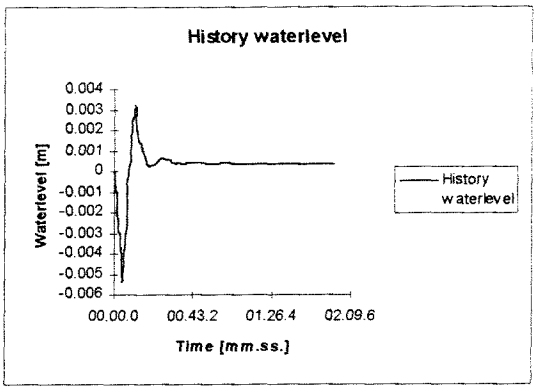

Figure 12.3: History water level

12.3 Input description

12.3.1 WAVES input

Input grid
The bottom input is provided to HISWA on a grid. The dimensions of the input grid are chosen such that the grid covers the whole area of interest, which is the wave basin. The resolution for the input grid resolves the relevant spatial details (in this case especially the breakwaters, modelled as ridges) in the bottom profile.
The input grid is taken rectangular with dimensions 29.5 m in x-direction (parallel to the shore) and 14.1 m in y-direction (perpendicular to the shore i.e. the wave propagation direction). This area is divided into meshes of 0.5 m in x-direction and 0.1 m in y-direction. The origin of the input file is (x,y) = (100 m, 100 m).
The bottom depth input is provided by the bottom depth file. This bottom depth file contains depth values positive downwards measured from the still water line. The bottom depth values are derived from the initial profile.

Computational grid

The computational grid is a grid in three dimensions: x-, y- and θ-space. The grid is taken larger than the input grid to prevent lateral disturbances reaching the area of interest. On each lateral side the computational grid is taken approximately 10 m larger than the input grid. The upwave and downwave boundary locations are taken equal to the boundary locations of the TRISULA grid, so the dimensions of the computational grid are 50 m in x-direction and 14.2 m in y-direction.

This area is divided into meshes of 0.5 m in x-direction and 0.2 m in y-direction. The mesh-size in x-direction depends more or less on the chosen directional sector of wave propagation. Usually this sector is taken 120°, because increasing the size of this sector means a considerable decrease of the mesh-size Δx. Also in this case a sector of 120^0 is taken, subdivided into 20 meshes of 6°.

Then the following condition of numerical stability must be satisfied:

$$\frac{|\Delta x.c_{0y}|}{|\Delta y.c_{0x}|} \leq 1 \qquad (12.1)$$

With the absence of currents the θ-direction is equal to direction of wave propagation.
Then equation 12.1 reduces to:

$$\frac{\Delta x}{\Delta y} \leq cotg\,\theta \qquad (12.2)$$

where the maximum of θ must be less than 90°.

With Δy = 0.5 m, Δx = 0.2 m and θ = 120°/2 = 60° this stability criterium is satisfied.

Wave data

In Chapter 11 the wave data were already determined: the significant wave height H_s = 0.17 m and wave period T = 1.55 s. The waves approach to the beach perpendicularly which means a wave propagation direction θ_0 of 0°.

The distribution of wave energy over the directions takes place according to the directional spreading function $D(\theta) = (\cos\theta)^{ms}$ where *ms* is taken equal to 30, which means a directional spreading of 10.2 degrees.

Dissipation due to breaking

The dissipation coefficient and the breaker coefficients for shallow water and steepness are determined as: α = 8.0, γ_s = 2.0 and γ_d = 1.0.

Bottom friction coefficients
These coefficients determine the bottom friction in HISWA. Only in case of large travel distances of waves these coefficients have a significant influence, so not in this case. Therefore the coefficients c_{fc} and c_{fw} are taken equal to their default values, namely 0.005 and 0.01 respectively.

Boundaries
At the upwave boundary the wave data are described. At the lateral boundaries open boundaries are applied.

12.3.2 FLOW input

Input grid
The dimensions of the TRISULA input grid are 14.1 m in y-direction and 29.5 m in x-direction. The mesh sizes in y- and x-direction are taken equal to the mesh sizes in HISWA: the mesh size in y-direction is 0.10 m and in x-direction 0.50 m.
The grid enclosure on the water level points of the staggered grid cells defines the computational grid boundaries. Points outside this enclosure are defined as dry points.

Bottom friction
For a depth-averaged flow (2D) the shear stress on the bed induced by a turbulent flow is assumed to be given by a quadratic friction law:

$$\tau_b = \rho \frac{g}{C_{2D}^2} |\underline{U}|^2 \qquad (12.3)$$

in which $|\underline{U}|$ is the magnitude of the depth-averaged horizontal velocity.

The 2D-Chézy coefficient C_{2D} is determined according to White-Colebrook's formulation, which reads:

$$C_{2D} = 18 \log_{10}\left(\frac{12H}{k_s}\right) \qquad (12.4)$$

where H is the total water depth and k_s is the Nikuradse roughness length.

For the computation a k_s-value of 0.01 m is chosen.

Horizontal eddy viscosity (turbulence viscosity)
The horizontal eddy viscosity describes the turbulence closure in the simulation.
Delft3D-FLOW gives the options to choose a turbulence closure model. In this case a constant horizontal eddy viscosity is applied, which leads to parabolic (laminar flow) vertical velocity profiles. This turbulence model has the advantage of simplicity, but especially near the bottom the eddy viscosity is not well modelled (too high).
In case of a strong varying eddy viscosity in practise the flow field is often calibrated with the magnitude of the turbulence viscosity.
Also in this study the turbulent viscosity has been determined by calibrating. Varying the magnitude of ν, the simulated (initial) flow velocities were compared with the measured velocities until these velocities were of the same order of magnitude.
Finally the uniform horizontal eddy viscosity in the model is given the value 0.10 m^2/s.

Numerical stability
Numerical stability is achieved if the Courant number is smaller than 10:

$$\sigma \cdot \sqrt{gh} \frac{\Delta t}{\Delta y} \leq 10 \qquad (12.5)$$

With h = 0.57 m, g = 9.81 m/s^2 and Δy = 0.20 m and σ = 10 it is required that $\Delta t \leq 0.85$ s.
The time step used in Delft3D-FLOW is 0.6 seconds.

Boundaries
The lateral boundaries and the downwave boundary are modelled as closed boundaries. The sea-boundary is chosen as an open boundary to obtain a limited computational area. In nature, waves can cross this kind of boundary unhampered and without reflections. In the model this property is included in the boundary condition: a weakly reflective boundary condition of Riemann type is applied. For this type of boundary condition both the water level and velocity have to be known. Because the open boundary allows water entering the model, which leads to an increase of waterlevel of approximately 0.01 m after an initial run with FLOW, the water level at the sea-boundary is set to -0.01 m (1 cm below still water level).

12.3.3 TRSTOT input

Transport formula
In the transport module the Bijker formula is used. The values of the parameters used in this formula should be given by the user.

In the bed load formula a coefficient b has to be specified. This coefficient depends on the relative activity of the waves (breaking or not breaking). The ratio H_{rms} / h expresses this activity. Dependent on shallow or deep water two values of b should be given. In intermediate waterdepths b is linearly interpolated. In case of shallow water (H_{rms} / h $\geq$ 0.79) b has the value of 5, in deep water (H_{rms} / h $\leq$ 0.08) b = 2.

The sand, with a density of ρ = 2650 kg / m^3, has a diameter D_{50} of 75 μm and a diameter D_{90} of 100 μm. The fall velocity of these grains is w = 0.006 m/s.
The bottom roughness μ is assumed to be 0.02 m (which is the estimated size of the bed ripples as measured during the experiments), the porosity of the bed material ϵ = 0.4 and the kinematic viscosity of water is 1.0 * 10^{-6} m^2 / s.

12.4 Results

In this section the results of the simulations with a fixed bed are given.
Some of the results are presented in figures which can be found in Volume II (figure numbers indicated with A). These pictures are generated with GPP, a graphical program which is able to use output data of Delft2D-MOR. Note that in these pictures the axis-system has somewhat changed. The y-axis begins at 100 m, which is the sea-boundary where the the waves are generated, and ends at 114 m, which is the land boundary. The x-axis begins at 100 m and ends at 129 m. Its orientation is as defined in Chapter 5. In some of the GPP-pictures contour lines of the initial bottom have been added with the purpose of showing the location of the breakwaters.
Other pictures (made in Excel) use the same axis-system as defined in section 5.5.
If reference is made to a figure or picture the coordinates are given with respect to the used axis-system.
The case of absence of breakwaters is indicated with code A3, the cases of two and three breakwaters are indicated with codes C3 and D3 respectively.

Note: The figure numbering in Volume II is not continuous!

12.4.1 Case A3: No breakwaters

Wave field and dissipation
The computed wave heights in cross-shore direction are equal for all cross-sections. For one section the wave heights are given in Figure 12.4:

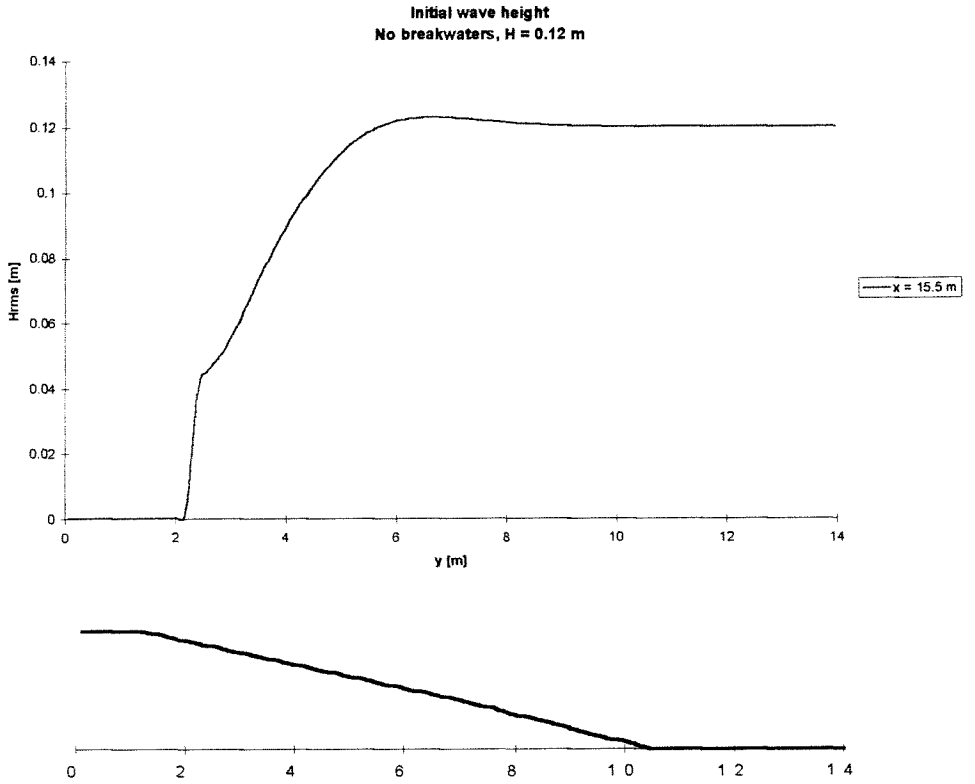

Figure 12.4: Initial wave height

Shoaling occurs in the region y = 14.0 m to y = 7.0 m, where dissipation is negligible as can be seen from Figure 12.5.

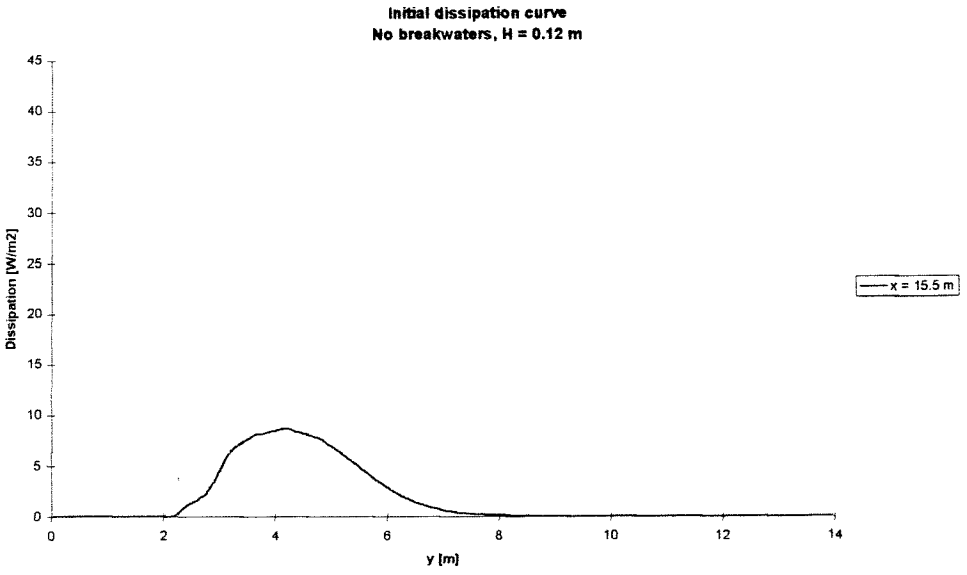

Figure 12.5: Initial dissipation

At approximately y = 7.0 m the breaker zone starts. Dissipation increases towards the beach and becomes zero at the shoreline (at approximately y = 2.0 m).

Water level

The water level is approximately constant at SWL (= 0.00 m) until the breaker zone where a wave set-up occurs. The computation of the water level is based on wave energy dissipation and wave forces. This explains why wave set-down is not computed: dissipation is (almost) absent outside the breaker zone. The initial water level is shown in Figure 12.6 below.

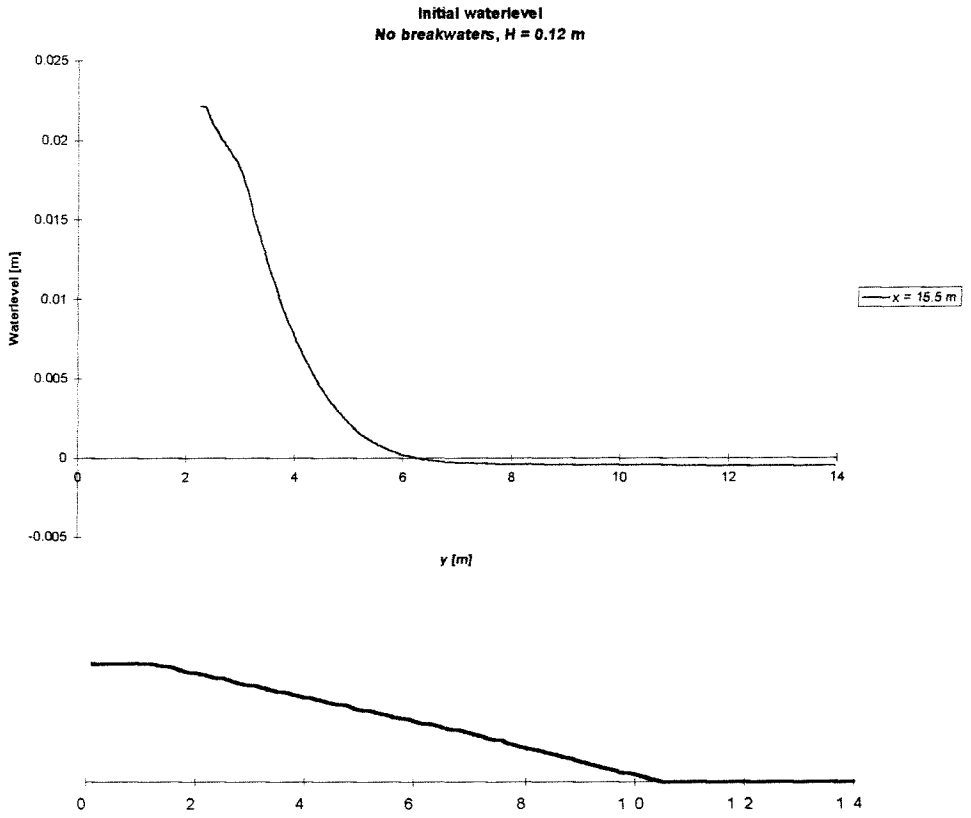

Figure 12.6: Initial water level

Flow field

The flow field (Figure A12-1) is somewhat strange. Because wave field and water level are uniform in cross-shore direction, theoretically there is no driving force for longshore currents. Apparently numerical inaccuracies (initial disturbances) are causing these deviations. The magnitude of the average flow velocities is very small, with higher velocities in the breaker zone.

The very low velocities are according to measurements, where flow velocities were so small that the accuracy of the EMS (measurent equipment, see Chapter 5) was questionable.

Return flow field

The return flow in Delft3D-FLOW (with mass flux computations included) is defined as the total flow (computed by solving the momentum and continuity equations) minus the mass flux (see Chapter 5 and 8), and is averaged over the total water depth. The return flow mainly determines sediment transport.

The return flow field (Figure A12-2) shows a pattern that can be expected. All flow directions are from the beach towards the sea. In the breaker zone the magnitude of the return flow is much higher than outside this zone which shows the big influence of breaking waves on the return flow.

Sediment transport

The sediment transport pattern (Figure A12-3) follows the pattern of the return flow field, which is correct: the undertow is mainly responsible for the transport of sediment. Throughout the whole breaker zone the sediment transport rates are small, outside the breaker zone these rates become zero.

It is remarkable that the Bijker formula, in the first place developed for longshore sediment transport computations, is able to describe onshore-offshore sediment transport as well. Usually the formula is applied to longshore sediment transport computations.

However, it should be noticed that this formula applied in cases where onshore-offshore transport is clearly present only gives first approximations. One of the reasons for this is that the Bijker formula uses return flow velocities averaged over the total water depth.

12.4.2 Case C3: Two breakwaters

Wave field and dissipation

Clearly the wave field is influenced by the breakwaters, as can be seen from Figure A12-6 and Figure 12.7.

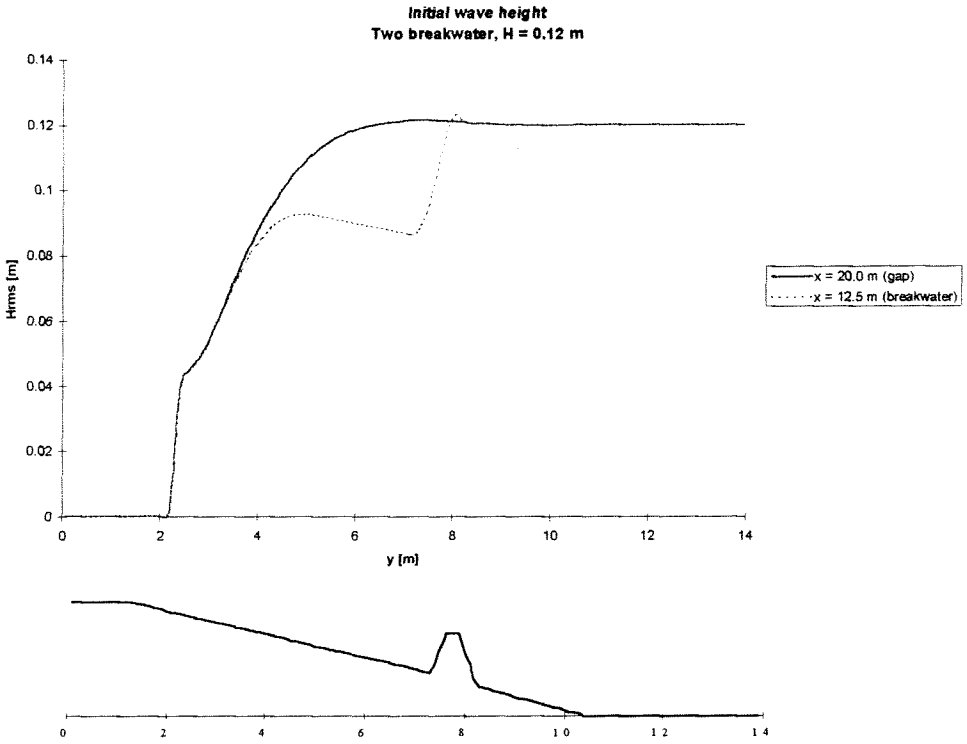

Figure 12.7: Initial wave height at x = 12.5 m and x = 20.0 m

In front of the breakwaters the wave height increases (due to shoaling on the breakwater), the wave height reaches its maximum at the breakwater crest and the wave breaks. Behind the breakwater zone wave energy enters the shadow zone of the breakwaters. At approximately y = 110 m (in Figure A12-10) the influence of the breakwaters on wave height is not present anymore: wave heights are approximately equal in longshore direction.

At the breakwater crests the amount of dissipation is very high. The shore-breaking waves dissipate much less, but this smaller amount of dissipation occurs over a longer distance. In Figure 12.8 this is shown:

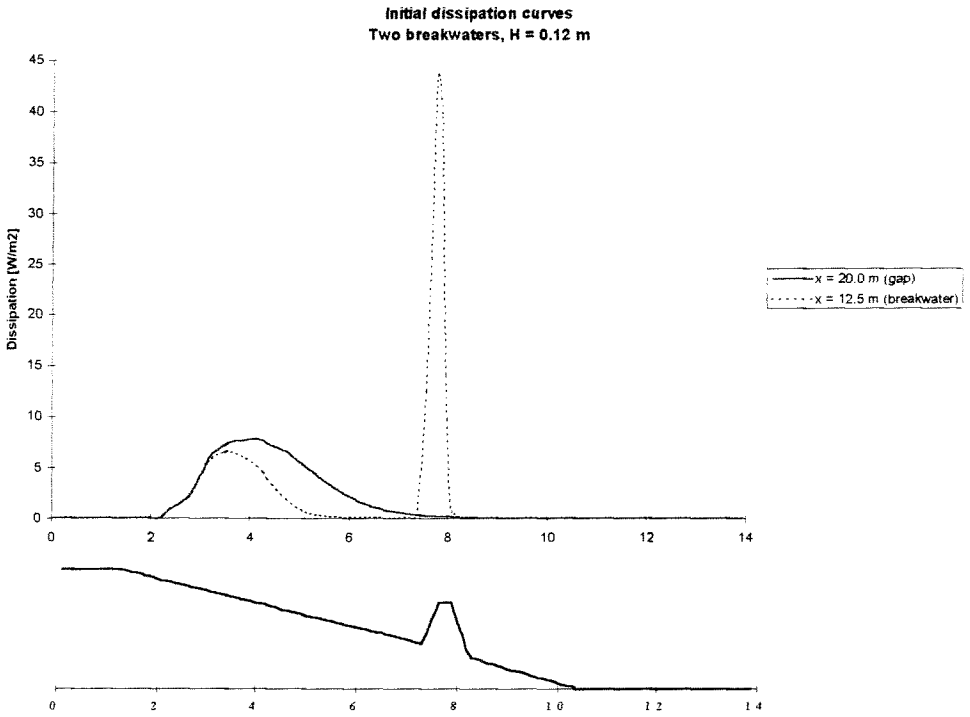

Figure 12.8: Initial dissipation at x = 12.5 m and x = 20.0 m

Because of this large amount of dissipation at the breakwaters and the decreased waves in their vicinity diffraction occurs in the area behind the breakwater. Wave energy is transferred from the regions with higher waves to the regions with lower waves.
When looking at the wave height and dissipation in a cross-section over a breakwater (Figure 12.8) it can be seen that the influence of the breakwater is very direct. The waves feel the breakwater and break immediately. In nature waves show the inertia phenomenon: when waves pass over a submerged breakwater they do not break immediately, but at a certain distance from the breakwater. For this reason the large, concentrated amount of dissipation at the crest of the breakwater, as computed in HISWA, is not realistic. A more realistic dissipation pattern would be a less concentrated, more spreaded dissipation with its peak at a certain distance behind the breakwater (where the waves break).
The shoaling of the waves behind the breakwater is not realistic either. The broken waves immediately start to shoal again. It is questionable whether in practise the broken waves propagate like 'normal' waves again. In practice a quasi-stationary breaking mode would occur, in which waves propagate like bores (Stive '88).
Theoretically the area under the two dissipation curves in Figure 12.8 should be equal, because in all cross-shore sections an equal amount of wave energy has to be dissipated. Probably the areas under the curves are equal, although that is hard to see.

Water level

According to the computations the water level is influenced in the breakwater zone. Over the breakwater wave set-up is present which is clearly bigger than the wave set-up induced by the dissipating waves in the cross-sections through the gaps, as can be seen from Figure 12.9.

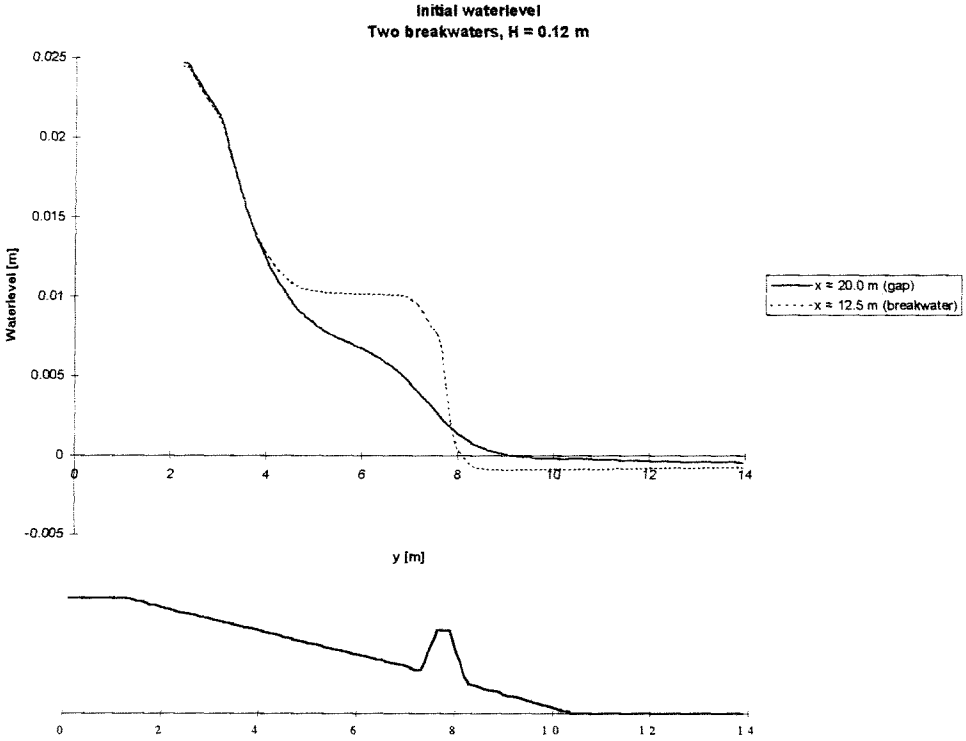

Figure 12.9: Initial water level at x = 12.5 m and x = 20.0 m

The large amount of dissipation at the breakwater crests induces this relatively large wave set-up. According to the computations waves stop breaking behind the breakwaters and the wave set-up does not increase until waves break near the shoreline (at approximately y = 4.0 m).
In the cross-sections through the gaps waves start dissipating behind the breakwaters, which results in wave set-up. From y = 4.0 m to the shoreline (y = 2.0 m) the water level is equal throughout the whole region.
The water level gradients in longshore direction results in longshore currents from regions with high water levels to regions with low water levels. Obviously, behind the breakwater zone currents are directed from behind the breakwaters towards the gaps.

Flow field

The influence of the breakwaters on the flow field is clearly visible (see Figure A12-7). The flow field is not dominated by wave-induced currents anymore. Due to gradients in the water level, caused by differences in wave set-up, circulation flow patterns occur. The flow behind the breakwaters bends into longshore flow in the direction of the gaps, where the water levels

are lower. In the gaps the flow is directed seawards and flow velocities increase there. In the cross-sections over the middle of the breakwaters hardly any longshore currents are present. In these sections the flow circulation cells are separated.
The circulation pattern in the area of the large breakwater and the 6 m-gap has a bigger order of magnitude than elsewhere in the basin. It is clearly visible that longshore flow velocities are significantly higher here, but the seaward directed flow velocities through the 6 m-gap are lower than in the 3 m-gap inbetween the breakwaters.
The longshore flow velocities near the breakwaters are significant, but decrease rapidly closer to the shoreline.
In addition to the currents induced by water level gradients, the dissipation of wave energy behind the breakwater generates currents in the direction of wave propagation. The differences in flow velocities close behind the large breakwater (stronger at the ends, weaker in the middle) can be explained by the strong attraction of flow by the gaps.

Return flow field
Figure A12-8 shows that the computed return flow is mainly directed seawards, but only one or two meters away from the shoreline it is obviously forced towards the gaps. The undertow is (partly) blocked by the presence of the breakwaters and has to find its way through the gaps.

Sediment transport
The sediment transport pattern shows great resemblance with the return flow pattern: near the shoreline is offshore directed sediment transport present which is more and more directed towards the gaps going seawards (see Figure A12-9).
Clearly visible is the transport of sediment from close behind the breakwaters. Since it seems that there is no sediment transport towards this area erosion will occur here. The significantly high transport rates close behind the breakwaters are caused by the large amount of dissipation that is concentrated at the breakwaters. This wave dissipation is responsible for the development of wave forces that induce currents directed in the wave propagation direction (shorewards).

12.4.3 Case D3: Three breakwaters

Wave field and dissipation

The wave height pattern shows great resemblance with case C3, as can be seen from Figure A12-10 and Figure 12.10.

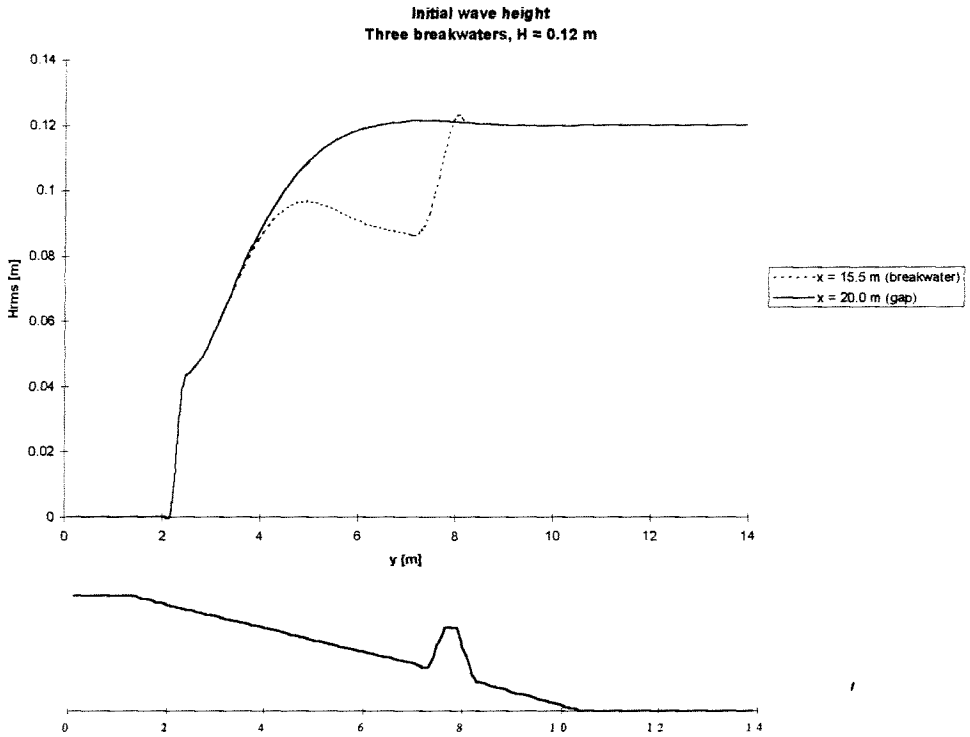

Figure 12.10: Initial wave height at x = 15.5 m and x = 20.0 m

The wave height remains more or less constant until the waves reach the breakwaters, where the wave height suddenly increases a little (because of shoaling on the breakwaters). The waves reach the maximum height and partly break there, which leads to smaller wave heights. Behind the breakwaters the wave height increases again, because of shoaling, until the breaker zone is reached, at y = 4.0 m approximately. Hardly any dissipation occurs at the seaward side of the breakwaters and 1 or 2 m at the landward side (see Figure A12-11 and Figure 12.11):

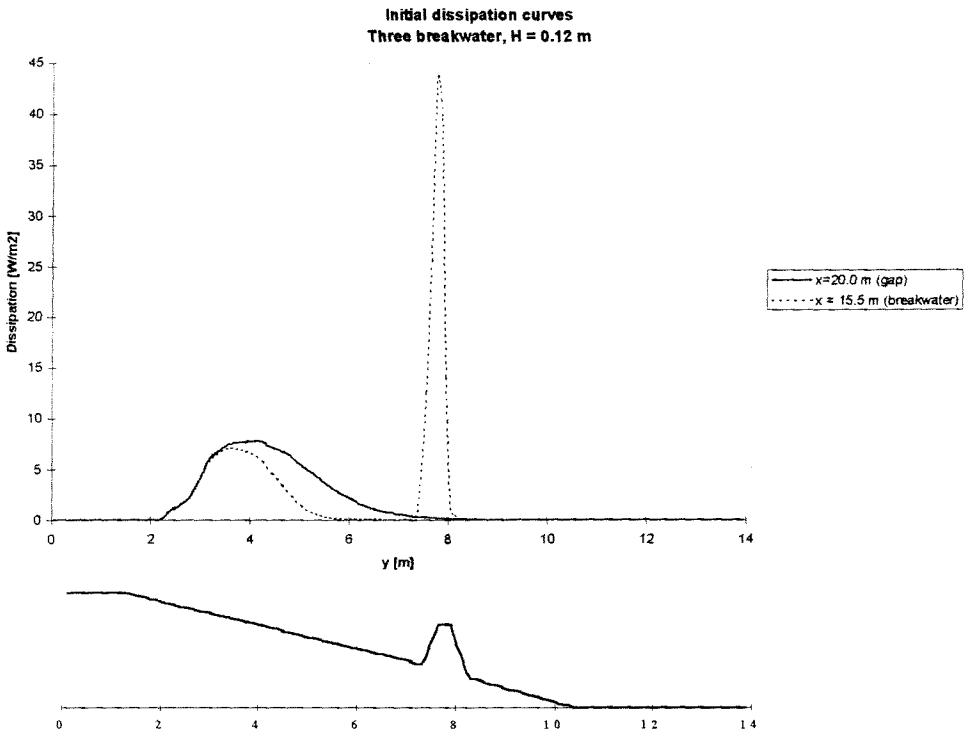

Figure 12.11: Initial dissipation at x = 15.5 m and x = 20.0 m

The breakwaters obviously induce a lot of dissipation. It can be seen that the breaker line is around y = 4.0 m. The magnitude of dissipation in the breaker zone is far less than in the breakwater zone.

Water level

The water level pattern is about the same as in case C3 as can be seen from Figure A12-12 and Figure 12.12. (For explanation reference is made to section 12.4.2):

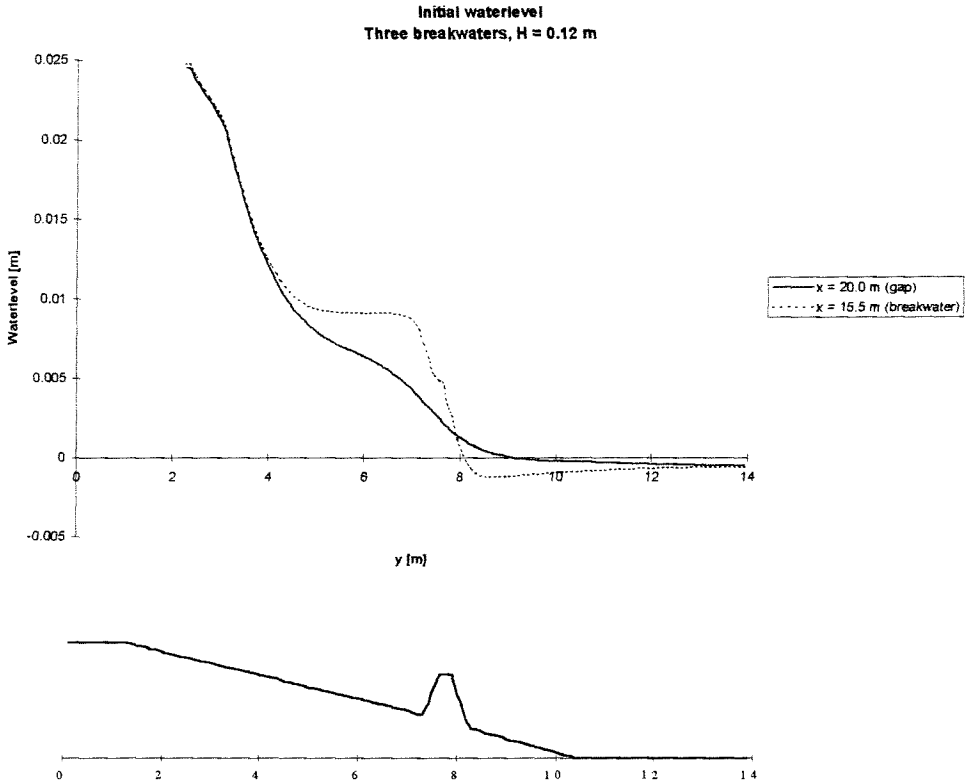

Figure 12.12: Initial water level at x = 15.5 m and x = 20.0 m

Flow field

Also in this case the influence of the breakwaters on the flow field is expressed in the presence of flow circulation patterns and the dissipation induced currents close behind the breakwaters (see Figure A12-13). Compared to case C3 the most striking difference is in the area between x = 100.0 m and x = 110.0 m. Longshore current velocities are smaller in case D3 which can be seen as the influence of the smaller gap width here compared to case C3: where in case C3 the 6 m-gap attracts currents this influence is much smaller in case of the smaller gap in D3. In both cases the flow velocities in the gaps are approximately equal.

Return flow field

Also the return flow field differs from case C3 in the region x = 100 - 110 m especially (see Figure A12-14). Much stronger (longshore) currents occur in case C3 and the currents in shoreward direction tend to bend earlier than in case D3. Again this difference can be explained by attraction of flow by the big gap in case C3.

Sediment transport

The differences in the sediment transport pattern can be explained by the differences in flow patterns as described above. In case C3 sediment transport rates are much higher near the big gap compared to case D3 (see Figure A12-15). The erosion rate behind the big gap in case C3 will certainly be much higher. In the region from x = 118 m to 129 m the sediment transport pattern and rates are approximately equal in both cases.

13 2DH-simulation of hydrodynamic and morphological processes in the wave basin without breakwaters

13.1 Introduction

In this chapter the 2DH-simulation without breakwaters is described. Only the results of the computer simulations at t = 7.5 hours are presented here, except for results concerning morphology, when also results after 0.5 hours of simulation are presented.
These simulation results are used for the determination of the effect of the presence of breakwaters on morphology in the configurations as described in Chapter 5. Besides, these results can be compared to the experimental results in case of absence of breakwaters in order to give an opinion about the model's ability to simulate the morphological effects in the wave basin.
Comparison of computed and measured wave heights, currents, water levels and sediment transports is difficult, because differences in computed and measured morphological developments in the basin are big.
In section 13.2 the used process tree is given. This process tree shows the way the simulation is carried out. (For a general description of the process tree reference is made to Chapter 6).
In section 13.3 the input for Delft2D-MOR is described.
The results of the simulation are given in section 13.4. Finally, in section 13.5 a brief conclusion is given.

13.2 Used process tree

The process tree of this computation is presented below in Figure 13.1:

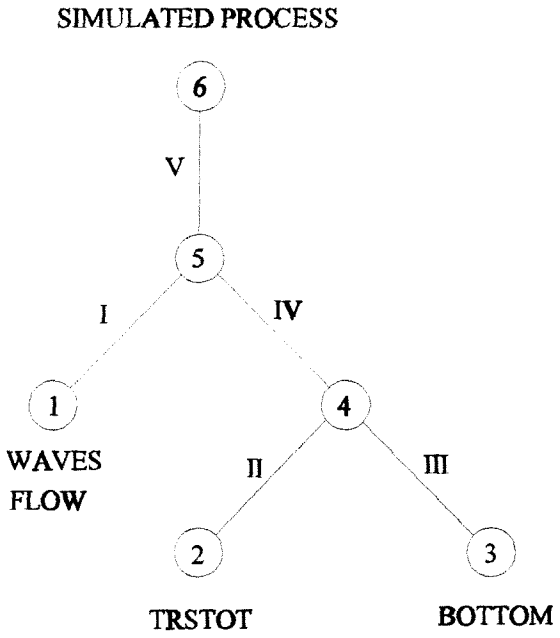

Figure 13.1: Process tree

First WAVES is called for the computation of the (initial) wave field. For this computation only a zero time step is needed, because the wave field is stationair.
Next FLOW is called in order to compute the current field and the waterlevel. After 200 time steps of 0.6 seconds (i.e. 2 minutes process time), the current field and waterlevel is stationair and the computation ends.
Wave-current interaction is not taken into account, therefore feed back of the computed current field to HISWA does not take place.
The current field is used as input for the module TRSTOT, which computes the sediment transport rates, which are used as input for the module BOTTOM.
TRSTOT and BOTTOM are called 30 times in a row, without a call of WAVES or FLOW (only the flow is adapted at a fast method: Q = constant).
This is because only after 30 time steps (determined by BOTTOM) the bottom changes are significantly important to call WAVES and FLOW and compute a new wave and flow field.
After TRSTOT has computed the average sediment transport rates, BOTTOM computes the the bottom change. With this new bathymetry BOTTOM adapts the flow velocities (discharges remain constant). The adapted flow field is used again by TRSTOT to compute new sediment transport rates and so on.
After 30 calls of TRSTOT and BOTTOM it is checked whether the process simulation end time has been reached or exceeded. If so, the computation is ended. If not, WAVES and FLOW (for the computation of new discharges) and, after that, TRSTOT and BOTTOM are called again: a new computation cyclus is started.

13.3 Input description

The same input is used as defined in Chapter 12.

13.4 Results

In this section the results of the simulation without breakwaters are given.
Some of the results are presented in figures which can be found in Volume II (figure numbers indicated with A). These pictures were generated with GPP, a graphical program which is able to use output data of Delft2D-MOR. Note that in these pictures the axis-system has somewhat changed. The y-axis begins at 100 m, which is the sea-boundary where the the waves are generated, and ends at 114 m, which is the land boundary. The x-axis begins at 100 m and ends at 129 m. Its orientation is as defined in Chapter 5. In some of the GPP-pictures contour lines of the initial bottom profile have been added with the purpose of showing the location of the breakwaters.
Other pictures (made in Excel) are generated with the same axis-system as defined in Chapter 5.
If reference is made to a figure or picture coordinates are given with respect to the used axis-system.
(The case of absence of breakwaters is indicated with code A3, the cases of two and three breakwaters are indicated with codes C3 and D3 respectively).

The simulation of case A3 (and also of C3 and D3) was carried out with a different grid enclosure. It was found that the bottom module computed very small time steps at locations close to the shoreline. In order to reduce computation time the shore boundary was shifted to y = 2.25 m. Therefore wave height, dissipation and water level curves presented in this chapter have been truncated at this location, so these should be treated carefully.

Note: The figure numbering in Volume II is not continuous!

Wave field and dissipation
After 7.5 hours the wave height pattern has clearly changed. Heavy erosion in the area near the shoreline has led to the formation of a scour hole, causing the water depth to increase. The increase of water depth in this area has led to a less steep wave decay pattern as can be seen from Figure 13.2.

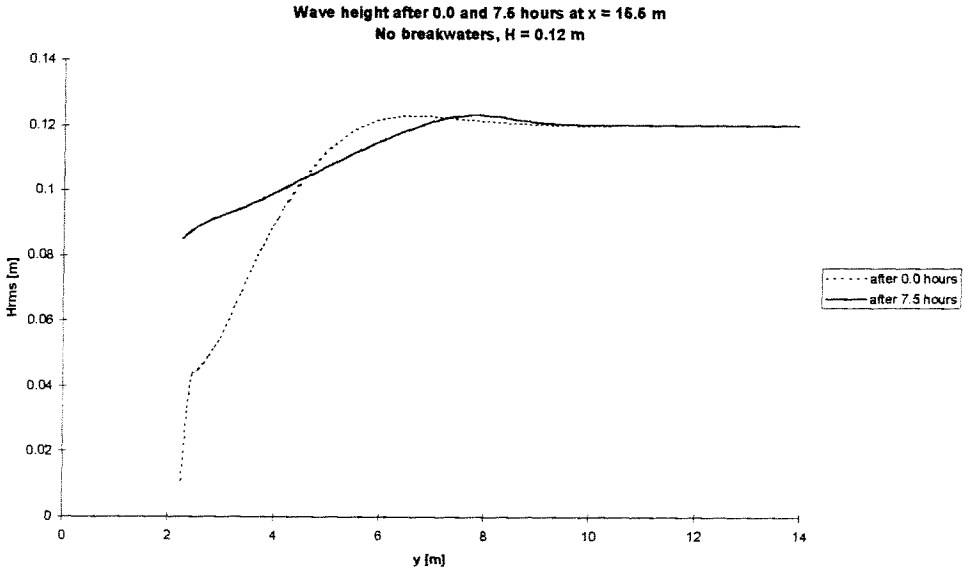

Figure 13.2: Wave height after 0.0 and 7.5 hours at x = 15.5 m

The dissipation patterns in Figure 13.3 confirm this statement. Obviously the dissipation pattern has been smoothed, causing a less steep wave decay pattern after 7.5 hours.

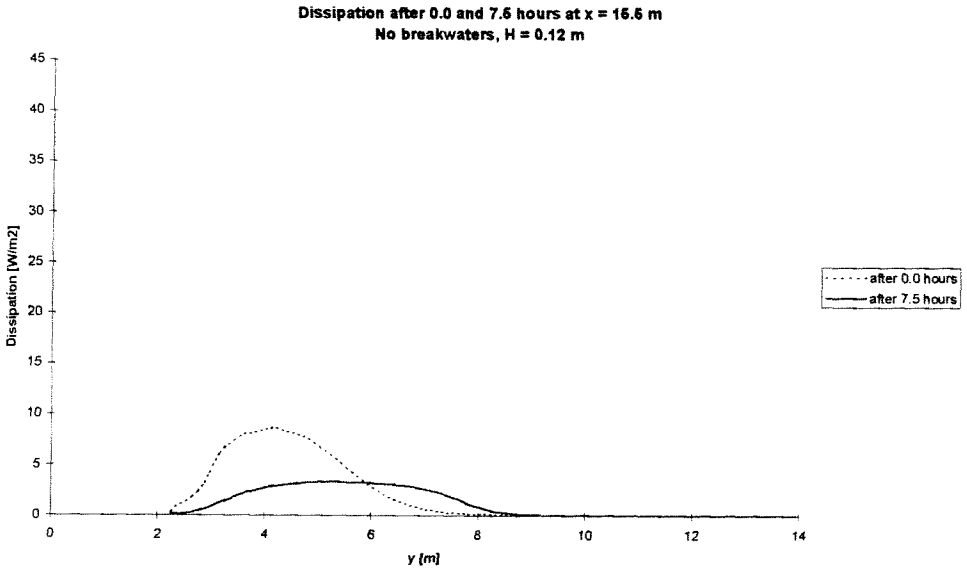

Figure 13.3: Dissipation after 0.0 and 7.5 hours at x = 15.5 m

It should be noticed that the dissipation curves are truncated at y = 2.25 m and that the amount of dissipation is non-zero there. From Figure 13.2 it can be seen that after 7.5 hours still a lot of wave energy has to be dissipated beyond this point, which explains the inequality of the

areas under the dissipation curves of 0.0 hours and 7.5 hours.

Water level

The water level has been influenced by the change of the dissipation pattern (see Figure 13.4). The wave set-up (in the breaker zone) has decreased due to the decrease of dissipation from y = 4 m to y = 2 m approximately. Since wave set-up in this model is determined by wave dissipation, this development is logical.

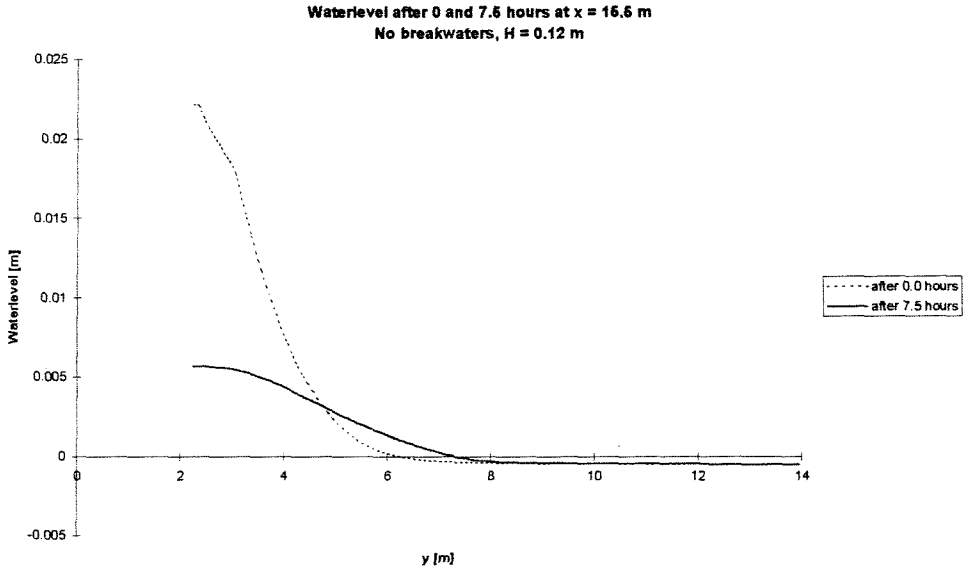

Figure 13.4: Water level after 0.0 and 7.5 hours at x = 15.5 m

Flow field

From Figure A13-4 it can be seen that flow velocities after 7.5 hours are still very small. Numerical inaccuracies near the boundary at x = 128.5 m lead to a kind of circulation flow pattern with relatively higher velocities. However after 7.5 hours of simulation these inaccuracies have not influenced the flow pattern throughout the whole basin. Therefore it is possible to discuss and use the results of these computations as long as they are not taken from the influenced zone.

Return flow field

The return flow field is about the same as the initial return flow field, except for the breaker line (at y = 107, 108 m) where the transition of flow velocities from small to very small is not so abrupt. This is probably due to the smoothing of the dissipation in this area after 7.5 hours. The small flow velocities never exceed 0.05 m/s. Figure A13-5 shows the return flow field, which has been disturbed near the boundary at x = 128.5 m (as was the case in the initial computation, see Chapter 12).

Sediment transport

The sediment transport is directed towards the sea throughout the whole basin. The transport rate is not much changed during 7.5 hours, as can be seen from Figure A13-6.

Morphology

Figure A13-7 shows the initial bathymetry, Figure A13-8 the bathymetry after 7.5 hours. In Figures A13-9 and A13-10 the computed and measured erosion/accretion after 7.5 hours is given respectively (erosion and accretion are in cm).

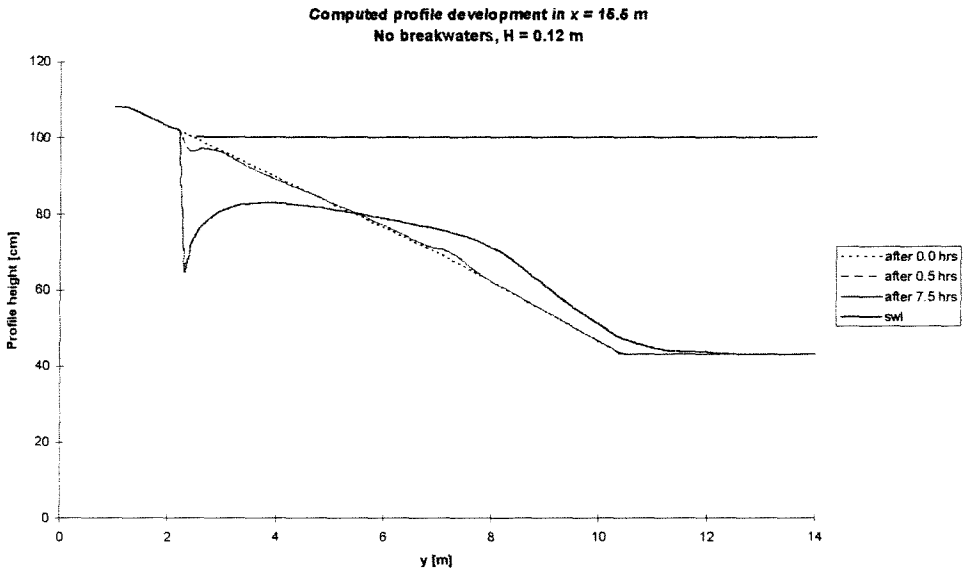

Figure 13.5: Computed profile development at x = 15.5 m

The effect of the more or less constant sediment transport from the shore towards the sea is clearly visible. The eroding (breaking) wave and current action near the shoreline leads to the formation of a scour hole (which is not filled with sediment from the beach). Accretion occurs in the area from y = 6.0 m to y = 12.0 m where flow velocities (and sediment transport rates) are lower or zero, hence unable to transport the sediment more seawards.
Figure 13.5 gives a clear view of the morphological development in time in cross-section x = 15.5 m (which is representative for all cross-sections). Because longshore currents are absent, the balance of erosion and accretion in one cross-section should be in equilibrium. This seems to be the case when looking at Figure 13.5.
The profile development in the experiments shows good resemblance with the model results in the accreting part of the cross-section (see Figure 13.6).

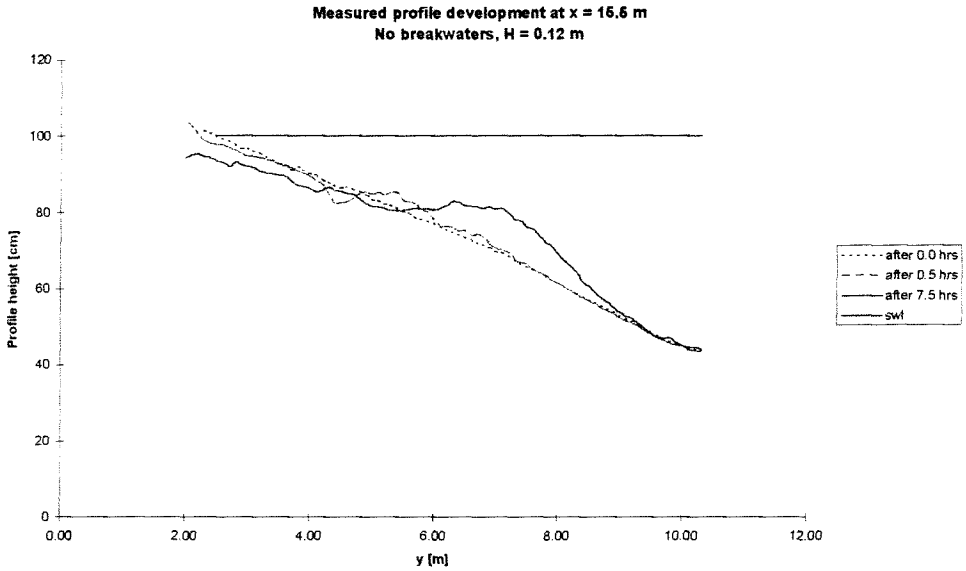

Figure 13.6: Measured profile development at x = 15.5 m

In the experiment sediment has been transported from the shore towards the sea, leading to erosion in the upper part of the profile and accretion more seawards.
The major difference between experiment and model results is the more uniform erosion (retreat of the shoreline) in the experiment, while erosion in the model leads to a scour hole, caused by the non-erodible beach beyond the shoreline.

13.5 Conclusions and remarks

Generally the results of the simulation show some resemblance with experimental results. Small flow velocities are generated, resulting in small sediment transport rates. The sediment transport is directed seawards which is according to expectations.
The computed morphological development corresponds in some respect to the measured development. The main difference lies in the fact that sand from the beach beyond the shoreline is not brought into the model. This leads to unrealistic erosion patterns near the shoreline.

14 2DH-simulation of hydrodynamic and morphological processes in the wave basin with two breakwaters

14.1 Introduction

In this chapter the 2DH-simulation with two breakwaters is described. These simulation results are used for the determination of the morphological effects of the presence of breakwaters in this configuration. For this purpose the results can be compared to the experimental results and to the results of the simulation without breakwaters (see Chapter 13).
In section 14.2 the used process tree is given. This process tree shows the way the simulation is carried out. (For a general description of the process tree reference is made to Chapter 6).
In section 14.3 the input for Delft2D-MOR is described.
The results of the simulation are given in section 14.4. Finally, in section 14.5 a conclusion is given together with some general remarks.

14.2 Used process tree

The process tree of this computation is the same as in the former computation without breakwaters. For an explanation about this process tree reference is made to Chapter 13.

14.3 Input description

The same input is used as described in Chapter 13. Of course only the bottom input has changed: breakwaters are added as profile elevations with a fixed bed.

14.4 Results

In this section the results of the simulation with two breakwaters are given. For an explanation about the axis-system of the figures reference is made to section 13.4.
Note: The figure numbering in Volume II is not continuous!

Wave field and dissipation
The wave field has changed much during 7.5 hours, especially in cross-sections through the gaps, as can be seen from Figure 14.1. From y = 12.0 m to y = 8.0 m, where only a little amount of shoaling is present in the initial state, the shoaling of waves is significant. This is due to the formation of shoals at the seaward side of the gaps between the breakwaters. The waterdepth has decreased there, leading to an increase in shoaling. (This increase of wave height at the shoals was also found during the experiments).

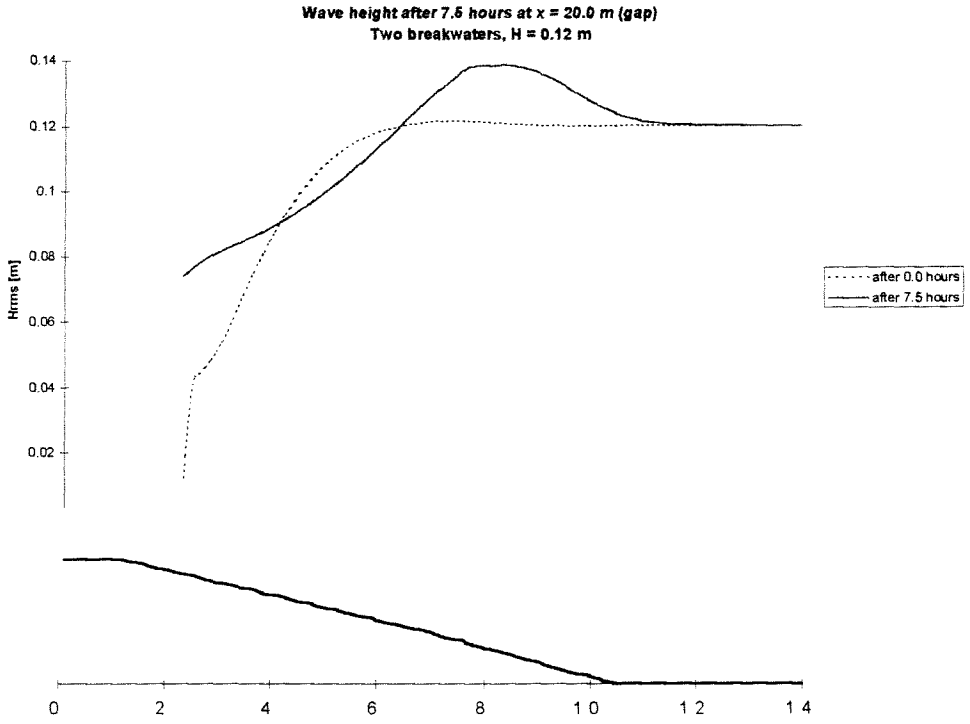

Figure 14.1: Wave height after 0.0 and 7.5 hours at x = 20.0 m

At approximately y = 8.0 m the waves already break at the shoal, having reached their maximum height, inducing dissipation (Figure 14.2):

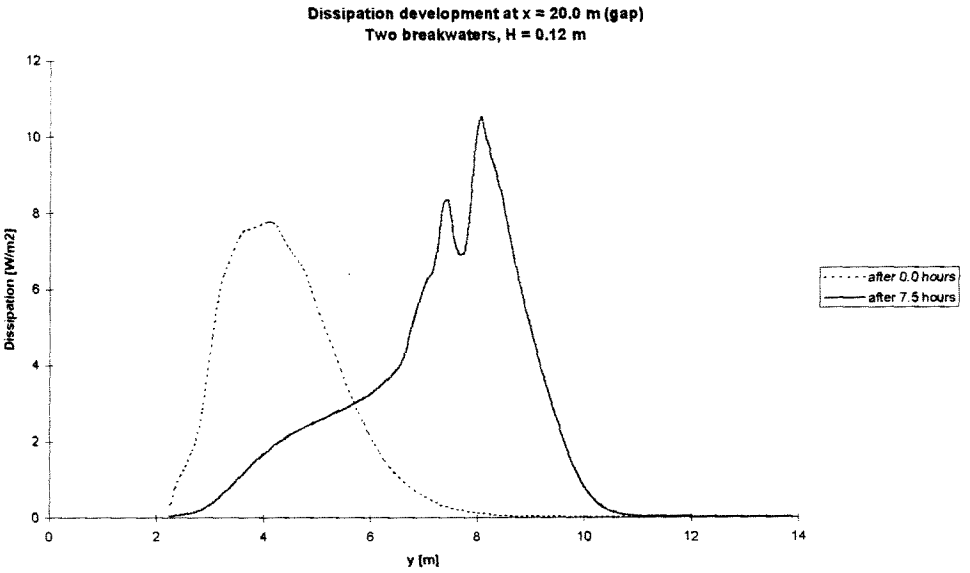

Figure 14.2: Dissipation after 0.0 and 7.5 hours at x = 20.0 m

Because after 7.5 hours most wave energy is dissipated at the shoal, dissipation in the breaker zone is not recognizable as a peak anymore (as it is in the initial state).

In cross-sections over the breakwaters (Figure 14.3) changes in the wave height pattern are relatively small. Only near the shoreline changes are significant. The maximum wave height there has been increased due to the increase in waterdepth near the shoreline because of erosion:

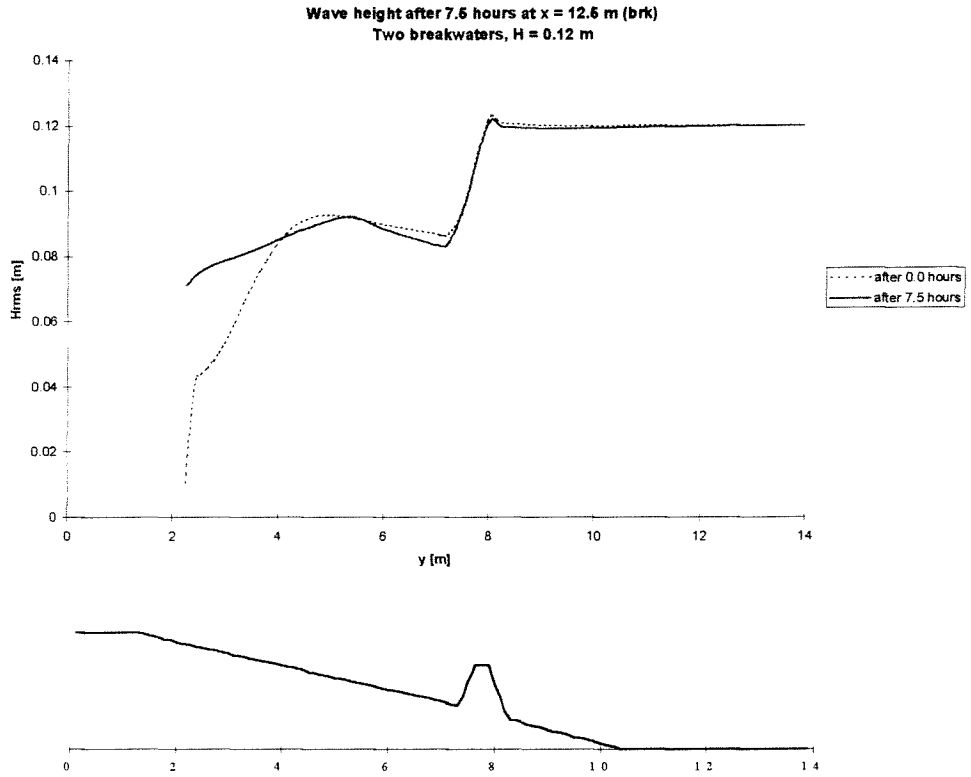

Figure 14.3: Wave height after 0.0 and 7.5 hours at x = 12.5 m

The wave breaking there is less prominent, inducing less dissipation as can be seen from Figure 14.4:

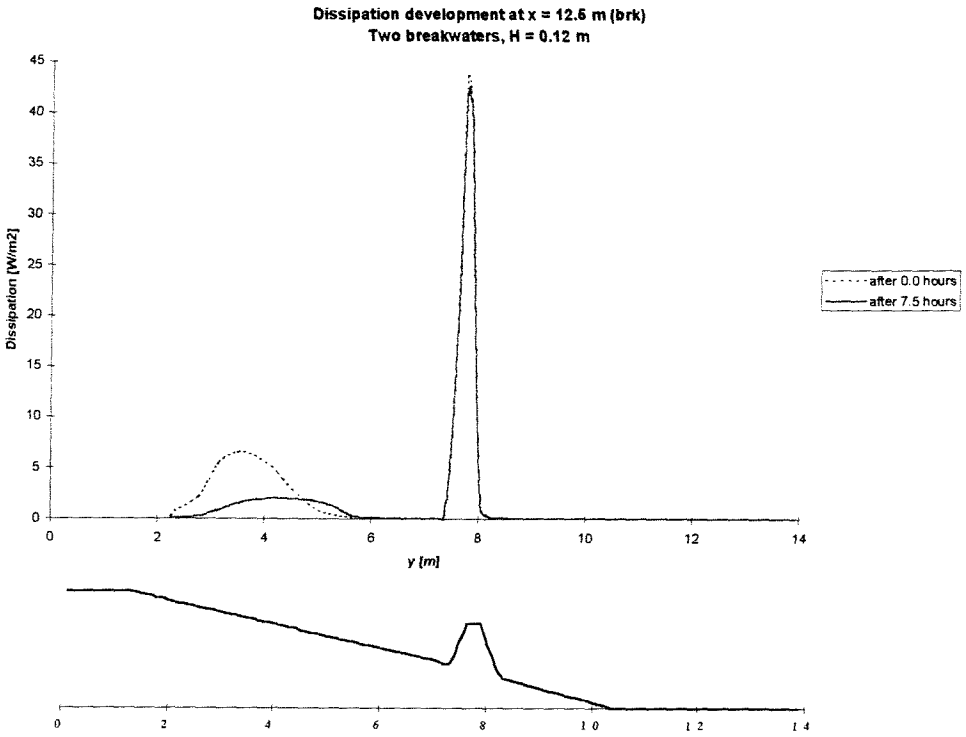

Figure 14.4: Dissipation after 0.0 and 7.5 hours at x = 12.5 m

The areas under the dissipation curves do not seem to be equal as they should be. For an explanation for this reference is made to chapter 13.

Water level

In Figure A14-3 the contourmap of the water level after 7.5 hours is given.
In the breaker zone the wave set-up is significantly smaller than in the initial state due to the decrease of dissipation in that area. In cross-sections through the gaps (Figure 14.5) the shift of the dissipation peak from close to the beach seawards does not seem to have much influence on wave set-up in the gap, where the wave set-up is just a little bit bigger:

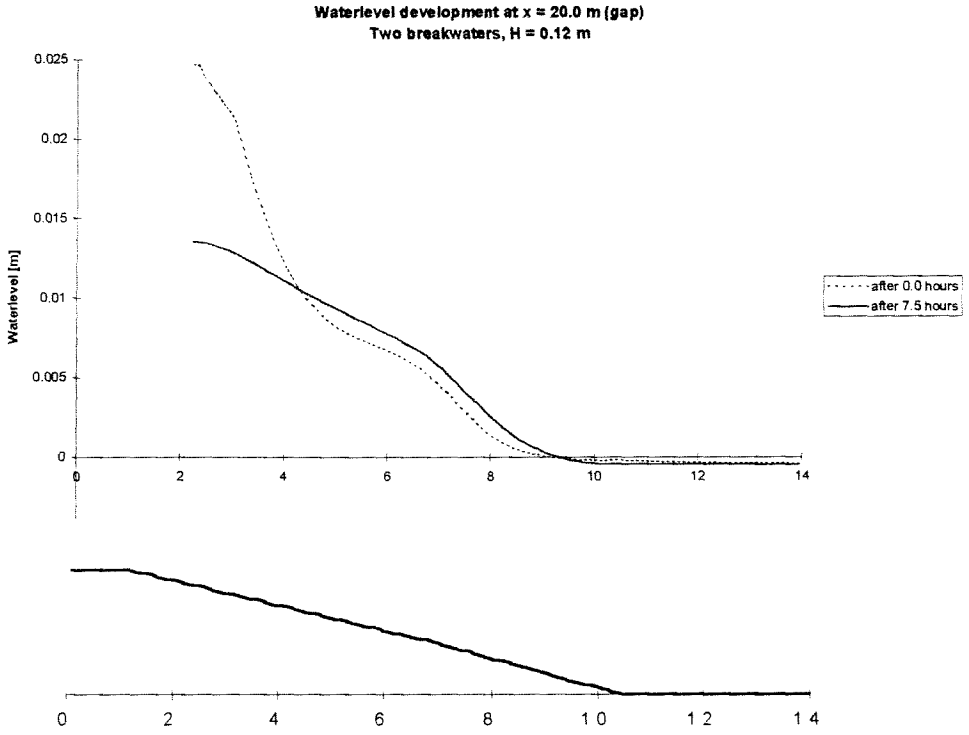

Figure 14.5: Water level after 0.0 and 7.5 hours at x = 20.0 m

In cross-sections over the breakwaters (Figure 14.6) only from y = 4.0 m to the shoreline (at y = 2.0 m) the wave set-up change is significant as could be expected from the dissipation figure (Figure 14.4).

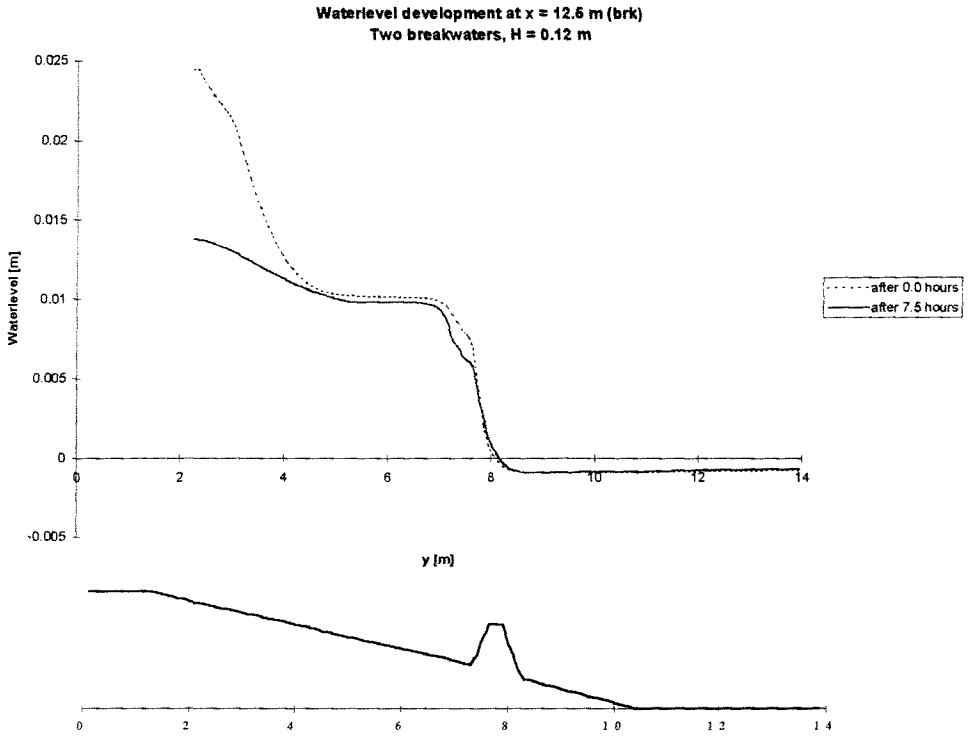

Figure 14.6: Water level at 0.0 hours and 7.5 hours at x = 12.5 m

Flow field

The flow field (Figure A14-4) has not much changed after 7.5 hours compared to the initial flow field. The flow circulation patterns are still present. Flow velocities in the gaps have decreased a little as well as longshore currents in the vicinity of the breakwaters. Due to erosion near the shoreline longshore currents are present here after 7.5 hours, while these were absent or very small in the initial state.
Compared to the case without breakwaters (A3) flow velocities are much higher due to the wave forcing initiated by dissipation over the breakwater and the waterlevel gradients that are driving forces for currents. (This also holds for the return flow field).

Return flow field

The return flow field is given in Figure A14-5. Changes, if present, are very small. The return flow over the breakwaters is a little stronger and also in this case longshore currents are present near the shoreline.

Sediment transport

The sediment transport pattern (Figure A14-6) shows some differences compared to the initial state, mainly caused by the movement of sediment: in the area between breakwaters and

shoreline, especially near the breakwaters ends, the transport rate has decreased. Sediment transport rates increased from almost zero to a significant magnitude in the seaward areas of the gaps due to the fact that after a given time sediment is available to be transported there. It is clear that compared to the case without breakwaters sediment transport rates are much higher, obviously resulting in more rigorous morphological changes.

Morphology

Figure A14-7 shows the initial bathymetry and Figure A14-8 the computed bathymetry after 7.5 hours. In Figures A14-9 and A14-10 the computed and measured erosion/accretion pictures are given (with erosion and accretion in cm).

Very clearly the influence of the relative large sediment transport rates just behind the breakwaters can be seen (see also Figure 14.7).

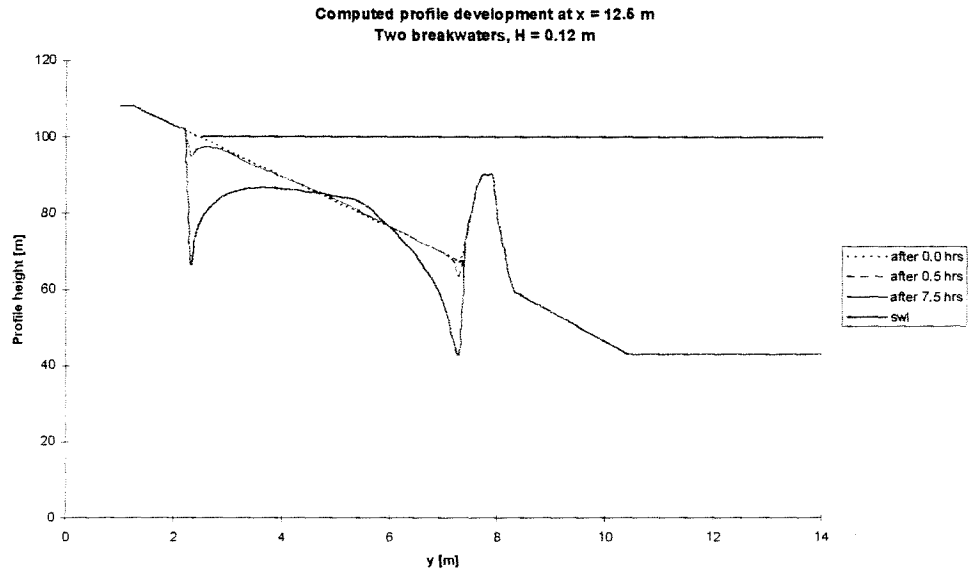

Figure 14.7: Computed profile development at x = 12.5 m

Large scour holes have been developed there. The same holds for the area near the shoreline. Sand has been transported from there towards the sea, but has not been replaced by sand from the beach causing a big erosion area near the shoreline, which of course in practice would be much smaller.

Figure 14.8 also shows that the sand balance in the cross-section is negative indicating that sand has been transported in longshore direction. In fact in this cross-section is hardly any accretion which means that almost all eroded sediment is transported to somewhere else.

The computed erosion/accretion picture (Figure A14-9) clearly shows that indeed sand is transported from behind the breakwaters (where erosion occurs) towards the gaps and further seawards.

When comparing Figure 14.8 and Figure A14-10 with Figure 14.7 and Figure A14-9 it can be seen that the difference between measured and computed profile development is very big.

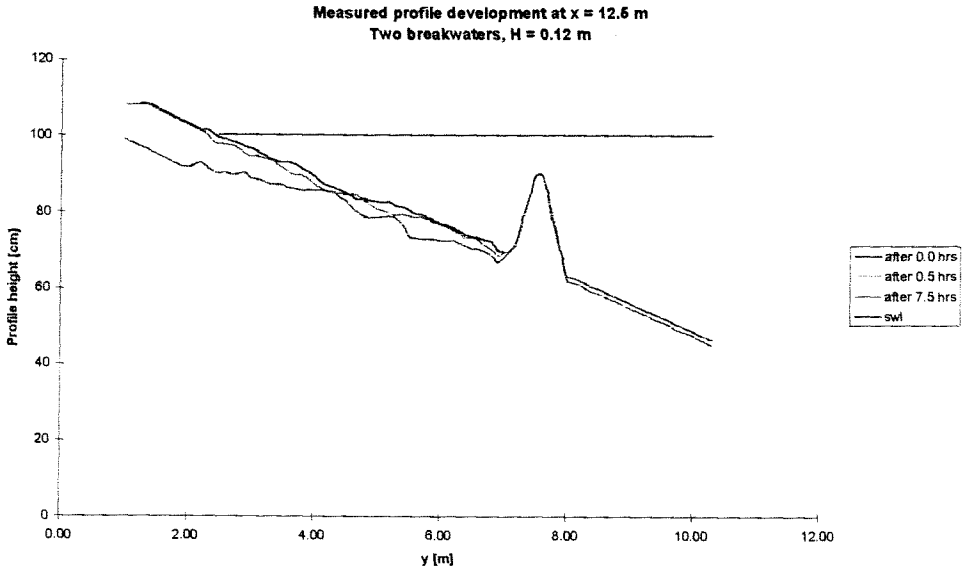

Figure 14.8: Measured profile development at x = 12.5 m

The large erosion holes behind the breakwaters were not present in the experiments. This indicates that wave dissipation and turbulence initiated by wave breaking is not concentrated close behind the breakwaters (as it is computed in HISWA). Obviously dissipation and turbulence were spread over a longer distance behind the breakwaters, causing a less concentrated eroding wave action.
In the experiments an erosion area near the shoreline is absent, but erosion took place over the whole area behind the breakwater. The presence of the erosion area near the shoreline as computed by DELFT2D-MOR can be explained by the disability of the model to bring the sand from the beach into the model. Sand transported from close to the shoreline to somewhere else is not (partially) replaced by sand from the beach, as it is the case in practise.
Figure 14.9 shows that the sand balance in a cross-section throug a gap (x = 20.0 m) is positive. Obviously the eroded material from close to the shoreline has been transported through the gap seawards together with eroded material from behind the breakwater:

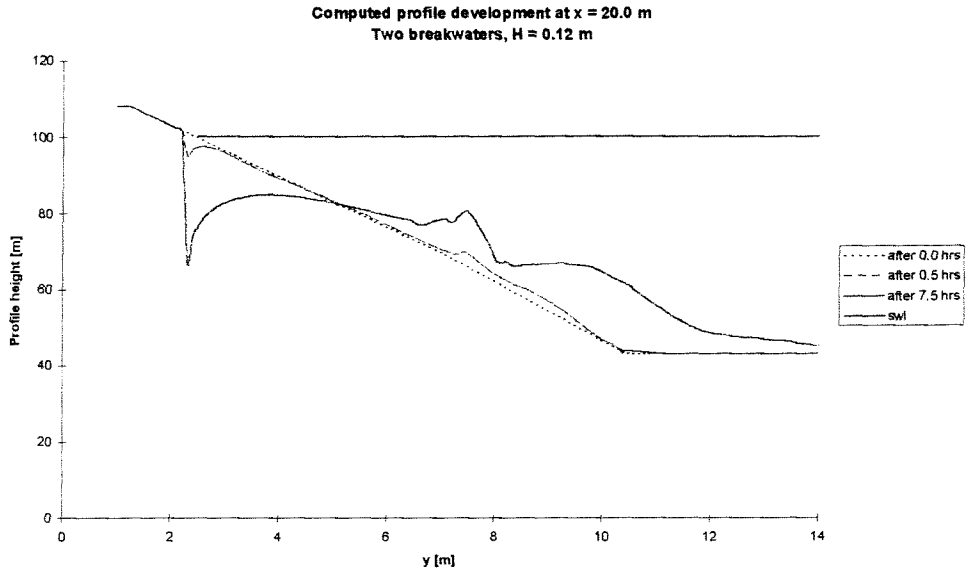

Figure 14.9: Computed profile development at x = 20.0 m

Correspondence of the computed profile development as shown in Figure 14.9 with the measured profile development (Figure 14.10) is better: erosion near the shoreline and accretion in or behind the gaps can be distinguished in both computation results and measurements. However, the magnitude of erosion and especially accretion (due to the large amount of erosion behind the breakwaters) in this cross-section differ much.

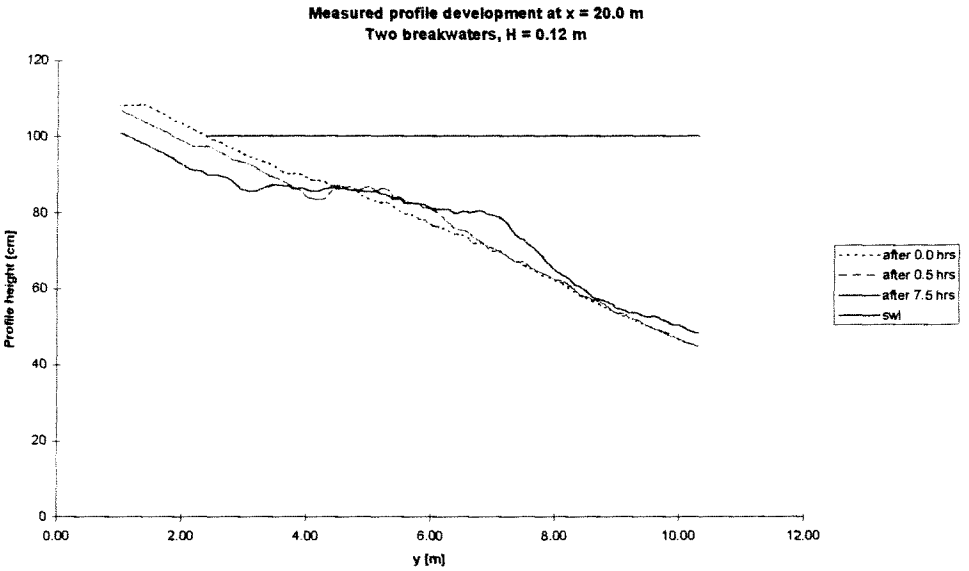

Figure 14.10: Measured profile development at x = 20.0 m

Compared to the simulation results in case of absence of breakwaters much more sediment has been transported shorewards after 7.5 hours as can be seen from the erosion/accretion pictures A13-9 and A14-9.

14.5 Conclusions and remarks

Flow velocities and (locally) sediment transport rates have become higher with the presence of the two breakwaters on the profile, resulting in a bigger sediment transport seawards. From this it could be concluded that the breakwaters in this configuration have a negative influence on morphological processes in the nearshore zone. This would be according to what was found by De Later (1996).
However this conclusion should be drawn very carefully when only looking at the simulation results. The model is not able to describe the (morphodynamic) processes near, at or beyond the shoreline which leads to inaccuracies. The most influencing inaccuracy of the computations near the shoreline is the disability of the model to bring sand from the beach beyond the shoreline into the model as stated before in Chapter 13. Besides, the dissipation over the breakwaters is likely to be too big and too much concentrated close behind the breakwaters which leads to strong wave forces and currents. This results in very high sediment transport rates, leading to large scour holes behind the breakwaters which were not developed during the experiments.

15 2DH-simulation of hydrodynamic and morphological processes in the wave basin with three breakwaters

15.1 Introduction

In this chapter the 2DH-simulation with three breakwaters is described. These simulation results are used for the determination of the morphological effects of the presence of breakwaters in this configuration. Therefore the results can be compared to the experimental results and to the results of the simulation without breakwaters (see Chapter 13) and with two breakwaters (see Chapter 14).
In section 15.2 the used process tree is given. This process tree shows the way the simulation is carried out. (For a general description of the process tree reference is made to Chapter 6).
In section 15.3 the input for Delft2D-MOR is described.
The results of the simulation are given in section 15.4. Finally, in section 15.5 a conclusion is given together with some general remarks.

15.2 Used process tree

The process tree of this simulation is the same as in the former computations (see Chapter 13).

15.3 Input description

The same input is used as described in Chapter 12. The bottom input has changed: three breakwaters have been added as profile elevations with a fixed bed.

15.4 Results

In this section the results of the simulation with two breakwaters are given.
For an explanation about the axis-system of the figures reference is made to Chapter 13.
Note: The figure numbering in Volume II is not continuous!

Wave field and dissipation
The wave and dissipation field have changed significantly during 7.5 hours of simulation due to morphological development of the bathymetry (see Figures A15-1 and A15-2). Accretion in the gaps has led to an increase in shoaling seaward of this accretion and dissipation due to wave breaking when waves reach their maximum height. This can be seen from Figure 15.1 and 15.2:

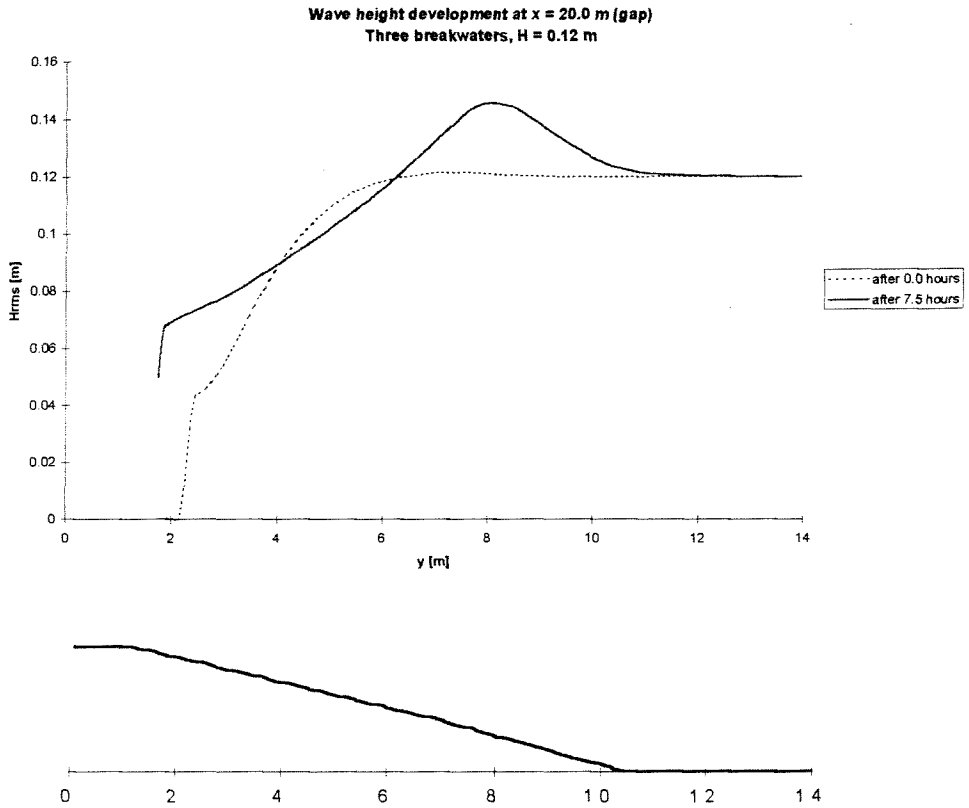

Figure 15.1: Wave height at x = 0.0 and 7.5 hours at x = 20.0 m

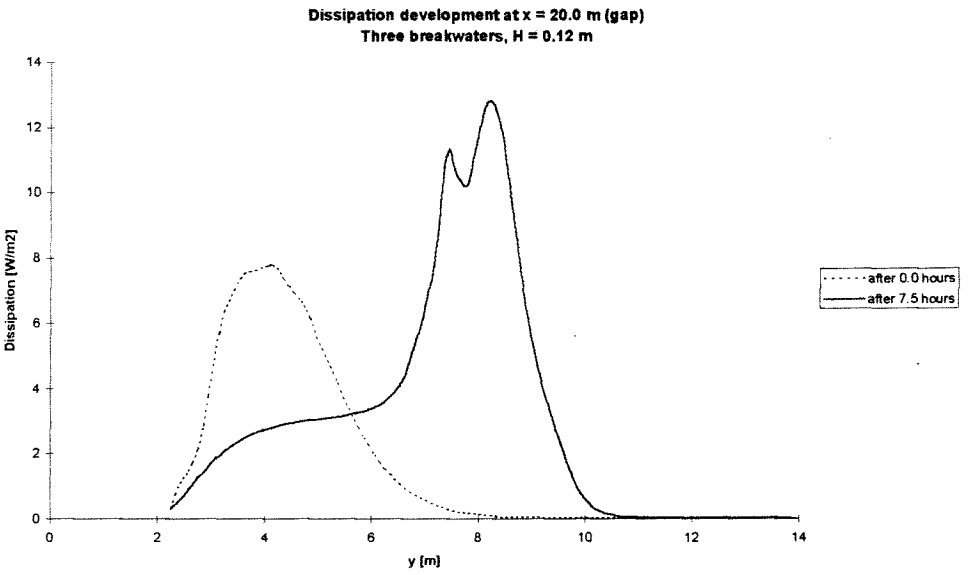

Figure 15.2: Dissipation after 0.0 and 7.5 hours at x = 20.0 m

The wave height and dissipation patterns in the gap after 7.5 hours show great resemblance with the wave height and dissipation patterns after 7.5 hours in case C3 (see Figures 14.1 and 14.2). This is according to what could be expected. In both cases (C3 and D3) shoals develop in and seawards of the gaps (at approximately y = 8.0 m), which have the same influence on wave height.

The wave height pattern in cross-sections over the breakwaters has not changed much (see Figure 15.3).

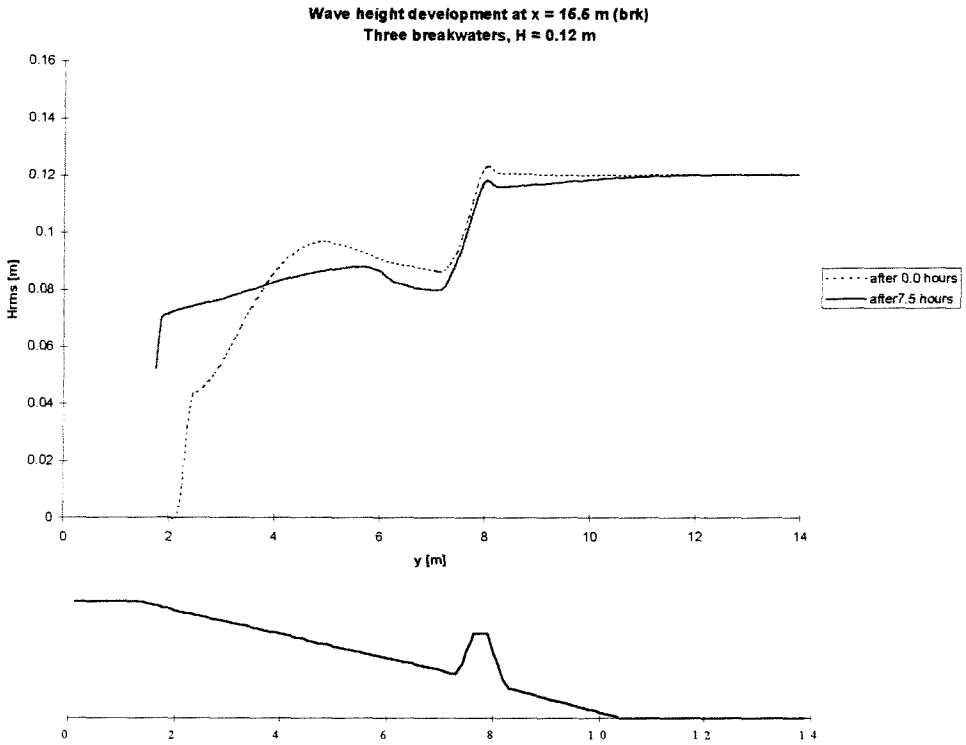

Figure 15.3: Wave height after 0.0 and 7.5 hours at x = 15.5 m

The large amount of erosion behind the breakwaters has not influenced wave height or dissipation much at these locations (see also Figure 15.4), because already in the initial state the water depth was large enough for the waves not to be influenced by the bottom.
Comparison of the wave height pattern in a cross-section over a breakwater with the wave height pattern in case A3 (see Figure 13.2) shows that the effect of the breakwaters is the reduction of wave height in the vicinity of the breakwaters. This effect is strong close behind the breakwaters, but due to shoaling of waves in case D3 and case C3 (see Figure 14.3) after breaking at the breakwaters this effect vanishes closer to the shoreline.

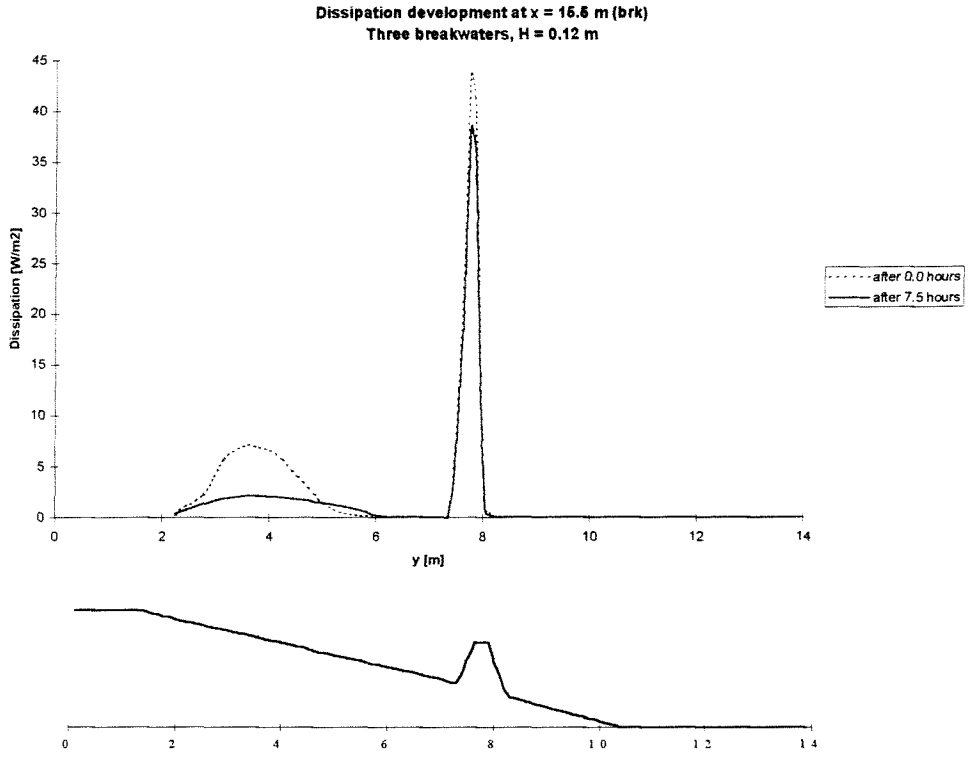

Figure 15.4: Dissipation after 0.0 and 7.5 hours at x = 15.5 m

Water level

In Figure A15-3 the contour map of the water level after 7.5 hours is shown.
Especially close to the shoreline the differences in wave set-up between the initial state and the situation after 7.5 hours is significant (see Figure 15.6 and 15.7). The dissipation peak there, caused by the breaking waves, has been moved more landward.
The water level at 0.0 and 7.5 hours in case D3 (Figures 15.6 and 15.7) show great resemblance with case C3 (see Figures 14.5 and 14.6). This is not surprising, because also the dissipation patterns in cross-sections through the gaps and over the breakwaters are almost equal. (Dissipation is one of the major causes for wave set-up).
Comparison of the water level figures of case C3 and D3 with case A3 (Figure 13.4) shows that there are quite some differences. In cases C3 and D3 the water level in cross-sections through the gaps after 7.5 hours rises at the location of the shoal (approximately y = 8.0 m) where dissipation is present. In case A3 dissipation is not or hardly present at that location and therefore the rise of the water level is still minimal.
In cross-sections over the breakwaters in cases C3 and D3 the difference in water levels with case A3 is even bigger. The large amount of dissipation at the breakwaters induces a rather abrupt wave set-up, which is of course not present in case A3.
Closer to the shoreline the water levels are approximately equal in all cases.

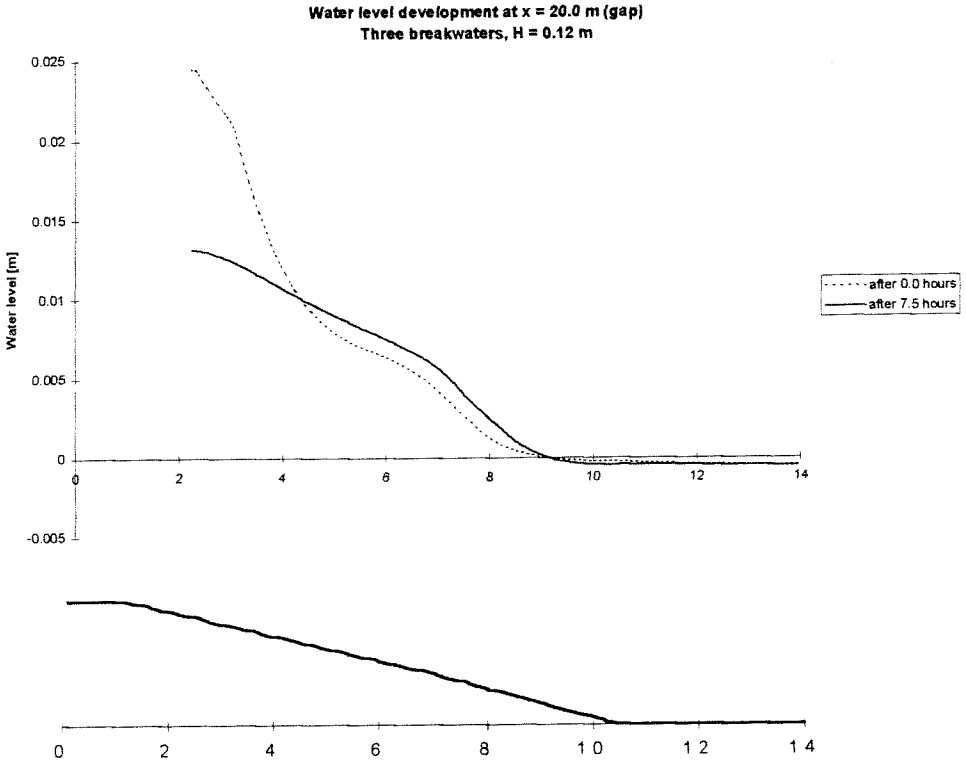

Figure 15.5: Water level after 0.0 and 7.5 hours at x = 20.0 m

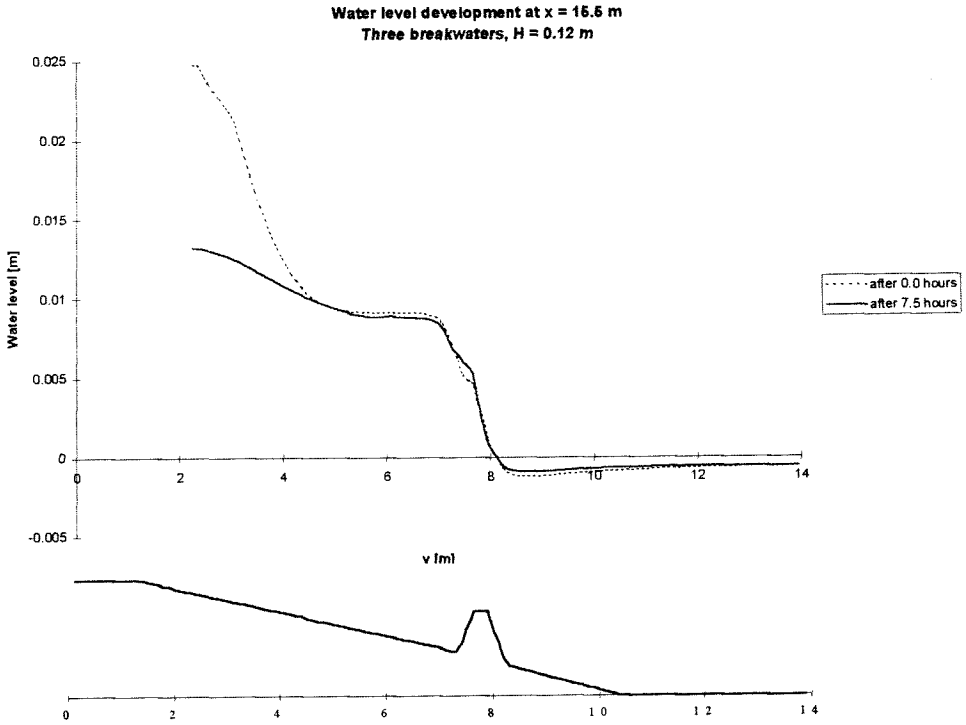

Figure 15.6: Water level after 0.0 and 7.5 hours at x = 15.5 m

Flow field
In general the flow field (Figure A15-4) has not been changed much compared to the initial flow field. In the gaps flow velocities are somewhat smaller. Just behind the breakwaters near the breakwater ends flow velocities are smaller due to a small decrease in wave forcing.

Compared to case A3 flow velocities are much higher (which also holds for the return flow velocities) due to the big wave forces because of dissipation behind the breakwaters. The water level gradient, caused by wave set-up differences, is another driving force for currents.

Compared to case C3 the longshore flow velocities are smaller when looking at the region x = 100 m to x = 110 m. Obviously in case C3 the 6 m-gap attracts a bigger part of the flow behind the breakwater than the 3 m-gap inbetween the breakwaters.
In case D3 all gaps are approximately 3 m wide and all breakwaters have the same lengths leading to an (approximately) equal distribution of flow through the gaps.

Return flow field
The return flow field (Figure A15-5) seems not to be influenced by morphological changes very much. Only near the shoreline flow velocities are somewhat smaller.

Comparison with case A3 (see Figure A13-5) and D3 (see Figure A14-5) shows the same phenomena as mentioned above in the discussion of the flow field.

Sediment transport
The sediment transport field (Figure A15-6) has hardly been influenced by morphological changes.
Locally, sediment transport rates are much higher compared to case A3 (see Figure A13-6) which leads to more rigorous profile developments.
From comparison of case D3 with case C3 (see Figure A14-6) it can be seen that in the region x = 100 m to x = 110 m sediment transport rates (especially the longshore rates) are much higher in case C3 close to the 12 m-breakwater end. This difference in magnitude of sediment transport rates is mainly caused by the difference in the return flow field.
It can be expected that the scour hole in the vicinity of the 12 m-breakwater in case C3 is larger than the scour hole in the vicinity of the 3 m-breakwater in case D3.

Morphology
Figure A15-7 shows the initial bathymetry, Figure A15-8 the bathymetry after 0.5 hours and Figure A15-9 the bathymetry after 7.5 hours. Already after 0.5 hours some trends are recognizable: an eroding bottom close behind the breakwaters and the transport of sand towards the gaps. This is according to the initial state of the sediment transport pattern in which a relatively large sediment transport rate is directed from behind the breakwaters towards the beach and relatively large rates transport sand from the area behind the breakwaters seaward.

The morphological development further in time shows the continuation of the trends. Close to the beach heavy erosion occurs. This can be expected because of the eroding action of breaking waves close to the shoreline, but there is another cause too. As stated before the sand from the beach that is located above the waterline is not brought into the model. In practice this sand would be part of the morphological process and probably would slow down the erosion process near the shoreline. In Figure A15-10 the overview of (computed) erosion and accretion is given, while in Figure A15-11 the measured erosion/accretion picture is shown (erosion and accretion in cm). Behind the breakwaters deep holes (until 25 cm erosion) have been formed while seaward of the gaps large shoals (until 25 cm accretion) have been developed. Inbetween the scour holes behind the breakwaters and the eroded area near the shoarline a bar-like accretion has been developed. In this area accretion occurs. From Figure A15-6 (sediment transport field) it can be seen that hardly any sediment transport is present there. Sand is transported from behind the breakwaters and from the area closer to the beach into this area which explains the accretion (see Figure 15.7).

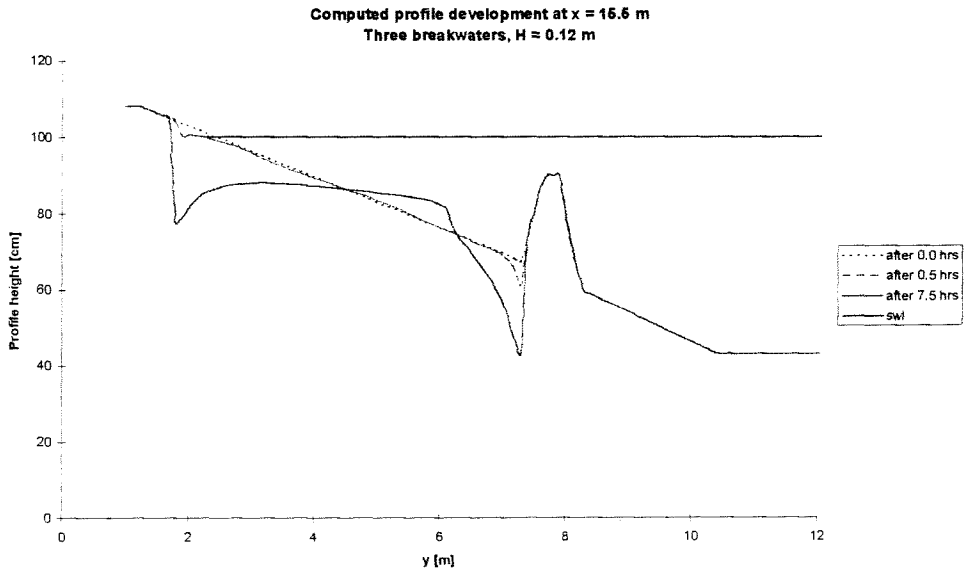

Figure 15.7: Computed profile development at x = 15.5 m

From Figure 15.7 it can also be seen that the sand balance is negative, which implies longshore transport of sediment (which is redirected through the gaps seawards).

The difference with the measured profile development is big. This can be seen from Figure 15.8 clearly. This figure shows hardly any profile changes except for erosion near the shoreline. The sand balance is negative though, which means that also during the experiments sand was transported by longshore currents.

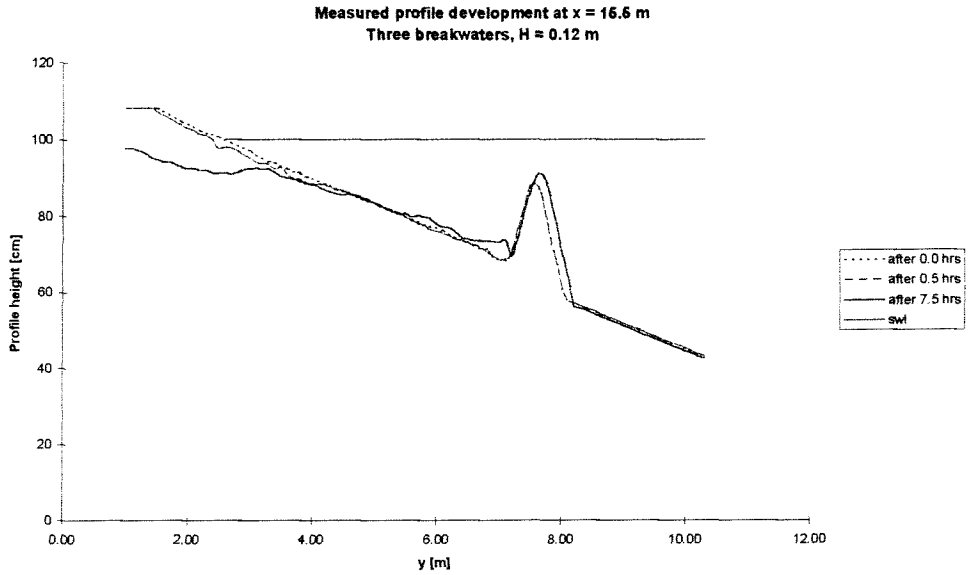

Figure 15.8: Measured profile development at x = 15.5 m

In the computations sand has been transported through the gaps indeed, which can clearly be seen from Figure 15.9. The sand balance is positive which implies transport of sediment towards the gap.

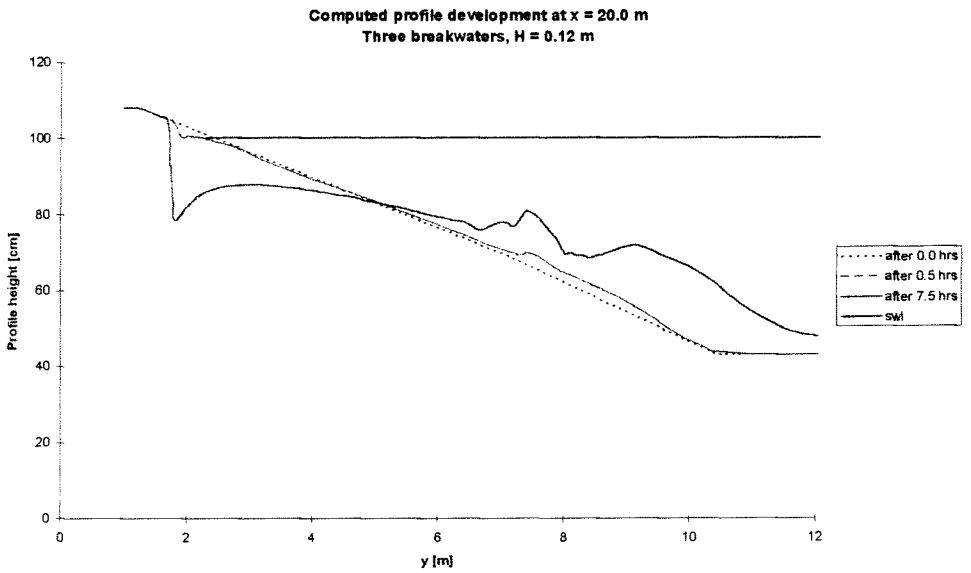

Figure 15.9: Computed profile development at x = 20.0 m

This is also the case in the experiments, as can be seen from Figure 15.10.

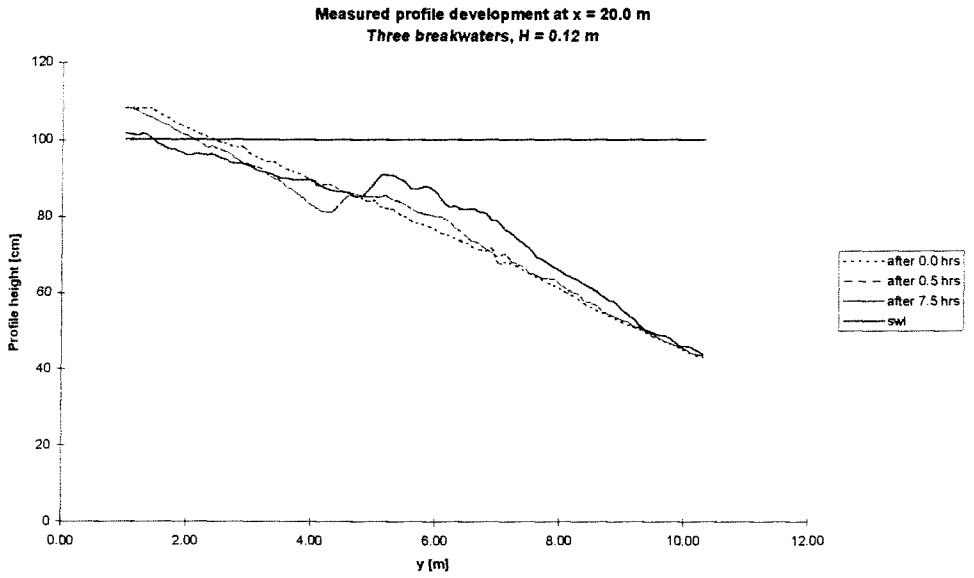

Figure 15.10: Measured profile development at x = 20.0 m

In the experiments the shoal developed more shoreward than in case of the simulation probably due to the computation of higher sediment transport rates in the gap than was the case in the experiment.
In the simulation the volume of sand that is transported seawards trough the gap is bigger than in the experiment which is caused by the larger amount of erosion in the profile behind the breakwaters in the simulation.

Compared with the computed profile development in case of absence of breakwaters (see Chapter 13) the presence of three breakwaters in this configuration has a negative effect: more sediment has been moved shorewards which results in bigger erosion areas at the landside of the breakwaters.

Compared to case C3 the computed profile development shows great resemblance as can be seen from Figures A14-8 and A15-9 and Figures A14-9 and A15-10. The major differences are the larger amount of erosion behind the 12 m-breakwater and the larger shoal in and seawards of the 6 m-gap in case C3. This is what could be expected from the sediment transport figures of cases C3 and D3.

15.5 Conclusions and remarks

When looking at the results of this simulation it can be concluded that the model computes sediment transport from behind the breakwaters through the gaps seawards, which was also found during the experiments. However the computed profile development shows big differences with the measured profile development, and therefore it can be concluded that the effects of three breakwaters on beach profile development in a wave basin are difficult to be simulated yet. This is mainly due to the fact that sand from the beach is not brought into the model and

the computation of very high sediment transport rates behind the breakwaters, caused by the very concentrated amount of dissipation over the breakwater (as mentioned before in Chapter 13 and 14).
From the experiments it was concluded that this configuration of breakwaters has a negative effect on morphology. This negative effect is obviously when intercomparing simulation results of A3 and D3, but since the differences between measurements and simulation are very big it is difficult to draw the same conclusion.
Compared to case C3 it seems that the configuration of breakwaters in case D3 has less negative effects. Probably the combination of a relatively long breakwater and a relatively wide gap in case C3 is not a good combination.

16 General discussion of the simulation results

The simulation of case A3 (see Chapter 13) has led to reasonable results. Flow velocities and sediment transport rates are small, as was the case in the experiments. The computed morphological changes show good resemblance with measurements. Only near the shoreline differences occur as a result of model shortcomings.

The simulations of case C3 and D3 (Chapters 14 and 15) show the same phenomena.
In the basin flow circulation patterns are present due to water level gradients caused by wave set-up differences. Flow velocities and sediment transport rates are locally much higher than in case A3. This is in good agreement with measurements where also bigger velocities were measured compared to case A3.
Differences in morphological development are big though. Large erosion areas are present close behind the breakwaters and, again, large erosion areas near the shoreline. These results are not in good agreement with measurements.

A lot of probable causes of these differences can be given. These causes are related to wave field and dissipation, flow field, sediment transport and morphology.
Causes of differences due to inaccuracies in numerical modelling are not treated here.

Wave field and dissipation
The generation of the wave field was done by the determination of the significant wave height H_s, wave period T, wave propagation direction θ_0, directional spreading of wave energy, the breaker indexes γ_s and γ_d and the dissipation coefficient α.

The first problem lies in the fact that (most of) these parameters are defined for irregular waves. The mean regular wave height H_m that was generated during the experiments has to be described with the irregular wave height parameter H_s. This has been done by equating H_m with H_{rms} ($= H_s / \sqrt{2}$), which is a rather rough estimate (see section 11.2) and likely to be inaccurate.
Directional spreading of wave energy is only present in case of irregular waves, but in the simulations this parameter is used for the modelling of diffraction due to the breakwaters because HISWA does not take diffraction into account (see section 11.5). In areas where wave height variations are large within a horizontal scale of a few wave lengths (which is more or less the case behind the breakwaters) the generated wave field by HISWA will not be accurate immediately behind obstacles. Introduction of directional spreading of wave energy is needed to compensate for this inaccuracy a little. Wave energy is spreaded over directions within a certain domain such that wave energy is able to enter the shadow zones of the breakwaters. In this approach of course diffraction is only modelled roughly as can be seen from a comparison between a computer model that simulates diffraction (CREON) and HISWA (see section 11.5 and Appendices).

Other problems are caused by the execution of the measurements. Wave measurements on a fixed bed are not available and therefore the initial wave field is not known. The wave measurements were carried out on a movable bed at different points of time in different cross-sections. In the five or six measured cross-sections only at four points measurements were carried out. (The reason for this is that in these experiments the focus was on morphology and not on wave heights. In some other experiments carried out in the framework of the Dynamics of Beaches project the focus was on other aspects (e.g. wave heights, water levels). From these experiments sufficient wave data could be obtained, but these were not available at the moment of writing this thesis).
The wave data obtained in this way are not useful for the generation of an overall picture of the wave field at one point of time. The method of interpolating measured bottom profiles at different points of time and relating the wave data to these interpolated bottom profiles (as described in section 15.6) is highly inaccurate. Moreover, it does not solve the problem of the availablity of wave data at only four points per cross-section. The generation in HISWA of a reasonably corresponding wave field is therefore impossible.

Wave measurements can be influenced by the presence of long waves in the wave basin. These long waves cause the water level to fluctuate around its mean level with a bigger period. Wave height measurement equipment also measures this fluctuation that is added to the wave heights. In order to have reliable wave data (wave heights) this fluctuation should be recognized and removed from the wave data.
Long waves are also responsible for wave set-up which is superimposed on the wave set-up caused by the smaller waves. This wave set-up influences the wave heights, because of its effect on water depth.
No investigation has been carried out to the presence of these long waves.

The breaker index γ_s and dissipation coefficient α have been determined making use of the available wave data (see section 11.6). Variation of these parameters led to different wave height patterns in cross-shore direction. Values of the parameters that generated a wave height pattern that fitted the wave data best were taken as wave input ($\gamma_s = 2.0$ and $\alpha = 8.0$). The thus obtained parameters are not physically correct. The correctness of these values is questionable. Especially the high value of α causes much (probably too much) dissipation when breaking occurs (at the breakwaters and in the breaker zone).

From the simulation results it can be seen that the computed dissipation is very much concentrated just behind the breakwaters. This leads to relative large wave forces behind the breakwaters inducing relatively high flow velocities and sediment transport rates that cause the formation of large erosion holes behind the breakwaters.
In practice (and in the experiments) the breakwater induced wave dissipation has probably been more spread over a distance behind the breakwaters. Moreover, the inertia of the waves will cause them to break at a certain distance from the breakwaters. For these reasons in practice the strong eroding wave and current action close behind the breakwaters is not present or at least weaker.

The wave breaking of irregular waves and regular waves differ. Irregular waves (modelled in HISWA) do not have a breaker line where practically all waves break. Waves with smaller heights break closer to the shoreline than higher waves.
Regular waves (generated in the experiments) have got, according to the definition, equal wave heights given an equal water depth. In theory these waves all break at the same location.

Flow field

The magnitude of the initial flow field in the simulations was obtained by variation of the horizontal eddy viscosity ν_h. Another parameter that influences the magnitude of the flow field is the roughness length k_s in White-Colebrook's formulation for bed-level shear stress. This roughness length was chosen 0.01 m.
The obtained flow velocities were compared to flow data, only available at five or six cross-sections at four points per cross-section. If the computed flow velocities matched the measured velocities reasonably, the horizontal eddy viscosity was given the value that was used to generate the flow field.
This calibration method of the FLOW-model is probably inaccurate, because of the few flow data available.

Sediment transport

The formula used for the computation of sediment transport is Bijker's formula. Usually this formula gives fair results, but as it is based upon a couple of assumptions it will only give approximations of the real sediment transport rates. In Van der Velden (1995) a list of comments on the Bijker formula is given. One of these comments is about the factor B (in these simulations being 5 in the breaker zone and 2 outside the breaker zone). This coefficient has received much discussion. This disagreement reflects the possible inaccuracies of the sand transport computations.
Another inaccuracy can be caused by the assumed value of the bottom roughness. Bijker suggested using a roughness equal to half the height of the ripples on the bottom. With ripples of 0.02 m this yields a bottom roughness of 0.01 m. This value has been chosen as input in the Bijker formula, not knowing exactly the height of the ripples that were present during the experiments.

Morphology

The morphological changes are based upon the computed sediment transports. These sediment transports are determined from the given flow field. The flow field is updated after 30 times of sediment transport and bottom change computations, so that the flow field is able to adapt to the changed bathymetry. This computation method will be more accurate when the number of sediment transport and bottom computations before the flow field is updated decreases. However this will lead to a longer computation time.

The computed morphology in the simulation is always inaccurate because of the shortcoming of the model to include the beach beyond the shoreline in the computations. This is due to the fixed land-sea boundary. A rise of the water level (because of wave set-up) does not yield the movement of this boundary landwards. At points where there is a waterlevel of 0 m (more approximate: 0.01 m or less) no waves, flow or sediment transport is computed, which means that sand from the beach beyond these points (shore line) can never be transported and brought into the computations.

17 Sensitivity analysis

17.1 Introduction

From the simulation results it was concluded that the model is not yet able to predict very well the morphological processes in the wave basin with the presence of submerged breakwaters. Because only a limited amount of measurements on the wave field in the experiments was available to generate a wave and flow field in the model, it is possible that the chosen values of some wave and flow parameters are not optimal.
In this chapter the influence of parameters and other modelling apects on the simulation results are checked or discussed. In the sections 17.2, 17.3 and 17.4 the influence of the shallow water breaking index γ_s and the dissipation coefficient α is determined. Next, in section 17.4 the length of the breakwater crest is enlarged in order to create a bigger spread out of dissipation over the breakwater.
Finally, in section 17.5 conclusions are drawn.

17.2 Shallow water breaking index γ_s

17.2.1 Introduction

For a definition of this parameter refernece is made to section 7.5.
In the simulations as described in Chapters 12 to 15 the value of this parameter had been given the value 2 (in combination with $\alpha = 8$ it seemed to describe the wave field reasonably well). Here different values of γ_s are chosen while $\alpha = 8$. Computations are carried out with $\gamma_s = 1$, 3 and 4 respectively. (Obviously the index loses its physical meaning in the case of high values). Only the influence of these changes on the initial wave field, flow field and sediment transports is investigated. Therefore initial computations are sufficient. All computations are carried out with the initial bottom profile of experiment D3 (three breakwaters)..
The input for the model is the same as defined in section 12.4.

17.2.2 Results

Wave field and dissipation
As can be seen from Figure 17.1 a higher value of γ_s results in a smaller wave height decay over the breakwaters. The reason for this is that the maximum wave height at a given water depth increases with increasing values of γ_s according to the definition of this parameter.
With $\gamma_s = 1$ (and $\alpha = 8$) the wave height pattern is by no means near the measured wave height pattern. This is due to the combination of a low value of γ_s, yielding a relative small maximum wave height at a certain depth (which forces the waves to dissipate relatively more), and the

high value of α, responsible for the large amount of wave dissipation.
The wave height patterns with $\gamma_s = 3$ or 4 do not differ much from the curve with $\gamma_s = 2$.
Dissipation over the breakwater becomes less with increasing γ_s (see Figure 17.2), because of the increasing maximum wave height at that location.

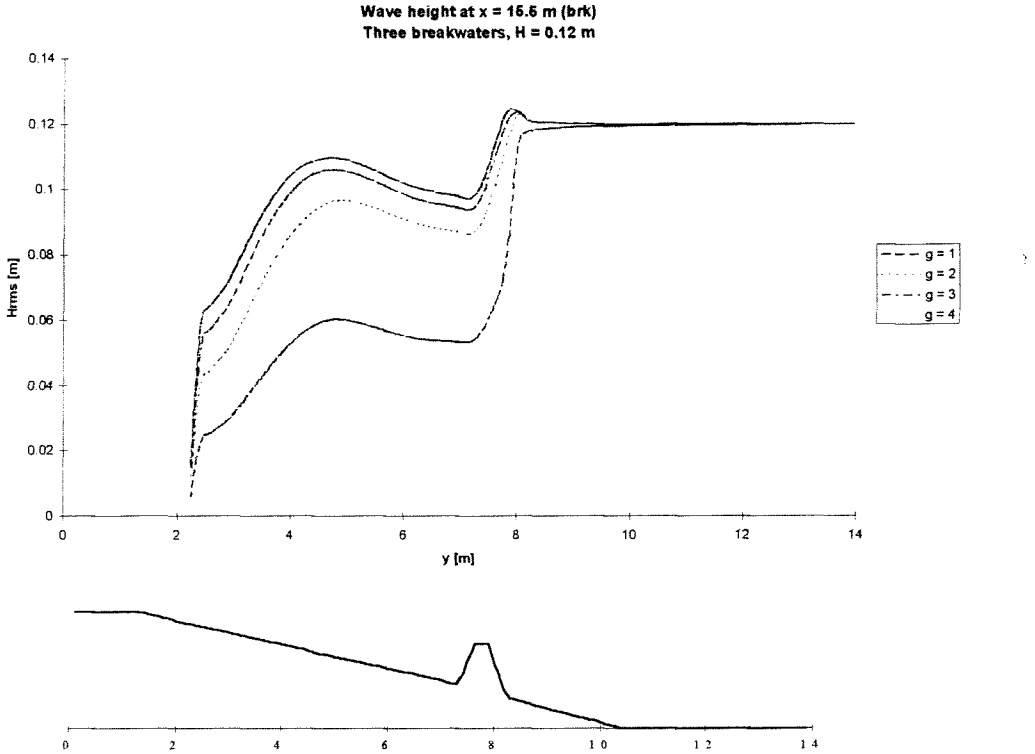

Figure 17.1: Wave height at x = 15.5 m (breakwater)

From Figure 17.2 it can also be seen that an increase of dissipation over the breakwater is compensated by a decrease of dissipation near the shoreline (the total dissipation must be constant):

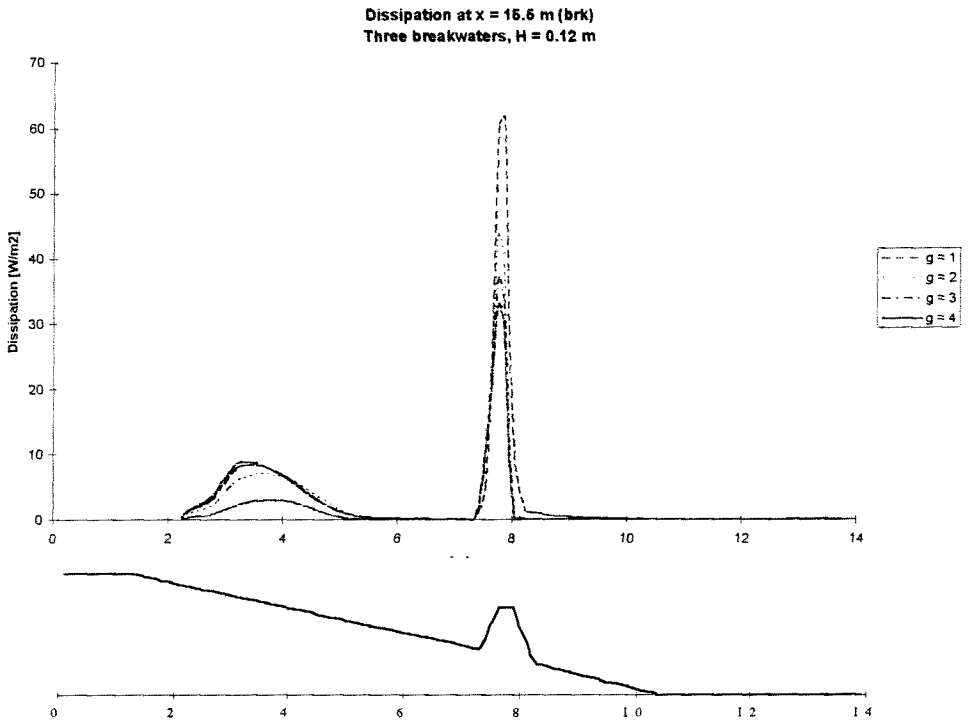

Figure 17.2: Dissipation at x = 15.5 m

Figure 17.3 shows the more concentrated dissipation pattern with increasing γ_s.
A higher value of γ_s means a bigger maximum wave height at a certain water depth, causing the shift of the 'breaker line' shorewards:

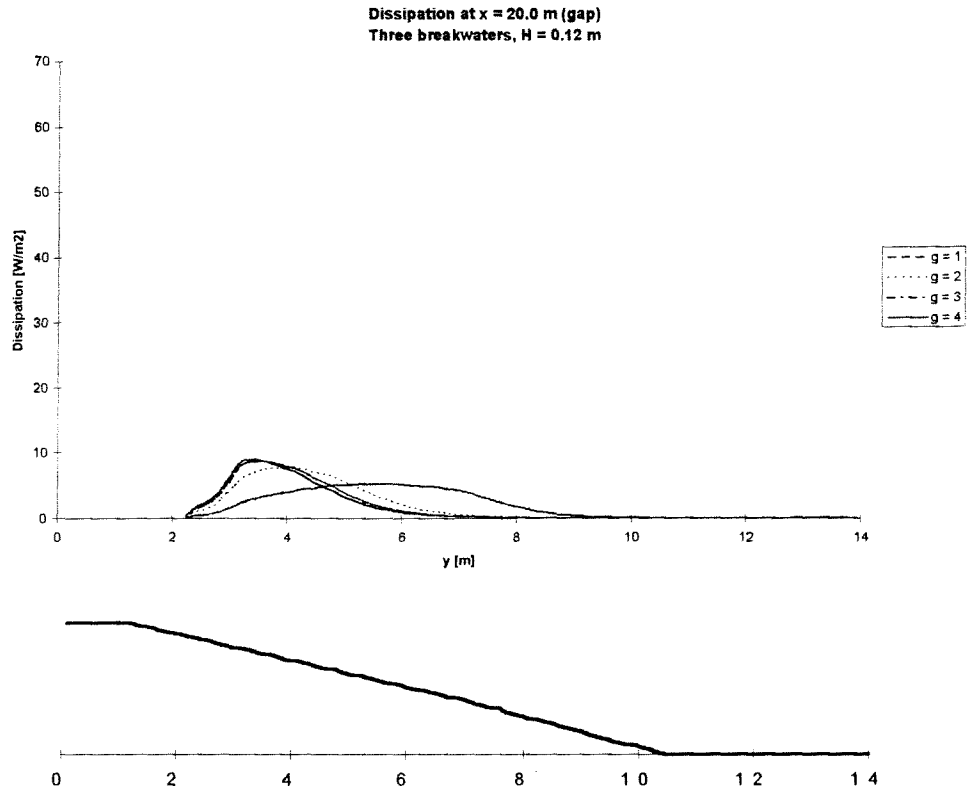

Figure 17.3: Dissipation at x = 20.0 m (gap)

Flow, return flow and sediment transport field

Only the results in case of γ_s = 1 and 4 are given. These are plotted in Figures A17-1 to A17-6. The average flow velocities increase slightly with decreasing γ_s due to the increase of dissipation and wave forcing behind the breakwater. Differences in the return flow fields are bigger. Behind the breakwaters the large velocities in case of γ_s = 1 disappear in case of γ_s = 4, while near the shoreline return flow velocities increase significantly.
From Figures A17-5 and A17-6 it can be seen that the significant increase of return flow velocities near the shoreline results in clearly larger sediment transport rates there.
Near the breakwaters and the gaps sediment transport rates do not seem to be influenced much by larger or smaller return flow velocities there.

From these results it can be concluded that with variation of γ_s the morphological changes in time are most influenced near the shoreline where an increase of γ_s will lead to an increase of erosion in that area.

17.3 Dissipation coefficient α

17.3.1 Introduction

For the definition of this parameter reference is made to section 7.1.6.
In the simulations as described in chapter 12 to 15 the value of this parameter had been given the value 8 (in combination with $\gamma_s = 2$). In practice this value is very high and has no physical significance. The high value of α is obviously a main reason for the high amount of dissipation which occurs over the breakwaters, so decreasing this value will decrease the amount of dissipation over the breakwaters, decrease the wave force and flow field and possibly reduce the amount of erosion behind the breakwaters).
Computations are carried out with α = 1, 2, 3 and 10 respectively. Again only the influence of these changes on initial wave heights, flow field and sediment transports is investigated. Therefore initial computations are sufficient.

17.3.2 Results

The relation of α with wave height and dissipation is clear from Figures 17.4 and 17.5. An increase of α means an increase of dissipation and a decrease of wave height. It can be seen that a value of 8 or 10 does not change the dissipation pattern much anymore (the dissipation curves are almost identical). However, the difference in wave heights and dissipation between low and high values of α is big.

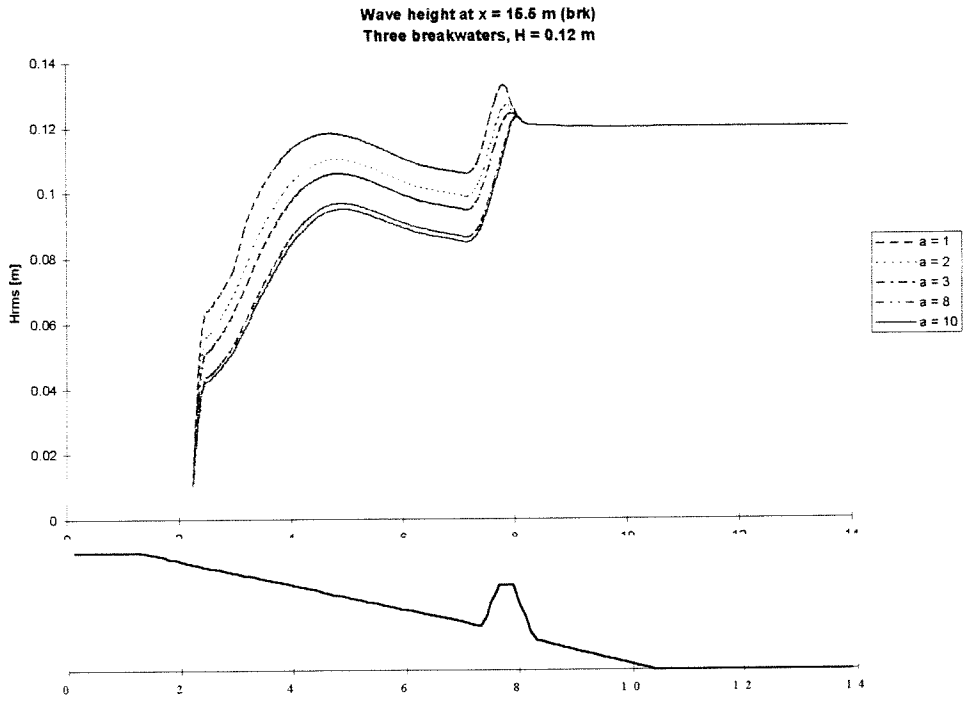

Figure 17.4: Wave height at x = 15.5 m (breakwater)

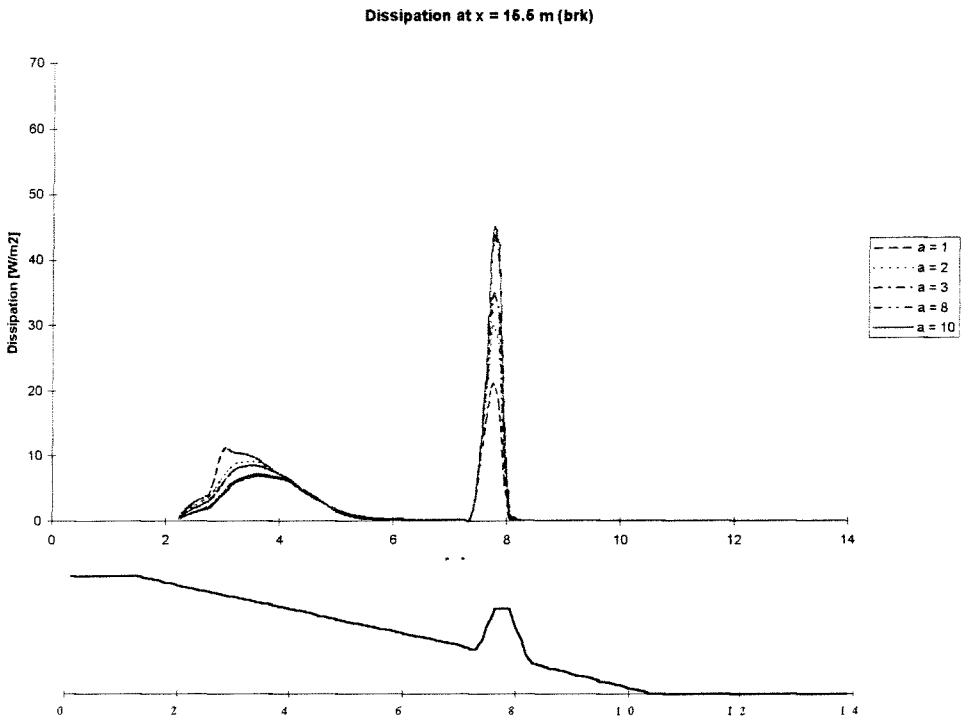

Figure 17.5: Dissipation at x = 15.5 m

Flow, return flow and sediment transport field

Only the results of computations with α = 1 and 10 are given in Figures A17-7 to A17-12. The flow fields (Figures A17-7 and A17-8) differ in magnitude. Flow velocities in case of α = 10 are significantly higher, apparently caused by the larger amount of dissipation over the breakwaters.

The sediment transport field also changes significantly with varying α. With α = 10 the sediment transport rates near the breakwaters and the gaps increase compared to the case with α = 1, while sediment transport rates near the shoreline significantly decreased

It seems that variation of α influences the morphological changes in time much. Increase of α will yield an increase of erosion behind the breakwaters and a decrease of erosion near the shoreline.

17.4 Breakwater crest enlargement

17.4.1 Introduction

The modelling of the breakwaters with wider crests can have advantages. At wider crest waves will dissipate over a longer distance. In that case probably a smaller value of α can be chosen to induce the same amount of dissipation as in the case of $\alpha = 8$. This has the advantage of simulating the processes in the wave basin with a more physically correct value of α.
In this computation a value of $\alpha = 2$ is chosen. The value of γ_s remains 2.
The same input is used as in former initial computations. A breakwater crest of 0.30 m is applied, 10 cm wider than in other computations.

17.4.2 Results

In Figure 17.6 the dissipation curve in case of a wider crest and $\alpha = 2$ is given. Also the initial dissipation curve with $\alpha = 8$ is shown for comparison.

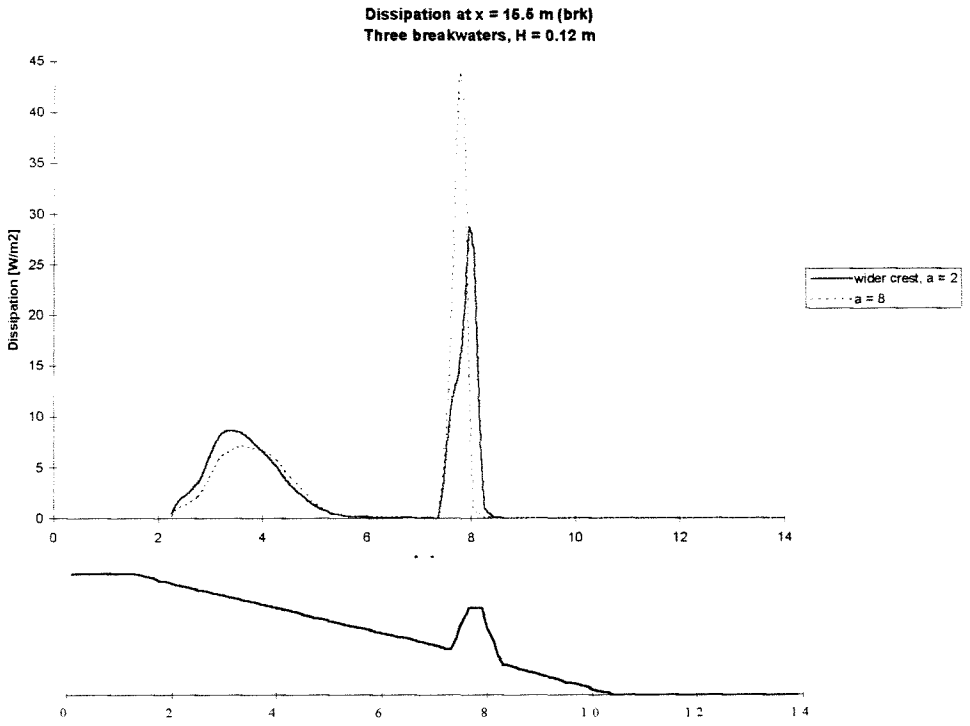

Figure 17.6: Dissipation at x = 15.5 m

From this figure it can be seen that dissipation is present over a longer distance. The lower peak is caused by the lower value of α. The total dissipation over the breakwater is still smaller than in former computations, but it is clear that with a wider crest (or a somewhat bigger value

of α) it must be possible to induce the same amount of dissipation as in former computations. From this it is concluded that the application of a wider breakwater crest can be of interest to be able to simulate with smaller values of α.

18 Conclusions and recommendations

From the results of the simulations as described in this report and the brief analysis of some parameters a number of conclusions can be drawn.
Delft2D-MOR is able to describe some hydrodynamic processes reasonably well. The flow circulation pattern caused by water level gradients (and side-walls) shows agreement with measurements: the flow behind the breakwaters bends into the direction of the gaps. The strong concentrated currents through the gaps induce flow circulation seaward of the breakwater zone.
In areas where wave dissipation is present currents are induced by wave forcing. This is also simulated by the model.
The return flow (Eulerian flow) is, as can be expected, mainly directed towards the sea, especially near the shoreline. Because this return flow is responsible for sediment transport, the sediment transport pattern should follow the return flow pattern, which is the case.

Simulation results in general show some big differences with what can be expected, and with measurements. The computed strong sediment transport rates close behind the breakwaters are incorrect. This is partly due to the concentrated wave dissipation over the breakwaters resulting in wave forces that induce strong currents. Another major cause for this can be the relatively low resolution of the computational grid. FLOW carries out interpolation of velocities computed at velocity-points such that these interpolated velocities are known at water level points. If a water level point is located close behind the breakwater, then the relatively high velocity computed at the breakwater (slope or crest), because of the small water depth there, influences the relatively low velocity further behind the breakwater where the water depth is bigger. This results in unrealistic high velocities close behind the breakwater, which causes unrealistic high sediment transport rates.
A computation with a higher resolution of the computational grid will probably give better results.

Problems occur with the application of HISWA in case of regular waves and submerged breakwaters. Regular waves are a very different phenomenon from irregular waves, and it is difficult (or impossible) to find suitable values for irregular wave parameters in order to describe the regular wave propagation and breaking. Moreover HISWA does not take into account diffraction. In case of big submergence of the breakwater crests this is not a problem, but with decreasing submergence the influence of diffraction on the wave field behind the breakwaters grows and so the need to model diffraction grows. Application of a directional spreading of wave energy in HISWA to approximate the effects of diffraction will always lead to deviations.

In HISWA it is difficult to model submerged breakwaters. Application of the standard HISWA obstacle function, with which it is possible to describe the submerged breakwater in terms of transmission, leads to inaccuracies in the flow field. Dissipated wave energy is only taken out

of the system and is not used for inducement of wave forces and currents. Modelling the breakwaters as profile elevations with a fixed bed is an option to avoid this problem, but another problem rises: the transmission relation cannot be used.
Adaption of the obstacle function in HISWA, such that it computes wave forces from dissipation over the obstacle, would be useful.

HISWA does not compute a very realistic wave height pattern over a submerged breakwater. Immediately behind the breakwater wave energy dissipation is set to zero and waves start shoaling again. In practice the behaviour of waves will be different. Waves will show the inertia phenomenon: waves break at a certain distance from the breakwater. Besides, probably these broken waves will not develop into 'normal' waves again, but propagate like bores.
In HISWA this wave behaviour should be modelled better in order to obtain realistic wave height patterns over submerged obstacles. Besides, it would be useful if HISWA, like CREON, could also model regular waves.

The available wave and flow data from the experiments were not sufficient to create a picture of the wave and flow fields that were present during the experiments. Therefore the determination of values of parameters that influence wave and flow field (γ_s, α, ν_h) was very difficult and probably inaccurate. It is possible that the choice of other values of these parameters will give better results.
The use of sufficient wave and flow data can make the determination of these values of parameters more accurate.

The simulation results show that the disability of the model to include the sediment from the beach into the computations causes an unrealistic erosion pattern near the shoreline. This is due to the fact that originally dry points in FLOW remain dry throughout the simulation. Solution of this problem will surely give better results.
If the model is able to check gradients in the bottom profile, it would be possible to adjust the bottom profile at locations where irrealistic large gradients occur. This would avoid the building of unrealistic 'walls' in the bottom profile near the shoreline, as was the case in the simulations.

From experiments it was found that the presence of the breakwaters have negative effects on profile development. This can also be concluded from simulation results.
This conclusion would be more worthy if deviations of simulation results from experimental results were not so big.

After simulations with an enhanced version of Delft2D-MOR and with sufficient measurement data it may be possible to judge the effect of different configurations of submerged breakwaters on the beach better.

Acknowledgements

I would like to express my thanks to dr. ir. J.A. Roelvink who guided me into the world of modelling and assisted me in using the computer model Delft2D-MOR.
My thanks go to all who have contributed to this study, especially dr. ir. J. van de Graaff and ir. S. van der Biezen for their supervision and assistance.

I would like to mention Lucia Torrini with whom I had useful co-operation and discussions. Thank you for your support!

Especially I would like to thank my family and Simone for their support throughout my whole study and in particular during graduation.

References

Battjes, J.A., 1992	Collegehandleiding b76 Korte Golven; Delft University of Technology, Department of Civil Engineering
Battjes, J.A. and Janssen, J.P.F.M., 1979	Energy loss and set-up due to breaking of random waves In: Proc. 16th International Conference on Coastal Engineering, 1978, Hamburg
Booij, N. and Holthuijsen, L.H., 1992	User Manual HISWA; Delft University of Technology, Department of Civil Engineering
Chiaia, L., L. Damiani, A. Petrillo, 1992	Evolution of a beach with and without a submerged breakwater: experimental investigation; Proc. 23rd International Conference on Coastal Engineering, ASCE, pp. 1959-1971
Dean R.G. et al, 1995	Full scale monitoring study of a submerged breakwater; Dynamics of Beaches Project
Delft Hydraulics, 1996	Manual Delft 3D-flow; Delft Hydraulics
Delft Hydraulics, 1996	An introduction to Delft 2D-MOR; Delft Hydraulics
Gao, Q. and Radder A.C., 1997	User Manual CREON
Later, J. de, 1996	Effect of submerged breakwaters on a beach profile exposed to regular waves in a wave basin; Delft University of Technology, Department of Civil Engineering
Prinos, P., A.S. Arcilla, N. Christensen, J. van de Graaff, M. Hogedal, A. Lewis, B. O'Connor, F. Riveroand J. De Rouck, 1995	The Dynamics of Beaches Project; Proc. Coastal Dynamics, ASCE, pp. 571-582
Sawaragi, T., 1992?	Detached breakwaters
Seelig, W.N., 1979	Effect of breakwaters on waves: laboratory test of wave transmission by overtopping; Proc. of the Conference on coastal structures

References (continued)

Stelling, G.S., 1984 — On the construction of computational methods for shallow water flow problems; Rijkswaterstaat communications, No. 35

Stive, M.J.F., 1988 — Cross-shore Flow in Waves Breaking on a Beach; Delft Hydraulics Communication No. 395, 1988

Svendsen, I.A., 1984 — Mass flux and undertow in the surf zone; Coastal Engineering, Vol. 8, pp. 303-329

Velden, E.T.J.M. van der, 1994 — Coastal Engineering (lecture notes), Volume II; Delft University of Technology, Department of Civil Engineering

Appendix A1

General information about wave conditions and basin lay-out in experiment A3

Experiment A3

Initial waterdepth:	0.57 m
Initial wave height:	0.12 m
Period:	1.55 s
Angle of incidence of waves:	0

Lay-out:

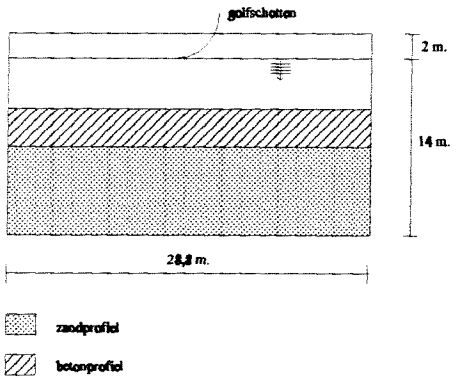

Slope sand profile:	1:15
Slope concrete profile:	1:13
Sand:	D_{50} = 75 μm

Appendix A2

General information about wave conditions and basin lay-out in experiment C3

Experiment C3

Initial waterdepth:	0.57 m
Initial wave height:	0.12 m
Period:	1.55 s
Angle of incidence of waves:	0

Lay-out:

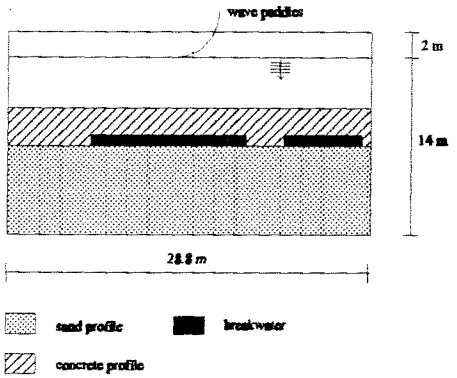

Slope sand profile:	1:15
Slope concrete profile:	1:13
Sand:	D_{50} = 75 μm

Breakwaters

stone diameter:	D_{n50} = 0.812 m
length:	12 m and 6 m
slope:	1:1.5
submergence:	0.10 m

Appendix A3

General information about wave conditions and basin lay-out in experiment D3

Experiment D3

Initial waterdepth:	0.57 m
Initial wave height:	0.12 m
Period:	1.55 s
Angle of incidence of waves:	0

Lay-out:

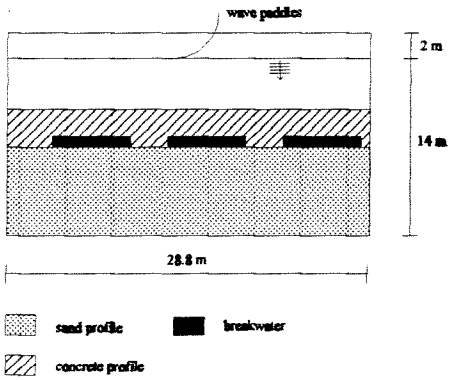

Slope sand profile:	1:15
Slope concrete profile:	1:13
Sand:	D_{50} = 75 μm

Breakwaters

stone diameter:	D_{n50} = 0.812 m
length:	6, 6 and 6 m
slope:	1:1.5
submergence:	0.10 m

Appendix B

Description of the computer model CREON

Introduction

This description of CREON was taken from Gao, Q. and Radder, A.C. (1997).
The model CREON has been designed to model wave property changes, such as wave direction, amplitude and wave length, as waves propagate over a varying bottom.
CREON is based on the concept of parabolic approximation as suggested by Radder (1979). This has been extended to a wide angle approximation. The model can only be applied to the place where bottom changes are small compared to the wave length. The effect of the current on wave propagation (Doppler shift) has been incorporated in the model as suggested by Booij ('81).

To simulate the combined effect of refraction and diffraction for an irregular wave field, a superposition of different directions is considered. Also, a careful treatment of the lateral boundary conditions is necessary to prevent undesirable side effects. The model CREON is an extension of the model CREDIZ with directional spreading effect. It is intended to be used for various sea conditions and in complicated coastal areas.

Basic equations

The parabolic equation for waves propagating at a fairly wide angle is approximated by:

$$\frac{\partial P\phi}{\partial x} - ik\sqrt{1-\epsilon^2}P\phi + R\phi = 0$$

where ϕ represents the potential function, k is the wave number, ϵ is the sine angle of wave propagation direction. P and R contain the y-direction derative, and R also contains additional physical effects such as dissipation and current.

A perfect boundary condition is considered with a known incident wave field ϕ_{inc}. It is given by:

$$\frac{\partial \phi^m}{\partial y} + k\sigma\phi^m = \frac{\partial \phi^m_{inc}}{\partial y} + k\sigma\phi^m_{inc} + k\sum_{l=0}^{m-1} \rho_l(\phi^l - \phi^l_{inc}) e^{\int_{x_l}^{x_m} k\delta dx}$$

in which σ and ρ are so-called non-local coefficients, δ is the coefficient containing the effect of wave dissipation, m is the grid number in x-direction.

The equation for the internal boundary is:

$$\frac{\partial \phi}{\partial y} = -iP_a k\phi$$

where P_a is an adjustable coefficient, defining an absorption mechanism for coastal lines or internal boundaries.

Physical effects of dissipation

Wave breaking

Wave dissipation due to breaking is computed by:

$$W_b = -\frac{\alpha}{\pi} \frac{\omega_r Q_b H_m^2}{H_{rms}^2}$$

in which $H_{rms} = H_s / \sqrt{2}$, H_s is the significant wave height, H_m is the breaking wave height and Q_b is the fraction of breaking or broken waves, defined as:

$$H_m = \frac{2\pi\gamma_d}{k} \tanh\left(\frac{\gamma_s}{2\pi\gamma_d} kd\right)$$

$$Q_b = \exp\left(-\frac{(1-Q_b)}{b^2}\right)$$

with $b = H_{rms} / H_m$ and d is the depth, γ_d and γ_s are coefficients of breaking height in deep and shallow water respectively.

Bottom friction

The dissipation due to bottom friction is calculated by:

$$W_f = \frac{s_0^2}{2g}\left(\frac{8}{3\pi} f_w s_0 H_s + 2f_s |V|\right)$$

with:

$$s_0 = \frac{\omega_r}{\sinh(kd)}$$

where v is the current velocity, g the gravity acceleration, ω_r the relative wave frequency, f_w the coefficient of wave-induced stress, f_s the coefficient of wave-current-induced stress.

Other effects

Other effects incorporated in CREON are the Doppler effect, the non-linear effect (modelled by wave effect on the dispersion relation) and effects of obstacles on the wave field (modelled in the same way as in HISWA).

Input and output

Input

CREON calculates wave heights based on the RMS-value, but as input the model only knows the significant wave height at the up-wave boundary. The model will discretize and transform them to proper variables. In output, the model will also generate resultant wave heights and mean wave directions.

If the incoming wave height is H_s, then wave component a_i in direction θ_i is calculated according to:

$$a_i^2 = \frac{1}{8} H_s^2 D(\theta_i) \Delta\theta_i$$

where $D(\theta_i)$ defines the wave distribution in θ-domain.

Output

The direction of a wave component is obtained from:

$$\theta_f = \frac{CC_g \frac{\partial S_t}{\partial y}}{CC_g \frac{\partial S_t}{\partial x}}$$

It differs from the direction of wave energy flux, which is calculated by:

$$\theta_t = \frac{CC_g \frac{\partial S_t}{\partial y} + \omega_r V \sin(\theta)}{CC_g \frac{\partial S_t}{\partial x} + \omega_r V \cos(\theta)}$$

where C is the wave phase speed and c_g the group speed. S is the local phase, V and θ_v represent current and its diffraction respectively.
The mean wave direction is given by:

$$\bar{\theta} = \arctan \frac{\sum_{i=N}^{N} a^2_i \sin(\theta_i)}{\sum_{i=N}^{N} a^2_i \cos(\theta_i)}$$

and the significant wave height is given by:

$$H^2_s = 2 \sum_{i=N}^{N} H^2_i$$

where H_i is the wave height. (The summation is with regard to the wave components).

Appendix C

Shoaling computation with HISWA, CREON and linear theory

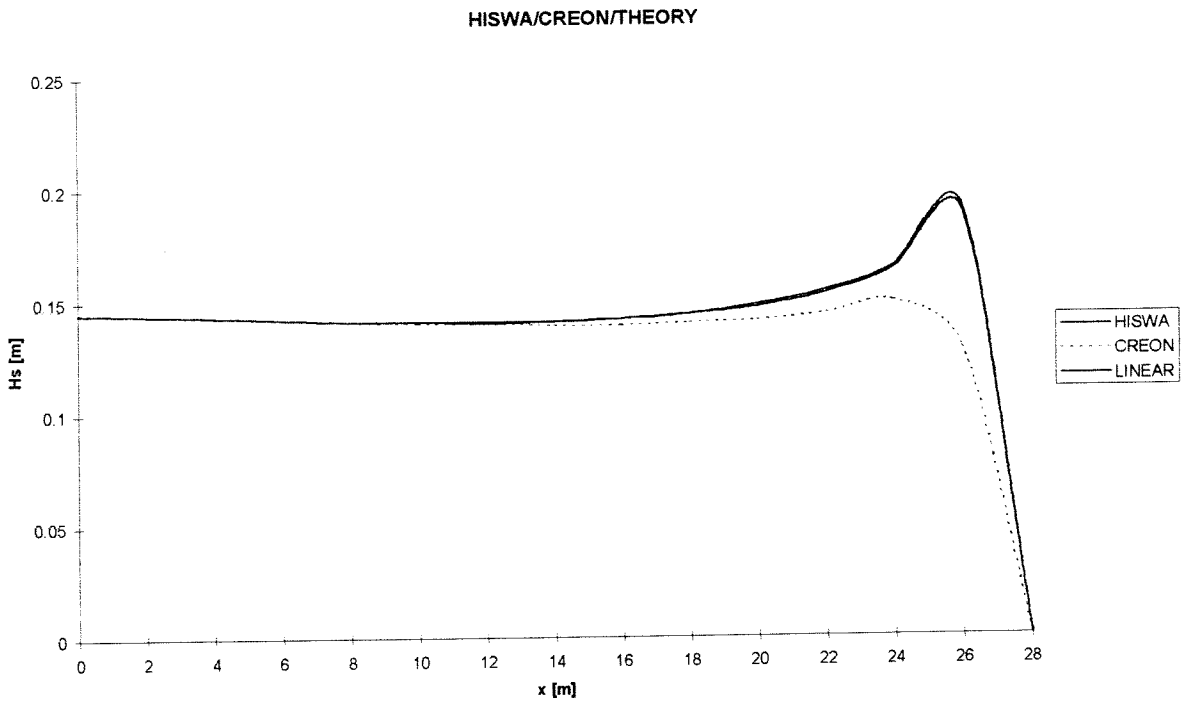

Appendix D

CREON diffraction computation

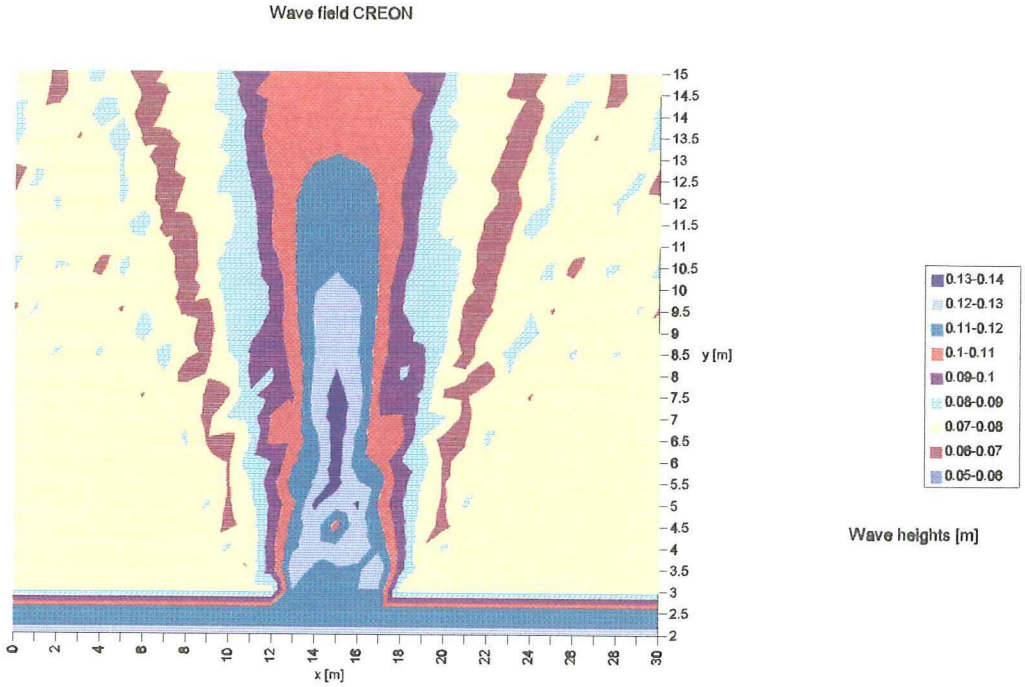

HISWA computation with ms = 10

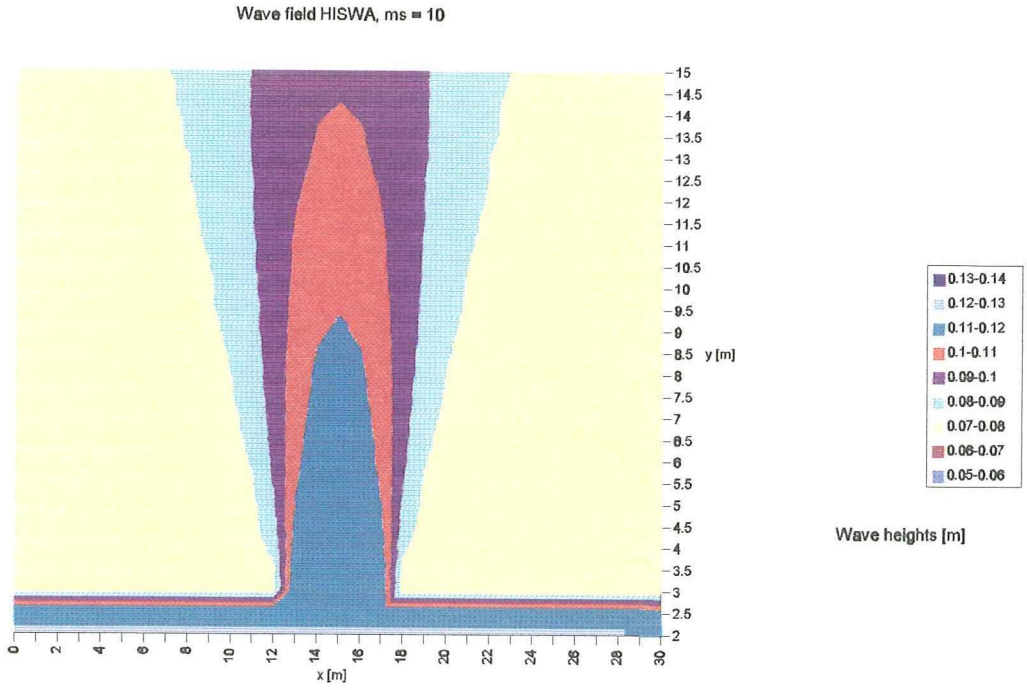

Appendix D (continued)

HISWA computation with ms = 20

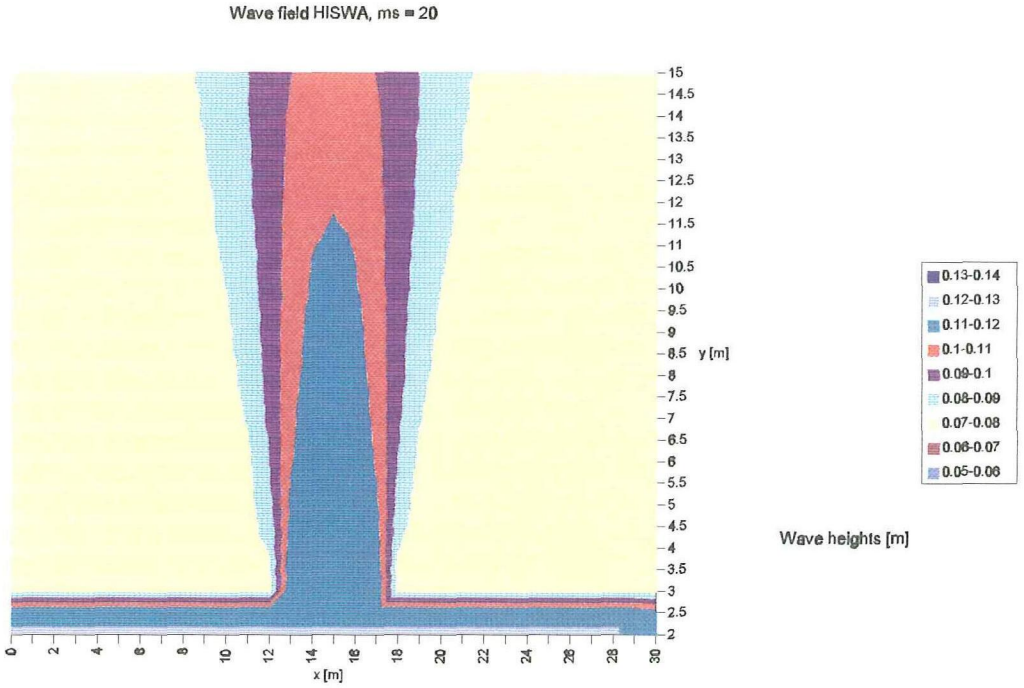

HISWA computation with ms = 30

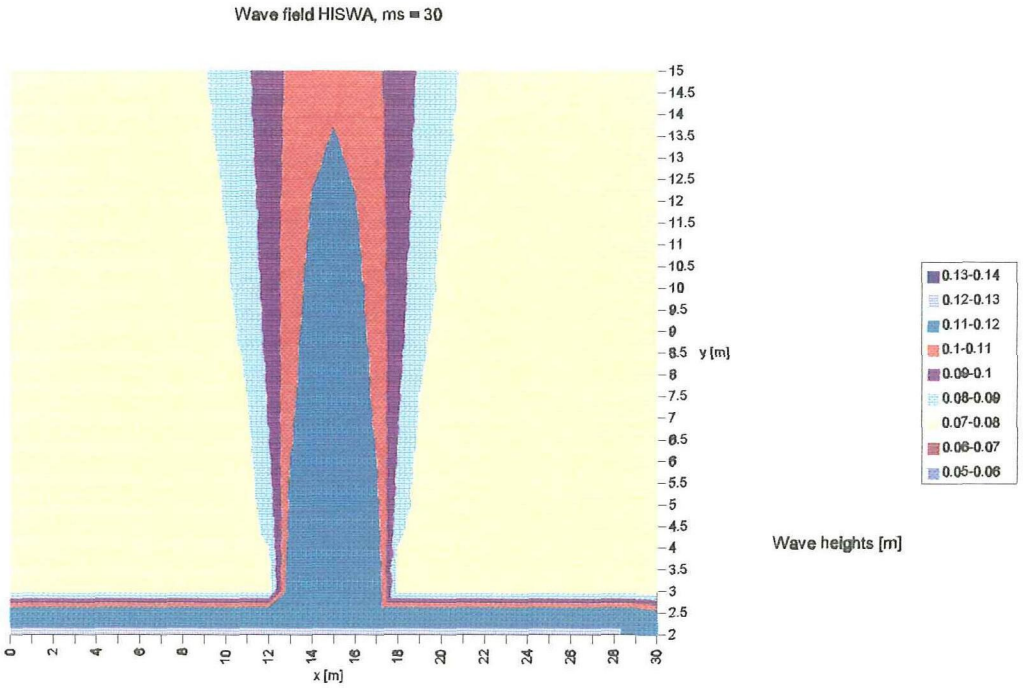

Modelling the effects of submerged breakwaters in a wave basin

2DH-simulations of tests with Delft2D-MOR

Volume II: Figures

J. Schaap

Master thesis
August 1997

Delft University of Technology
Faculty of Civil Engineering

Supervision:

prof. ir. K. d'Angremond
dr. ir. N. Booij
dr. ir. J. van de Graaff
dr. ir. J.A. Roelvink
ir. S.C. van der Biezen

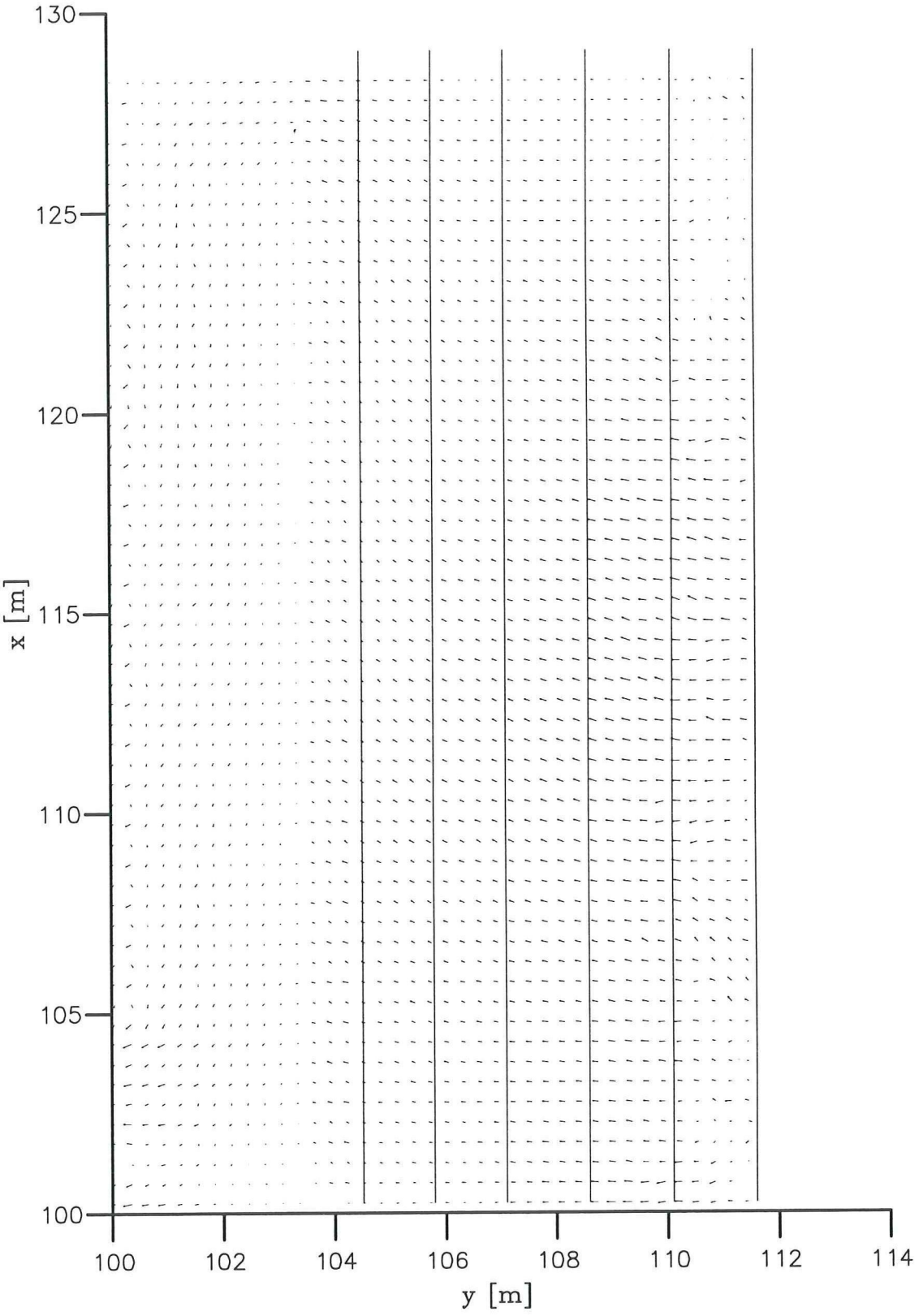

Initial flow field	A3	H=0.12 m
	Flow velocities [m/s]	
Delft University of Technology	DELFT3D	A12–1

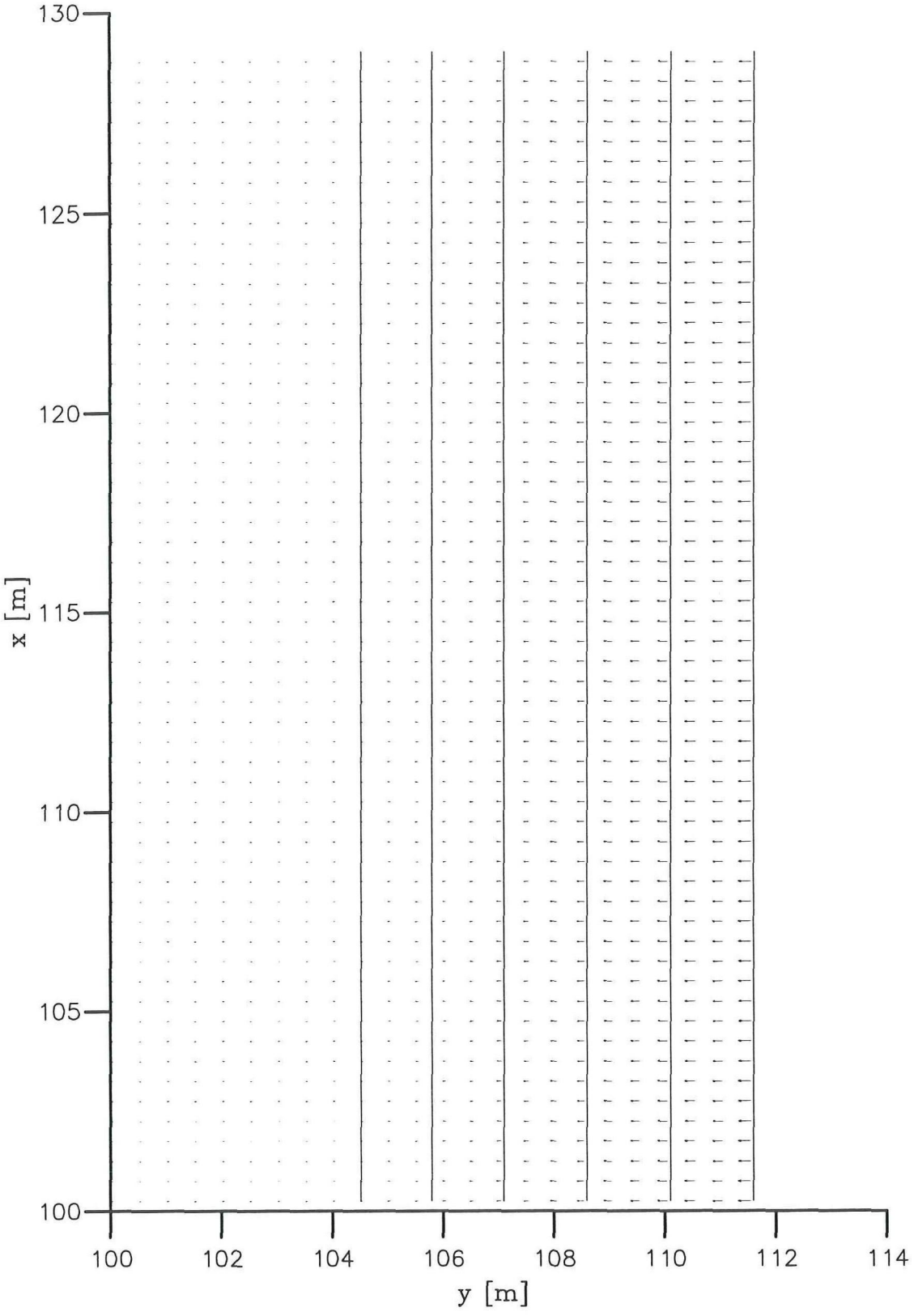

Initial return flow field	A3	H=0.12 m
	Flow velocities [m/s]	
Delft University of Technology	DELFT3D	A12–2

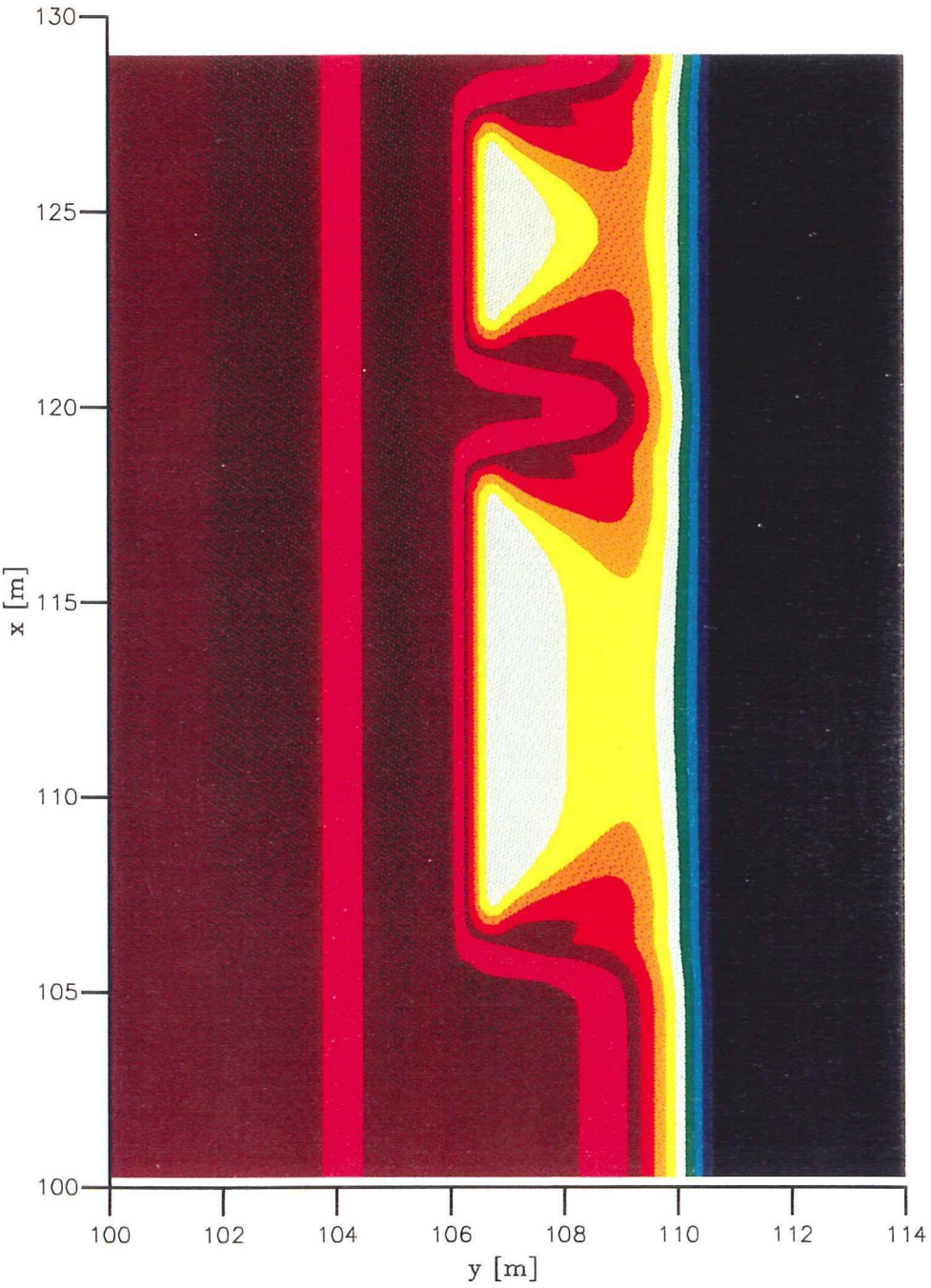

Initial wave field	C3	H=0.12 m
	Wave heights [m]	
Delft University of Technology	DELFT3D	A12-6

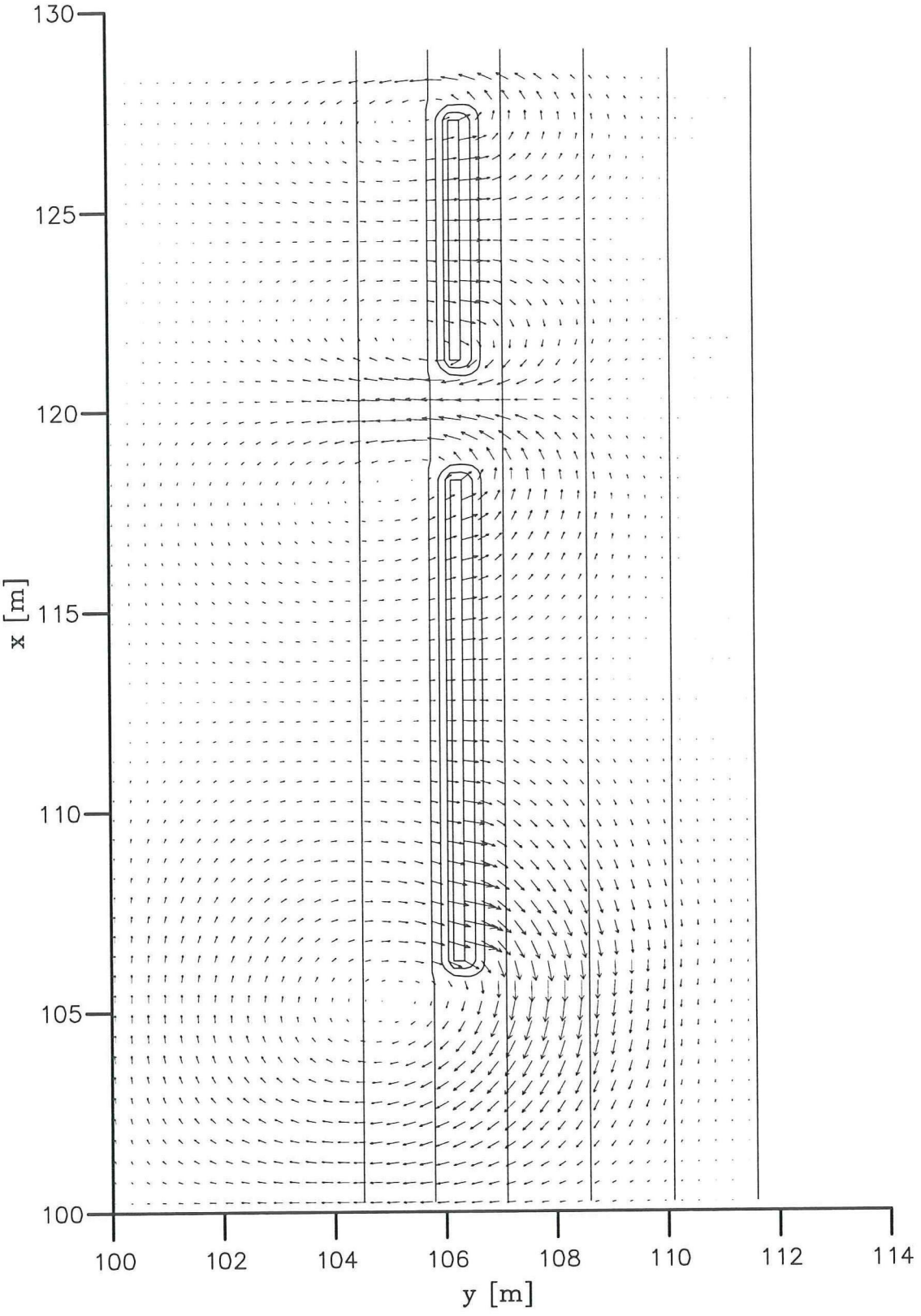

Initial flow field	C3	H=0.12 m
	Flow velocities [m/s]	
Delft University of Technology	DELFT3D	A12–7

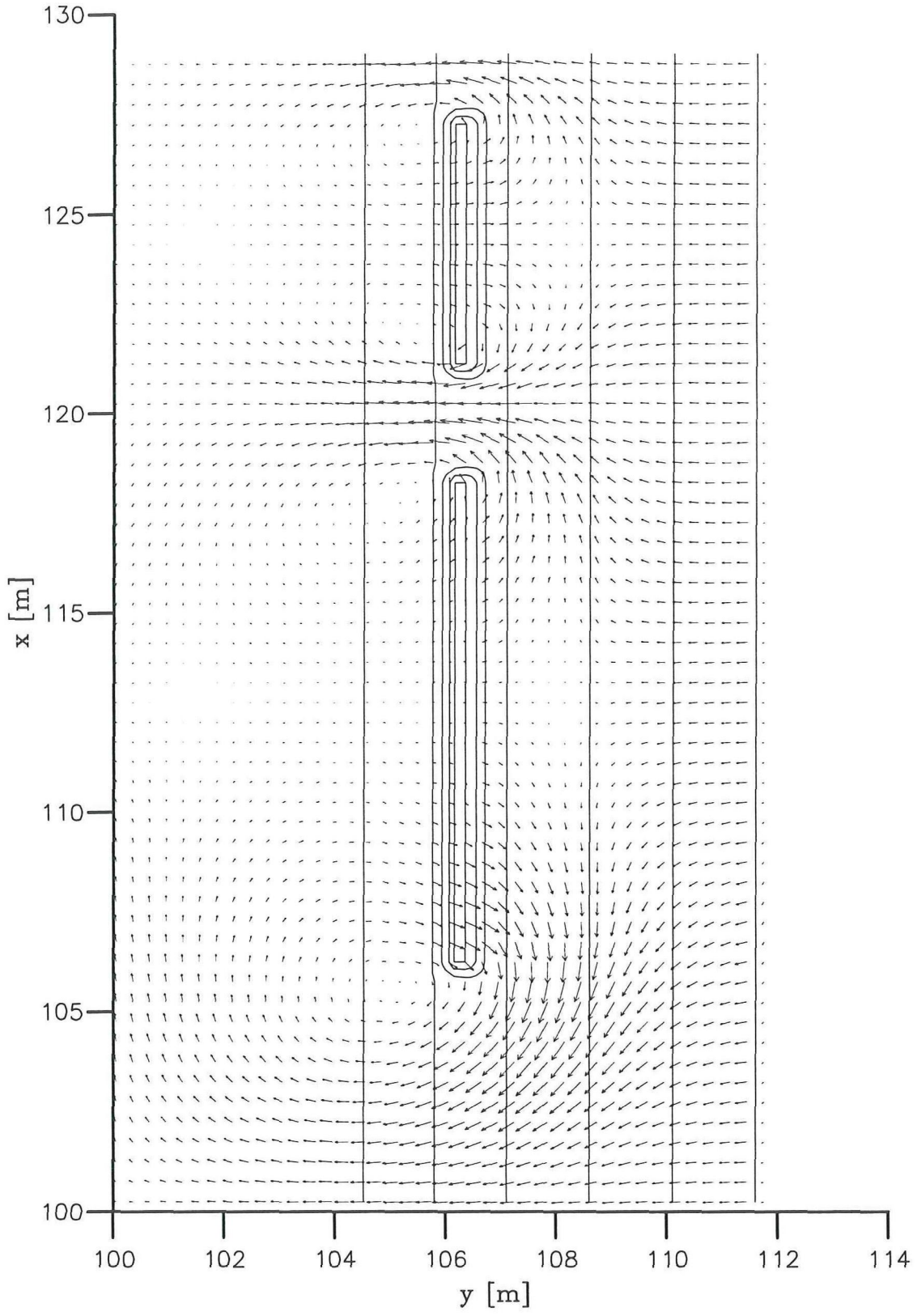

Initial return flow field	C3	H=0.12 m
	Flow velocities [m/s]	
Delft University of Technology	DELFT3D	A12–8

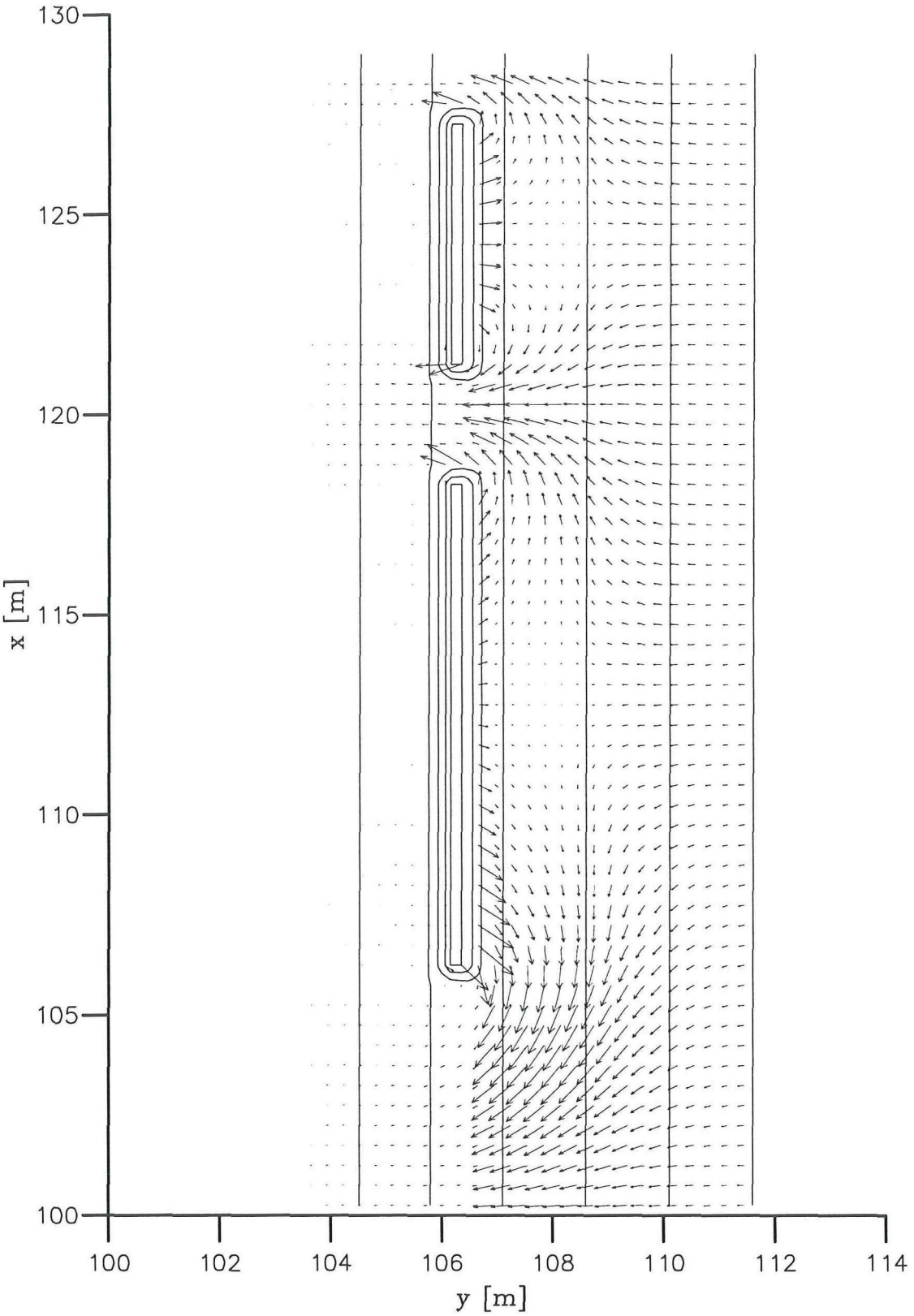

Initial sediment transport field	C3	H=0.12 m
	Sed. transport [m2/s]	
Delft University of Technology	DELFT3D	A12-9

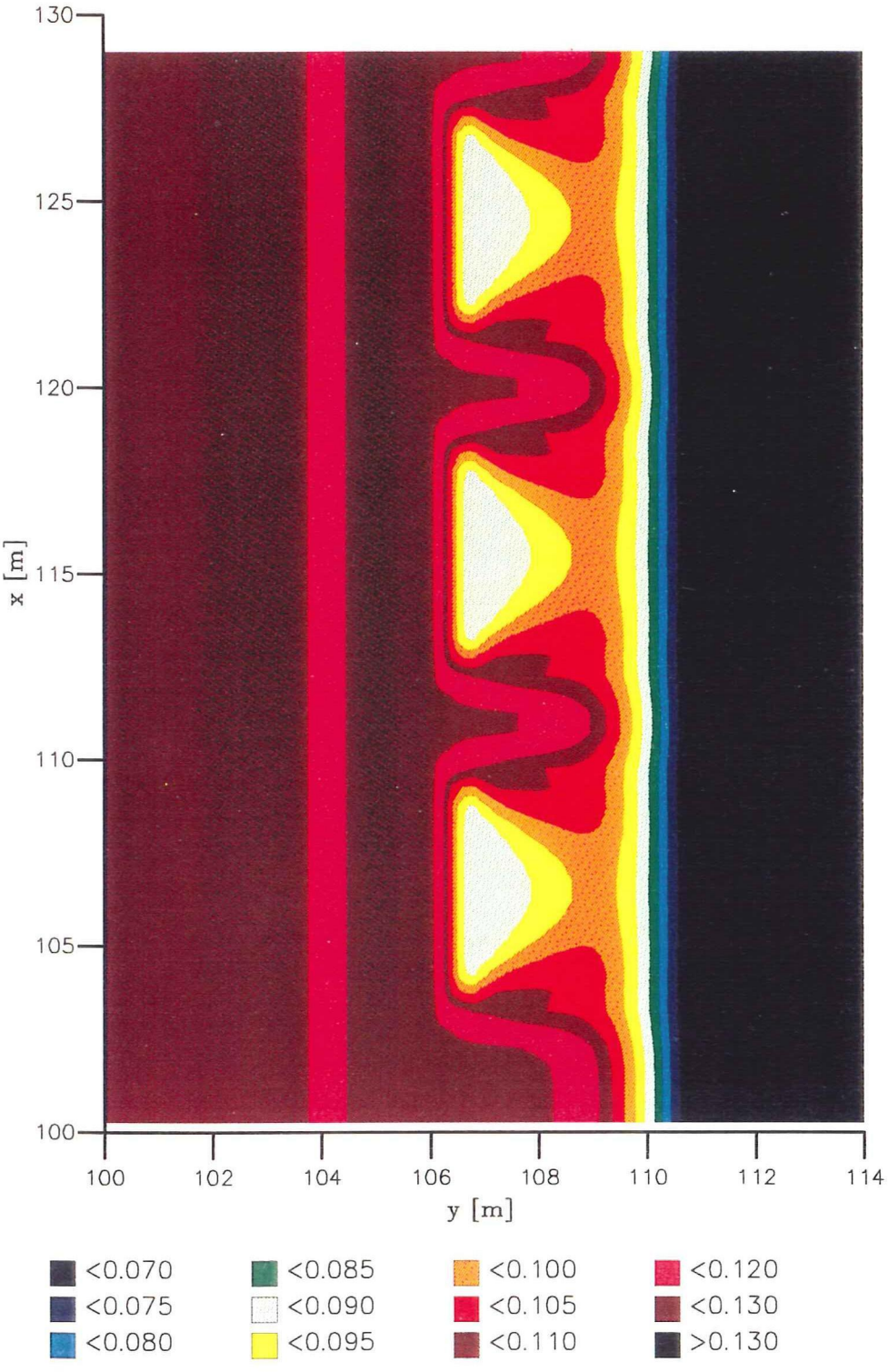

Initial wave field	D3	H=0.12 m
	Wave heights [m]	
Delft University of Technology	DELFT3D	A12–10

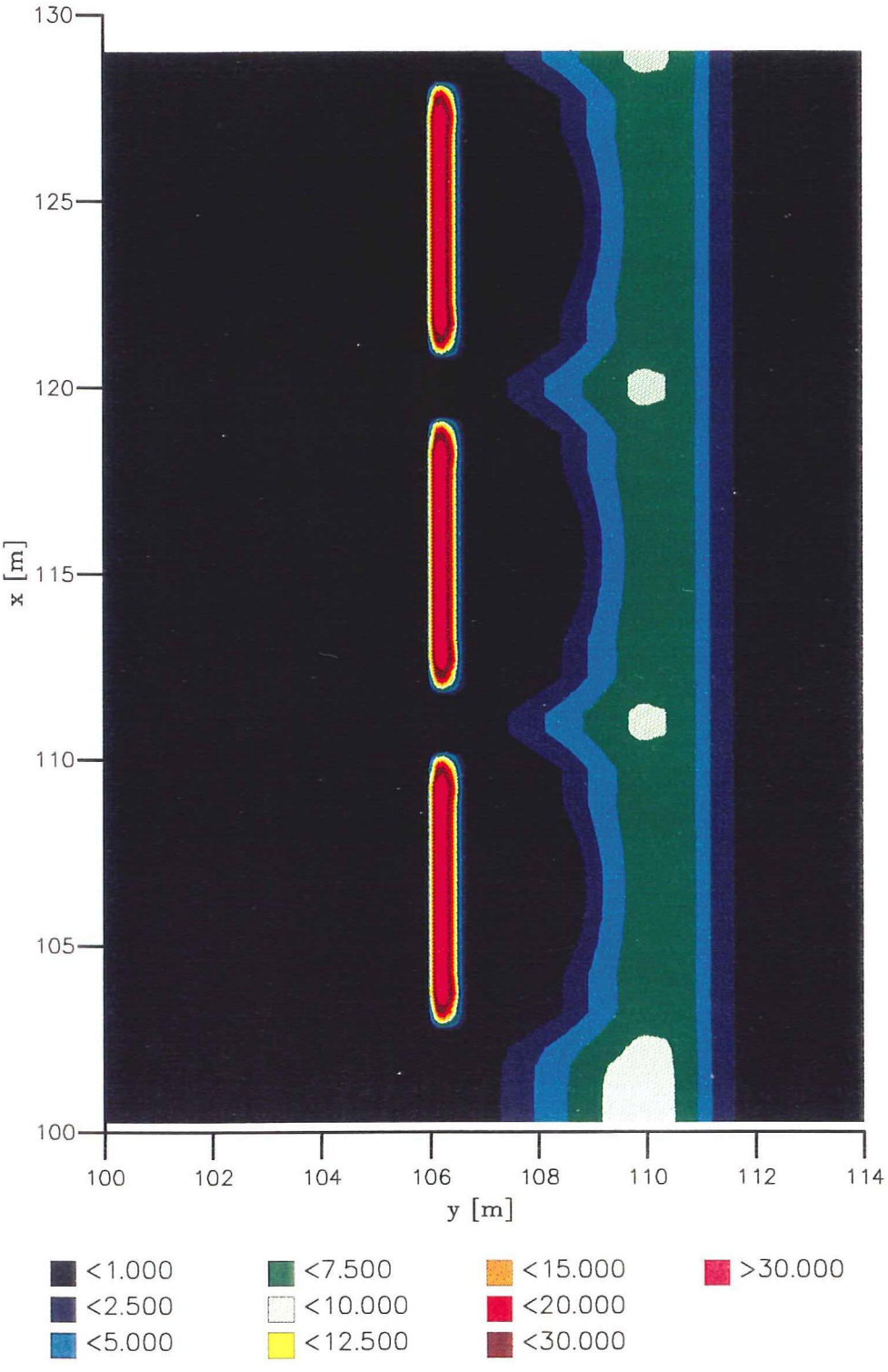

Initial dissipation	D3	H=0.12 m
	Dissipation [W/m2]	
Delft University of Technology	DELFT3D	A12-11

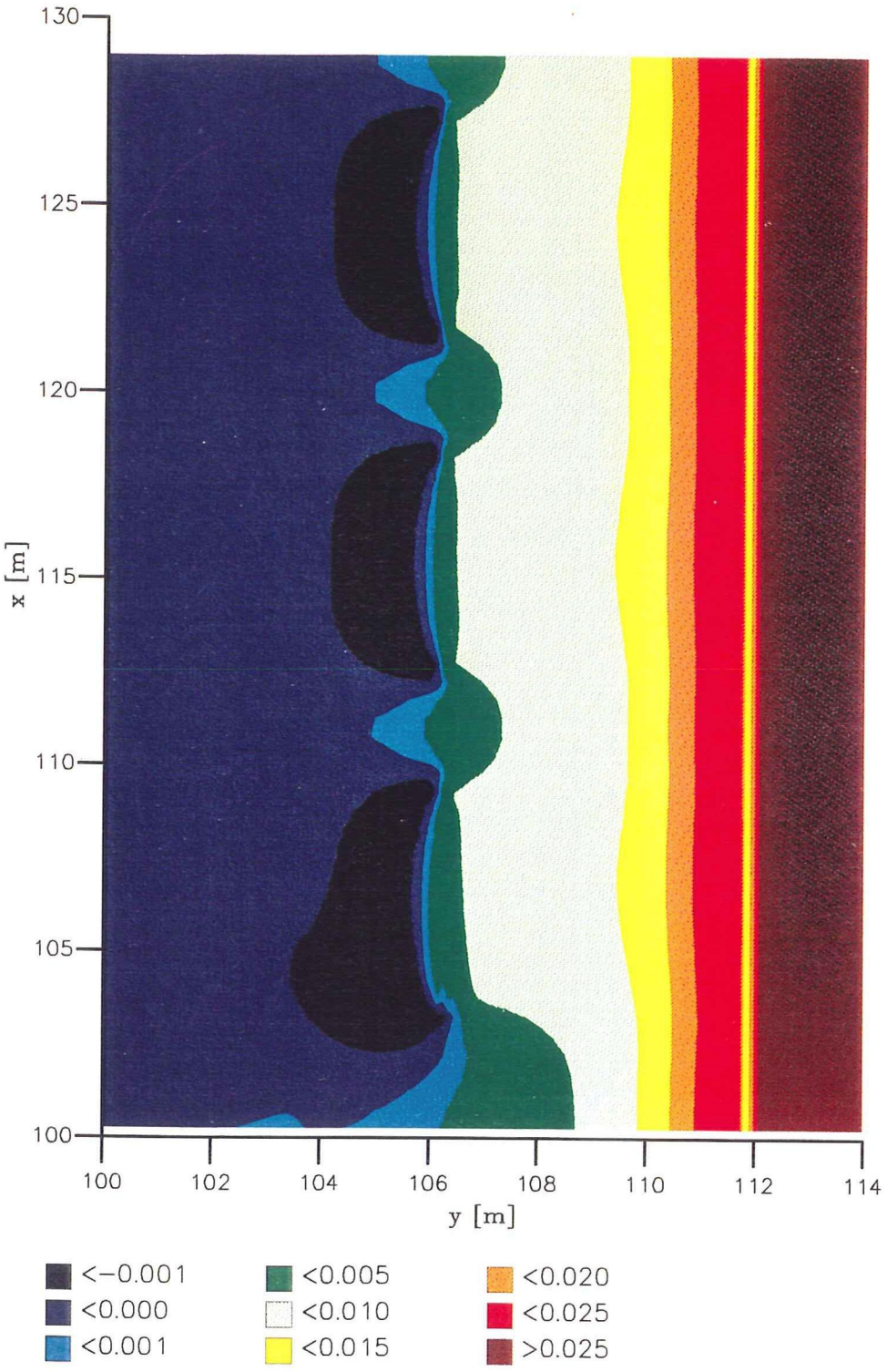

Initial water level (water levels positive upwards)	D3	H=0.12 m
	Water levels [m]	
Delft University of Technology	DELFT3D	A12−12

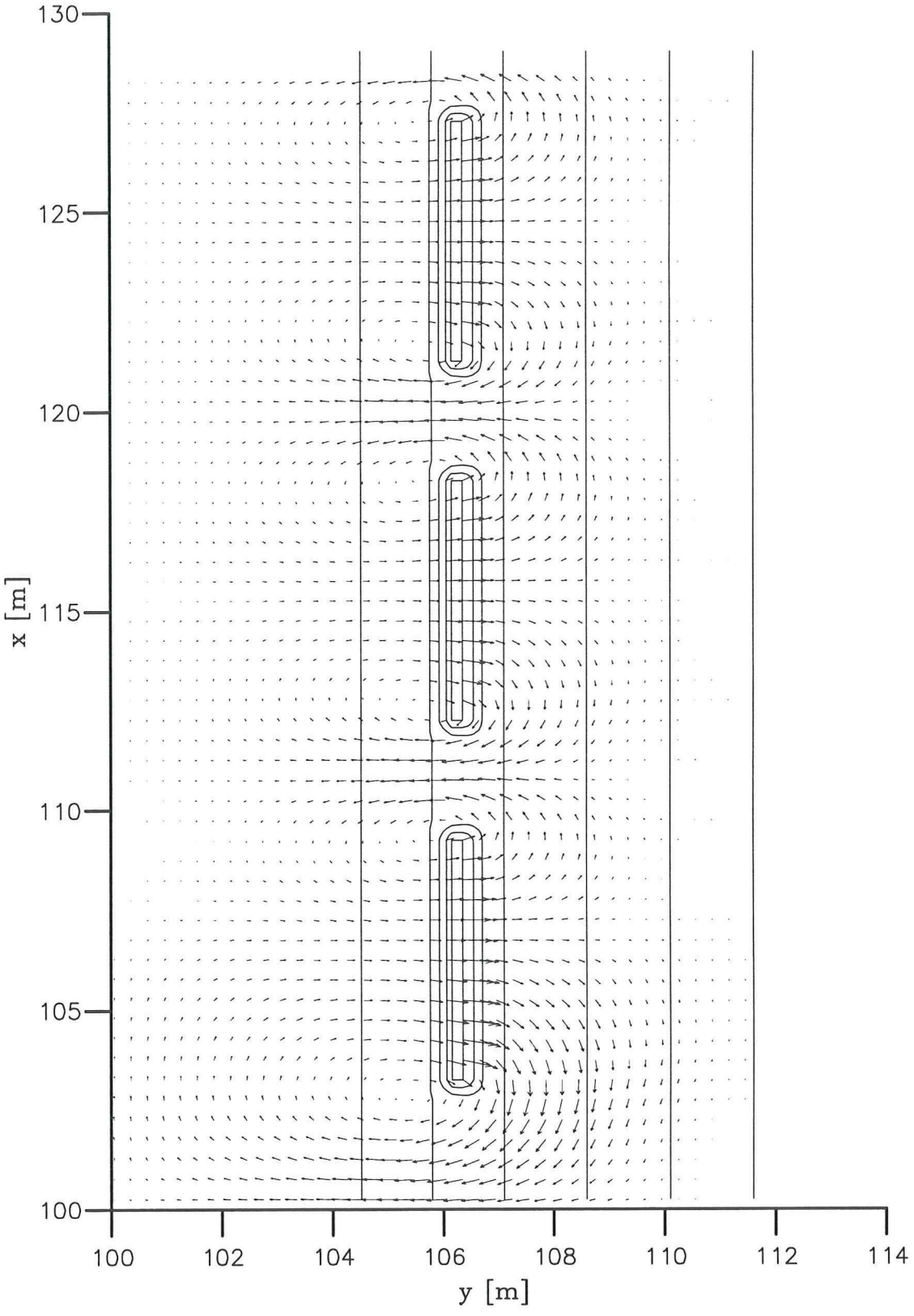

Initial flow field	D3	H=0.12 m
	Flow velocities [m/s]	
Delft University of Technology	DELFT3D	A12–13

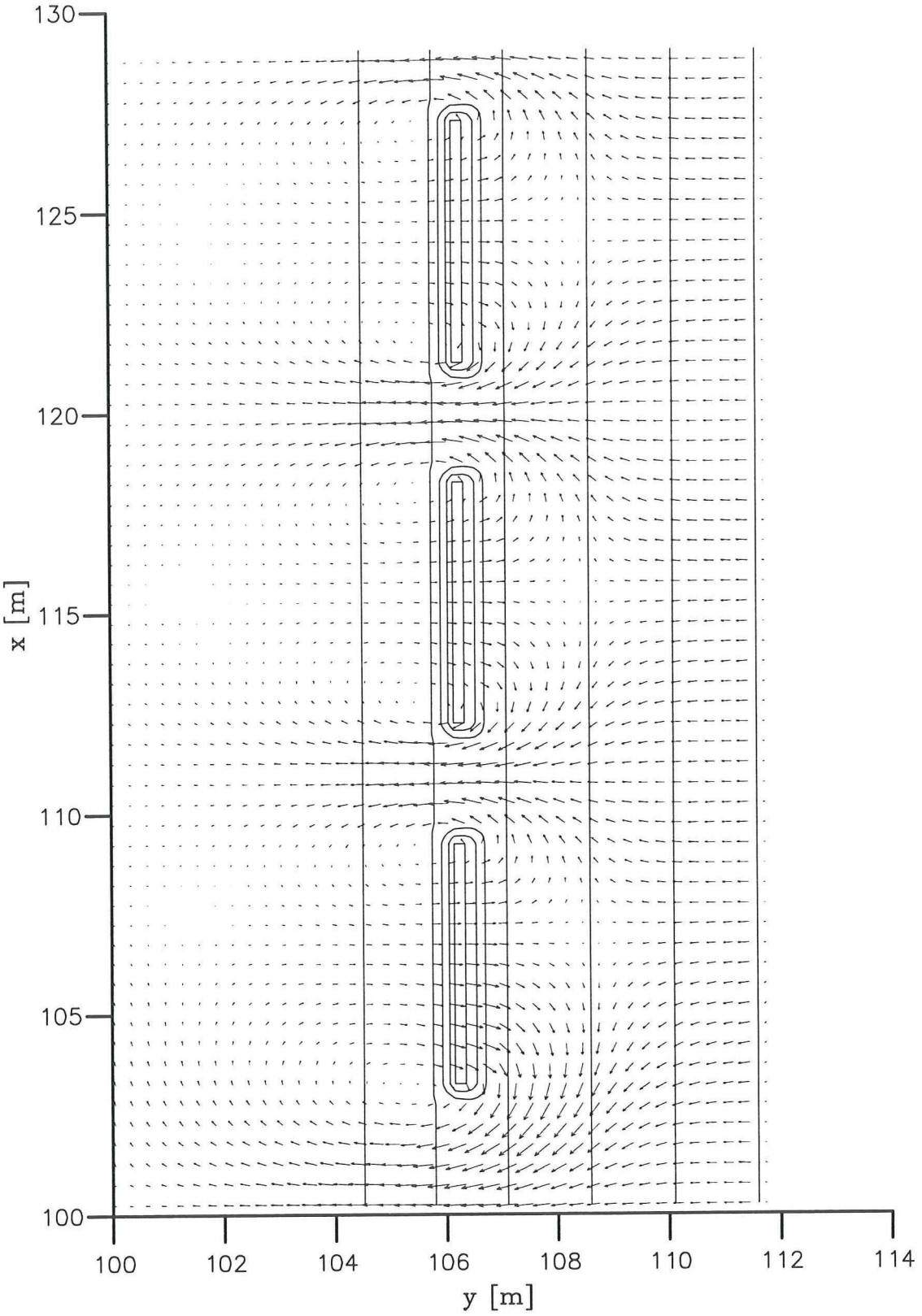

Initial return flow field	D3	H=0.12 m
	Flow velocities [m/s]	
Delft University of Technology	DELFT3D	A12–14

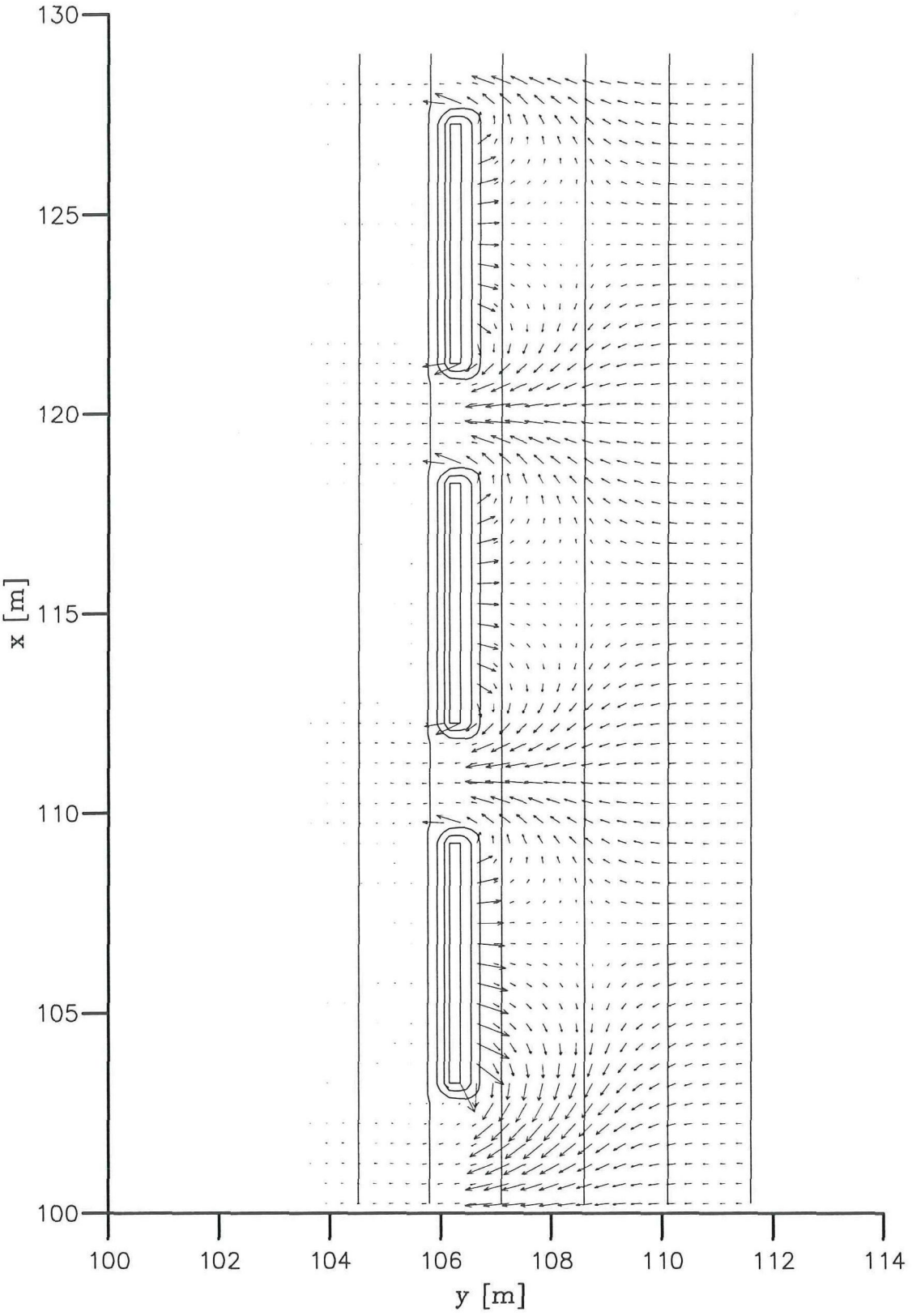

Initial sediment transport field	D3	H=0.12 m
	Sed. transport [m2/s]	
Delft University of Technology	DELFT3D	A12–15

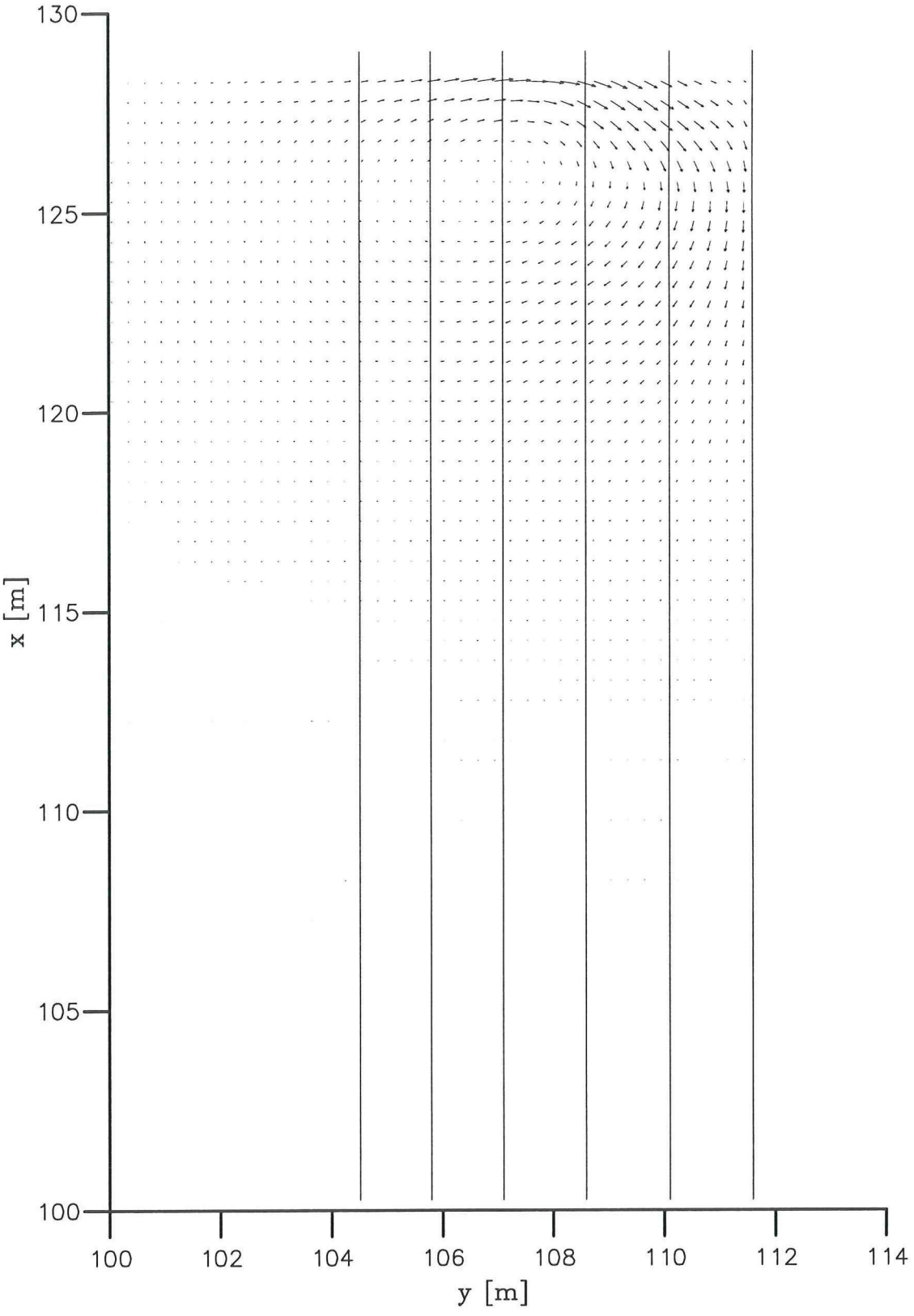

Flow field after 7.5 hours	A3	H=0.12 m
	Flow velocities [m/s]	
Delft University of Technology	DELFT3D	A13–4

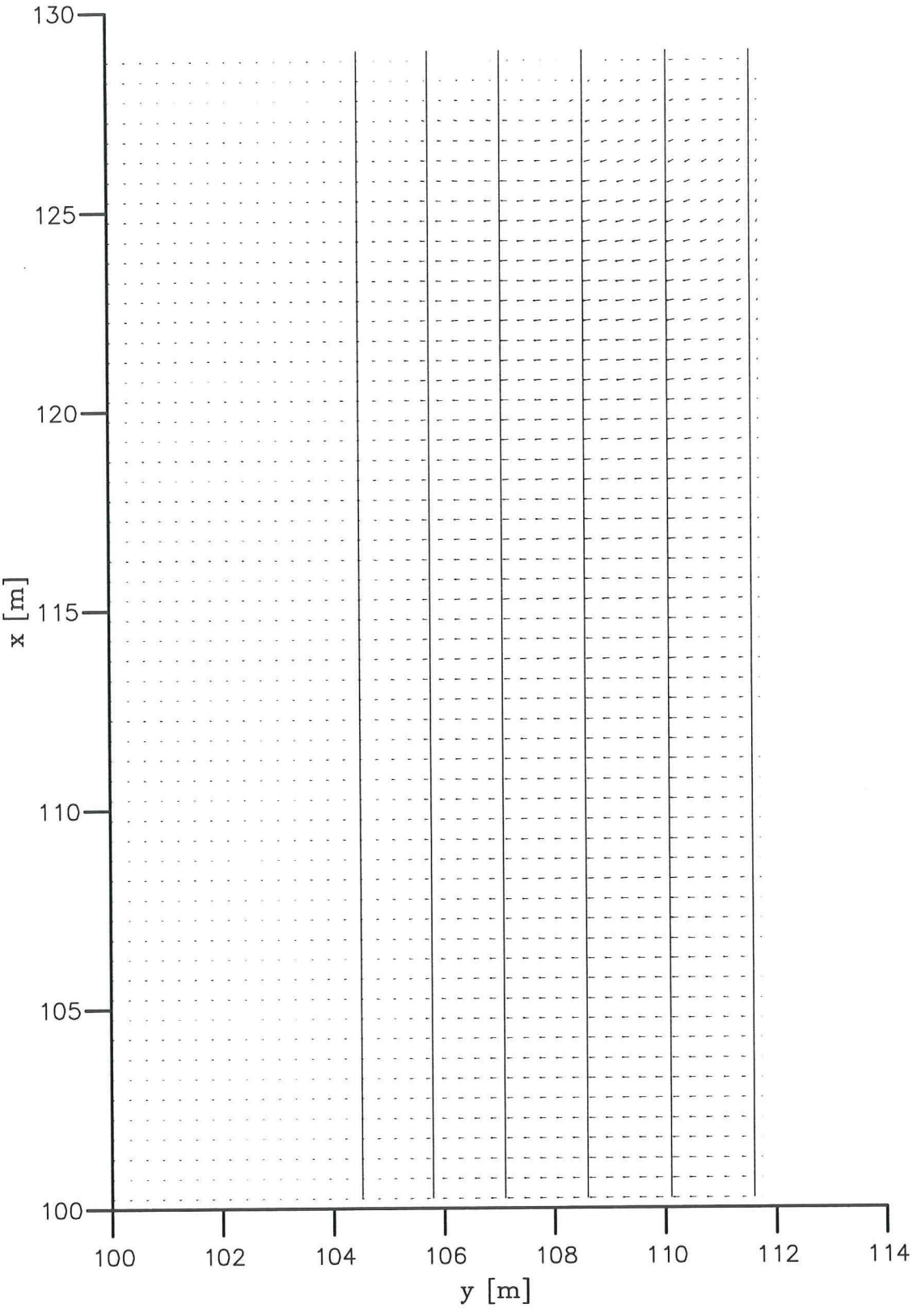

Return flow field after 7.5 hours	A3	H=0.12 m
	Flow velocities [m/s]	
Delft University of Technology	DELFT3D	A13–5

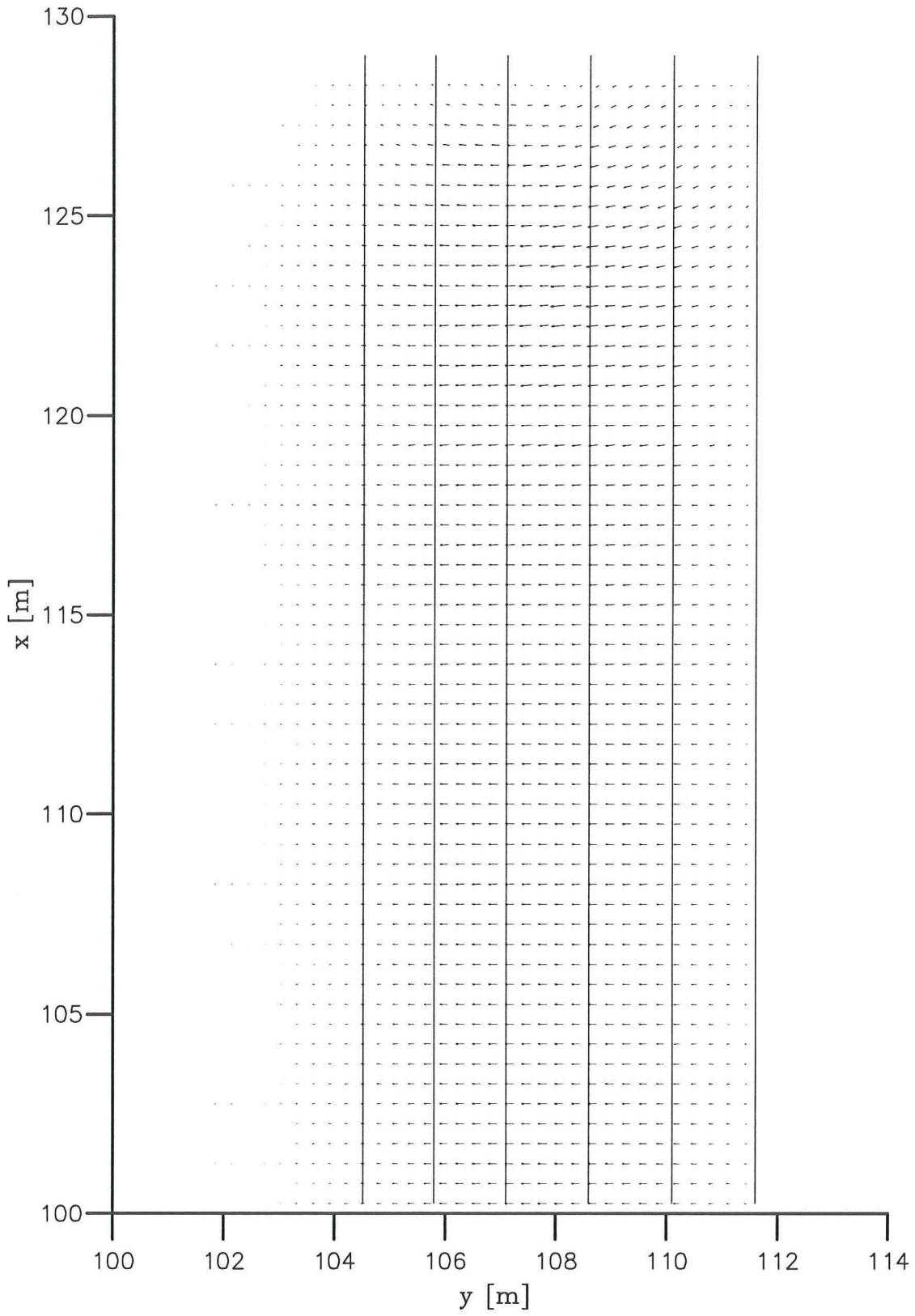

Sediment transport field after 7.5 hours	A3	H=0.12 m
	Flow velocities [m/s]	
Delft University of Technology	DELFT3D	A13–6

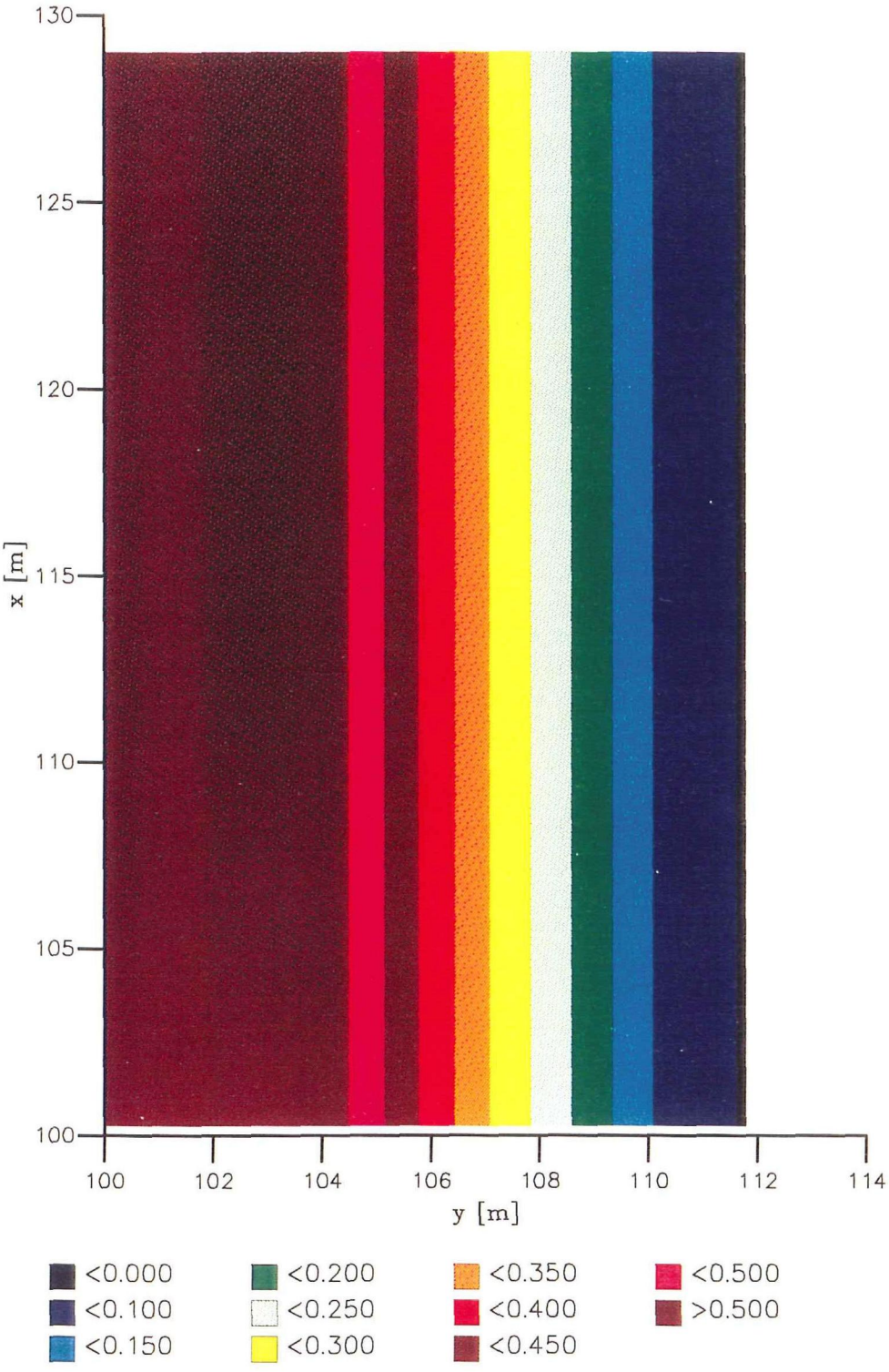

Initial bathymetry (bottom depths positive downwards)	A3	H=0.12 m
	Bottom depths [m]	
Delft University of Technology	DELFT3D	A13-7

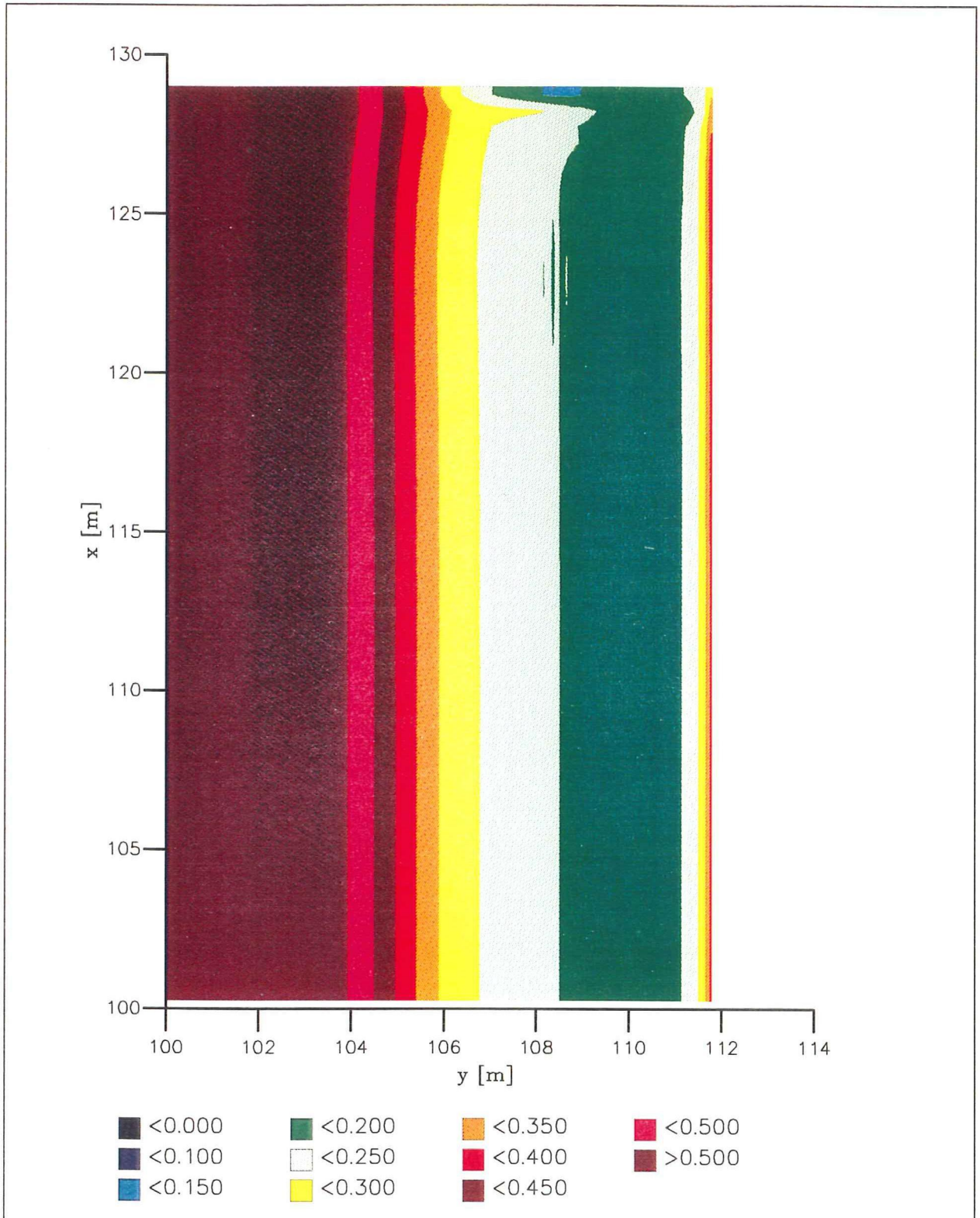

Bathymetry after 7.5 hours (bottom depths positive downwards)	A3	H=0.12 m
	Bottom depths [m]	
Delft University of Technology	DELFT3D	A13–8

Computed erosion/accretion after 7.5 hours
No breakwaters, H = 0.12 m

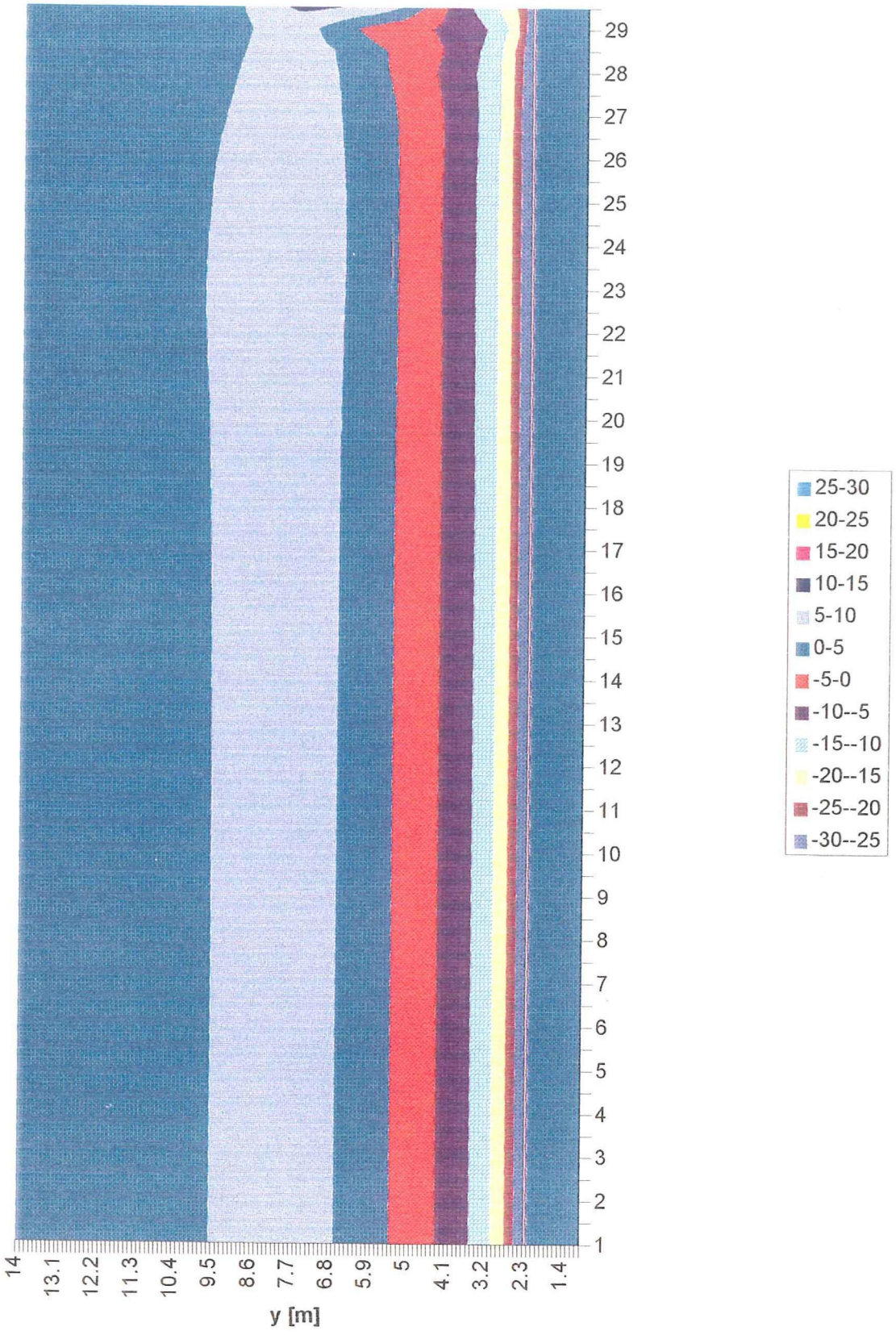

Measured erosion/accretion after 7.5 hours
No breakwaters, H = 0.12 m

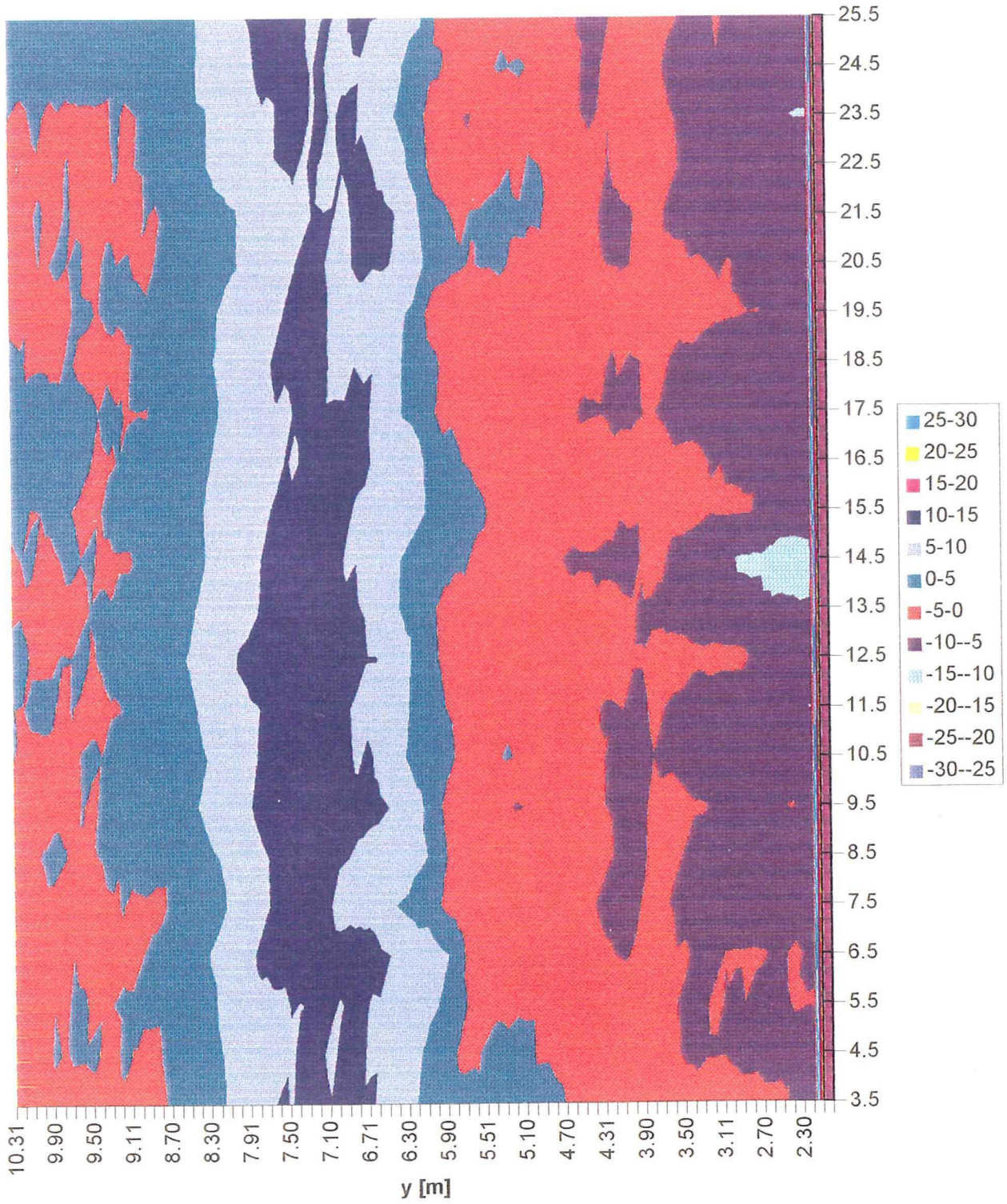

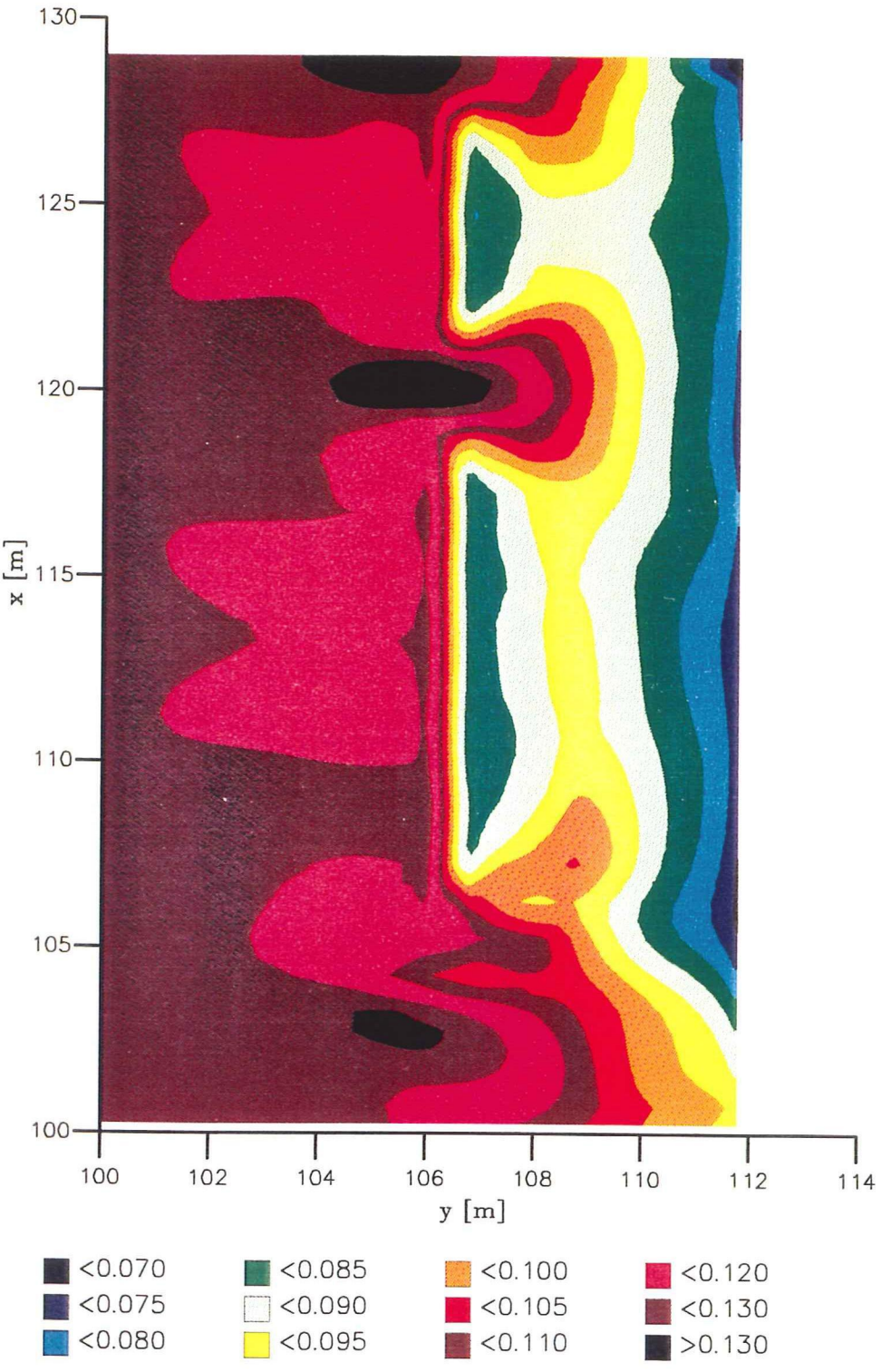

Wave field after 7.5 hours	C3	H=0.12 m
	Wave heights [m]	
Delft University of Technology	DELFT3D	A14–3

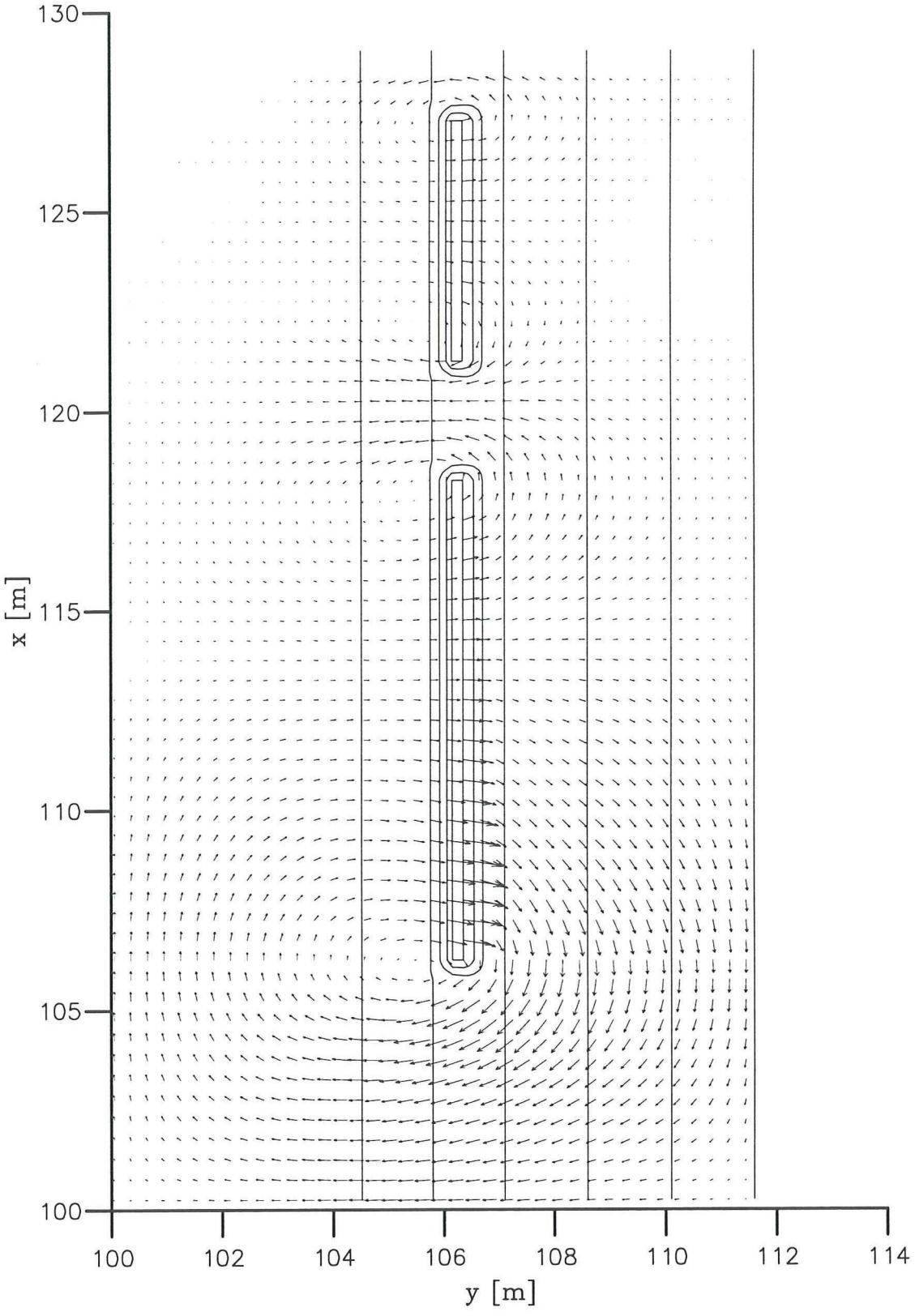

Flow field after 7.5 hours	C3	H=0.12 m
	Flow velocities [m/s]	
Delft University of Technology	DELFT3D	A14–4

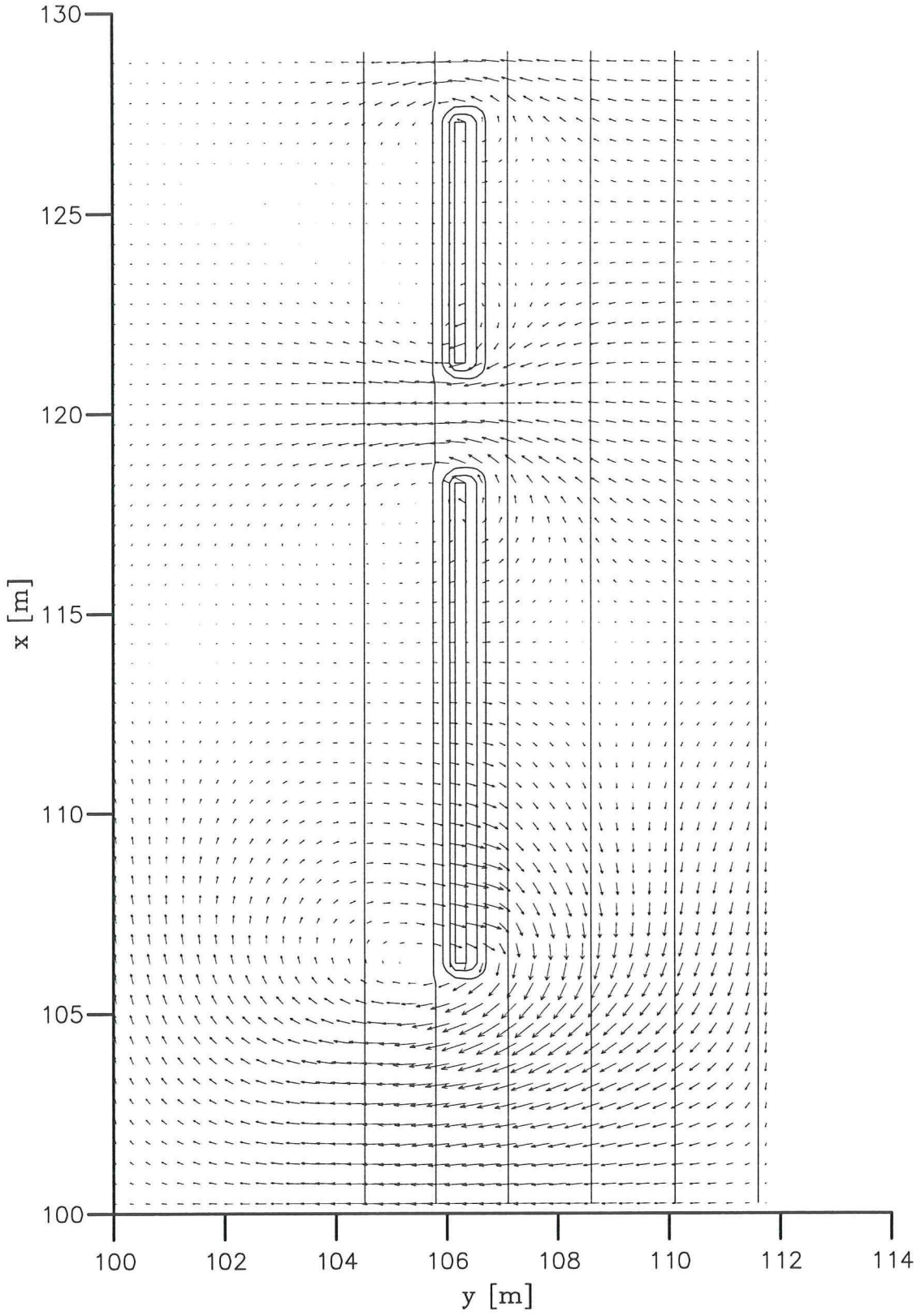

Return flow field after 7.5 hours	C3	H=0.12 m
	Flow velocities [m/s]	
Delft University of Technology	DELFT3D	A14–5

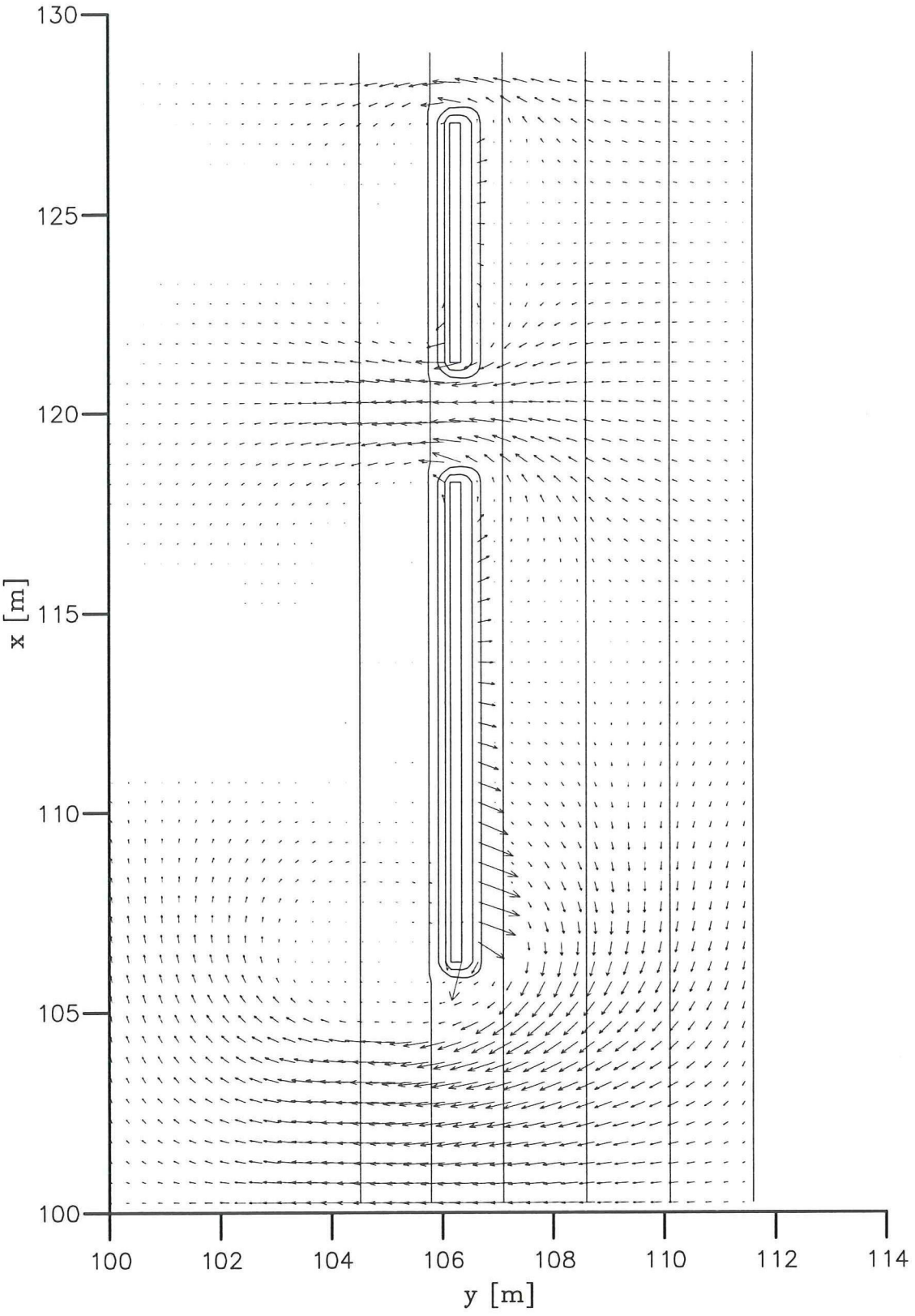

Sediment transport field after 7.5 hours	C3	H=0.12 m
	Sed. transport [m2/s]	
Delft University of Technology	DELFT3D	A14–6

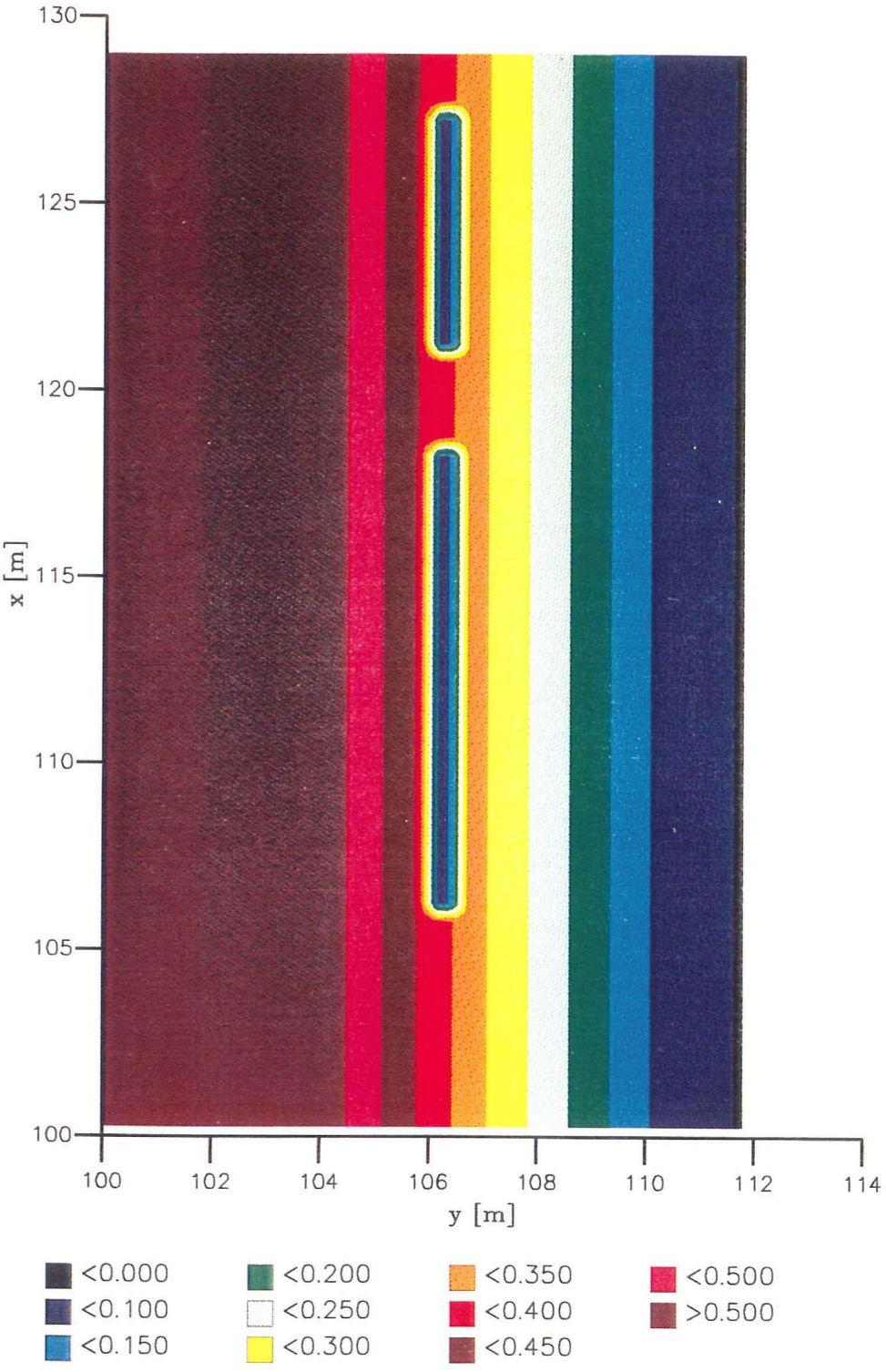

Initial bathymetry (bottom depths positive downwards)	C3	H=0.12 m
	Bottom depths [m]	
Delft University of Technology	DELFT3D	A14–7

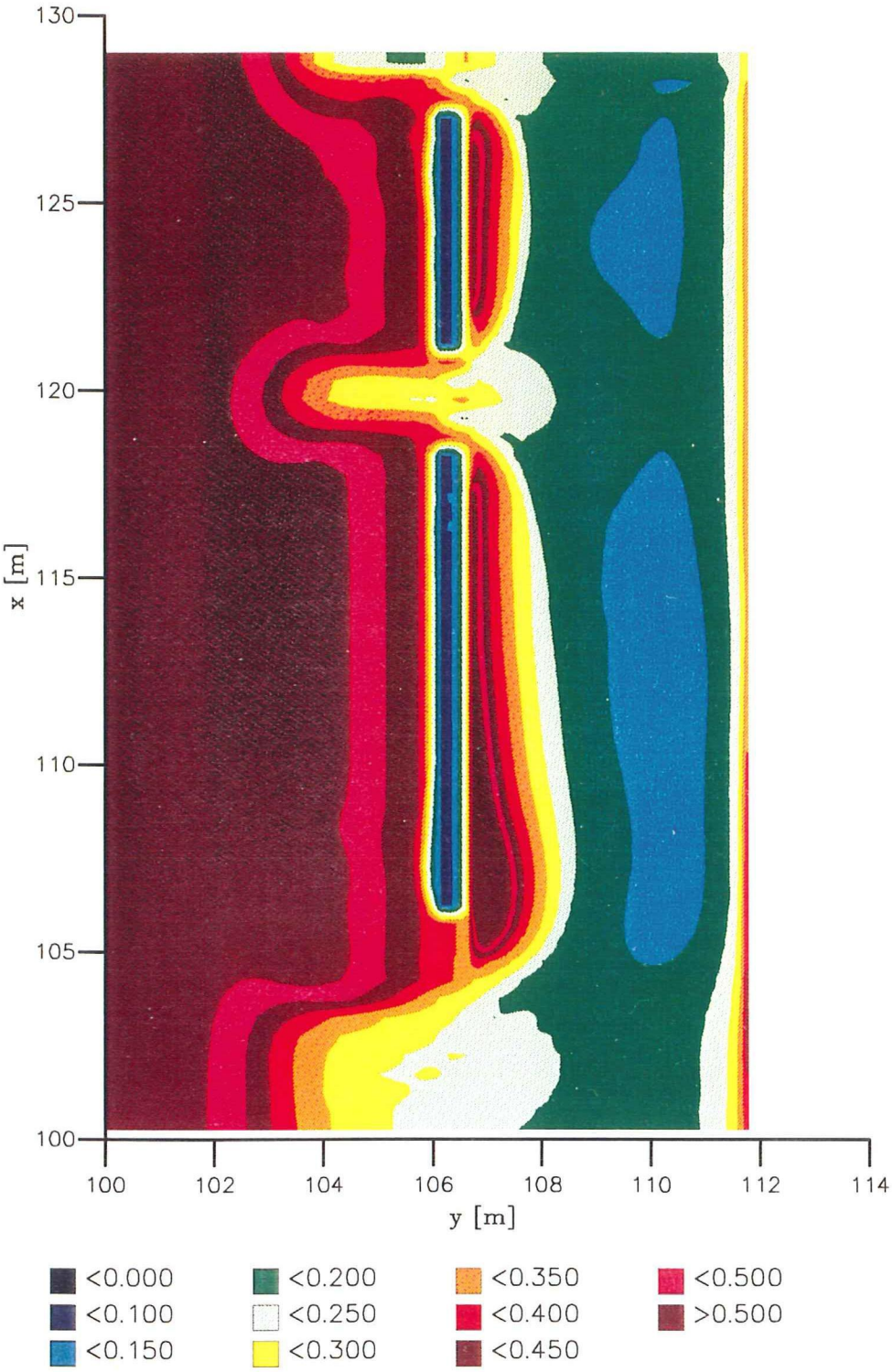

Bathymetry after 7.5 hours (bottom depths positive downwards)	C3	H=0.12 m
	Bottom depths [m]	
Delft University of Technology	DELFT3D	A14–8

Computed erosion/accretion after 7.5 hours
Two breakwaters, H = 0.12 m

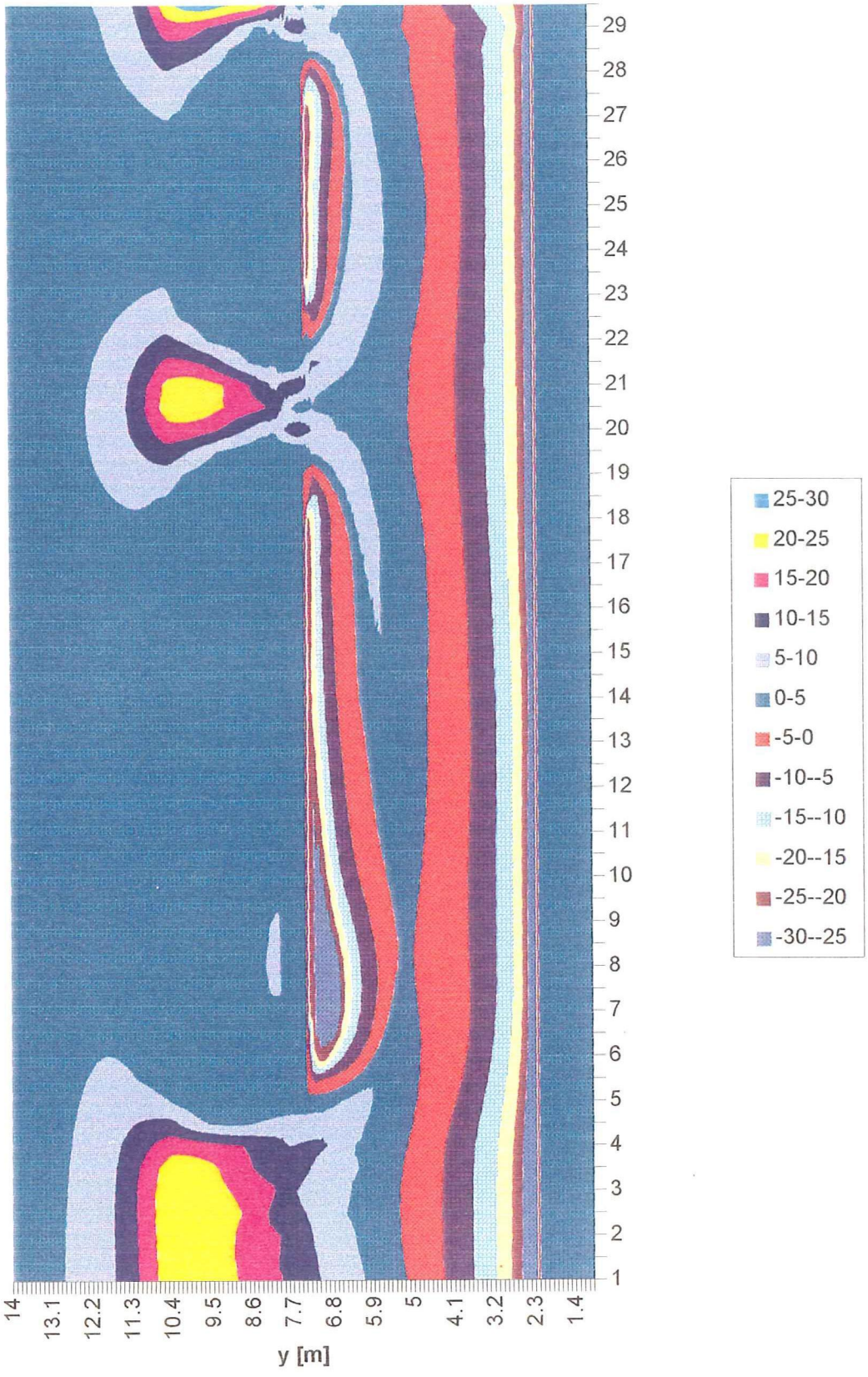

Measured erosion/accretion after 7.5 hours
Two breakwaters, H = 0.12 m

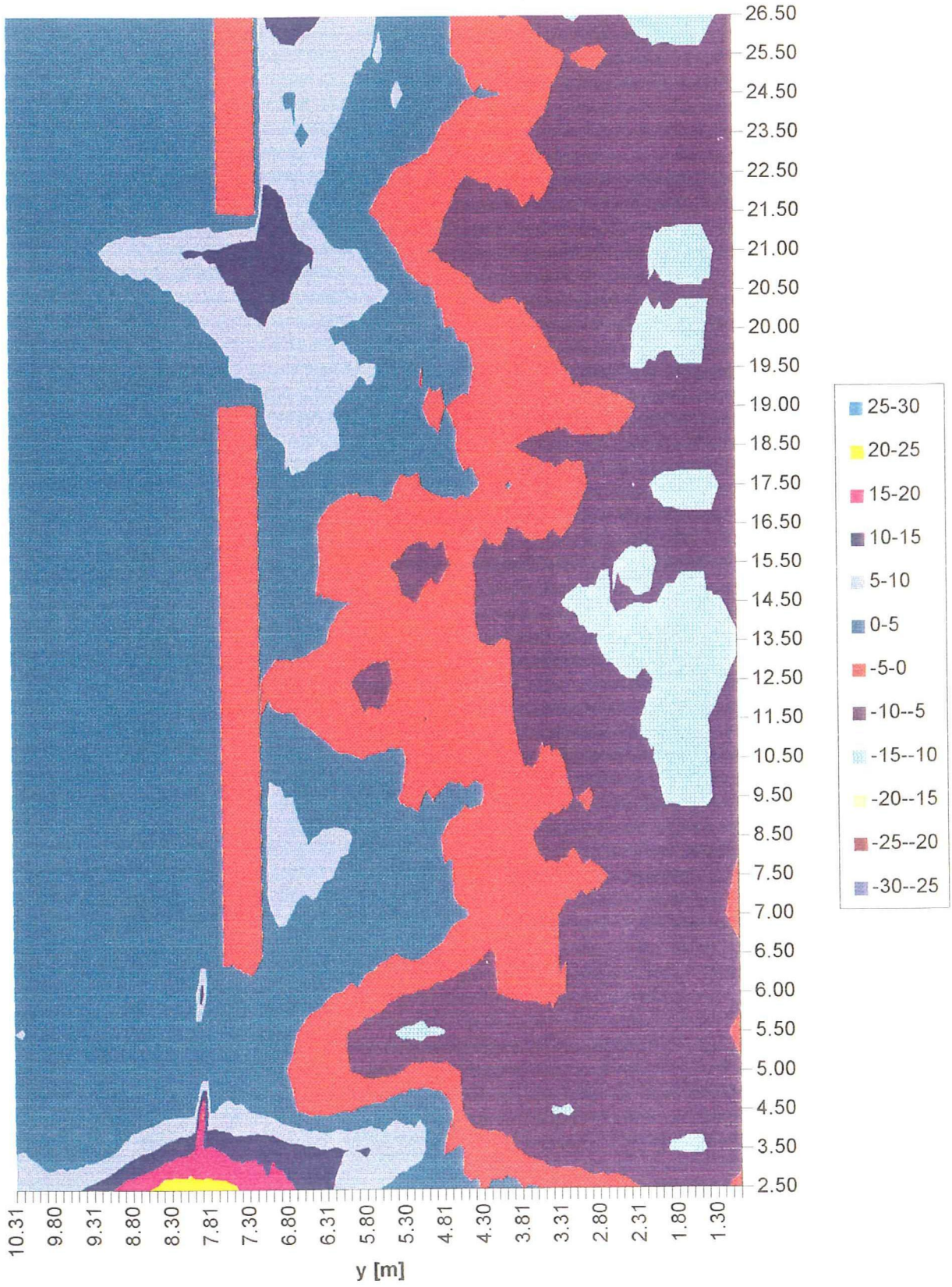

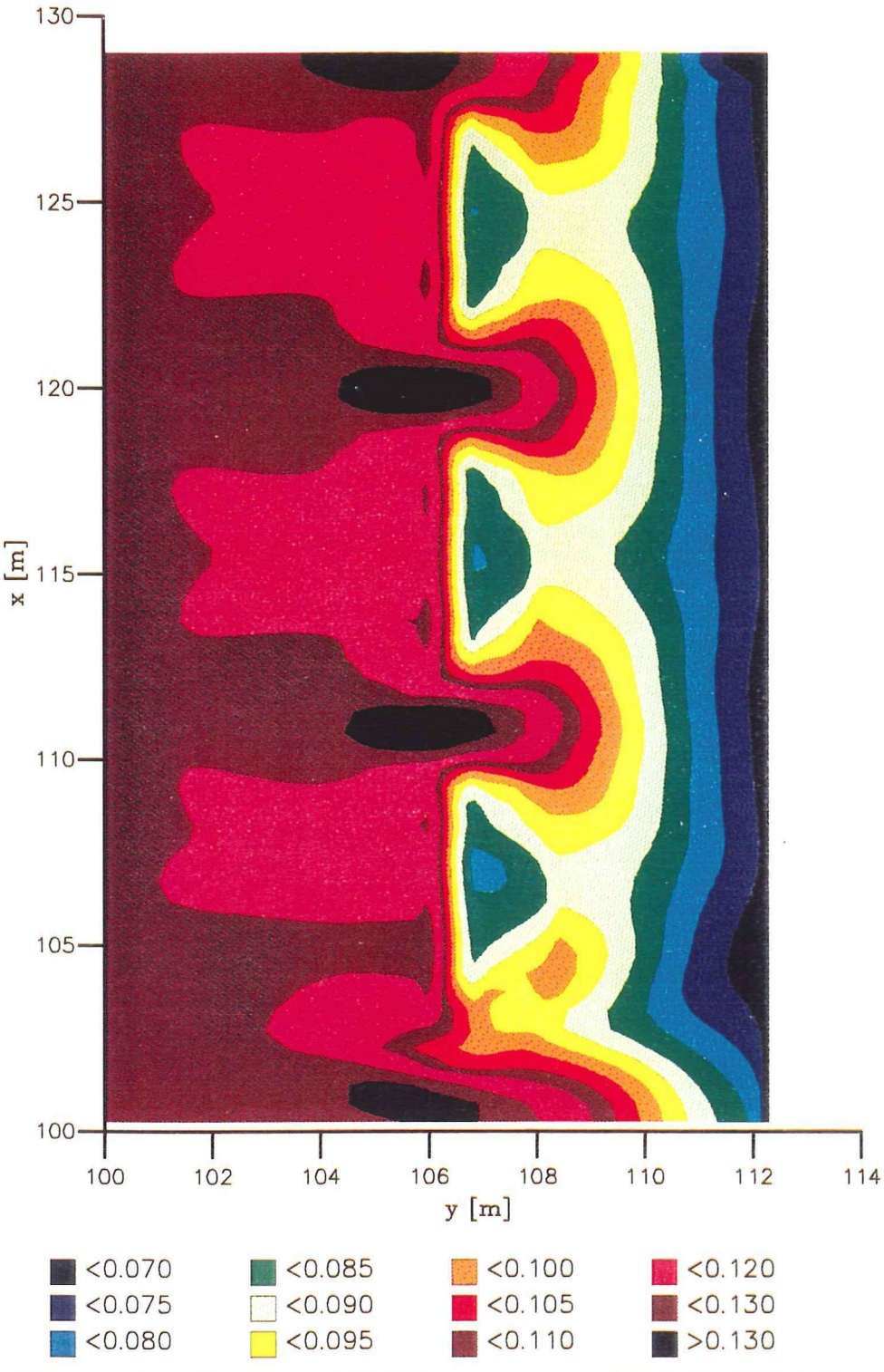

Wave field after 7.5 hours	D3	H=0.12 m
	Wave heights [m]	
Delft University of Technology	DELFT3D	A15–1

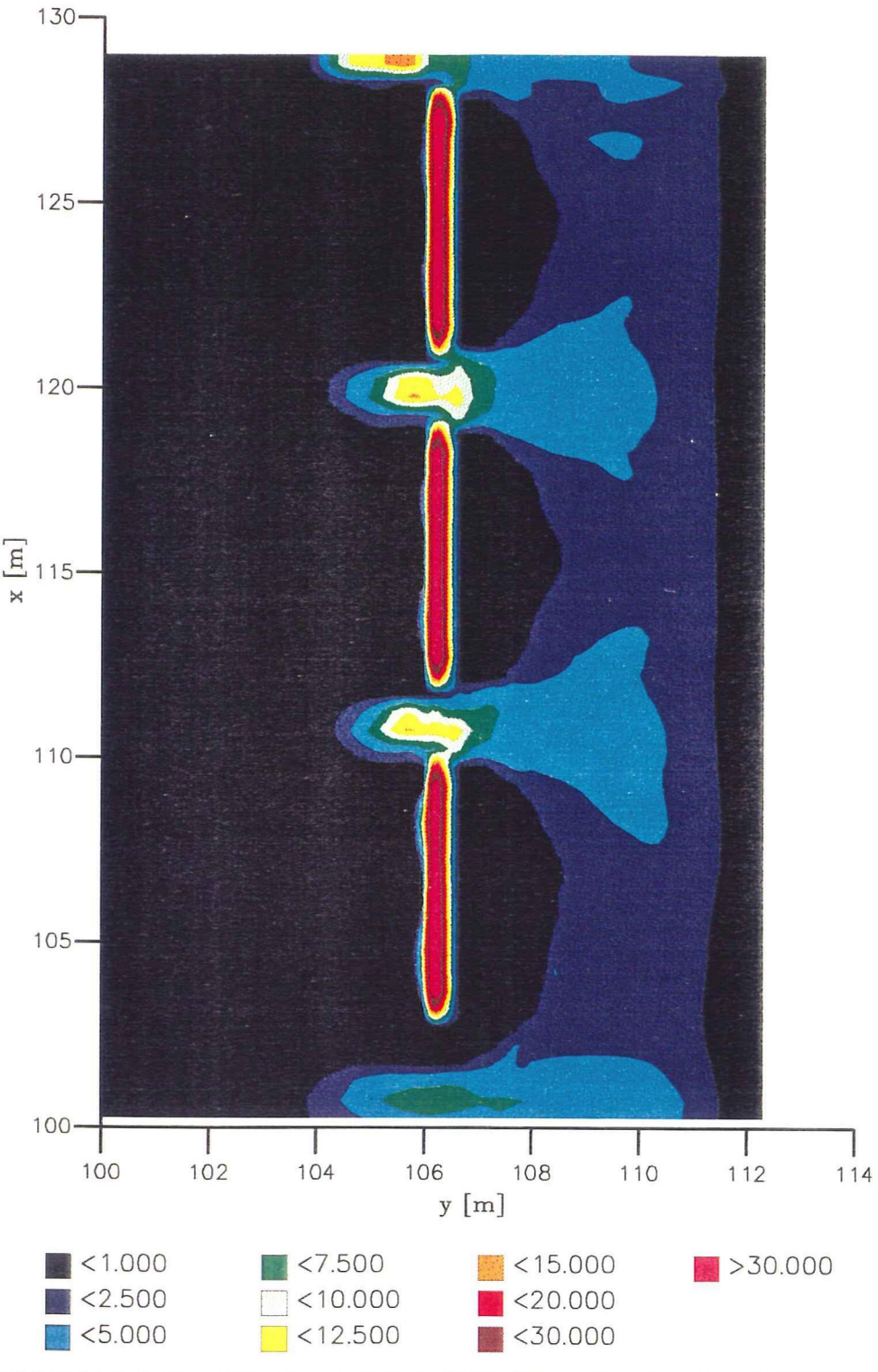

Dissipation after 7.5 hours	D3	H=0.12 m
	Dissipation [W/m2]	
Delft University of Technology	DELFT3D	A15-2

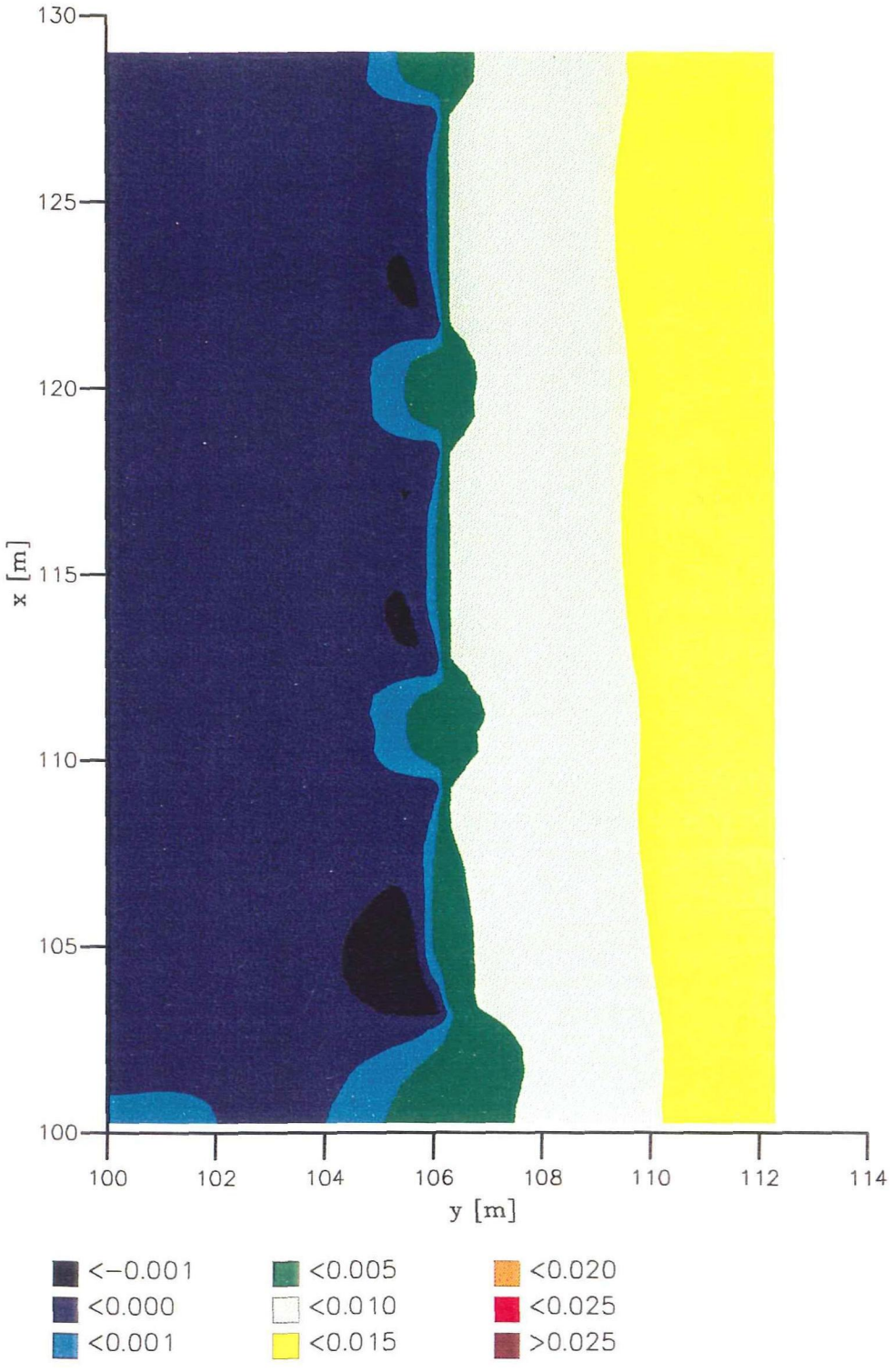

Water level after 7.5 hours (water levels positive upwards)	D3	H=0.12 m
	Water levels [m]	
Delft University of Technology	DELFT3D	A15−3

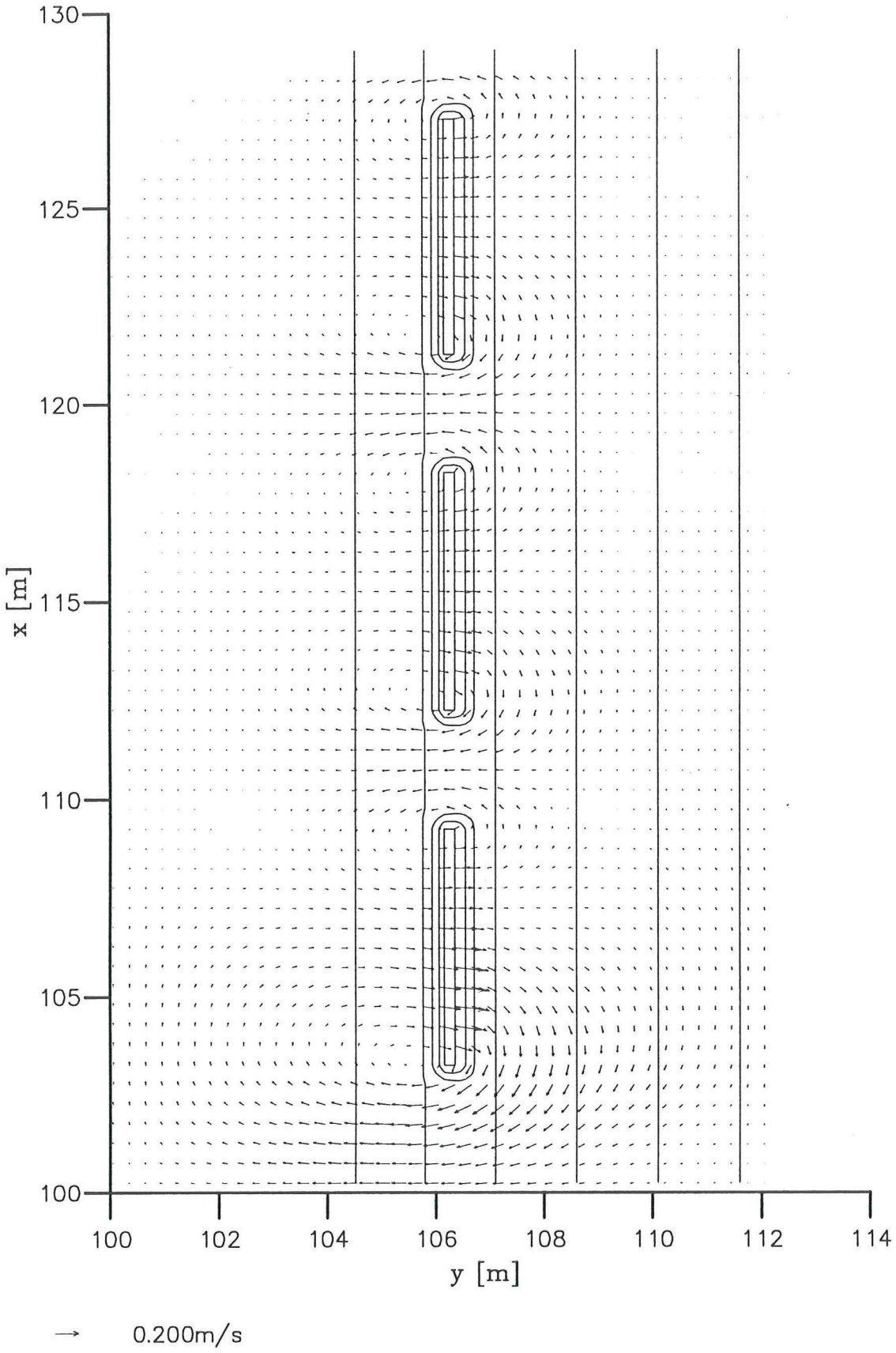

Flow field after 7.5 hours	D3	H=0.12 m
	Flow velocities [m/s]	
Delft University of Technology	DELFT3D	A15-4

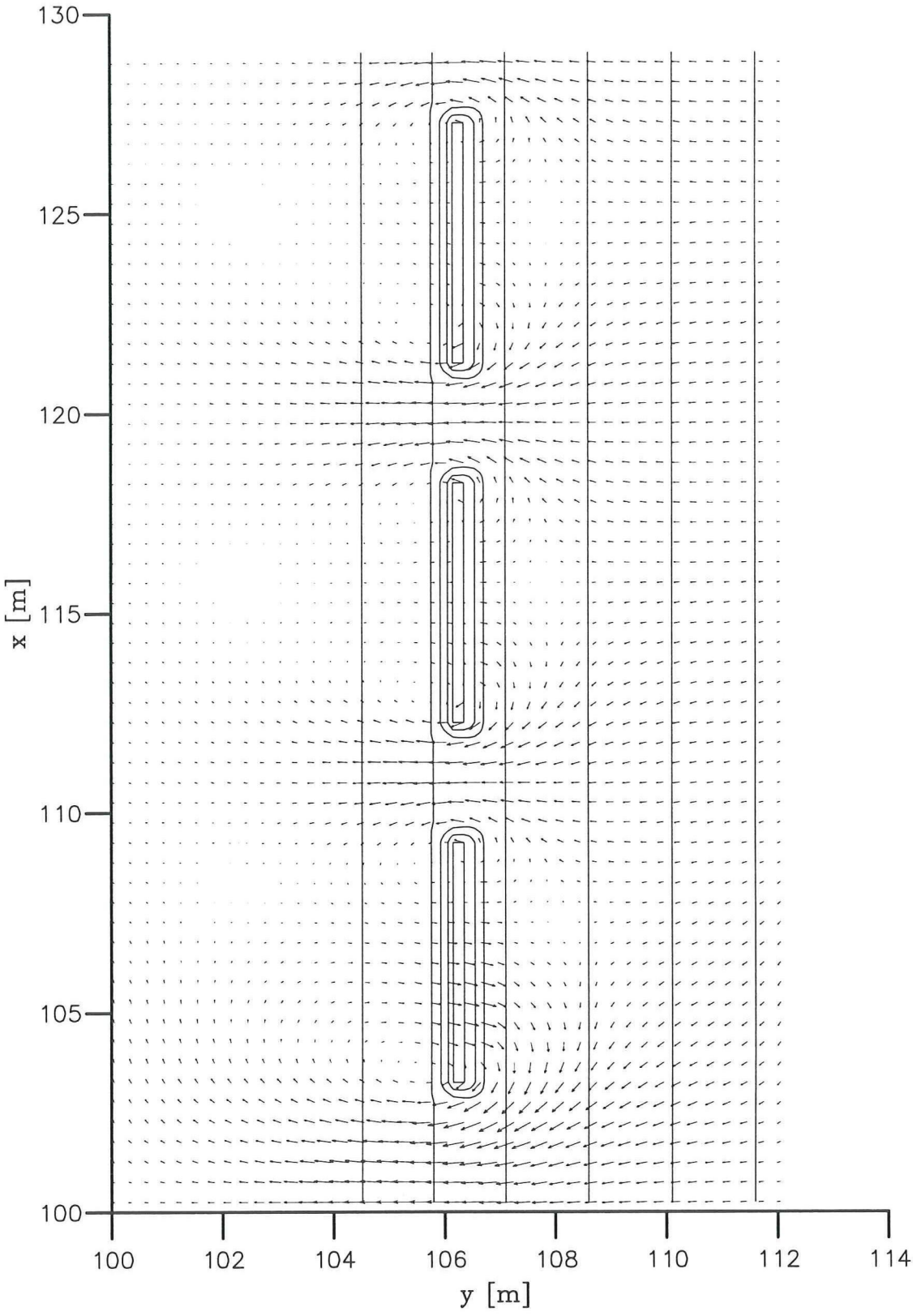

Return flow field after 7.5 hours	D3	H=0.12 m
	Flow velocities [m/s]	
Delft University of Technology	DELFT3D	A15–5

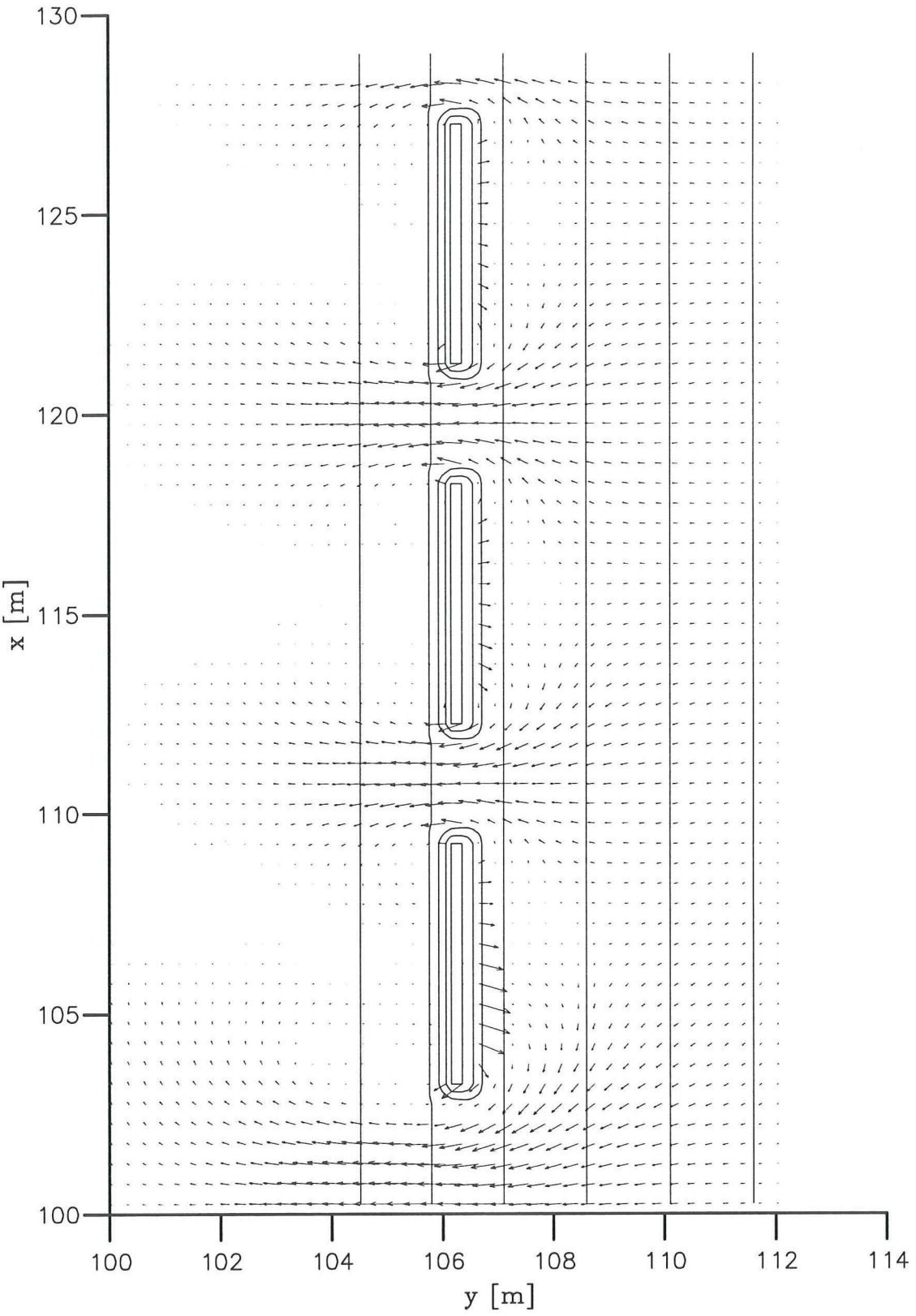

Sediment transport field after 7.5 hours	D3	H=0.12 m
	Sed. transport [m/s]	
Delft University of Technology	DELFT3D	A15–6

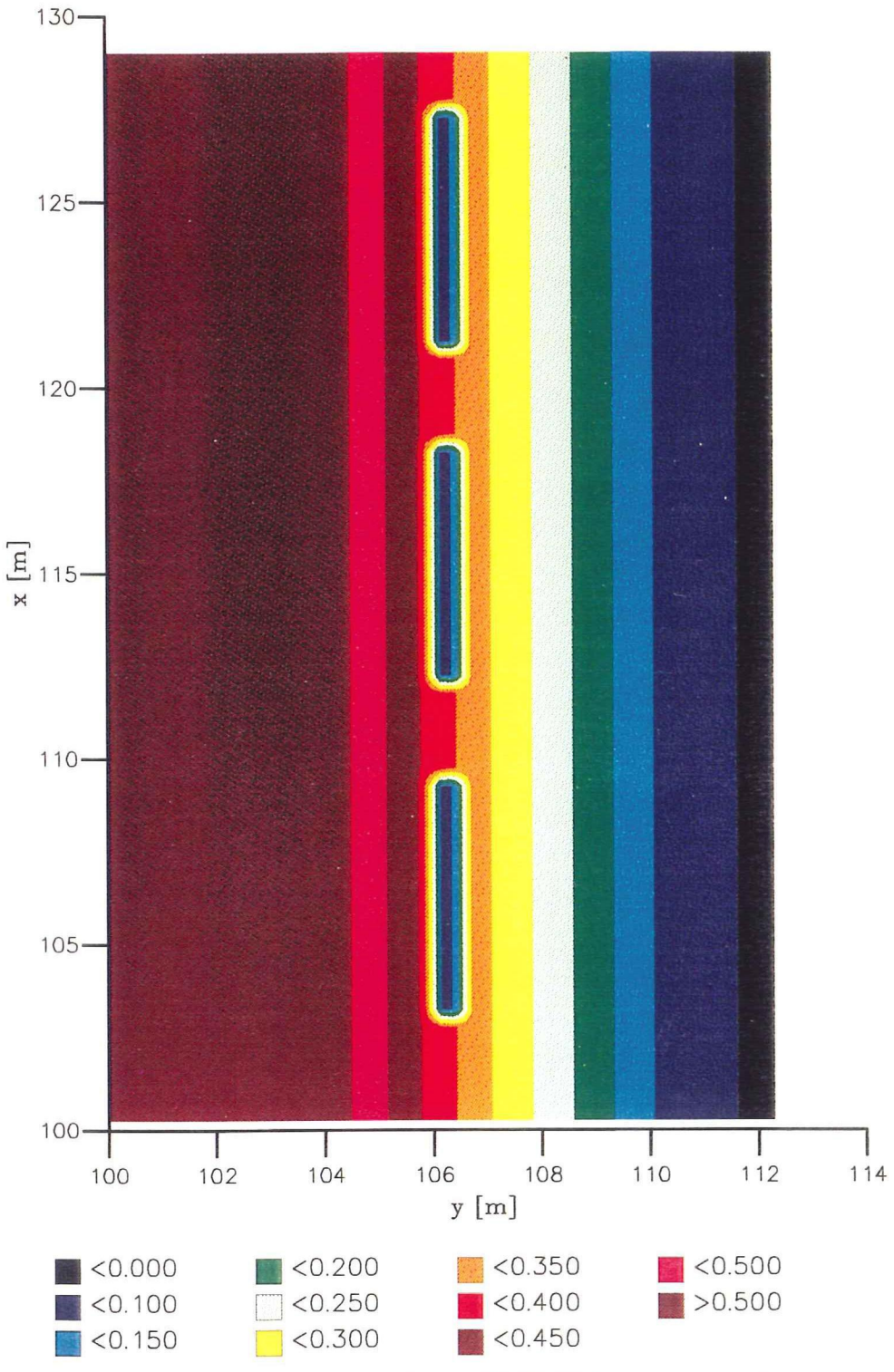

Initial bathymetry (bottom depths positive downwards)	D3	H=0.12 m
	Bottom depths [m]	
Delft University of Technology	DELFT3D	A15-7

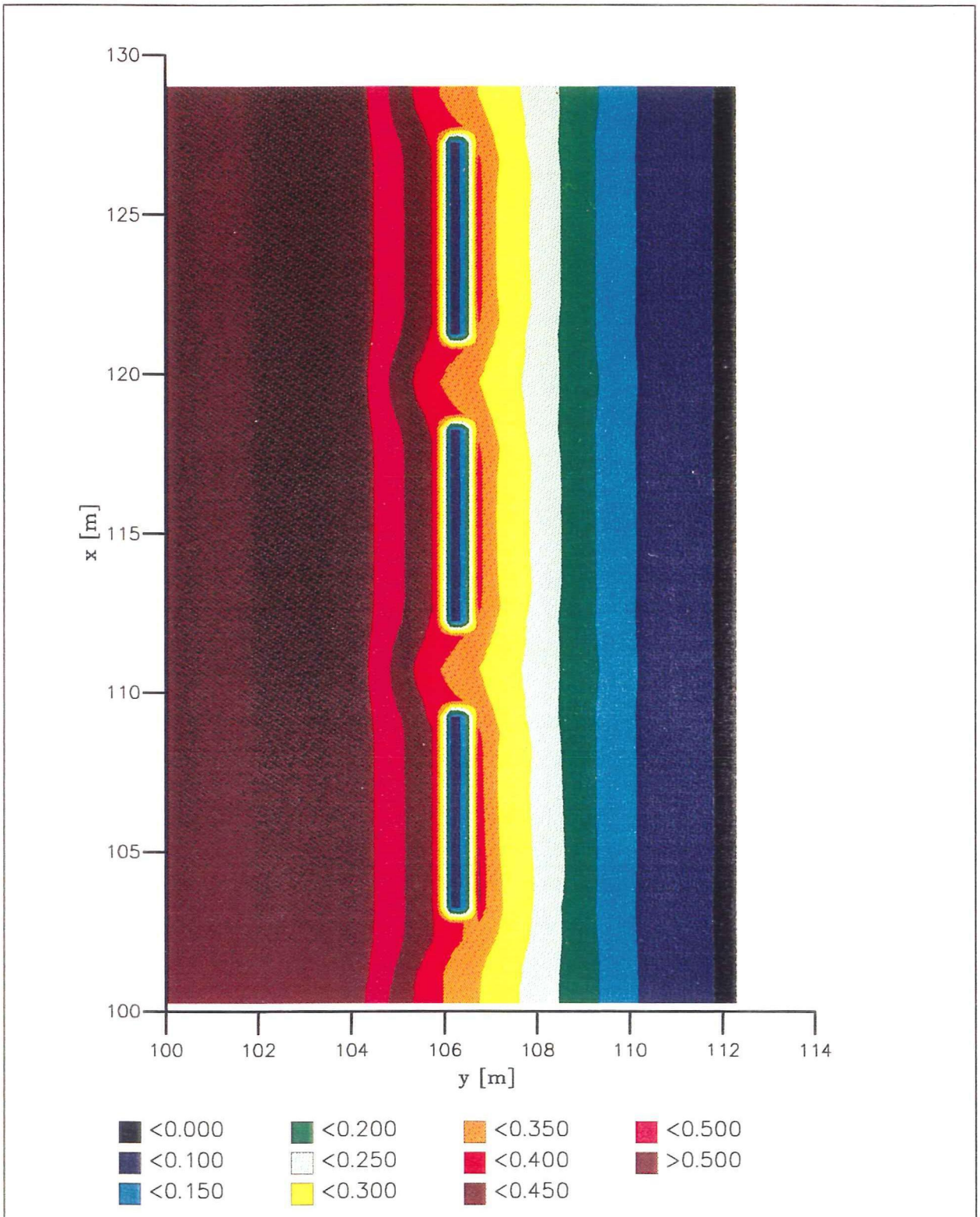

Bathymetry after 0.5 hours (bottom depths positive downwards)	D3	H=0.12 m
	Bottom depths [m]	
Delft University of Technology	DELFT3D	A15-8

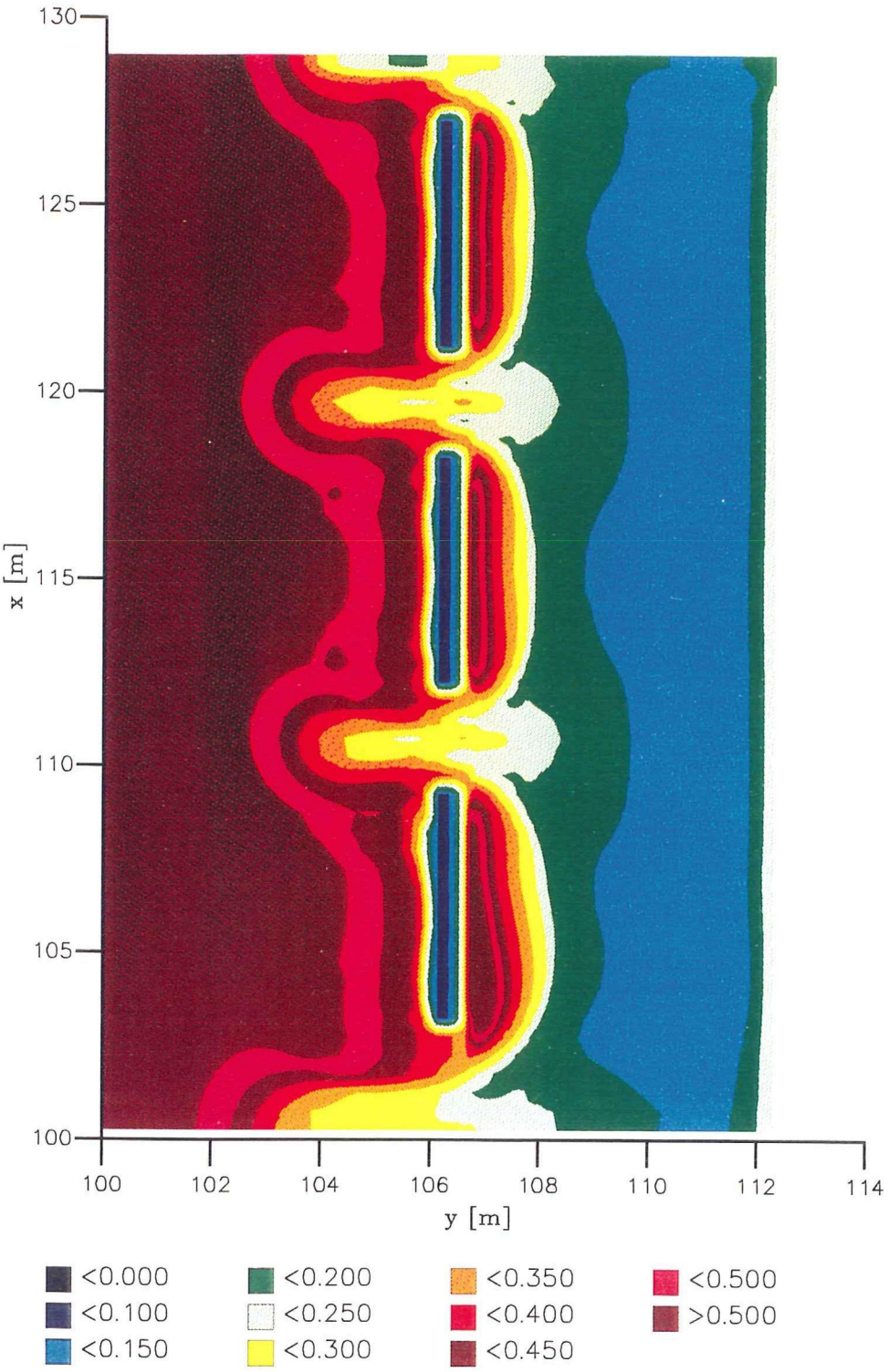

Bathymetry after 7.5 hours (bottom depths positive downwards)	D3	H=0.12 m
	Bottom depths [m]	
Delft University of Technology	DELFT3D	A15–9

Computed erosion/accretion after 7.5 hours
Three breakwaters, H = 0.12 m

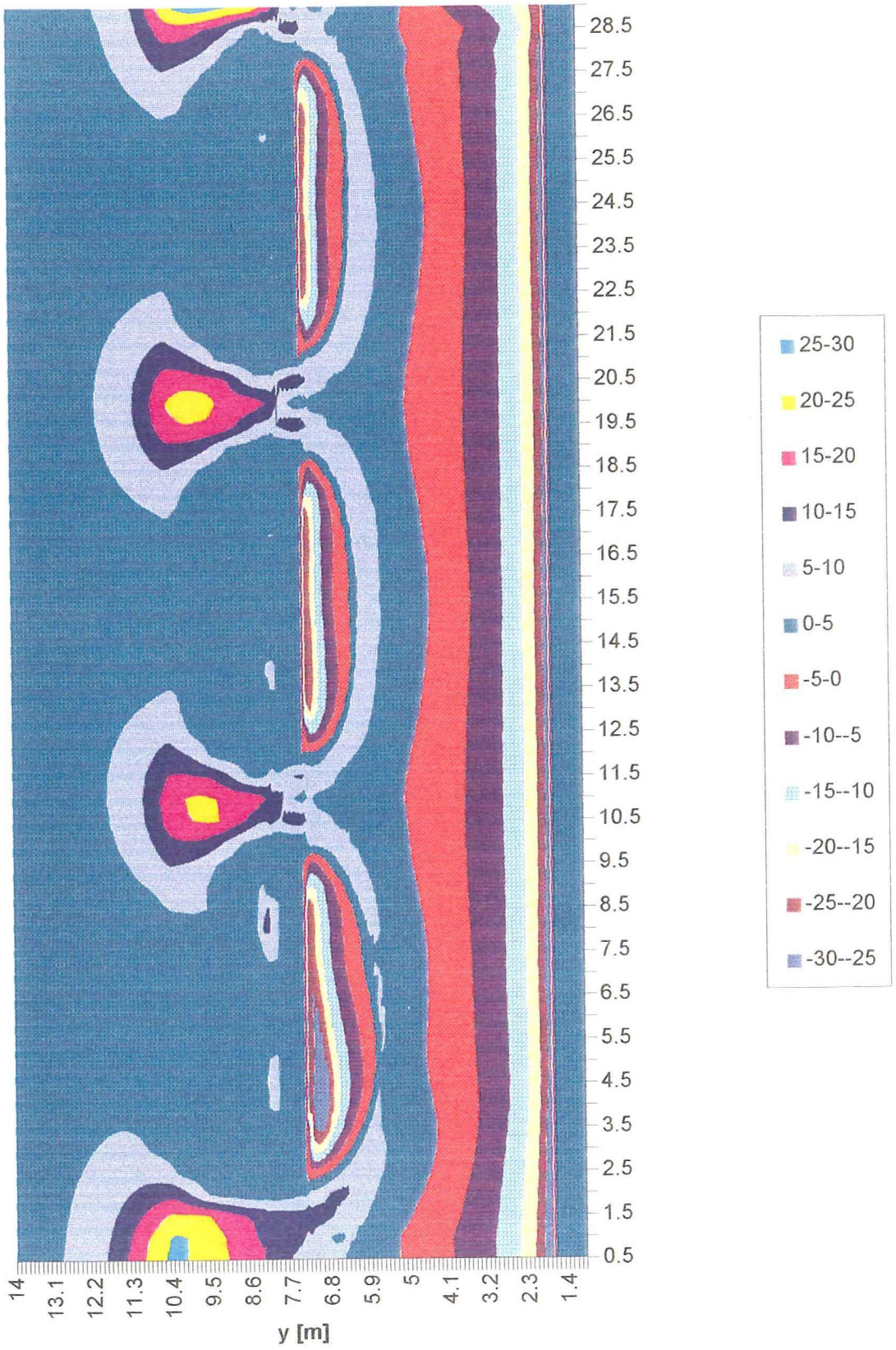

Measured erosion/accretion after 7.5 hours
Two breakwaters, H = 0.12 m

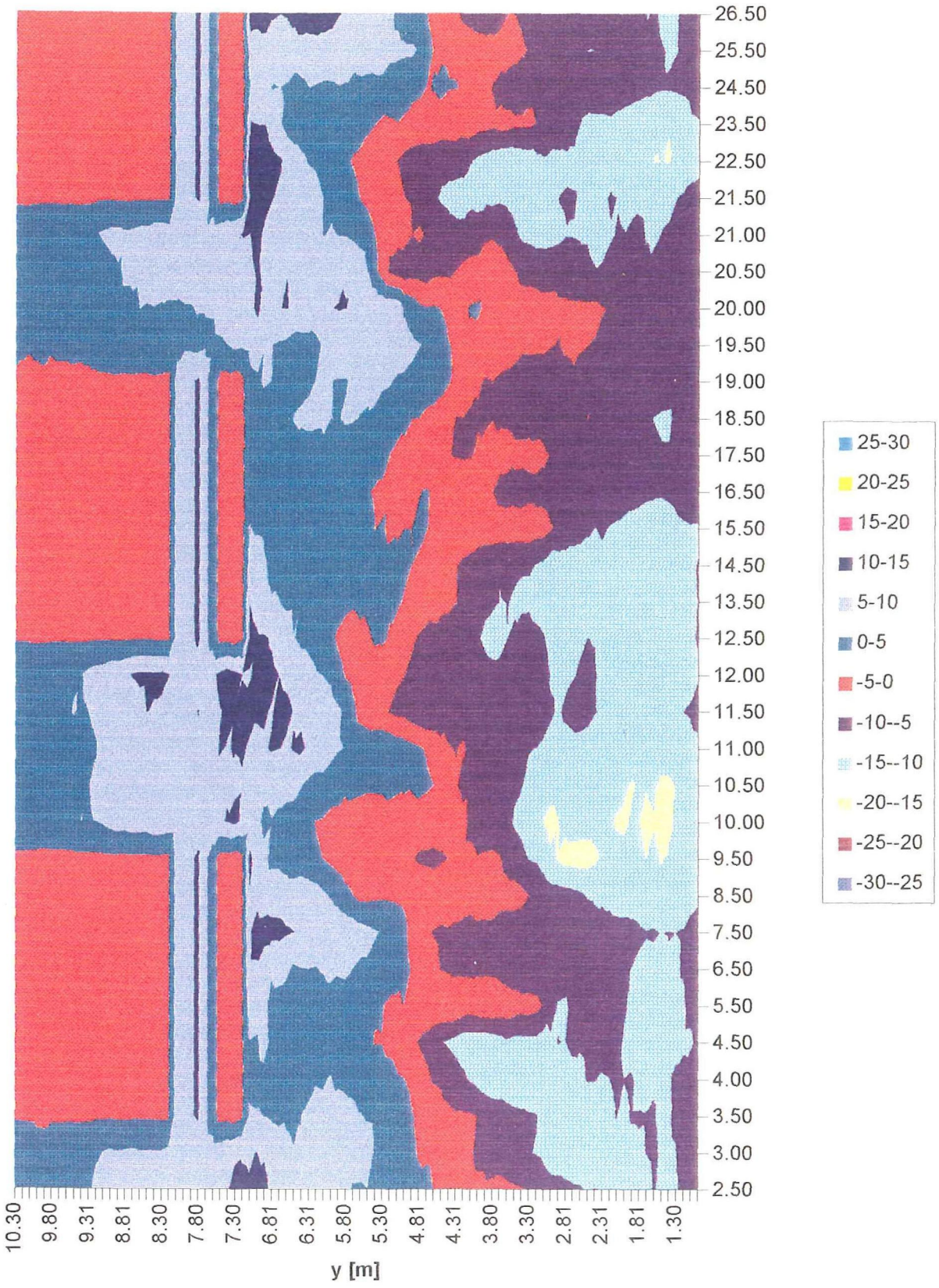

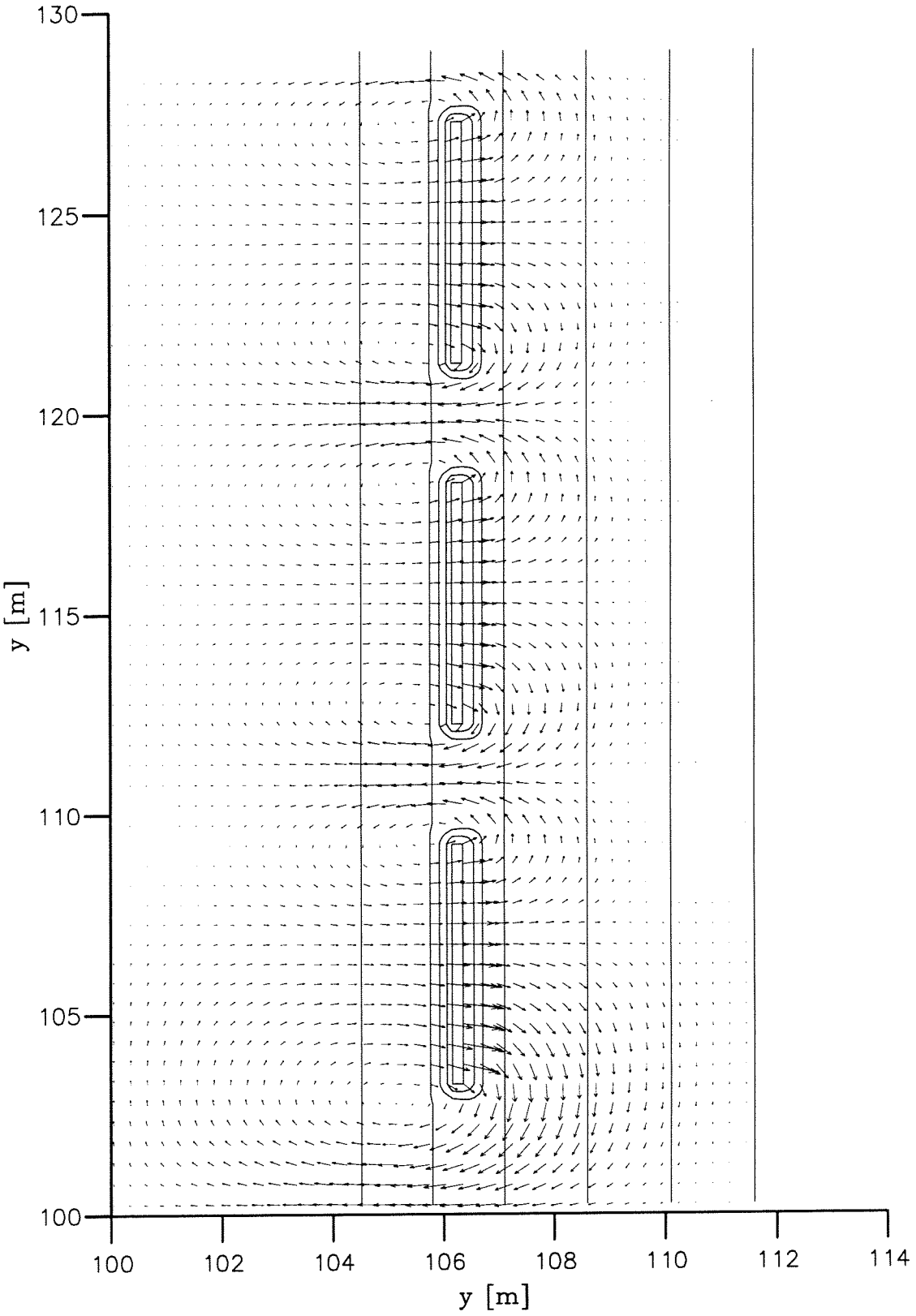

Initial flow field (gamma_s = 1)	D3	H=0.12 m
	Flow velocities [m/s]	
Delft University of Technology	DELFT3D	A17−1

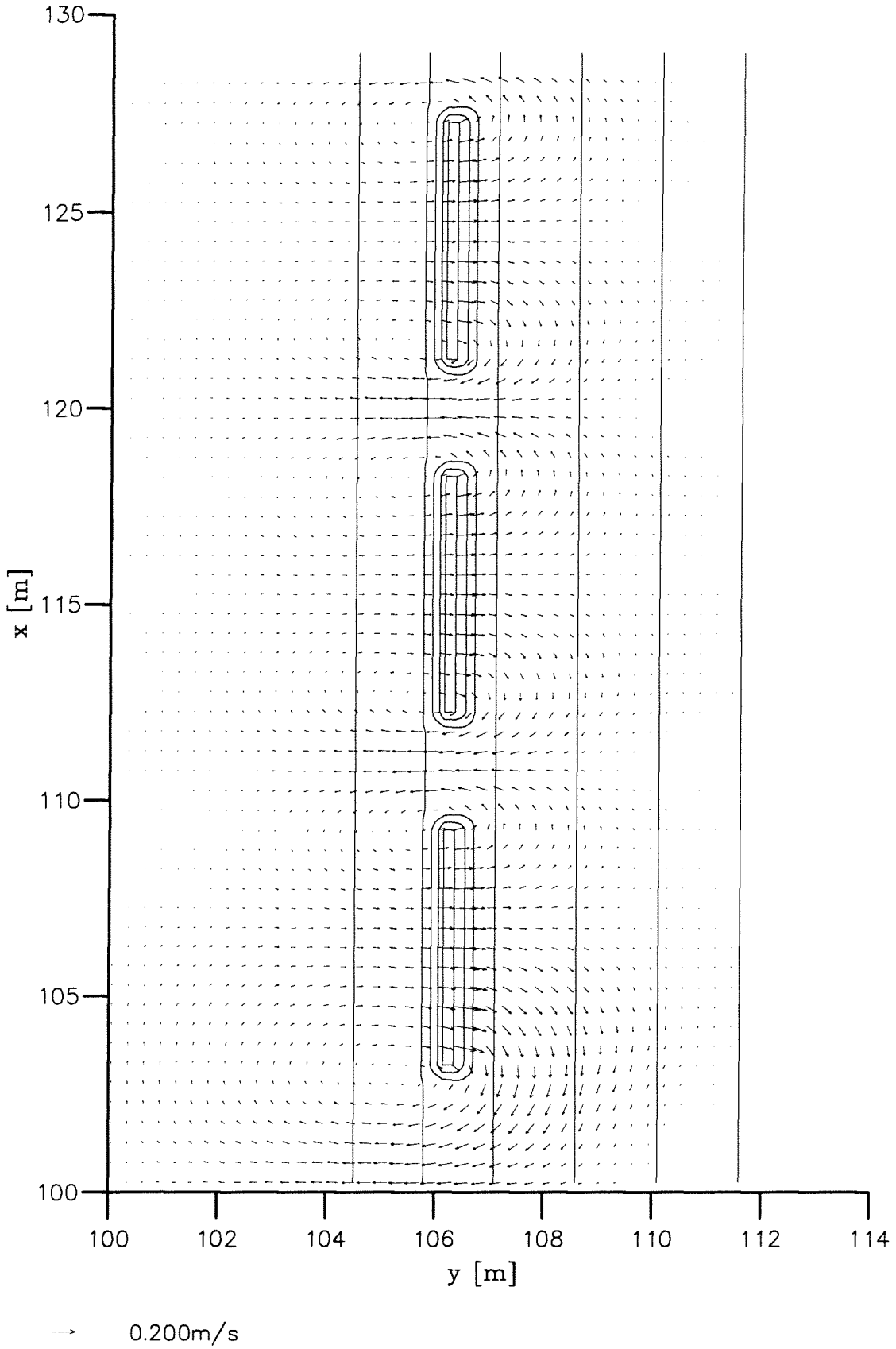

Initial flow field (gamma_s = 4)	D3	H=0.12 m
	Flow velocities [m/s]	
Delft University of Technology	DELFT3D	A17–2

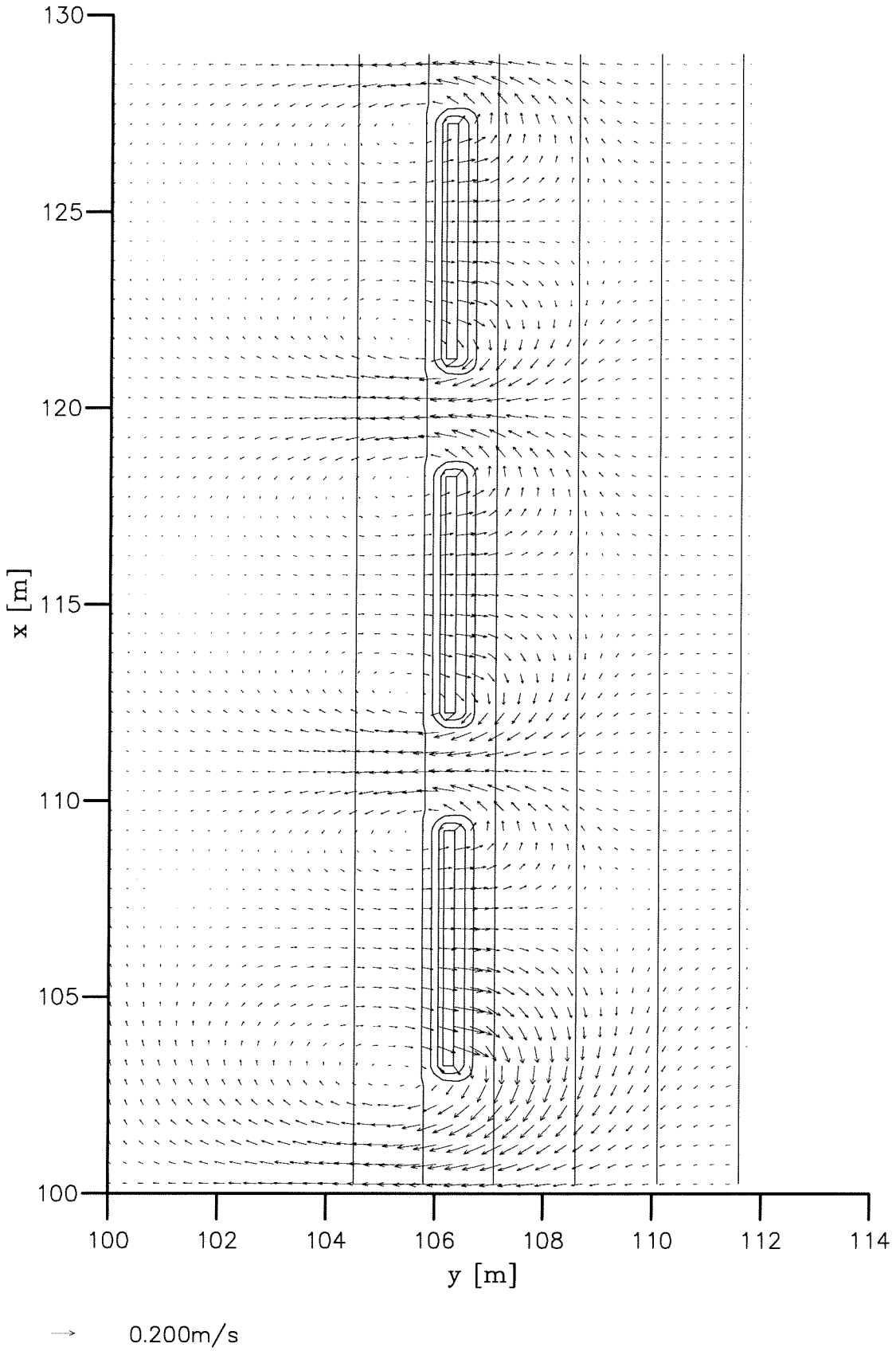

Initial return flow field (gamma_s = 1)	D3	H=0.12 m
	Flow velocities [m/s]	
Delft University of Technology	DELFT3D	A17–3

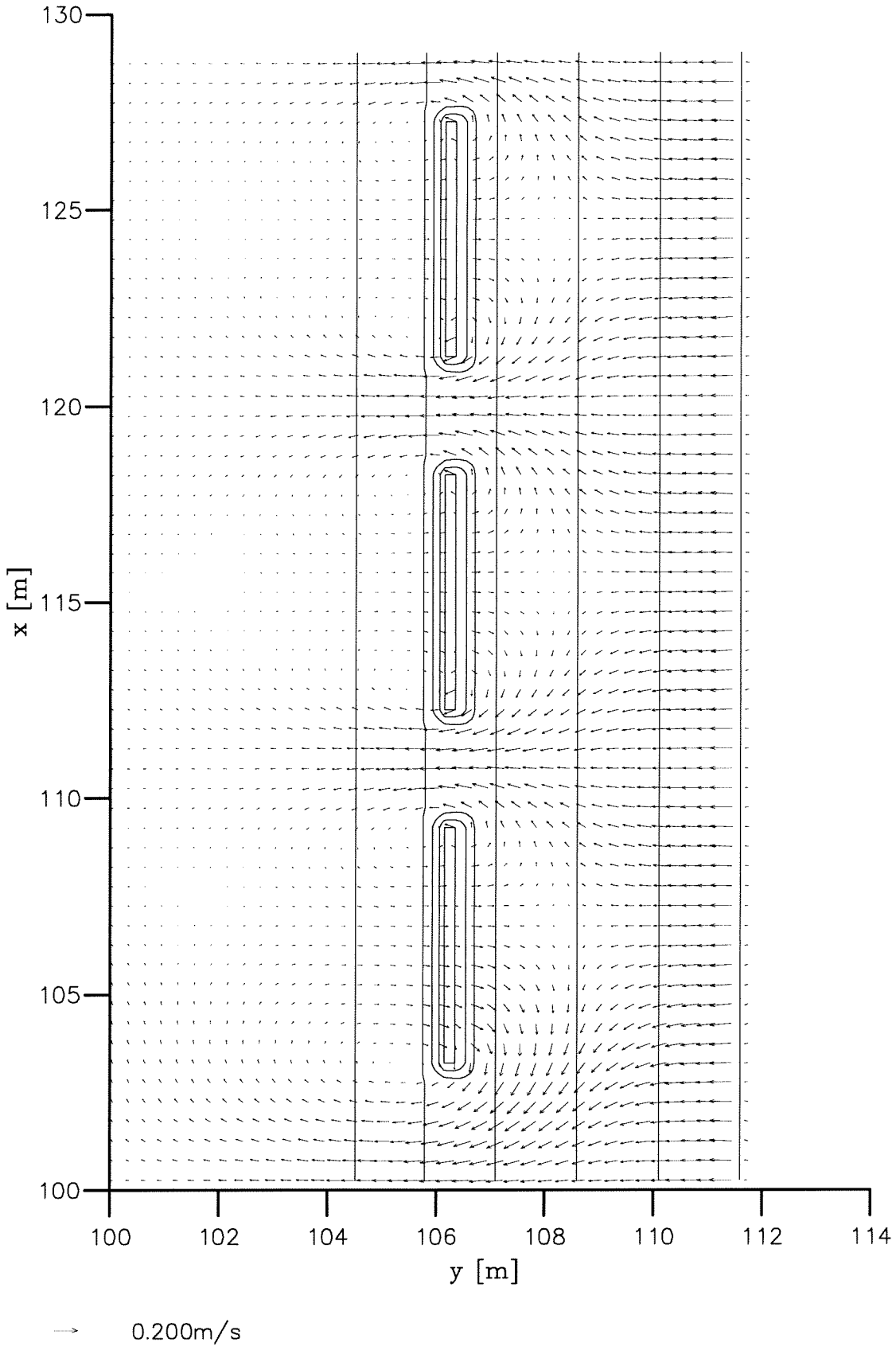

Initial return flow field (gamma_s = 4)	D3	H=0.12 m
	Flow velocities [m/s]	
Delft University of Technology	DELFT3D	A17–4

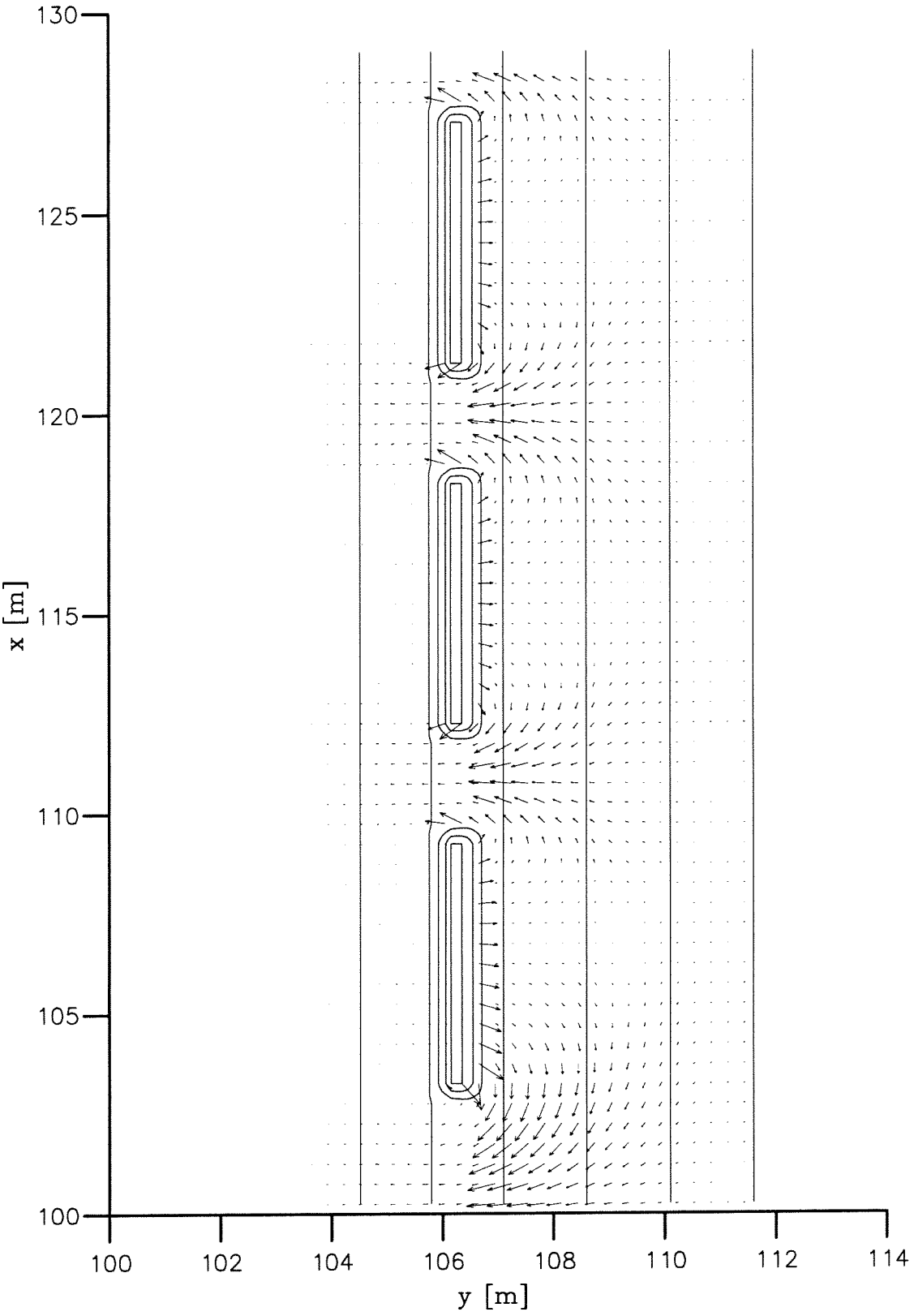

Initial sediment transport field (gamma_s = 1)	D3	H=0.12 m
	Sed. transport [m/s]	
Delft University of Technology	DELFT3D	A17–5

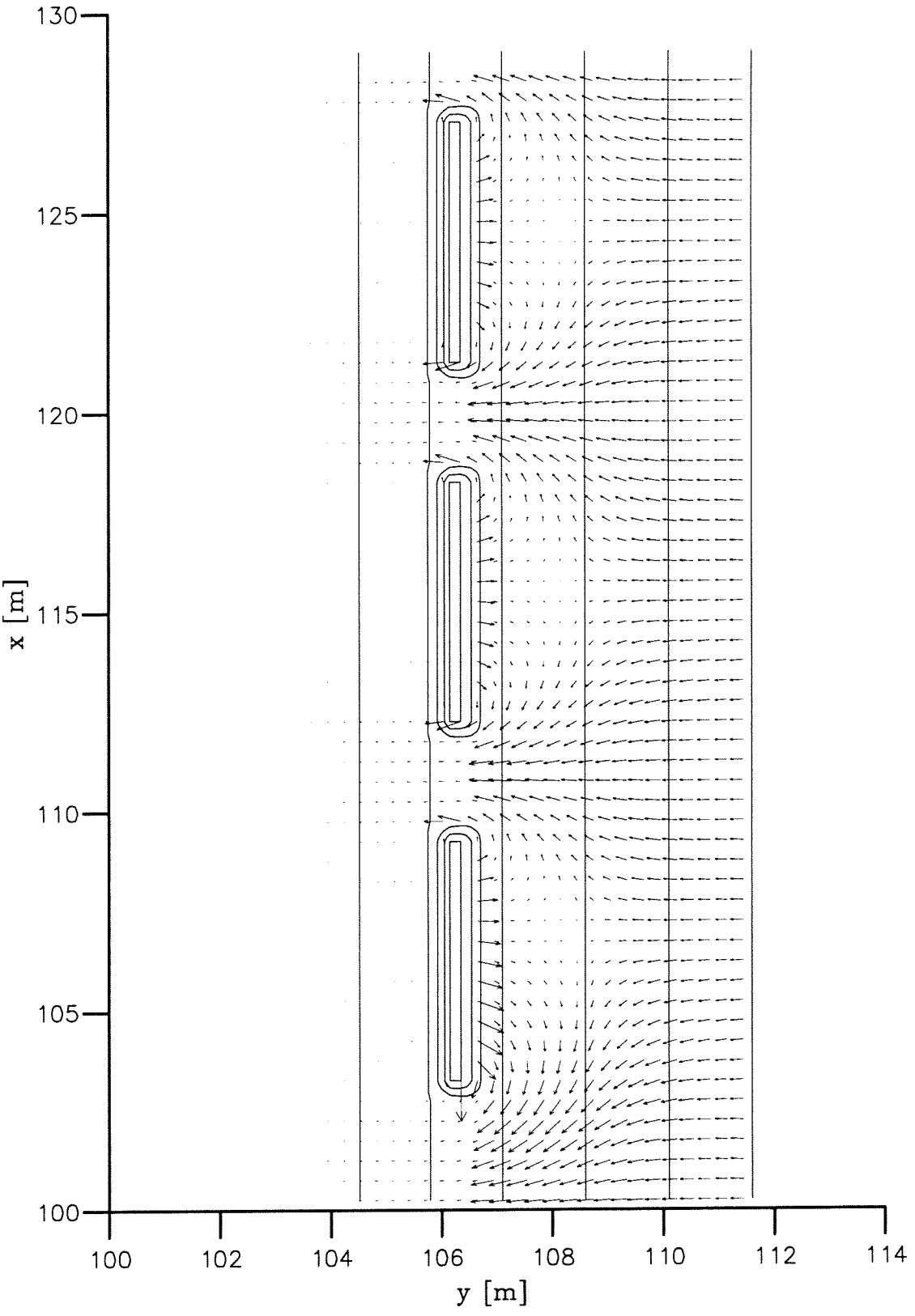

Initial sediment transport field (gamma_s = 4)	D3	H=0.12 m
	Sed. transport [m2/s]	
Delft University of Technology	DELFT3D	A17–6

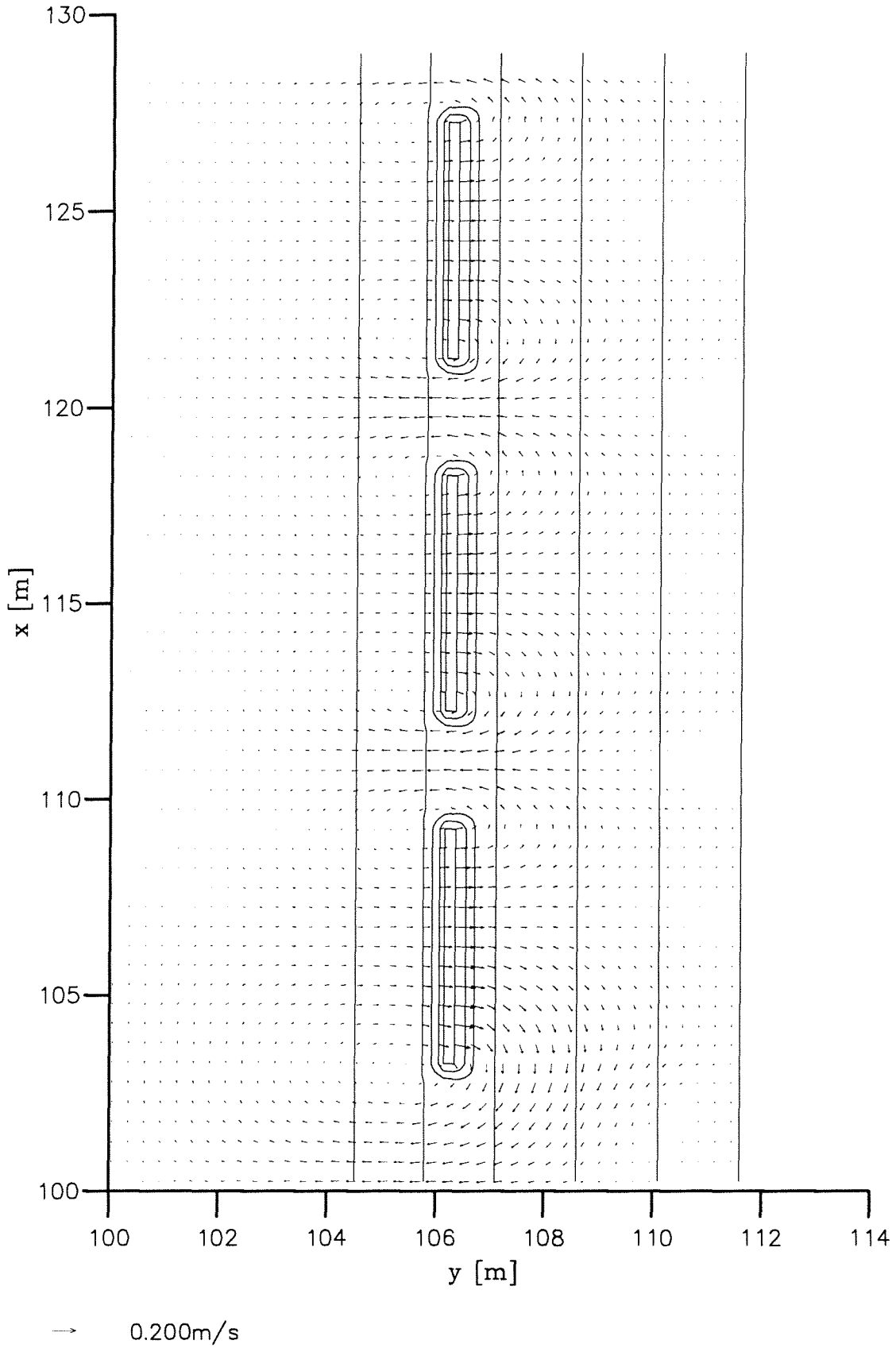

Initial flow field (alpha = 1)	D3	H=0.12 m
	Flow velocities [m/s]	
Delft University of Technology	DELFT3D	A17–7

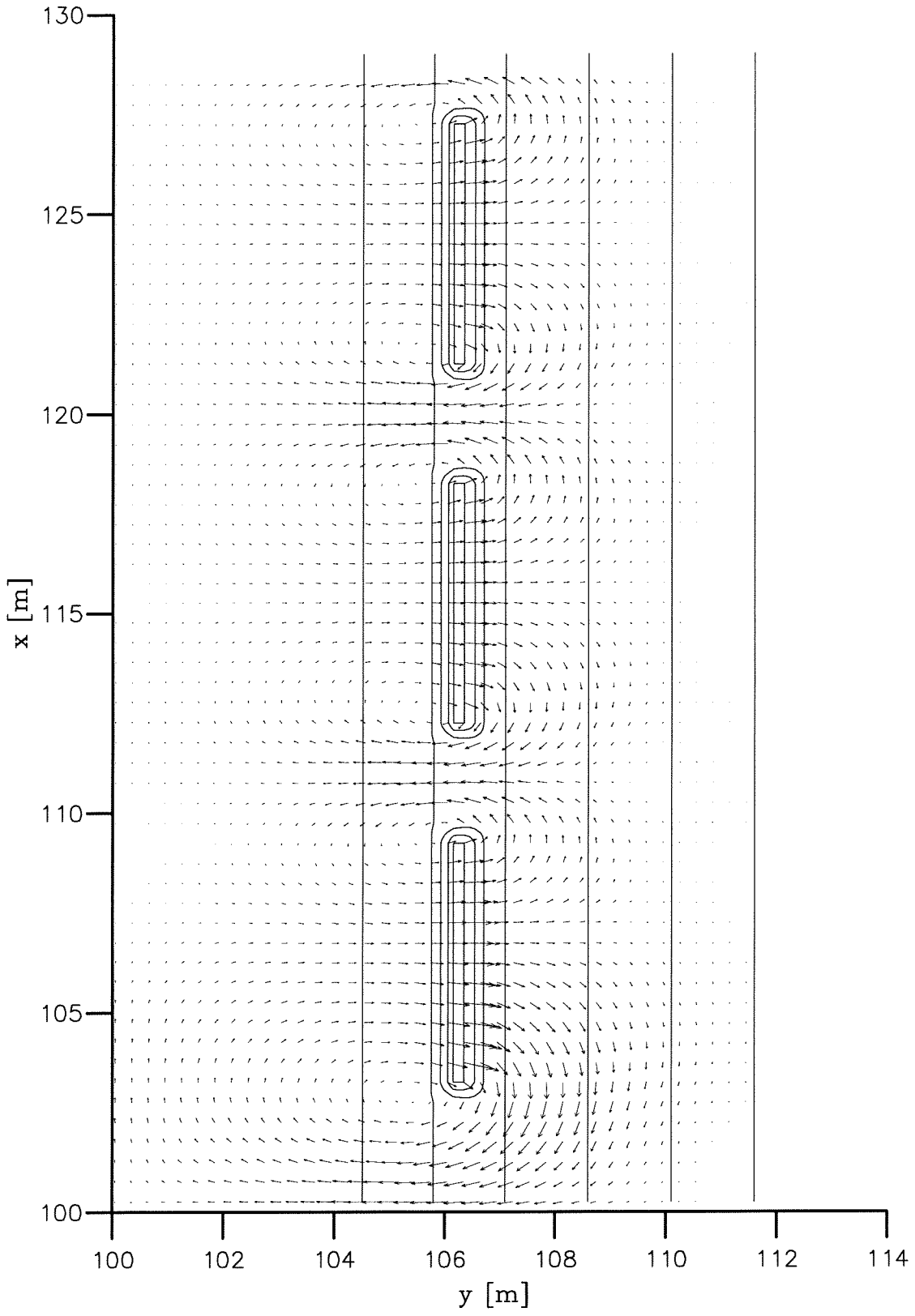

Initial flow field (alpha = 10)	D3	H=0.12 m
	Flow velocities [m/s]	
Delft University of Technology	DELFT3D	A17–8

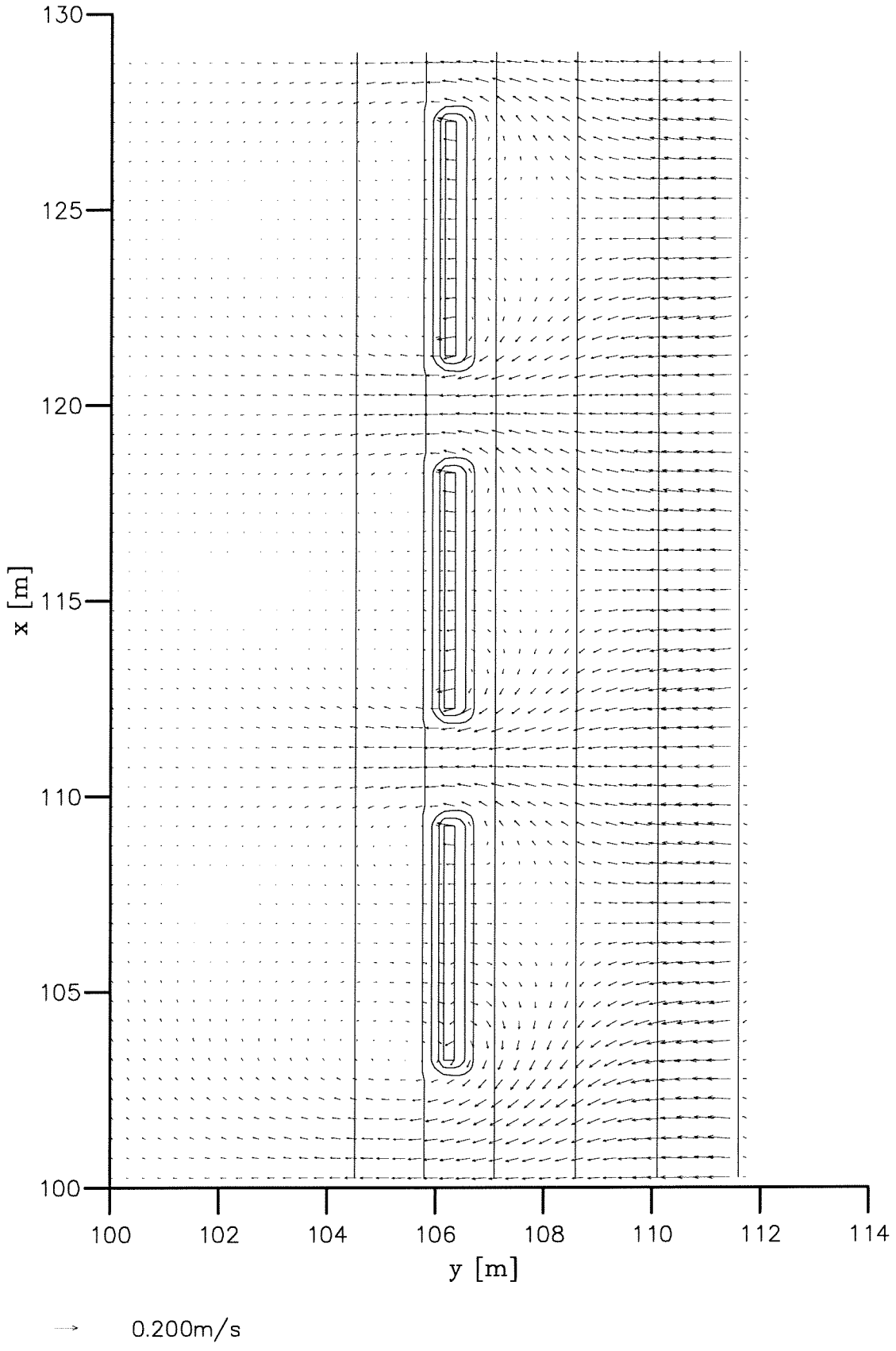

Initial return flow field (alpha = 1)	D3	H=0.12 m
	Flow velocities [m/s]	
Delft University of Technology	DELFT3D	A17–9

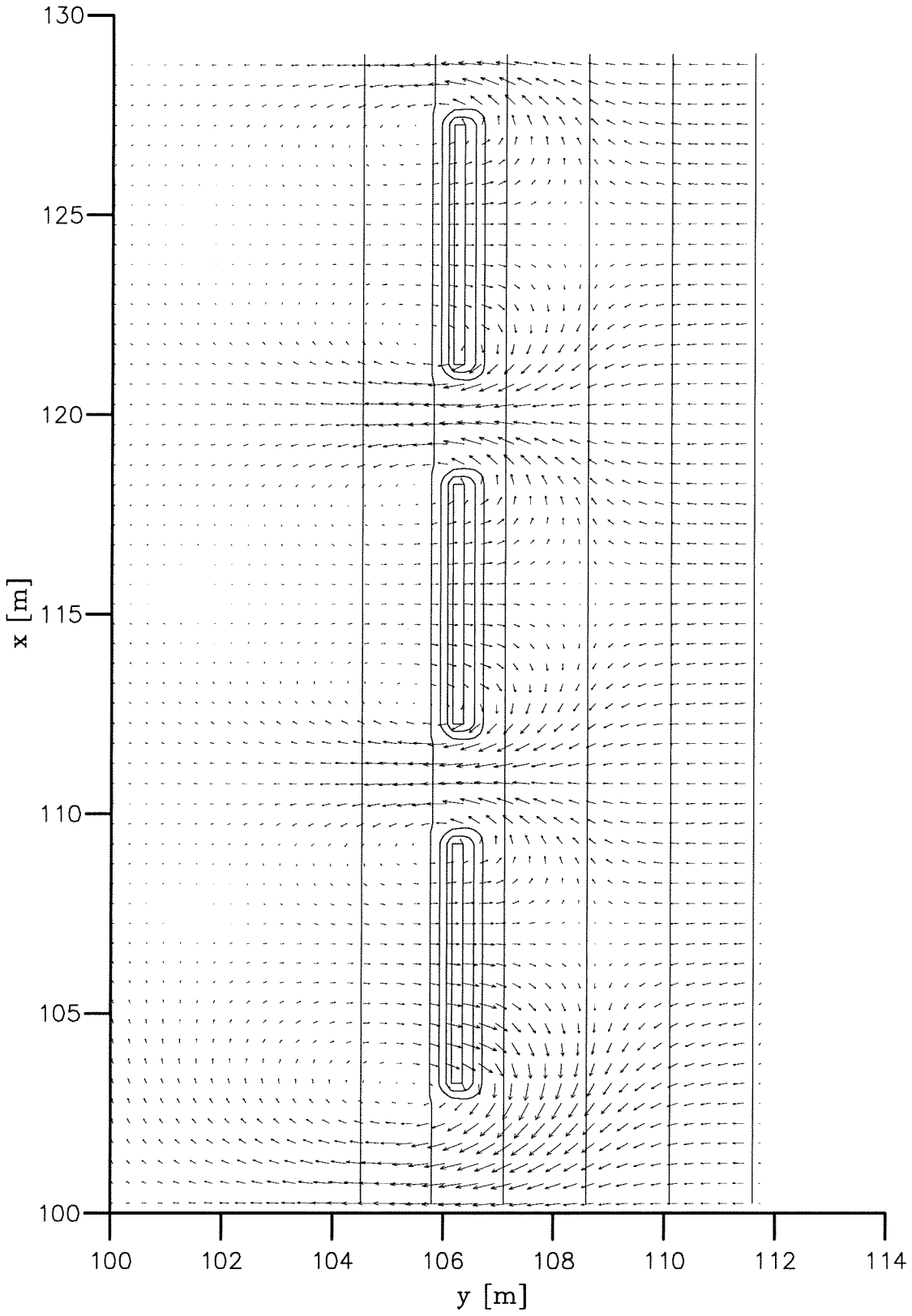

Initial return flow field (alpha = 10)	D3	H=0.12 m
	Flow velocities [m/s]	
Delft University of Technology	DELFT3D	A17–10

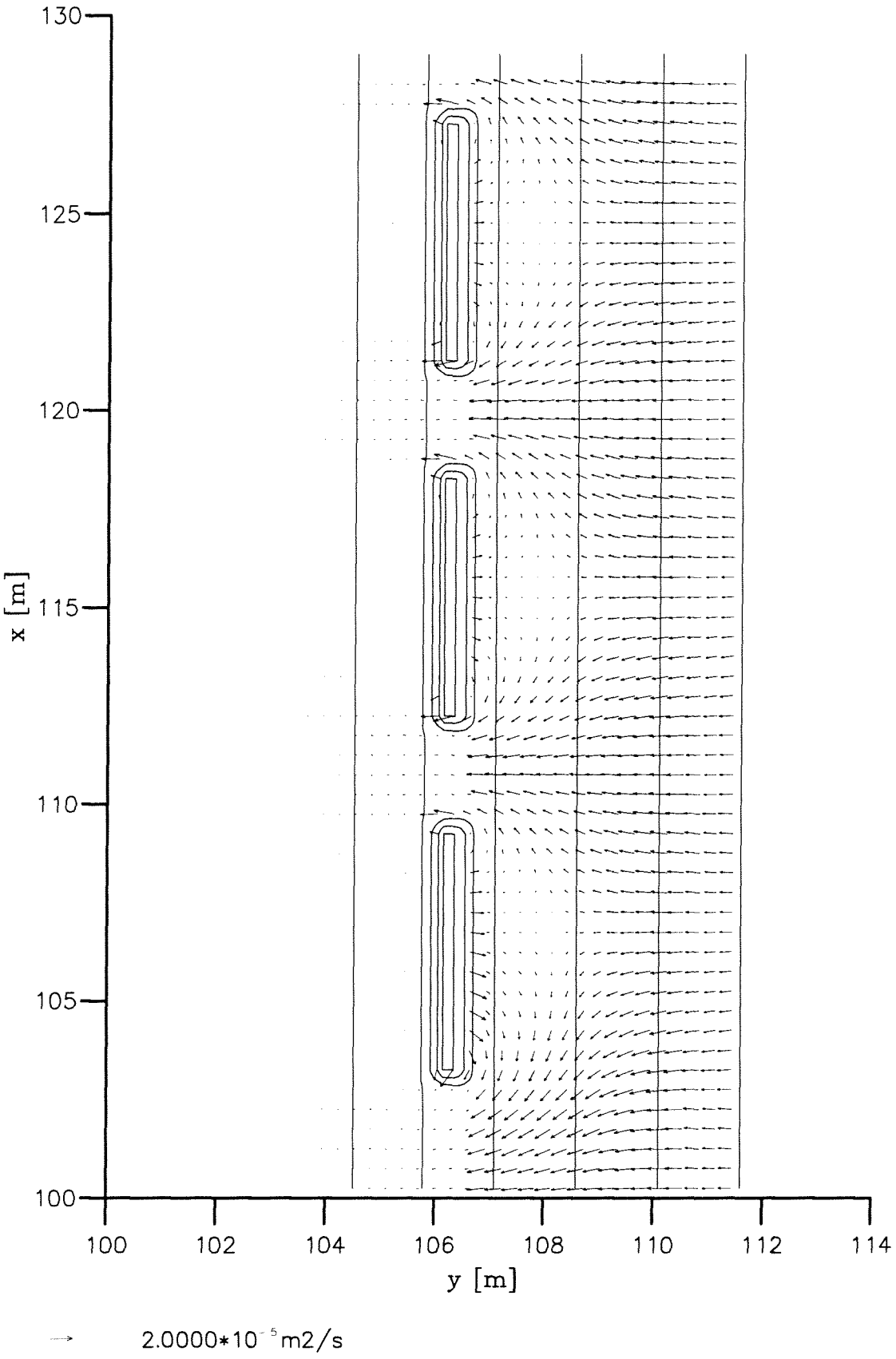

Initial sediment transport field (alpha = 1)	D3	H=0.12 m
	Sed. transport [m2/s]	
Delft University of Technology	DELFT3D	A17-11

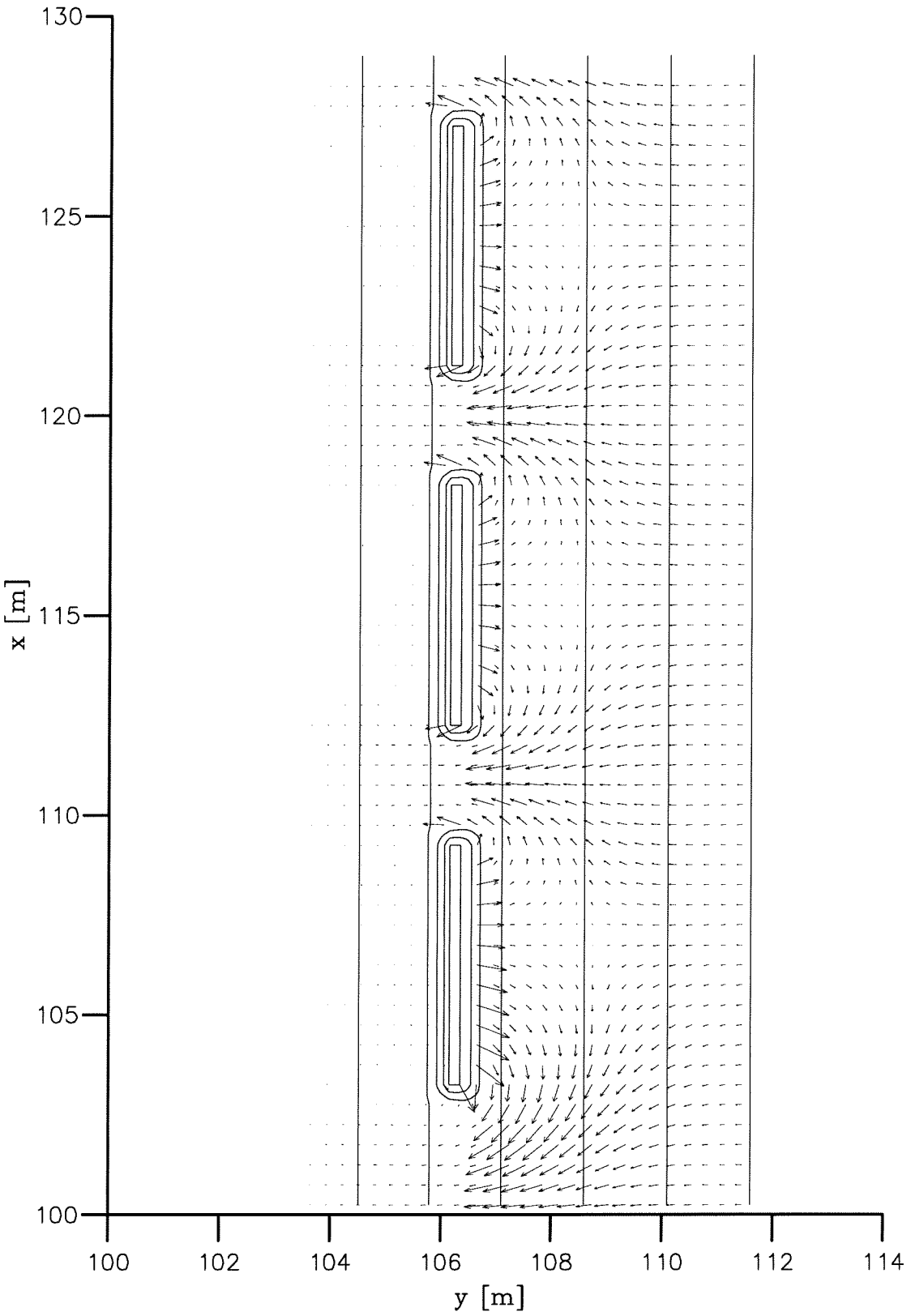

Initial sediment transport field (alpha = 10)	D3	H=0.12 m
	Sed. transport [m2/s]	
Delft University of Technology	DELFT3D	A17–12

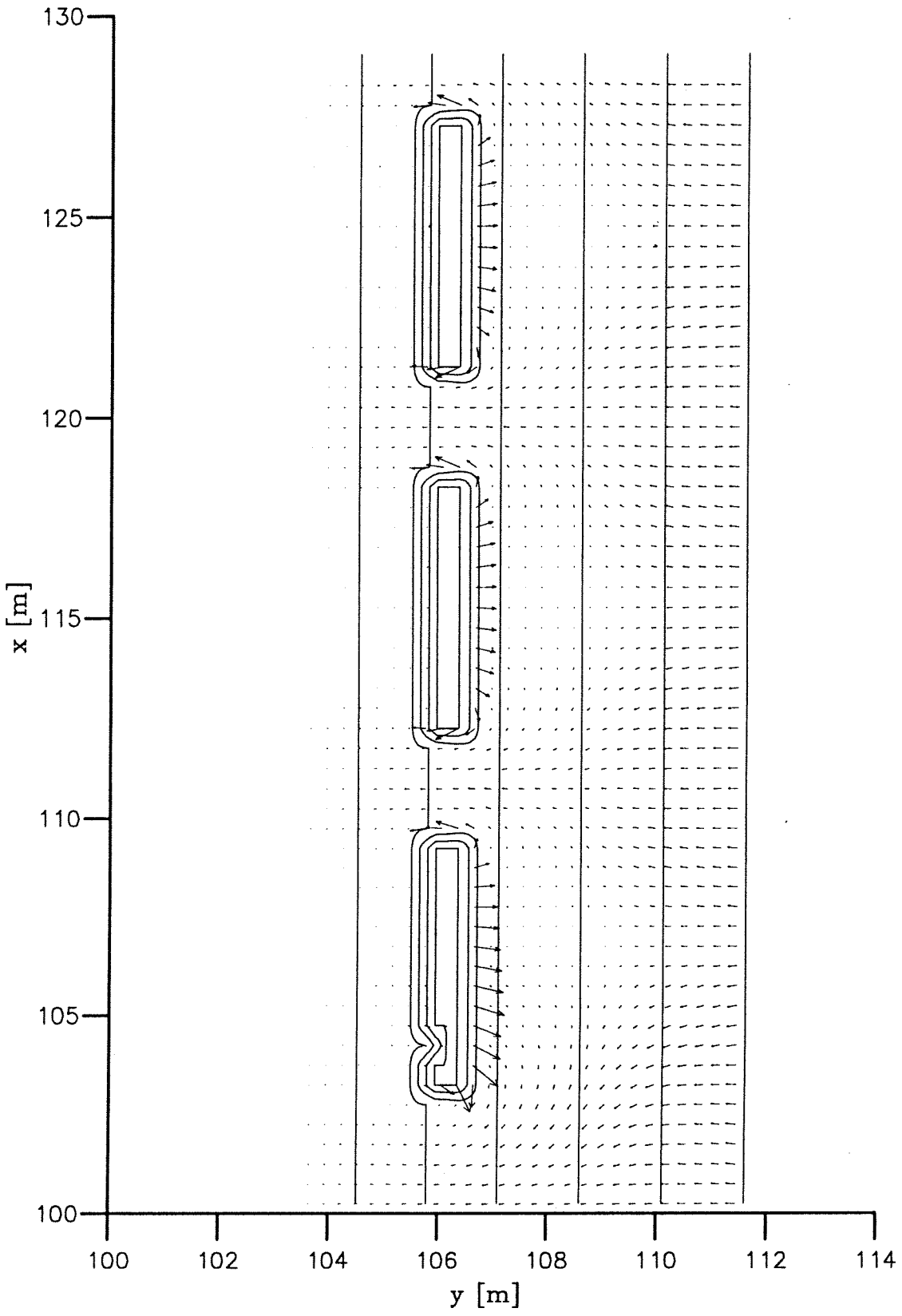

Initial sediment transport field (breakwaters with wider crests)	D3	H=0.12 m
	Sed. transport [m/s]	
Delft University of Technology	DELFT3D	A17–19